UNIVERSITÄT
DUISBURG
ESSEN

Offen im Denken

Chemoproteomics as a versatile approach for the study and identification of the target enzymes of neratinib in *Arabidopsis thaliana*

Inaugural-Dissertation

zur

Erlangung des Doktorgrades

- Dr. rer. nat. -

der Fakultät für

Biologie

an der

Universität Duisburg-Essen

vorgelegt von

Sabrina Ninck

aus Düsseldorf

Essen, Juni 2020

Die der vorliegenden Arbeit zugrundeliegenden Experimente wurden in der Abteilung für Chemische Biologie am Zentrum für Medizinische Biotechnologie der Universität Duisburg-Essen im Zeitraum von Dezember 2015 bis Dezember 2019 durchgeführt.

1. Gutachter: Prof. Dr. Markus Kaiser
2. Gutachter: Prof. Dr. Bettina Siebers
3. Gutachter: Prof. Dr. Steven Verhelst

Vorsitzender des Prüfungsausschusses: Prof. Dr. Peter Bayer

Tag der mündlichen Prüfung: 09.09.2020

DOI: 10.17185/duepublico/72944
URN: urn:nbn:de:hbz:465-20231106-095302-0

Teile dieser Arbeit sind in den folgenden Veröffentlichungen enthalten:

Halder V., Ninck S., Krahn J. H., Bormann J., Bhandari D. D., Gupta M. D., Heilmann G., Kaschani F. and Kaiser M. (submitted). The pan-HER kinase inhibitor Neratinib augments salicylic acid-mediated plant immunity by covalent targeting of an Arabidopsis epoxide hydrolase.

Folgende Publikationen wurden während der Promotion veröffentlicht:

Zeitschriftenartikel

Beisser D., Kaschani F., Graupner N., Grossmann L., Jensen M., Ninck S., Schulz F., Rahmann S., Boenigk J. and Kaiser M. (2017). Quantitative Proteomics Reveals Ecophysiological Effects of Light and Silver Stress on the Mixotrophic Protist *Poterioochromonas malhamensis. PLoS One*, 12(1): e0168183

Zweerink S., Kallnik V., Ninck S., Nickel S., Verheyen J., Blum M., Wagner, A. Feldmann I., Sickmann A., Albers S. V., Braesen C., Kaschani F., Siebers B. and Kaiser M. (2017). Activity-based protein profiling as a robust method for enzyme identification and screening in extremophilic Archaea. *Nat Commun,* 8, 15352

Grosse-Holz F., Madeira L., Zahid M. A., Songer M., Kourelis J., Fesenko M., Ninck S., Kaschani F., Kaiser M. and van der Hoorn, R. A. L. (2018). Three unrelated protease inhibitors enhance accumulation of pharmaceutical recombinant proteins in *Nicotiana benthamiana*. *Plant Biotechnol J*, 16(10), 1797-1810

Buchkapitel

Zweerink S., Pollmann T., Ninck S., Kaschani F. and Kaiser, M. (2017). Activity-Based Protein Profiling with Natural Product-Derived Chemical Probes in Human Cell Lysates. *Activity-Based Proteomics: Methods and Protocols*, 23-46

„Zwei Dinge sind zu unserer Arbeit nötig: Unermüdliche Ausdauer und die Bereitschaft, etwas, in das man viel Zeit und Arbeit gesteckt hat, wieder wegzuwerfen."

Albert Einstein (1879-1955)

Table of contents

List of figures

List of tables

Index of abbreviations

Abbreviations of words

4-MU	4-methylumbelliferone
4-MUG	4-methylumbelliferyl-β-D-glucuronide
A. thaliana	*Arabidopsis thaliana*
ABC	Ammonium bicarbonate
ABP	Activity-based probe
ABPP	Activity-based protein profiling
ACN	Acetonitrile
A*f*BP	Photoaffinity-based probe
APS	Ammonium persulfate
as-1	Activation sequence-1
AtEH7	*Arabidopsis thaliana* epoxide hydrolase 7
ATP	Adenosine triphosphate
Bis-Tris	Bis(2-hydroxyethyl)amino-tris(hydroxymethyl)methane
BODIPY	Dipyrromethene boron difluoride
BSA	Bovine serum albumin
CHMP	Committee for Medicinal Products for Human Use
CI	Confidence interval
CID	Collision-induced dissociation
CoA	Coenzyme A
CpdX	Compound X
CRL3	Cullin-RING ligase 3
CuAAC	Copper(I)-catalysed [3+2]-azide-alkyne-cycloaddition
Cy	Cyanine
DIGE	Difference gel electrophoresis
DMEM	Dulbecco’s Modified Eagle’s Medium
DMSO	Dimethyl sulfoxide
DNA	Deoxyribonucleic acid
DPBS	Dulbecco's PBS
DRB	5,6-dichloro-1-β-(D)-ribofuranosylbenzimidazole
DTT	Dithiothreitol
E. coli	*Escherichia coli*
ECL	Enhanced chemiluminescence

EDTA	Ethylenediaminetetraacetic acid
EET	Epoxyeicosatrienoic acid
EGFR	Epidermal growth factor receptor
EH	Epoxide hydrolase
ER	Endoplasmic reticulum
ErbB	Erythroblastosis oncogene B
ESI	Electrospray ionisation
ETD	Electron-transfer dissociation
FA	Formic acid
FCS	Fetal calf serum
FDA	Food and Drug Administration
FDR	False discovery rate
FT-MS	Fourier transform MS
GuHCl	Guanidine hydrochloride
GUS	β-glucuronidase
HAC	Histone acetyltransferase
HER	Human epidermal growth factor receptor
HF	High-fidelity
His-tag	Polyhistidine-tag
HRP	Horseradish peroxidase
HT	High-throughput
IAM	Iodoacetamide
IC_{50}	Half-maximal inhibitory concentration
ICS	Isochorismate synthase
IGD	In-gel digestion
IMAC	Immobilised metal affinity chromatography
IPTG	Isopropyl β-D-thiogalactopyranoside
JA	Jasmonic acid
LC	Liquid chromatography
LDS	Lithium dodecyl sulfate
LFQ	Label-free quantification
LOX	Lipoxygenase
mRNA	Messenger RNA
mEH	Microsomal EH
MeSA	Methylated SA

MOPS	3-(*N*-morpholino)propanesulfonic acid
MS	Mass spectrometry
MS/MS or MS^2	Tandem MS
MSA	Multiple sequence alignment
MW	Molecular weight
MWCO	Molecular weight cut-off in daltons
N. benthamiana	*Nicotiana benthamiana*
Ner	Neratinib
Ni-IDA	Ni(II)-iminodiacetic acid
NPR	Nonexpressor of pathogenesis-related gene
NZA	N-Z-Amine
o/N	Overnight
OBD	On-bead digestion
OD_{600}	Optical density at a wavelength of 600 nm
OPDA	12-oxo-phytodienoic acid
PAGE	Polyacrylamide gel electrophoresis
PAL	Phenylalanine ammonia-lyase
PBS	Phosphate-buffered saline
PCR	Polymerase-chain-reaction
PEG	Polyethylene glycol
Pen/Strep	Penicillin/Streptomycin
PR	Pathogenesis-related
PTM	Post-translational modification
PVDF	Polyvinylidene fluoride
RNA	Ribonucleic acid
RT	Room temperature
RuBisCO	Ribulose-1,5-bisphosphate carboxylase
SA	Salicylic acid
SABP2	SA-binding protein 2
SAG	SA 2-O-β-D-glucose
SAMT	SA-methyl transferase
SAR	Systemic acquired resistance
SDS	Sodium dodecyl sulfate
SEC	Size-exclusion chromatography
sEH	Soluble EH

SGE	Salicylate glucose ester
S-NEPC	(2*S*,3*S*)-*trans*-3-Phenyl-2-oxiranylmethyl 4-nitrophenyl carbonate
SOB	Super Optimal Broth
STSA	StageTip-solution A
STSB	StageTip-solution B
SUMO3	Small ubiquitin-like modifier 3
TAMRA	Carboxytetramethylrhodamine
TBE	Tris-borate-EDTA
TBS	Tris-buffered saline
TBS-T	TBS-Tween
TBTA	Tris((1-benzyl-4-triazolyl)methyl)amine
TCEP	Tris(2-carboxyethyl)phosphine
TEMED	*N*,*N*,*N*′,*N*′-Tetramethylethylenediamine
TF	Transcription factor
TGA	TGACG sequence-specific
TK	Tyrosine kinase
TKI	Tyrosine kinase inhibitor
Tris	Tris-(hydroxymethyl)-aminomethane
UV	Ultraviolet
UV/vis	UV-visible
WT	Wild-type

1- and 3-letter abbreviations for amino acids

A	Alanine
Asp	Asparagine
Cys, C	Cysteine
Glu	Glutamine
His	Histidine
Ile	Isoleucine
Ser	Serine
Trp	Tryptophan
Tyr	Tyrosine

Abbreviations of units

µg	Microgram
µL	Microlitre
bp	Base pairs
g	Gram; g-force (relative centrifugal force)
h	Hour(s)
kb	Kilobase
kDa	Kilodalton
L	Liter
min	Minutes
mL	Millilitre
ng	Nanogram
rpm	Revolutions per minute
sec	Seconds
U	Unit
v/v	Percent by volume
w/v	Percent by weight

Zusammenfassung

Die Chemoproteomik ist eine vielseitig einsetzbare Methode für das Studium und die Identifikation von Enzymen. Diese Methode beruht auf der Verwendung von sogenannten chemischen Sonden, die aus einem niedermolekularen Inhibitormolekül bestehen, welches mit einer Reportergruppe verknüpft ist. Als Inhibitoreinheit wird meist ein kovalenter Hemmstoff ausgewählt, welcher eine Bindung der chemischen Sonde an dessen Zielenzyme vermittelt und auf diese Weise deren Identifikation ermöglicht. Als Reportergruppe finden fluoreszente oder affinitätsmarkierte funktionelle Gruppen Anwendung, welche die Detektion oder Anreicherung dieser Zielenzyme realisieren. Angereicherte Zielenzyme können in einem zweiten Schritt mittels massenspektrometrischer Untersuchungen identifiziert werden.

In der vorliegenden Arbeit wurden die molekularen Zielenzyme des Tyrosinkinase-Hemmers Neratinib, einem pan-Inhibitor der humanen epidermalen Wachstumsfaktor Rezeptor-Familie, der an einen konservierten Cysteinrest innerhalb der ATP-Bindestelle bindet, in *Arabidopsis thaliana* untersucht. Neratinib wurde im Zuge eines chemischen Screens mit Arabidopsis-Keimlingen als Aktivator des Salicylsäure-Signalwegs, der unter anderem die Resistenz von Pflanzen gegen Pathogene vermittelt, identifiziert. Um die Zielenzyme von Neratinib und somit mögliche neue Modulatoren dieses Signalwegs zu identifizieren, wurde eine chemische ’click‘ Sonde verwendet, bei der das Neratinib-Molekül mit einem Alkinrest als funktionelle Gruppe modifiziert wurde, sodass in einer zweiten Reaktion eine Reportergruppe eingebracht werden kann. Nach Verifizierung der funktionellen Integrität dieser Sonde in humanen HeLa Gebärmutterhals-Krebszellen wurde diese in Arabidopsis-Protoplasten eingesetzt. Dabei wurde eine einzige prominente Proteinbande detektiert, die nach einem in-Gel-Verdau und massenspektrometrischer Analyse als Epoxid Hydrolase 7 (AtEH7) identifiziert wurde. AtEH7 wurde weiterhin als spezifisches Zielenzym von Neratinib in Arabidopsis-Keimlingen nachgewiesen. Die kovalente Bindung von Neratinib an AtEH7 wurde mittels Expression des rekombinanten Proteins in *Escherichia coli* und anschließender enzymkinetischer Untersuchungen sowie Markierungsstudien mit der Neratinib-basierten Sonde bestätigt. Zur Identifizierung der Bindestelle von Neratinib an AtEH7 wurde ferner eine ortsspezifische Mutagenese der drei vorhandenen Cysteinreste durchgeführt, nachdem eine Inhibition der Markierung

von AtEH7 mit der Neratinib-basierten Sonde durch eine Vorinkubation mit dem Cystein-Alkylierungsreagenz Iodoacetamid gezeigt werden konnte. Die generierten AtEH7 Mutanten wurden ebenfalls mittels enzymkinetischer Assays und Markierungsstudien mit der chemischen Sonde überprüft, wodurch Cys186 als Bindestelle von Neratinib validiert werden konnte.

Abstract

Chemoproteomics is a powerful method for the study and identification of enzymes. This method is based on the employment of a chemical probe which is made up of a small molecule inhibitor linked to a reporter group. As the inhibitory unit, in most cases a covalent-acting molecule is used that mediates the binding of the chemical probe to its target enzymes and thus enables their identification. As reporter groups, fluorescent or affinity-labelled functional groups are used that realise the detection or enrichment of these target enzymes. In a second step, the enriched target enzymes can be identified by mass spectrometric analysis.

In the present work, the molecular target enzymes of the tyrosine kinase inhibitor neratinib, a pan-inhibitor of the human epidermal growth factor receptor family that binds to a conserved cysteine residue within the ATP binding site, were investigated in *Arabidopsis thaliana*. Neratinib was identified as an activator of the salicylic acid signalling pathway from a chemical screen with Arabidopsis seedlings, which, amongst other, mediates the resistance of plants to pathogens. To enable the identification of the target enzymes of neratinib and thus of potential new modulators of this signalling pathway, a chemical 'click' probe was used, in which the neratinib molecule was modified with an alkyne moiety as a functional group, allowing a reporter group to be introduced to the probe in a second step. After confirming the functional integrity of this probe in human HeLa cervical carcinoma cells, the probe was applied to Arabidopsis protoplasts. From this labelling, a single prominent protein band was detected, which was identified as epoxide hydrolase 7 (AtEH7) by in-gel digestion and subsequent mass spectrometric analysis. AtEH7 was furthermore detected as a specific target enzyme of neratinib in Arabidopsis seedlings. The covalent binding of neratinib to AtEH7 was confirmed by expression of the recombinant protein in *Escherichia coli*, which was used for enzyme kinetic studies and labelling with the neratinib-based probe. To identify the binding site of neratinib to AtEH7, site-directed mutagenesis of all three cysteine residues was performed after a competition experiment with iodoacetamide demonstrated cysteine residues as potential binding sites of the neratinib-based probe. The resulting AtEH7 mutants were likewise screened using enzyme kinetic assays and chemical probe labelling, which permitted the validation of Cys186 as the binding site of neratinib.

1. Introduction

The identification of (direct) molecular target enzymes of small molecule inhibitors is still one of the major bottlenecks in chemical biology and drug discovery[1,2]. For the assessment of drug-phenotype relationships, high-throughput (HT) screening of small molecule inhibitors for their ability to induce a phenotype at the cellular or organismal level in various different species is often used, for example, by applying forward chemical genetics, especially in plant systems[3-5]. However, the identification of the enzyme(s) whose alteration is responsible for the observed phenotype remains the most challenging step[5]. To overcome the burdens of this difficult task, chemoproteomics has emerged as a versatile approach within the field of chemical biology to facilitate the process of target identification through the use of chemical probes[6,7]. In the rational design of such a chemical probe, the small molecule itself functions as a warhead to enable covalent or non-covalent binding to the target enzyme. If the warhead binds to the active site of a target enzyme, these probes are referred to as activity-based probes (ABPs) whereas the underlying methodology is called activity-based protein profiling (ABPP)[8]. To enable visualisation or purification of the targeted enzyme(s), a reporter group is attached to the warhead via a linker region. These chemical probes can then be applied *in vivo* at the cellular level or *in vitro* on protein extracts for target identification based on mass spectrometry (MS)[9].

1.1 Chemoproteomics

1.1.1 Chemical probes

The archetypical and most widely-known chemical probe is a fluorophosphonate-based ABP with broad-range specificity for serine hydrolases that was developed in the group of Benjamin Cravatt[8]. In the corresponding publication, the term ABPP was also introduced for the first time. Yet several different prototypes of chemical probes were published earlier. These are, for example, radiolabelled inhibitors[10-12], biotin-modified non-covalent inhibitors[13,14] or biotin-modified covalent inhibitors[15,16]. Until now, many different chemical probes have been developed that target different enzymes or multiple members of distinct enzyme classes such as cysteine proteases[17-19], protein kinases[20-23], serine/threonine[24] or tyrosine[25-27] phosphatases, metallohydrolases[28-31] or glycosidases[32-34], amongst others.

A ‘classical’ chemical probe is composed of three different entities: a warhead (reactive group) that binds to the target enzymes, a reporter group used for the detection or affinity enrichment of the target enzymes as well as a linker that connects the warhead with the reporter group (Fig. 1)[35].

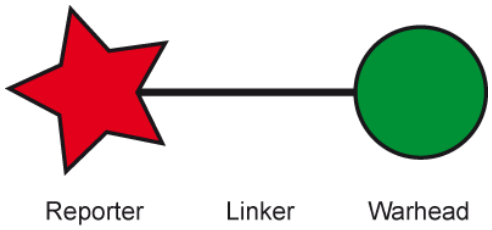

Fig. 1 Schematic representation of a chemical probe. Structural composition of a chemical probe, consisting of a warhead for binding to a target enzyme, a reporter group for target detection or enrichment and a linker for connecting the warhead and reporter moieties. Adapted from Cravatt *et al*., 2008[9].

The most challenging and at the same time most important step in the development of a chemical probe is the design of a suitable warhead. Warheads for chemical probes are usually selected based on bioactive natural compounds, synthetic analogues thereof or fully synthetic small molecules that are either known as inhibitors of selected enzymes or enzyme classes or are small molecules with yet unknown targets[36,37]. Structure activity relationship studies can be further taken into account to improve the design of the warhead or to find suitable attachment sites for the linker without changing the activity of the warhead[38,39]. One of the most important characteristics of a warhead is its reactivity. In general, the reactivity of the warhead needs to be high enough to enable the modification of target enzymes with the chemical probe whereas at the same time, it needs to be as low as possible to prevent unspecific modifications of off-target enzymes[40]. Chemical probes with broad-range activity therefore are equipped with inhibitors that show higher reactivity towards their target enzymes than inhibitors for specific enzymes which, in contrast, show only modest reactivity[41].To not be restricted to the use of electrophilic inhibitors that possess a covalent mode of action, photoaffinity-based probes (A*f*BPs) have been developed that are equipped with a photoreactive group. These photoreactive groups are used for the photo-crosslinking between the probe and a target enzyme[42]. Photoaffinity labelling for creating a covalent bond between a reagent and the active site of an enzyme has first been introduced by Singh *et al*. in the 1960s[43]. Photoreactive groups are designed to be stable and chemically inert under standard laboratory conditions[38,44]. Upon irradiation with ultraviolet (UV) light, the photoreactive group is activated and a reactive

radical intermediate such as a nitrene, a carbene or a diradical is formed that inserts into nearby X-H bonds like C-H bonds, N-H-bonds or O-H bonds as reaction partners, whereby different photoreactive groups show distinct reactivities towards the different kinds of X-H bonds[42]. By exploiting this reaction mechanism, enzymes that do not carry a reactive nucleophile at the binding site of the warhead for creating a covalent bond to the chemical probe through an irreversible nucleophilic attack can be targeted. Creation of a covalent bond to the labelled enzymes is essential for the use of chemical probes, as downstream target visualisation by in-gel fluorescence detection and identification after affinity enrichment is almost exclusively done under denaturing conditions under which non-covalent interactions between the warhead and the target enzyme do not persist[30,42]. However, due to the high reactivity of the photoreactive group, once activated, A*f*BPs often show higher non-specific labelling than chemical probes with a covalent mode of action since cross-linking between the photoreactive probe and nearby non-target enzymes, especially those which are highly abundant, is also very likely[42,45]. The risk of unspecific labelling is reduced by selecting photoreactive groups that form radical intermediates with shorter lifetimes than the warhead-enzyme interaction. In addition, photoreactive groups need to be rather small to not disturb the reversible binding mode of the warhead towards the target enzyme[42]. Several different photoreactive groups that meet this criteria such as aryl azides[46], diazirines[47] or benzophenones[48] have been introduced for the use in photoaffinity labelling to date, whereas benzophenones and diazirines are the most prevalent ones due to their photochemical properties[42,44]. Prominent examples of A*f*BPs for photoaffinity labelling are those that target Metalloproteases[28-30], as Metalloproteases do not mediate peptide bond hydrolysis via a covalent catalysis mechanism, but rather employ a divalent metal ion (usually Zn^{2+})-activated water molecule as a nucleophile[49].

As a linker of a chemical probe, long hydrocarbon (alkyl), polyethylene glycol (PEG) or peptide chains are used prevalently. Alkyl chains enhance the hydrophobicity of a chemical probe, thereby facilitating the uptake of the probe into living cells whereas PEG linkers are often employed to enhance the solubility of a probe in aqueous solvents. Peptide linkers can enhance the specificity of a probe to their target enzymes, for example in case of proteases[50]. Besides its function in optimising the characteristics of a probe, the linker ensures that the distance between the bulky reporter group and the binding site of the warhead, in most cases the active site of the target enzyme, is

large enough to prevent steric interactions. On the other hand, the linker ensures a good accessibility of the reporter group during target enrichment[35]. One of the more recent innovations are cleavable linkers. These are further differentiated into photocleavable, acid or base labile, reductively or oxidatively cleavable and enzymatically cleavable linkers as reviewed by Yang *et al.*[51]. Furthermore, isotopically heavy and light labelled linkers have been invented for direct MS-based quantitative profiling of target enzymes[52].

The reporter group is chosen based on the field of application of the probe. Reporter groups can be used for the visualisation of labelled proteins or for the enrichment of probe targets from a complex protein sample. For target visualisation on a polyacrylamide gel by fluorescence scanning or by fluorescence microscopy, different fluorophores like rhodamine, carboxytetramethylrhodamine (TAMRA), fluorescein, cyanine (Cy)-dyes or dipyrromethene boron difluoride (BODIPY)-dyes are chosen[35]. Some of the fluorescent dyes, like BODIPY- or Cy-dyes, are even suitable tags for the *in vivo* application of a probe as they are cell permeable and therefore enable the labelling of intact cells[35]. Earlier to the use of fluorescent tags, radioisotopes have been introduced into the inhibitory entity to allow the detection of radiolabelled target proteins by autoradiography on gel[17]. In contrast, biotin is the most commonly used reporter group for target enrichment via (strept-) avidin-coupled matrices[35]. It is also possible to combine a fluorescent reporter group with a biotin moiety, resulting in a so called trifunctional probe[53]. Such trifunctional probes are *inter alia* used for the visualisation of affinity-enriched proteins on a polyacrylamide gel with subsequent in-gel digestion (IGD) of the target enzymes and MS-based analysis.

Although some of the fluorophores used as reporter groups are cell permeable, most of the bulky and polar reporter groups have negative effects on the membrane permeability of the probe and its dissemination within living cells and organisms, thereby hampering the study of target enzymes under physiological conditions *in vivo*[54,55]. Due to these limitations of the ‘classical’ one-step probes that are already equipped with a detectable reporter group, ‘click’ probes that are employed in a two-step approach have been developed to overcome these constraints and to allow the study of proteins in their native state. The two-step approach basically relies on the ‘click’ chemistry between an azide and a terminal alkyne, hence these ‘click’ probes carry either one of these moieties covalently attached to the inhibitory entity[54]. In the

first step, the ‘click’ probe is applied for the labelling of the target enzymes in living cells or in cell extracts[56]. In the second step, a fluorescent, affinity-based or trifunctional ‘click’ tag carrying the complement azide or alkyne group is ‘clicked’ to the probe *in vitro* in a bioorthogonal reaction, as for instance, through a copper(I)-catalysed [3+2]-azide-alkyne-cycloaddition (CuAAC) which is one of the most effective and widely employed variants of the Huisgen 1,3-dipolar cycloaddition[56-58]. The copper(I)-catalysed ligation of azides and terminal alkynes has been introduced by Sharpless and co-workers[59] and was modified for the use with two-step chemical probes in the group of Benjamin Cravatt (Fig. 2)[54].

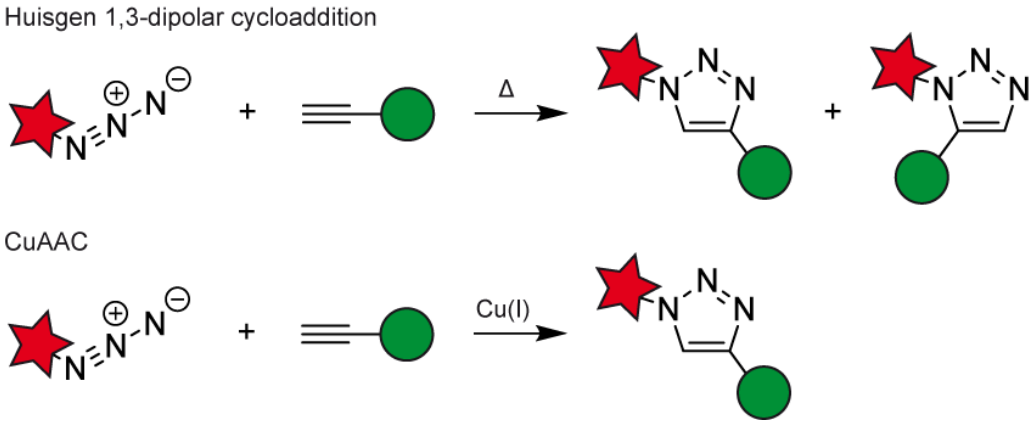

Fig. 2 Copper(I)-catalysed [3+2]-azide-alkyne-cycloaddition. Reaction scheme for the CuAAC between an azide and an alkyne. Unlike the uncatalysed Huisgen 1,3-dipolar cycloaddition that results in the formation of 1,4-substituted 1,2,3-triazoles and 1,5-substituted 1,2,3-triazoles in a molecular ratio of 1:1, the CuAAC only results in the formation of 1,4-substituted 1,2,3-triazoles. Adapted from Haldon *et al*., 2015[60].

To carry out a ‘click’ reaction, the probe-labelled target enzymes are mixed with the complementary ‘click’-tag, a copper(II)-salt, e.g. copper(II) sulfate, as the catalysing agent, a reducing agent such as sodium ascorbate or tris(2-carboxyethyl)phosphine (TCEP) and a ligand like tris(benzyltriazolylmethyl)amine (TBTA) that stabilises the copper(I) oxidation state under aerobic conditions[56,58,61]. The copper(I)-catalysed ‘click’ reaction can only be performed on extracted proteins *in vitro*, as copper is cytotoxic to living systems. Hence, attempts to improve the biocompability of the click reaction have been made, such as by using copper chelating azides[62]. Besides, copper-free methods that can additionally be implemented for *in vivo* ‘click’ reactions have been developed. These rely on a [3+2]-azide-alkyne-cycloaddition between azides and substituted cyclooctynes[63].

An overview about the different types of chemical probes employed in a chemo-proteomics experiment and the downstream sample processing steps for MS-based target identification is given in the following scheme (Fig. 3).

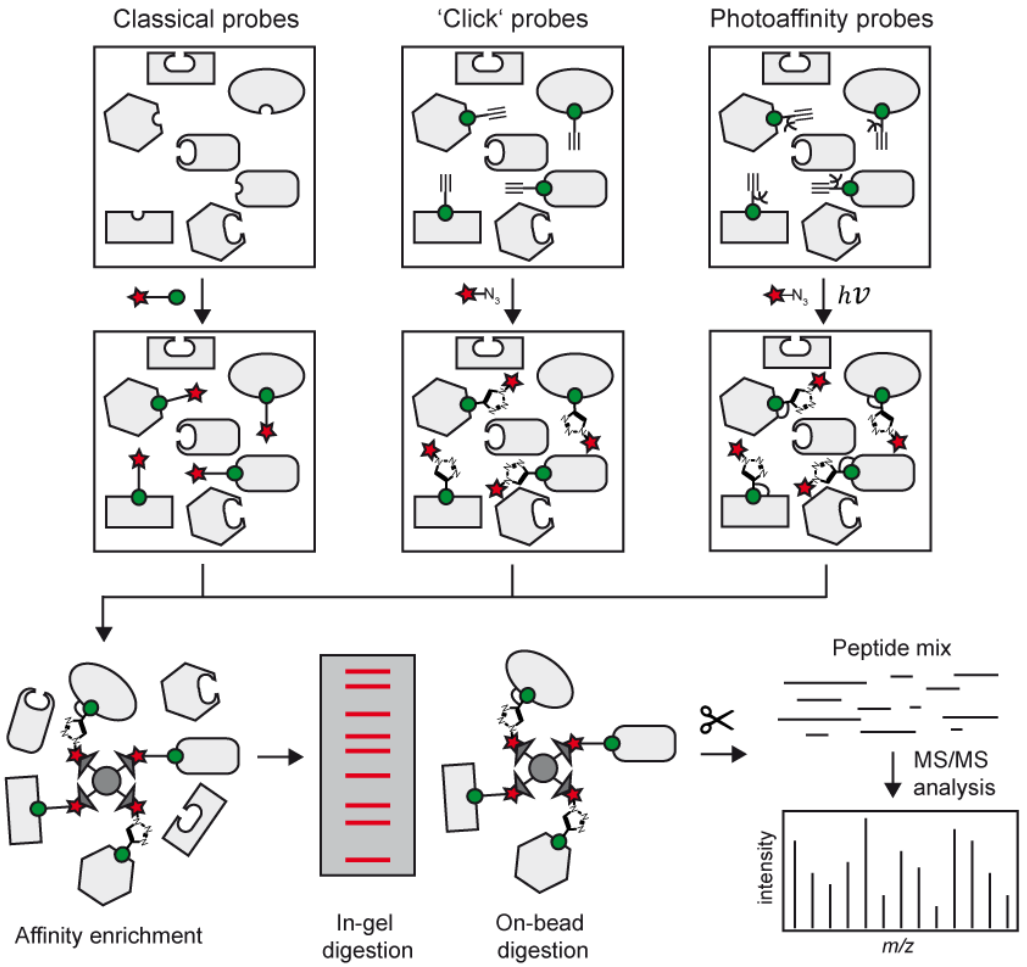

Fig. 3 Overview of a chemoproteomics experiment using different types of chemical probes. Classical one-step probes are almost exclusively used for the labelling of a proteome *in vitro* whereas two-step 'click' probes can be used for the *in vivo* or *in vitro* labelling of a proteome. The typical Cu(I)-catalysed 'click' reaction is performed in a second step *in vitro*. A*f*BPs, in most cases, are two-step probes that can be used for *in vivo* or *in vitro* labelling. In either case, the proteome has to be extracted under non-denaturing conditions to preserve the non-covalent interactions between the probe and the target enzymes before the photo-crosslinking and subsequent 'click' reaction are performed *in vitro*. However, it is likewise possible to perform the photo-crosslinking step in intact cells prior to the extraction of the proteome. After the target enzymes are covalently modified with a reporter-bound chemical probe, a matrix-assisted affinity enrichment of target enzymes is done, usually by exploiting the strong interactions between biotin and (strept-) avidin. Enriched target proteins are analysed on gel followed by IGD or are directly digested on-bead and the obtained peptide mix is analysed by tandem MS (MS/MS or MS^2) analysis. Adapted from Geurink *et al*., 2012 and Zweerink *et al*., 2017[42,64].

Labelling with a chemical probe can not only be distinguished by the type of the employed probe, but can further be classified by its type of use, resulting into a differentiation between a comparative or a competitive approach (Fig. 4).

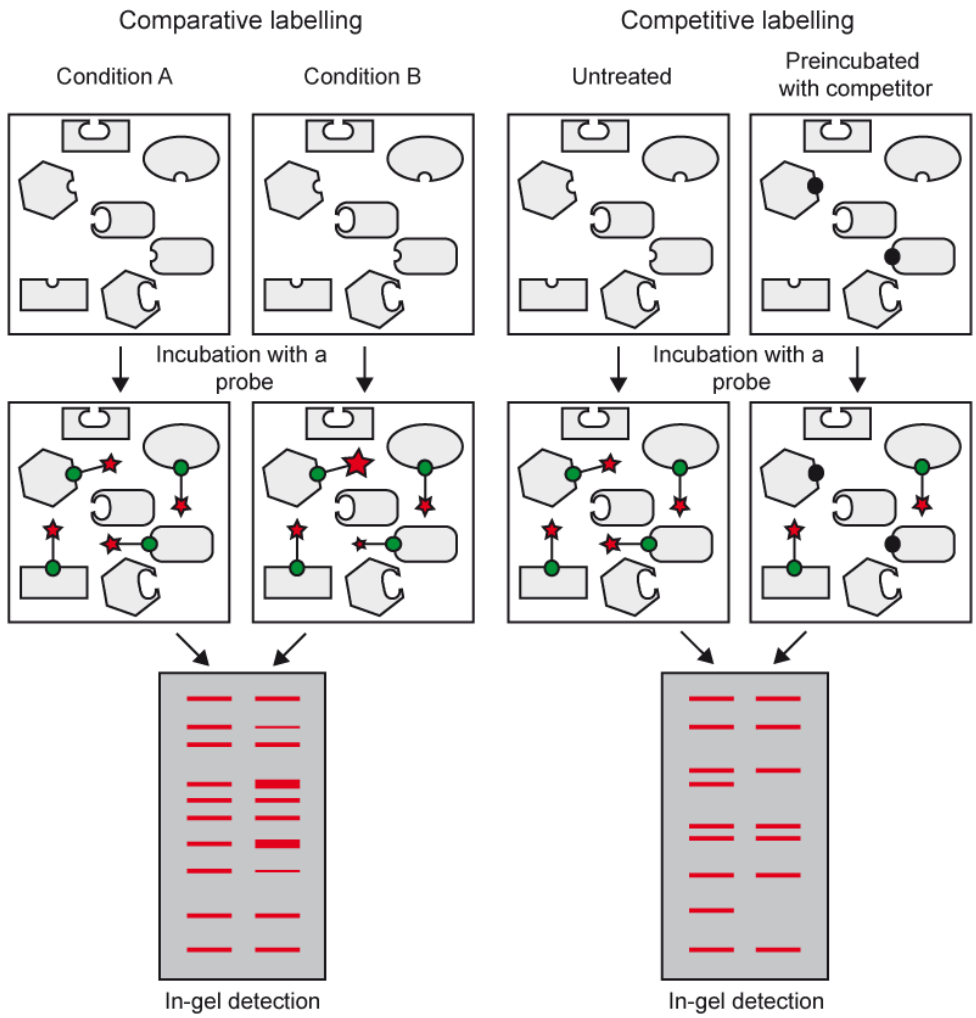

Fig. 4 Differences between comparative and competitive labelling approaches. The comparative labelling approach is used to investigate the effects of different conditions on a proteome. This is done by comparing the labelling pattern/intensities of a chemical probe between the different conditions using in-gel fluorescence detection. The competitive labelling approach serves for the identification of specific inhibitors. The labelling pattern of a chemical probe is compared between an untreated proteome and a proteome preincubated with the tested inhibitor, the so called competitor. An inhibition of probe labelling by the competitor can be detected through in-gel fluorescence analysis as a 'missing' or intensity-reduced protein band on a gel. Adapted from Cravatt *et al*., 2008[9].

The comparative approach allows for studying the influence of different factors, e.g. temperature, pH value or other chemicophysical factors, as well as different developmental stages, on the labelling pattern of a chemical probe. The effects of the differential treatments can be analysed through gel-based methods by comparing the observed labelling intensities. The competitive approach, in contrast, is used for the identification of specific inhibitors for a target protein. This is done by preincubation of a proteome or purified enzyme with a potential or known inhibitor prior to the labelling with a chemical probe. If the tested inhibitor acts as a competitor for the warhead of the chemical probe, probe binding is prevented[9]. Competition of the probe labelling by

a competitor can either be achieved through occupation of the same binding site or through binding to an allosteric site, resulting in a conformational change of the probe binding site[65]. Target enzymes of the tested inhibitors can be identified through gel-based analysis as a 'missing' protein band or a protein band with reduced intensity compared to the samples that were not pretreated with the tested inhibitor[9].

The field of application of chemical probes is not exclusive to protein extracts or human and other mammalian cell cultures but can rather be extended to the use in other unicellular organisms like eukaryotic pathogens[66,67] or prokaryotes such as bacteria[68] and archaea. Even though the latter often colonise harsh environments where they live under extreme conditions regarding temperature, pH, salinity or combinations thereof, it was shown that *in vivo* labelling of archaea with selected chemical probes is a robust method even under these limitations[64]. Chemical probes can be used to address a variety of different biological and medicinal questions. For instance, they are suitable tools for pharmaceutical drug development as they allow to determine the potency and selectivity of a lead structure under physiological conditions[69]. The thorough investigation of off-target effects of a drug candidate is highly important as such effects may have dramatic consequences for patients[70]. By using chemical probes, off-target effects can be assessed before a drug candidate enters clinical trials, thereby protecting study participants and preventing a cost-intensive late-stage dropout[70,71]. The drug candidates to be evaluated with the help of chemical probes can be directed either against proteins endogenous to the human body or against the proteins of disease-causing pathogens[69]. Consequently, chemical probes show a wide range of applications and are of special value in various research areas.

1.1.2 Mass spectrometry-based proteomics

In biology, the 'omics' disciplines deal with the comprehensive study of different types of biomolecules, whereby the field of proteomics deals with the study of all aspects of proteins, comprising their structure, expression, biochemical activity, localisation, interactions and cellular roles[72,73]. Chemical proteomics, also referred to as chemoproteomics, is a field of proteomics research that allows for evaluating the proteome-wide selectivity of chemical tools[74]. One of the major tools in chemoproteomics are the previously introduced chemical probes. In order to ascertain the selectivity of such chemical probes, i.e. to differentiate between specific and off-

target labelling, MS as the preferred methodology for the analysis of proteins within a complex sample is regularly employed for the identification of the target proteins of chemical probes[74,75].

The history of MS dates back to the 19th century when the first gas discharge experiments were carried out and Eugen Goldstein detected the canal rays[76,77]. The first 'modern' MS was engineered by Arthur Jeffrey Dempster and published in the year 1918[76,78]. In 1959, MS was used to identify peptides for the first time[79]. Since then, MS has rapidly evolved into a very powerful tool for peptide and protein identification, *inter alia*, due to the inventions of quadrupoles as mass filters[80], MS/MS[81], Fourier transform MS (FT-MS)[82], electrospray ionisation (ESI) for larger biomolecules[83] and the Orbitrap mass analyser[84] as key landmarks.

Protein identification can be achieved using two different approaches: The top-down approach and the bottom-up approach (Fig. 5). In the top-down approach, intact proteins are injected into a mass spectrometer and the masses of the intact protein and fragment ions of the protein are used for identification[85]. This identification is either based on a sequence database search or on *de novo* sequencing[86,87]. In the bottom-up approach, the proteins to be analysed are first digested into smaller fragments using different kinds of proteases, like trypsin, the most commonly used digestion enzyme for MS[88]. The obtained peptide mix is then injected into the mass spectrometer in the second step and proteins are identified based on peptide fragment ion masses and sequences. This is usually done by matching this information with predicted patterns based on the *in silico* digest of a reference database[85]. Even though the top-down approach gained increasing attention in recent years due to the advanced analysis of proteoforms, the bottom-up approach is still more widely employed since it is suitable for HT analyses of highly complex proteome samples[85,89,90]. If a complex mixture of proteins is analysed by bottom-up proteomics, this is either referred to as shotgun proteomics in case that all proteins within a sample are considered for analysis or as targeted proteomics when proteins of interest are preselected for analysis[91]. A proteomics analysis can further be differentiated into a qualitative or a quantitative analysis. While qualitative proteomics serves the identification of a protein, quantitative proteomics, in contrast, additionally enables the comparison of protein abundances between a set of samples that represents variant sampling conditions[92]. Qualitative

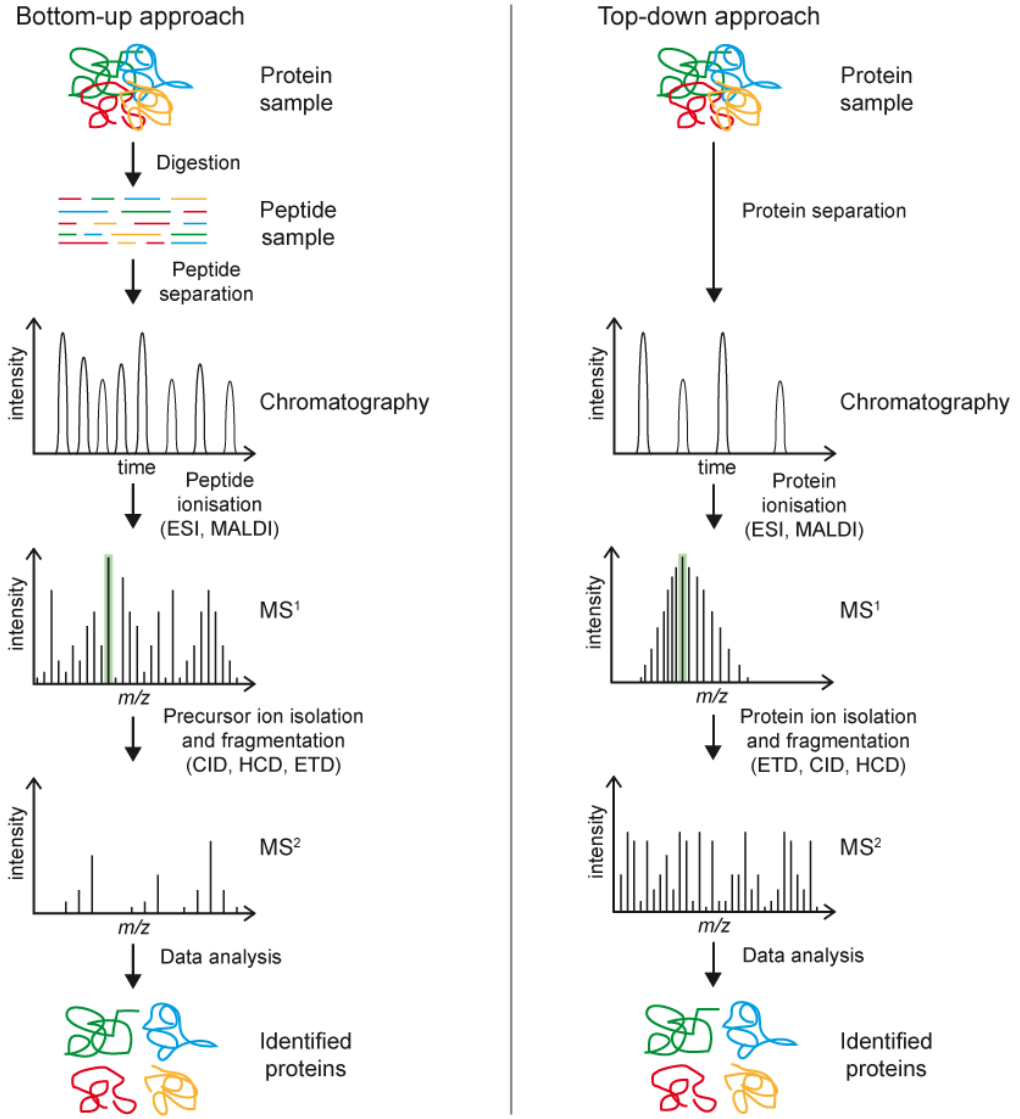

Fig. 5 Bottom-up and top-down proteomics. The two main approaches for the MS-based identification of proteins are the bottom-up and the top-down approach. In the bottom-up approach, proteins are first digested into peptides using proteases like trypsin, prior to chromatographic separation of peptides by liquid chromatography (LC) or gas chromatography (GC). Peptide ionisation by ESI or matrix-assisted laser desorption ionisation (MALDI) is needed for acquisition of an MS^1 spectrum of precursor ions. Precursor ions are selected for fragmentation by collision-induced dissociation (CID), higher energy collisional dissociation (HCD) or electron-transfer dissociation (ETD) based on their intensity and an MS^2 spectrum of the product ions is acquired. Proteins are identified by matching the information on peptide precursor ion masses and sequences with an *in silico* digested reference database. In the top-down approach, intact proteins are injected into the mass spectrometer after protein separation and ionisation. An MS^1 spectrum of protein ions is acquired prior to protein ion fragmentation, mostly by ETD, and acquisition of an MS^2 spectrum of the generated product ions. The proteins are identified by a database search or by *de novo* sequencing using intact protein and fragment ion masses. Top-down proteomics is superior over bottom-up proteomics for the differentiation between various proteoforms, since the detection of post-translational modifications (PTMs) using top-down proteomics is advanced. Adapted from Zhang and Ge, 2011 and Zhang *et al*., 2014[93,94].

proteomics can be used for the identification of direct or unspecific targets of a chemical probe by exploiting the covalent interaction between the target proteins and

the warhead of the probe. After the target proteins are captured by a chemical probe within a complex proteome, these target proteins are affinity-enriched prior to MS analysis using bottom-up proteomics for target identification[38]. Peptides for bottom-up MS analysis are *a priori* generated through direct on-bead digestion (OBD) or after elution of the proteins from the beads using either in-solution digestion (ISD) or IGD subsequent to gel-based visualisation of target proteins[95,96]. However, both methods have distinct advantages and disadvantages. An OBD can be used to analyse the complete target repertoire of a chemical probe, thereby determining its selectivity, whereas an IGD is especially suitable to analyse selected protein bands on a gel. While an OBD usually results in a high amount of (strept-) avidin being present in the sample which impairs the MS analysis[97], the release of peptides from the gel matrix through water extraction is incomplete for an IGD[98]. However, potential targets that were identified using either of the two methods can be matched with an observed phenotype, if present, and further be confirmed by generating knock-out mutants that are insensitive to labelling with the respective probe or by performing enzyme inhibition assays, for example[17].

The comparison of protein abundances using quantitative proteomics can be further distinguished into the determination of either relative or absolute protein abundances and has found growing application in recent years since several new quantification methodologies have been developed[92]. For the comparison of relative protein abundances, label-free quantification (LFQ) as well as label-based quantification strategies have been invented. The LFQ algorithm is implemented in several software tools for analysing MS datasets, like MaxQuant[99], and is either based on peak intensities or spectral counting[100]. The isotopic labels used for relative quantification can be introduced through metabolic incorporation at the organismal level, for example by using stable isotope labelling by amino acids in cell culture (SILAC)[101], or chemically at the protein or peptide level e.g. by using isotope-coded affinity tags (ICAT)[102], tandem mass tags (TMT)[103], isobaric tags for relative and absolute quantitation (iTRAQ)[104] or terminal amine isotopic labelling of substrates (TAILS)[105]. For the absolute quantification of protein abundances, isotopically labelled standard proteins or peptides are utilised with a methodology called AQUA[106]. The principle for relative and absolute quantification using metabolic or chemical stable isotope labels is therefore based on a defined mass shift between the different isotopes[92].

Beside these approaches for protein identification and quantification, a whole bunch of other application fields have emerged. These are, amongst others, the analysis of PTMs (phosphorylation, glycosylation, acetylation, biotinylation, nitrosylation, ubiquitination) as reviewed by Parker *et al.*[107] or structural proteomics (native MS, covalent labelling, hydrogen deuterium exchange (HDX)-MS, cross-linking MS) as reviewed by Leitner[108].

1.2 Neratinib

Neratinib (**Ner**; former name HKI-272, trade name Nerlynx®) is an approved, orally active chemical drug used in the adjuvant treatment of HER2-positive breast cancer[109,110]. It covalently targets several members of the human epidermal growth factor receptor (HER) tyrosine kinase (TK) family which is also referred to as the erythroblastosis oncogene B (ErbB) receptor family: HER1 (ErbB1), also known as epidermal growth factor receptor (EGFR), HER2 (ErbB2; Neu), and HER4 (ErbB4)[109,111]. Therefore, **Ner** is designated a pan-HER inhibitor[112]. The irreversible inhibition of the HER-receptor family is achieved via a Michael addition[113] between the β-carbon of the dimethylamino crotonamide warhead at the 6-position of **Ner** serving as a Michael acceptor and the nucleophilic sulfhydryl group of a conserved cysteine residue within the catalytic cleft of the adenosine triphosphate (ATP) binding pocket of the kinase domain, resulting in the formation of a stable N-S-bond[114].

Ner (Fig. 6) was first introduced by Wyeth LLC (now Pfizer) in the year 2004[109] as a second-generation tyrosine kinase inhibitor (TKI) of the HER-receptor family[115]. Second-generation TKIs such as **Ner**, afatinib or pelitinib, in contrast to first-generation TKIs like gefitinib, erlotinib or icotinib that continuously compete with high levels of endogenous ATP for binding, mainly possess an irreversible mode of inhibition and are therefore designed to be more potent than first-generation EGFR TKIs[115-118]. Additionally, they target multiple members of the HER-receptor family, whereas first-generation TKIs are selective for EGFR[118]. Furthermore, second generation TKIs are able to overcome an acquired resistance against first-generation TKIs, as for example observed for the T790M mutant of EGFR, which is frequently found in lung adenocarcinomas of patients that received treatment with gefitinib or erlotinib [115,119,120]. However, they also target wild-type (WT) EGFR, causing toxicity that is dose-limiting

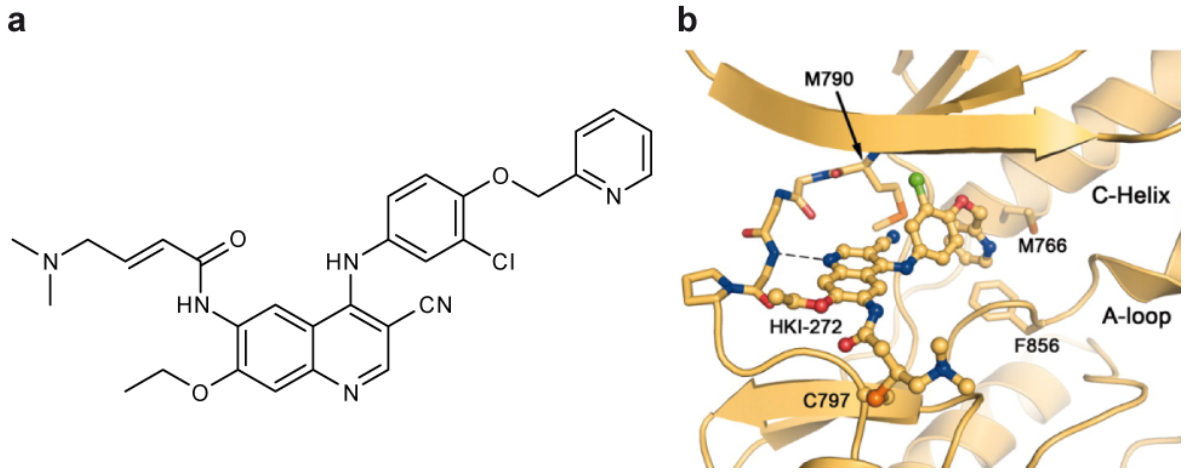

Fig. 6 Chemical properties of Ner. (a) Chemical structure of **Ner**. **Ner** is a 3-Cyano-4-anilinoquinoline-based TKI that irreversibly targets members of the HER-family via its Michael system. (b) Crystal structure of **Ner** (HKI-272) in complex with the EGFR T790M mutant. The β-carbon of the crotonamide warhead (Michael acceptor) of **Ner** is covalently bound to the nucleophilic sulfhydryl group of the Cys797 residue (Michael donor) within the ATP-binding pocket of EGFR. The binding of **Ner** results in a conformational change with the C-helix displaced, leading to an inactivation of the TK domain. The dashed line indicates a hydrogen bond between **Ner** and the hinge region of T790M EGFR. The aniline substituent of **Ner** is positioned within the enlarged hydrophobic pocket of the inactive conformation of the TK domain (Protein Data Bank (PDB)[121] code: 2JIV). Taken from Yun *et al.*, 2008[122]. Copyright (2008) National Academy of Sciences.

in medication. Therefore, third-generation TKIs that are selective for EGFR with activating or resistance mutations like the T790M mutation, but not inhibiting WT EGFR, are currently under development[123].

Chemically, **Ner** ((2*E*)-*N*-[4-[[3-Chlor-4-[(pyridin-2-yl)methoxy]phenyl]amino]-3-cyan-7-ethoxychinolin-6-yl]-4-(dimethylamino)but-2-enamide) is a 4-anilino-3-cyano quinoline derivative[115]. A number of different synthetic routes have been described for the synthesis of **Ner**[114,124,125]. These differ in the order in which the C4 and C6 side chains of **Ner** have been introduced[126]. The development of **Ner** arose from the need for a small molecule TKI that is more potent towards HER2 than previously developed small molecule TKIs which were found to show only poor inhibition of HER2 compared to EGFR[109]. **Ner** was determined to inhibit EGFR, HER2 and HER4 in an *in vitro* autophosphorylation assay with half-maximal inhibitory concentrations (IC_{50}) of 92 nM, 59 nM and 19 nM, respectively[112], whereas the further off-target repertoire of **Ner** in humans has been investigated by Davis *et al.*[127]. HER2 is overexpressed in about 20% of all breast cancer cases[128] and is also known to be overexpressed in several other types of cancer such as ovarian, gastric, bladder, lung, cervical, colorectal, oesophageal and endometrial cancer as reviewed by Iqbal and Iqbal[129], with a

predominance for epithelial malignancies[130]. Patients with HER2-positive breast cancer have a poor prognosis for progression of the disease, as has been already known for some time[128,131]. HER2, for which no ligand is known so far, only forms heterodimers with HER1, HER3 or HER4 under normal conditions (Fig. 7)[132,133].

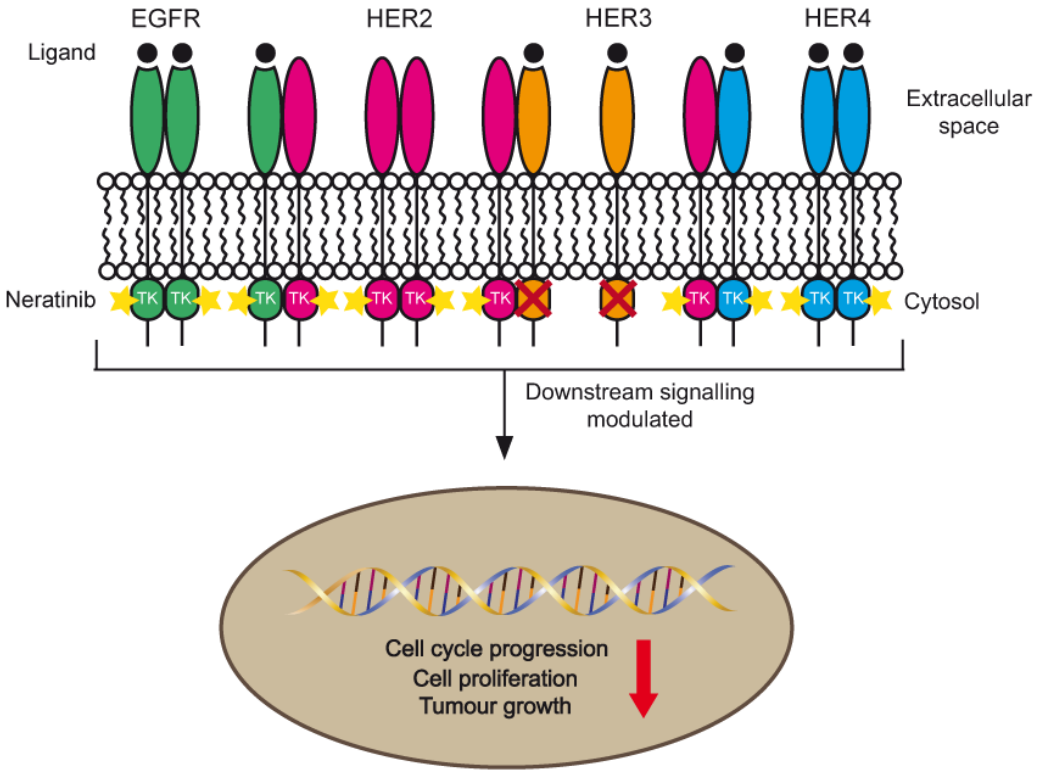

Fig. 7 HER receptor signalling cascade. The HER receptor family comprises four different members: EGFR (HER1), HER2, HER3 and HER4. A HER receptor consist of an extracellular ligand binding domain, a membrane spanning region as well as an intracellular TK domain. Upon binding of a receptor specific ligand, dimerisation of the receptors occurs. While EGFR as well as HER4 can form homodimers, HER2 and HER3 form heterodimers with other HER receptors, since HER2 has no known ligand and HER3 is not equipped with a functional TK domain. The overexpression of HER2 in various types of cancer however leads to a spontaneous homodimerisation of HER2, resulting in the activation of the downstream signalling cascade without regulation by a ligand. The treatment with **Ner** results in inhibition of tyrosine phosphorylation within the kinase domain, which prevents downstream signalling, ultimately resulting in decreased cell cycle progression, cell proliferation and tumour growth. Adapted from Pollock and Grandis, 2015, Richard *et al.*, 2016 and Collins *et al.*, 2019[134-136].

Overexpression of HER2, in contrast, leads to an unintended homodimerisation of the receptor, resulting in receptor autophosphorylation and activation of the downstream signalling cascade. This promotes cell cycle progression and therefore cell proliferation as well as tumour growth without the need for control by a ligand[114]. A treatment with **Ner** blocks HER-receptor dimerisation as well as tyrosine-phosphorylation through binding to the inactive conformation (type II inhibitor) of the receptor, thereby modulating the downstream signal transduction pathway[136,137]. The resulting decrease

in Cyclin D1 expression and retinoblastoma protein phosphorylation as well as the increase in p27 lead to an arrest of the cell cycle at the G1/S phase transition, finally translating into a decreased cell proliferation[109]. HER3, unlike the other members of the HER receptor family, has no functional TK domain and is therefore not targeted by **Ner**[138].

In July 2017, Nerlynx® (Puma Biotechnology, Inc.) was approved for a one-year adjuvant treatment of early-stage HER2-positive breast cancer in adults after HER2-specific antibody treatment with trastuzumab by the Food and Drug Administration (FDA) in the United States[110,139]. In Europe, the approval of Nerlynx® as a drug in cancer treatment was primarily not granted by the European Medicines Agency (EMA) Committee for Medicinal Products for Human Use (CHMP) in February 2018[140]. This rejection was based on the phase III ExteNET study, the same study on which the approval by the FDA was based on. On the one hand, **Ner** was found to show only low efficacy in the adjuvant treatment of HER2-positive breast cancer after administration of trastuzumab compared to the placebo, whereas at the same time, severe side effects of **Ner** treatment, especially diarrhoea, were observed[141]. However, at the end of June 2018, the CHMP revised this decision due to a re-examination[142] and Nerlynx® was granted marketing authorisation through Pierre Fabre Médicament in the European Union by the end of August 2018[143]. In February 2020, the FDA furthermore approved Nerlynx® in combination with capecitabine for the treatment of advanced or metastatic HER2-positive breast cancer in adults that received previous anti-HER2 treatment based on the phase III NALA trial[144,145].

1.3 Salicylic acid signalling in plants

Salicylic acid (SA) signalling is a major plant signalling pathway essential to plant immunity and disease resistance, with the small phenolic phytohormone SA acting as a key regulator. SA thereby mediates the defence of plants to various pathogens[146].

SA is synthesised from chorismate, a product of the shikimate pathway, via two different pathways in the plastids of a plant cell: The isochorismate synthase (ICS) or the phenylalanine ammonia-lyase (PAL) pathway, whereas the former one involving ICS1 is supposed to be the main synthetic route for SA synthesis[147]. *ICS1* transcription and thereby SA biosynthesis and accumulation are regulated by Ca^{2+}-signalling in the

cytosol of a plant cell as reviewed by Seyfferth and Tsuda[146]. Since free SA, at elevated levels, has cell toxic effects that can lead to cell death, SA is converted into inactive derivatives, *inter alia*, through glucosylation or methylation[148,149]. Glucosylated SA exists in the form of SA 2-O-β-D-glucose (SAG) as well as a salicylate glucose ester (SGE)[150]. In *Arabidopsis thaliana* (*A. thaliana*), two glucosyltransferases are known for the production of glucosylated SA. One of them produces SAG and SGE, while the other only produces SAG[151]. SAG is a storage form of SA, accumulating in the vacuole, which can be converted back into reactive SA by β-glucosidase activity upon a pathogen attack[150,152,153]. Methylated SA (MeSA) produced from SA by an SA-methyl transferase (SAMT) is a volatile derivative that is able to cross membranes[154,155]. Consequently, in the form of MeSA, SA can diffuse out of the plastids. On the one hand MeSA diffuses into the cytosol, where it is converted back into active SA by SA-binding protein 2 (SABP2) to induce the downstream SA signalling cascade, leading to a hypersensitive response (HR) and a local acquired resistance (LAR) at the site of infection[149,156,157]. On the other hand, MeSA further diffuses out of the cells and is transported through the phloem into systemic tissues, where it is likewise converted back into SA by SABP2, thereby inducing a systemic acquired resistance (SAR) in uninfected plant tissues, leading to an enhanced resistance in the whole plant[158]. MeSA is not only able to diffuse into systemic tissues, but is also emitted from the plant to induce immunity in neighbouring plants[154]. Furthermore, a diffusion of MeSA out of the cells additionally contributes to reducing the cytotoxic effect of free SA in the cells[149].

During SAR, elevated levels of free SA result in redox changes that lead to a disruption of oligomeric nonexpressor of pathogenesis-related gene (NPR) 1, an ankyrin repeats-containing protein, in the cytosol of plant cells in systemic tissues[159,160]. The release of monomeric NPR1 is caused by a reduction of the intermolecular disulphide bonds in oligomerised NPR1 by thioredoxins TRX-h3 and TRX-h5[160,161]. Nuclear translocation of monomeric NPR1 is then triggered by the NPR1 bipartite nuclear localization signal[160,162]. In the nucleus, NPR1 induces the transcription of *pathogenesis-related (PR)* genes through the formation of a coactivator complex with CBP/p300family histone acetyltransferases (HACs)[163]. This coactivator complex is recruited to the chromatin by the interaction with the TGACG sequence-specific TGA transcription factors (TF), a subclass of the basic leucine zipper TFs that bind to the SA-responsive

activation sequence-1 (as-1)-like element, which is part of the *PR-1* gene promoter[164-170]. The HAC-NPR1-TGA complex then initiates histone acetylation, resulting in epigenetic reprogramming, which mediates *PR* gene expression[163]. Transcription of *PR* genes is tightly controlled through the SA-induced modification of NPR1. *PR-1* gene transcription is normally repressed through an interaction of Ser55/Ser59-phosphorylated NPR1 with the transcription factor WRKY70, which binds to a negative *cis*-element WRKY box of the *PR-1* gene promoter[164,171-173]. Upon a pathogen-induced accumulation of SA, a dephosphorylation of Ser55/Ser59 takes place, enabling small ubiquitin-like modifier 3 (SUMO3) modification of NPR1, thus leading to a disruption of the NPR1/WRKY70 interaction[173]. Sumoylation by SUMO3 further enables NPR1 phosphorylation of Ser11/Ser15 residues which renders NPR1 more active and initiates TGA TF binding at the positive *cis*-element *as-1*[173,174]. Turnover of NPR1 in the nucleus is mediated by Cullin-RING ligase 3 (CRL3), an E3 ligase, with the SA-regulated NPR1 paralogs NPR3 and NPR4 acting as adapter proteins for CLR3, thereby assisting the subsequent NPR1 degradation[174,175]. In absence of a pathogen attack and the consequently low levels of SA in the cell, NPR1 is subjected to a CLR3-NPR4-mediated proteasomal degradation[173,174]. Since the transcription of SA-responsive genes upon a pathogen attack relies on the steady turnover of chromatin-associated NPR1 and the recruitment of fresh NPR1, Ser11/Ser15-phosphorylated and TGA-interacting NPR1 is likewise recognised by CRL3 with NPR3 functioning as the adaptor protein which provokes initial ubiquitination of NPR1, thereby still preserving the expression of *PR* genes through chromatin-association of NPR1[173,174,176]. A further polyubiquitination of NPR1 by an ubiquitin E4 ligase (UBE4) finally triggers proteasomal degradation of NPR1. Ubiquitination of NPR1 is counterbalanced by its deubiquitination through UBP6/7 deubiquitinases, which allows for a precise control of NPR1 activity and turnover during the SA-induced immune reaction[176]. Even though NPR1 was found to be the key mediator of SA-induced transcription of *PR* genes in SAR against bacteria and fungi[177], it was reported not to be crucial for the resistance to viruses in Arabidopsis[178,179]. An overview of the SA signalling cascade is depicted in the following Scheme (Fig. 8).

Due to the important role of SA in mediating plant defence against pathogens, various synthetic compounds have been studied for their potential to mimic the resistance-

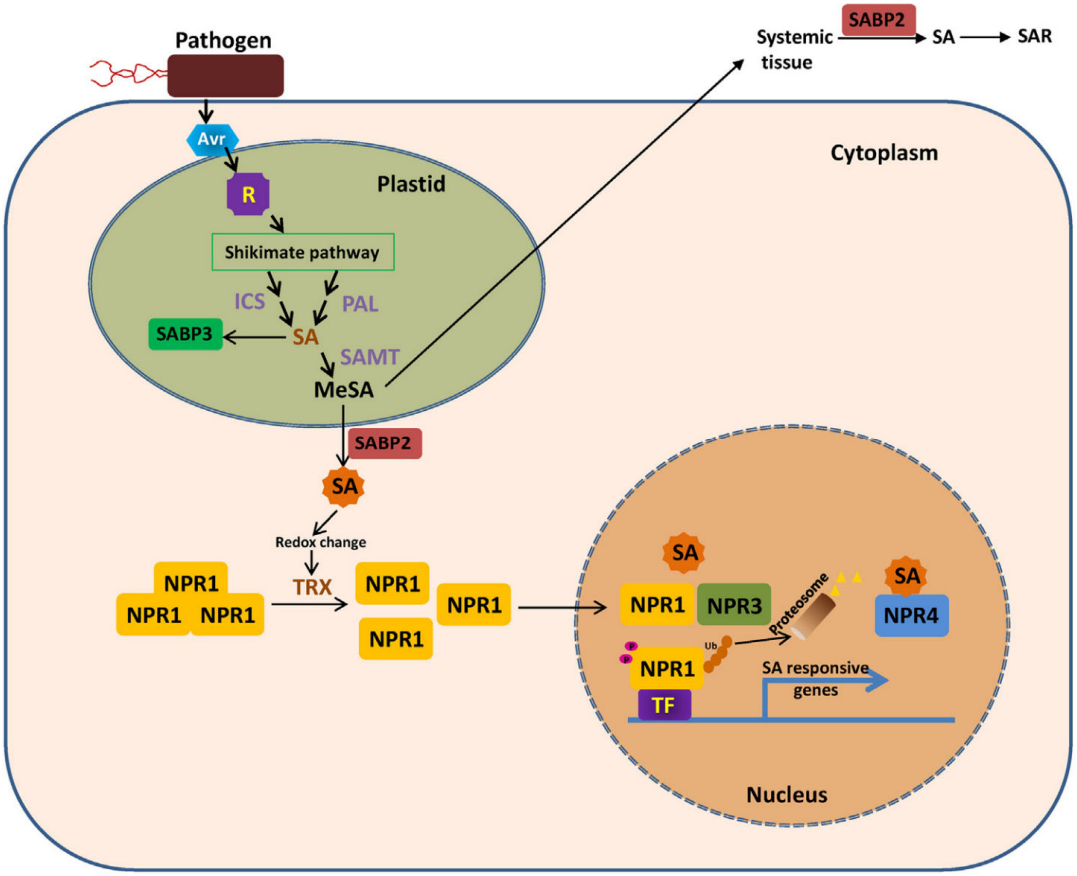

Fig. 8 Activation of SA signalling in plants. Upon a pathogen attack, biosynthesis of SA via the ICS/PAL pathways in the plastids is upregulated. Prior to diffusion into the cytoplasm, SA needs to be converted into MeSA. This step is catalysed by SAMT. In the cytoplasm, MeSA is converted back into SA by SABP2. The resulting increase in the total SA level in the cytoplasm leads to the disruption of oligomeric NPR1 into its monomers. NPR1 monomers migrate into the nucleus where they activate the transcription of SA-responsive defence genes including the *PR* genes through binding to TFs. TF binding is initiated through a switch in the phosphorylation status of NPR1. Since the constitutive turnover of phosphorylated NPR1 is needed for the expression of SA-responsive genes, phosphorylated NPR1 is recognised for NPR3-assisted ubiquitination by E3 and E4 ligases, causing proteasome-mediated degradation of NPR1. Taken from Kumar, 2014[149]. Copyright (2014) Elsevier Ireland Ltd. Reused with permission.

inducing effect of SA, as such compounds are valuable in agriculture for crop protection[149,180]. However, SA not only contributes to plant immunity, but has further important roles as a signalling molecule in a variety of different physiological processes such as seed germination, flowering, stomatal closure, thermogenesis, salt stress and clathrin-mediated endocytic protein trafficking or in response to drought, ozone and chilling as recorded by Kumar[149]. Plant hormone signalling pathways do not merely orchestrate such physiological processes alone. Instead, there exists an active crosstalk between the different plant hormone signalling pathways that act synergistic or antagonistic. For example, the SA signalling pathway together with the jasmonic acid (JA) signalling pathway forms the backbone of plant immunity signalling. Other

plant hormones, i.e. abscisic acid, auxins, cytokinins, ethylene and gibberelins have further been found to interact with the SA-JA backbone as reviewed by Pieterse *et al*.[181].

Since the understanding of SA signalling is still incomplete and SA plays an essential role in plant immunity and other important physiological processes, further attempts to identify novel SA-related genes, i.e. those that encode SA-binding proteins or those encoding modulators of SA levels remain indispensable[182]. Hence, HT screens aiming to unravel such genes using crosslinking with a photo-reactive SA analogue or by screening mutants have been conducted in the last years[183,184].

1.4 Plant epoxide hydrolases

Epoxide hydrolases (EHs) are enzymes that catalyse the cleavage of epoxides into their corresponding vicinal diols (1,2-diols) through the addition of water[185,186]. EHs are distributed across all living organisms ranging from microorganisms to insects as well as plants and mammals[187]. Even though the role of EHs has been extensively studied in mammals and insects, there is very low information available about the physiological role of EHs in plants[187,188].

An epoxide, also termed oxirane, is a quite reactive three-membered cyclic ether. The electrophilic reactivity of an epoxide towards nucleophiles is based on the highly polarised C-O bonds and the high strain energy of the three-atom ring[186,189,190]. Even though endogenously occurring epoxides exhibit a rather medium reactivity and are therefore quite stable under physiological conditions, foreign epoxides, which frequently occur as intermediates from the metabolism of xenobiotics, by contrast often show a particular toxic, mutagenic or carcinogenic potential due to their high reactivity towards biomolecules such as deoxyribonucleic acid (DNA), ribonucleic acid (RNA) or proteins[185,186,191]. Therefore, epoxides are under tight control by EHs that transform the reactive species to vicinal diols, resulting in a more stable and less reactive compound[191,192]. Different sub-types of EHs have been described from different organisms to date that fulfil diverse physiological functions. In mammals, for example, the microsomal EH (mEH), the soluble EH (sEH), also referred to as cytosolic EH, the leukotriene A_4 hydrolase, the microsomal cholesterol 5,6-oxide hydrolase, the hepoxilin A_3 hydrolase as well as EH3 and EH4 have been described, with mEH and

sEH being the longest known and most widely studied EHs[187]. mEH and sEH have been reported to possess activity on a broad range of substrates and homologues of these enzymes were furthermore found to exist in organisms other than mammals[186,193-196]. The described functions of EHs range from the aforementioned detoxification of xenobiotic epoxides (mEH, sEH), the catabolism of carbons from natural sources (microbial EH) to the regulation of physiological lipid-derived signalling molecules (sEH)[186,191].

Although the sequences of EHs vary considerably, their mechanism of action is highly conserved[186,197]. Most epoxide hydrolases including plant EHs belong to the α/β-hydrolase fold-containing family of enzymes[188,198]. The α/β fold is made up of eight β-strands with intermediary α-helices and is referred to as the core domain[199,200]. This core domain is covered by a cap (also referred to as lid or flap) domain mainly consisting of α-helices and an additional cap loop[190,197,200]. The core and cap domain are connected by an NC-loop and together form the EH active site pocket[191,197]. The cap-loop and the NC-loop, in contrast to the core and cap domain, are structurally variable regions[197]. All members of this family share a highly conserved catalytic triad with a 'charge-relay' mechanism responsible for substrate cleavage, consisting of a nucleophile, a general base and an acid (Asp-His-Asp/Glu)[191,198]. The nucleophilic Asp and the His residue are located in a hydrophobic space between the core and cap domain[197]. In addition to the catalytic triad, two tyrosine residues positioned within the lid domain and opposite to the nucleophilic side chain of Asp are involved in the initial alkylation step by supporting the recognition, positioning, activation and ring opening of the epoxide substrate[190,201].

The cleavage of epoxides into vicinal diols by an α/β fold EH is based on a two-step mechanism via the formation of a covalent alkyl-enzyme intermediate (Fig. 9). In the proposed reaction mechanism, the initial step is a nucleophilic attack of the carboxylic acid moiety of the aspartate residue on one of the two carbon atoms of the epoxide substrate, which is hydrogen bonded with and polarised by the two tyrosine residues. The attack results in the ring opening of the epoxide and thus in the formation of an alkyl-enzyme intermediate[186,202]. This step is designated the alkylation half-reaction. In the second step which is referred to as the hydrolytic half-reaction, the previously formed ester bond between the nucleophilic aspartate and the substrate is

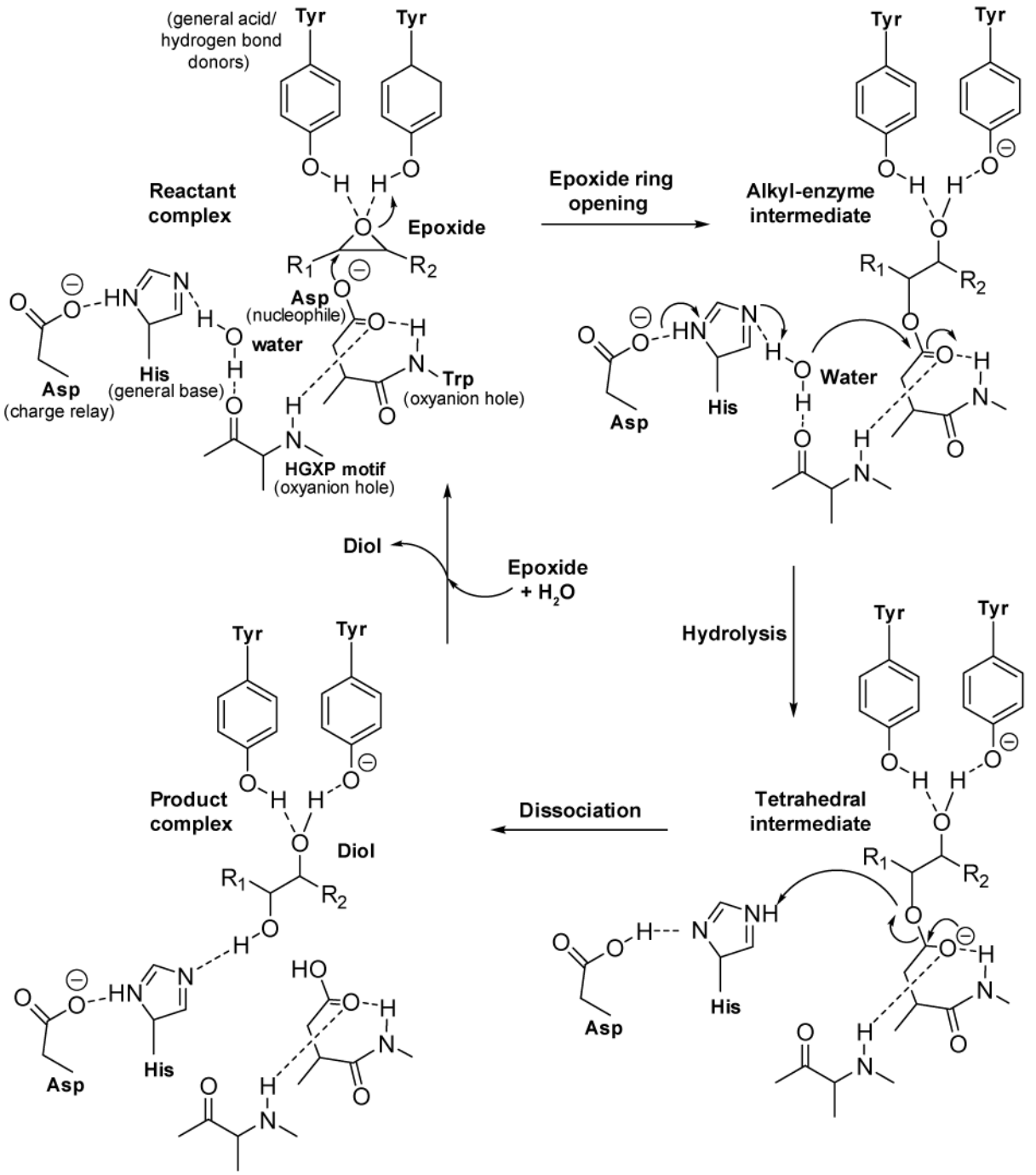

Fig. 9 Proposed reaction mechanism of a sEH. An epoxide is cleaved into a diol by an α/β-fold containing EH in a multistep reaction. The reaction mechanism involves a catalytic triad consisting of Asp-His-Asp/Glu as well as two tyrosine residues that support the recognition, positioning and ring opening of the epoxide substrate. In the first step, the ring opening of the epoxide occurs via an initial hydrogen bonding of the epoxide with the two tyrosine residues and the subsequent nucleophilic attack by an aspartate side chain on one of the carbons of the epoxide substrate, resulting in the presence of a covalent alkyl-enzyme intermediate. In the second step, a tetrahedral intermediate is formed through a histidine-assisted nucleophilic activation of a water molecule that attacks the carbonyl and leads to a hydrolysis of the ester bond between the nucleophilic aspartate and the substrate. The final dissociation of the oxyanion hole-stabilised tetrahedral intermediate results in a release of the diol product and recovers the free enzyme. Adapted from Hopmann and Himo, 2006 and Serrano-Hervás *et al*., 2017[203,204].

hydrolysed[202,205]. Here, a nucleophilic attack of a histidine-activated water molecule on the carbonyl occurs which leads to the formation of a tetrahedral intermediate[186,202,204]. The tetrahedral intermediate is stabilised by an oxyanion hole, whereby hydrogen bonds are formed between the oxyanion and two peptide backbone nitrogen atoms of amino acids, one of which is the X amino acid of the HGXP motif whereas the other one follows the nucleophilic Asp in the amino acid sequence of the EH[202]. Finally, a dissociation of the tetrahedral intermediate takes place, resulting in the release of the diol product and the free enzyme[203]. The formation of the alkyl-enzyme intermediate which occurs during the alkylation half-reaction via the formation of a Michaelis complex is reversible. The corresponding Michaelis complex exists in a rapid equilibrium with the substrate and free enzyme, while the hydrolysis of the ester bond is irreversible and thus represents the rate limiting step in this reaction[201,206].

Most publications about plant EHs report on sEHs, like the soybean EH or potato stEH1, which have been studied quite well with respect to their substrate specificity or regio- and enantioselectivity as well as their structure[196,207,208]. Fewer studies, however, additionally describe EH activity to occur in microsomal fractions[209-211]. EHs are present in different plant tissues like roots, leaves or fruits and have been detected at different developmental stages such as germinating seeds, seedlings or mature plants with their subcellular localisation not being restricted to the cytosol[212,213]. Like their mammalian counterparts, plant sEHs play a role in lipid metabolism, with epoxide containing fatty acids, i.e. epoxy fatty acids or epoxy-hydroxy fatty acids such as epoxystearic and epoxylinoleic acids or hepoxilins as their physiological substrates as reviewed by Newman *et al.*[212]. In contrast to mammalian sEHs, plant EHs often show a higher enantioselectivity with an apparent preference for *trans*-substituted epoxides over *cis*-substituted epoxides as substrates[207,214,215]. The cleavage of these lipid-derived epoxides results in a lower chemical reactivity, a modified biological activity and an increased water solubility of the substrate[212]. Due to the physiological functions of their lipidic substrates, plant EHs *inter alia* play a role in mediating stress responses, in cuticle formation or in general defence against pathogens. For example, an Arabidopsis sEH was reported to be induced by auxin and water stress[216], sEHs from soybean and Arabidopsis were reported to participate in the synthesis of cutin monomers[188,217], a tobacco sEH was induced during the resistance response to a virus infection[218] and finally, an EH from *Vicia sativa* was shown to act on potential

messengers involved in plant-pathogen interactions[219]. Plants, in contrast to other organisms express different EH isoforms that can occur in monomeric or dimeric forms[188,214,220]. However, it seems to remain underexplored whether these isoforms play a role in entirely different physiological processes independent of each other or whether they possibly co-orchestrate the same physiological processes and even act on the same physiological substrates.

1.5 Objectives

The aim of this work was to elucidate and subsequently validate the molecular targets of the pan-HER TKI **Ner** in *A. thaliana* using chemoproteomics. Previous work on this project was done by Dr. Vivek Halder at the MPIPZ in Cologne. To study the role of kinases involved in SA signalling, a chemical screen for SA agonists employing a library of 89 different kinase inhibitors was conducted using SA-responsive *PR1p::β-glucuronidase (GUS)* seedlings. From this screen, **Ner**, among few other compounds with known functions as broad-spectrum inhibitors or as inhibitors of DNA replication processes was identified to act as a strong activator of SA signalling in Arabidopsis. Concentration-dependent activation of SA signalling was further confirmed by measuring *PR-1* messenger RNA (mRNA) expression levels as well as SA levels in living plants after treatment with **Ner**. **Ner**, however, has never been evaluated *in planta* before and its mechanism of action in manipulating SA signalling is unknown. Therefore, this work was intended to unravel the target enzyme(s) by which **Ner** impacts on SA signalling.

To enable target identification studies, an alkyne-derivatised version of **Ner** (**≡Ner**) that can be applied as a chemical probe for the visualisation and affinity enrichment of target proteins was synthesised by Jan H. Krahn and Sarah Resch, University of Duisburg-Essen. Two structurally related control probes (**≡Ctrl1** and **≡Ctrl2**) were also synthesised by Sarah Resch and were included in these studies to control for indirect side effects of **≡Ner** that may lead to the activation of SA signalling (Fig. 10). The underlying experiments comprise the initial evaluation of **≡Ner** in HeLa cells to examine the functional integrity of the chemical probe, followed by the study of the target proteins of **≡Ner** in Arabidopsis. This was achieved through visualisation of the labelled proteins on gel after electrophoretical sample separation and further target

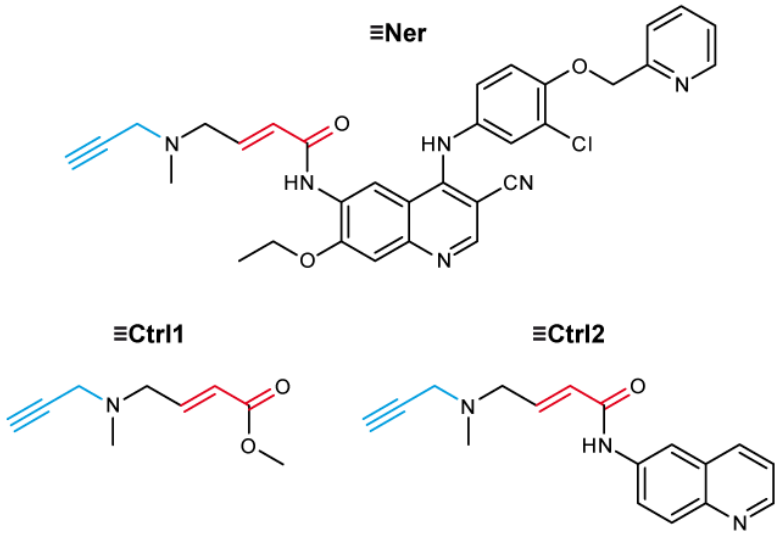

Fig. 10 Overview of chemical probes employed in this work. Chemical structures for the alkyne-modified chemical probes **≡Ner**, **≡Ctrl1** and **≡Ctrl2** are shown. The reactive Michael system that possesses covalent binding of the chemical probes to their target enzymes is depicted in red while the alkyne moiety is shown in blue.

identification by performing an IGD of the target proteins with trypsin, followed by an MS-based qualitative proteomics analysis. In addition, the selectivity of **≡Ner** should be determined by conducting an OBD of all captured target proteins with a subsequent LFQ-based MS analysis. For this analysis, the two control probes **≡Ctrl1** and **≡Ctrl2** were employed alongside **≡Ner**. In addition to those experiments aiming on the identification of the target proteins of **≡Ner** and thus **Ner**, a potential target was confirmed by using an Arabidopsis knock-out mutant line as well as the recombinantly expressed protein for chemical labelling with **≡Ner**. The recombinant protein was additionally utilised in enzyme kinetic assays with **Ner**. Further studies on the binding site of **Ner** to this target protein were carried out by generating and evaluating site-directed mutants.

2. Material and Methods

2.1 Material

2.1.1 Chemicals

A list of all used chemicals and their suppliers can be found in the appendix (Appendix 1, Tab. 13).

2.1.2 Consumable material

All used consumable material and their manufacturers are listed in the appendix (Appendix 2, Tab. 14).

2.1.3 Laboratory equipment

A list of used laboratory devices and their manufacturers as well as which type of device is reported in the appendix (Appendix 3, Tab. 15).

2.1.4 Buffers and solutions

The composition of all buffers and solutions that were used for this work are shown in the appendix (Appendix 4, Tab. 16).

2.1.5 Complete systems

The employed complete systems and their suppliers are displayed below (Tab. 1).

Tab. 1 List of complete systems. All complete systems used in this work are reported together with their respective supplier.

Complete system	Supplier
NucleoBond® Xtra Plus	Macherey-Nagel
NucleoSpin® Plasmid	Macherey-Nagel
NucleoSpin® Gel and PCR Clean-up	Macherey-Nagel
Roti®-Nanoquant, 5× solution	Carl Roth
Set of dATP, dCTP, dGTP, dTTP, 25 µmol each	Promega
SuperSignal® West Femto Maximum Sensitivity Substrate	Thermo Scientific
SuperSignal® West Pico Chemiluminescent Substrate	Thermo Scientific

2.1.6 Proteins and enzymes

All used commercial proteins and enzymes as well as their suppliers are listed below (Tab. 2).

Tab. 2 List of commercial proteins and enzymes. All proteins and enzymes used in this work are reported together with their respective supplier.

Protein or enzyme	Supplier
6×-His Tag monoclonal antibody (HIS.H8) HRP-conjugate Mouse/IgG2b, monoclonal	Invitrogen™ (Thermo Fisher Scientific)
BSA Protein Standard, 2 mg vials	Supelco (Merck)
BSA, molecular biology grade	VWR Chemicals
Cellulase Onozuka R-10 (1 U mg^{-1})	Merck
*Dpn*I (20 U μL^{-1})	New England Biolabs
Macerozyme R-10 (pectinase ca. 0.5 U mg^{-1}, hemicellulase ca. 0.25 U mg^{-1}, cellulase ca. 0.1 U mg^{-1})	Serva
PfuUltra HF DNA polymerase (2.5 U μL^{-1}) supplied with PfuUltra HF reaction buffer (10×)	Agilent Technologies
Trypsin protease, Pierce™ MS grade	Thermo Scientific (Thermo Fisher Scientific)
Trypsin protease, sequencing grade modified trypsin supplied with trypsin resuspension dilution buffer	Promega

2.1.7 Inhibitors

A list of all kinase inhibitors that were used for the experiments and their suppliers is reported below (Tab. 3). The chemical structures of all employed kinase inhibitors can be found in the appendix (Appendix 5, Fig. 37).

Tab. 3 List of employed kinase inhibitors. All kinase inhibitors used in this work are reported together with their respective supplier.

Kinase inhibitor	supplier
5,6-dichloro-1-β-(D)-ribofuranosylbenzimidazole	Santa Cruz Biotechnology
Afatinib	Santa Cruz Biotechnology
BAY 11-7082	Santa Cruz Biotechnology
Gefitinib	Santa Cruz Biotechnology
Genistein	Santa Cruz Biotechnology
Ner	Santa Cruz Biotechnology
Pelitinib	Sigma-Aldrich (Merck)

The utilised protease inhibitor cocktails and their suppliers are listed in the following table (Tab. 4).

Tab. 4 List of employed inhibitor cocktails. All inhibitor cocktails used in this work are reported together with their respective supplier.

Inhibitor cocktails	supplier
cOmplete™ Mini EDTA-free Protease Inhibitor Cocktail	Roche
MS-SAFE Protease and Phosphatase Inhibitor	Sigma (Merck)

2.1.8 Chemical probes and 'click' tags

To perform labelling experiments, the three chemical probes **≡Ner**, **≡Ctrl1** and **≡Ctrl2** were used (Fig. 10). **≡Ner** is an alkyne-tagged derivative of the TKI **Ner**. **≡Ctrl1**, the electrophilic linker with the alkyne tag and **≡Ctrl2**, the **≡Ctrl1** moiety linked to 6-aminoquinoline were used as inactive control probes for **≡Ner**. These probes carry a Michael system for covalent binding to target enzymes. The alkyne tag is used to attach a 'click' tag for probe detection or target affinity enrichment via 'click' chemistry.

For two-step ABPs, 'click' tags were employed to detect the labelled proteins. These click-tags and their suppliers are listed below (Tab. 5).

Tab. 5 List of 'click' tags. All 'click' tags used in this work are reported together with their respective supplier.

'Click' tag	Supplier
5/6-TAMRA-Azide-Biotin	Jena Bioscience
Cy3-Azide	Kaiser lab

2.1.9 Oligonucleotides

All used primers for site-directed mutagenesis of AtEH7 were self-designed and synthesised by the company Sigma-Aldrich (St. Louis, MO, USA). Primers were utilised at a final concentration of 250 nM per polymerase-chain-reaction (PCR). The sequences of these primers are depicted below (Tab. 6).

Tab. 6 Primers for site-directed mutagenesis of AtEH7. All primers used for site-directed mutagenesis of AtEH7 are reported together with their respective orientation and primer sequence (5'→3').

Primer	Orientation	Primer sequence (5'→3')
C111A	Forward	GTTGCGTGGTGGCTTGCTATGATCAGGCCTG
	Reverse	CAGGCCTGATCATAGCAAGCCACCACGCAAC
C152A	Forward	CGATGATTACTACATTGCGAGGTTTCAGGAGCCTGG
	Reverse	CCAGGCTCCTGAAACCTCGCAATGTAGTAATCATCG
C186A	Forward	GTAACCCACGTCCACCTGCAATTCCAAAGTCAGTTG
	Reverse	CAACTGACTTTGGAATTGCAGGTGGACGTGGGTTAC

Sequencing primers for mutant AtEH7 constructs were either self-designed and synthesised by the company Sigma-Aldrich (St. Louis, MO, USA) or provided by the sequencing service contractor Microsynth Seqlab (Göttingen, Germany; Tab. 7).

Tab. 7 Primers for sequencing. All sequencing primers used in this work are reported together with their respective orientation and primer sequence (5'→3').

Primer	Orientation	Primer sequence (5'→3')
AtEH7 sequencing primer	Forward	GCTTCGATTGGTTCAGGTCC
	Reverse	ACGTGCTTCTTCAAACCACC
Microsynth Seqlab sequencing primer	Forward (T7)	TAATACGACTCACTATAGGG
	Reverse (T7term)	TGCTAGTTATTGCTCAGCGG

2.1.10 Strains of organisms

For the experimental work, *A. thaliana* Columbia (Col-0) seedlings, as well as root cells and leave material were used to perform plant-based experiments. In addition, seedlings of the *A. thaliana* Col-0 derived mutant line *eh3-2* (SALK_149885C) were used. All plant material was provided by Dr. Vivek Halder, MPIPZ Cologne, Germany. Arabidopsis Col-0 seedlings were additionally supplied by Kyoko Morimoto, University of Oxford and Jan Schulze Hüynck, University of Cologne. Moreover, the human cervical carcinoma cell line HeLa (ATCC®/LGC Standards, Manassas, VA) was employed. Additionally, the *Escherichia coli* (*E. coli*) strains BL21 (DE3) (Novagen®, EMD Millipore, Merck KGaA, Darmstadt, Germany), TOP10 (Invitrogen™, Thermo Fisher Scientific Inc., Waltham, MA, USA) and DH5α (Invitrogen™, Thermo Fisher Scientific Inc., Waltham, MA, USA) were utilised (Tab. 8).

Tab. 8 *E. coli* strains. All *E. coli* strains used in this work are reported together with their respective genotype and reference.

Strain	Genotype	Reference
BL21 (DE3)	F^- *omp*T *hsd*S_B (r_B^-, m_B^-) *gal dcm* (DE3)	Studier and Moffatt1986[221]
DH5α	F^- Φ80*lac*ZΔM15 Δ(*lac*ZYA-*arg*F) U169 *rec*A1 *end*A1 *hsd*R17(r_k^-, m_k^+) *pho*A *sup*E44 *thi*-1 *gyr*A96 *rel*A1 λ^-	Hanahan 1985[222]
TOP10	F^- *mcr*A Δ(*mrr-hsd*RMS-*mcr*BC) φ80*lacZ*ΔM15 Δ*lac*X74 *rec*A1 *ara*D139 Δ(*ara-leu*)7697 *gal*U *gal*K λ^- *rps*L(Str^R) *end*A1 *nup*G	Invitrogen™

HeLa cells as well as *E. coli* strains were a gift from the group of Prof. Dr. Michael Ehrmann, University of Duisburg-Essen, Germany.

2.1.11 Resins for protein purification

A list of all employed resins for protein purification and their suppliers is shown below (Tab. 9)

Tab. 9 List of used resins for protein purification. All resins used in this work are reported together with their respective supplier.

Resin	Supplier
Pierce™ Avidin Agarose Beads	Thermo Scientific
Protino® Ni-IDA resin	Macherey-Nagel
Superdex™ 75 PG Hiload 16/60 column	GE Healthcare Life Sciences (now Cytiva)

2.1.12 Cell culture liquids

All cell culture liquids and their supplier are listed in the following table (Tab. 10).

Tab. 10 Cell culture liquids. All cell culture liquids used in this work are reported together with their respective supplier.

Cell culture liquid	Supplier
Gibco™ DMEM	Invitrogen™ (Thermo Fisher Scientific)
Gibco™ DPBS	Invitrogen™ (Thermo Fisher Scientific)
Gibco™ FCS	Invitrogen™ (Thermo Fisher Scientific)
Gibco™ Pen/Strep	Invitrogen™ (Thermo Fisher Scientific)
Gibco™ Trypsin-EDTA (0.05%), phenol red	Invitrogen™ (Thermo Fisher Scientific)

2.1.13 DNA and protein ladders and dyes

All ladders and dyes used for DNA or protein gelelectrophoresis as well as their supplier are displayed below (Tab. 11)

Tab. 11 List of commercial DNA and protein ladders or dyes. All commercial DNA and protein ladders or dyes used in this work are reported together with their respective supplier.

Ladder or dye	Supplier
1 kb DNA ladder	Amresco (VWR)
DNA loading dye, 6×	AppliChem
HD Green DNA dye	Intas
Spectra™ Multicolor Broad Range Protein Ladder	Thermo Scientific (Thermo Fisher Scientific)

2.1.14 Plasmids

For the recombinant protein expression and site-directed mutagenesis of the *A. thaliana* soluble epoxide hydrolase 7 (AtEH7; At4g02340, Gene ID: 828063), a plasmid containing the *eh7* gene cloned into the Gateway® Nova pET-59-DEST™ expression vector (Novagen®, EMD Millipore, Merck KGaA, Darmstadt, Germany) was provided by Dr. Mainak Das Gupta, MPIPZ Cologne. The vector carries an N-terminal polyhistidine-tag (His-tag)-configuration as well as an N-terminal thioredoxin 1 (TrxA)-configuration followed by a thrombin-cleavage site. A strep-tag II is included C-terminally. In addition, this vector holds a T7-promotor and an ampicillin resistance gene. The full-length sequence of the cloned *eh7*::pET-59-DEST plasmid is shown in the appendix (Appendix 6).

2.1.15 Software

In the course of this work, the software Microsoft Office 2016, ChemDraw Prime 16.0, Adobe CS4 Photoshop and Illustrator, Fiji 1.51j, GraphPad Prism version 5 and Endnote™ X9 have been used. SeqMan Pro™ and SeqBuilder™ (both from the DNASTAR Lasergene package, version 12.2.0) were used for displaying plasmid sequences and analysing sequencing data. Primers for site-directed mutagenesis were constructed using the PrimerX web-tool (Last update 08/2006) whereas SeqBuilder™ was additionally used for the construction of sequencing primers. PyMOL™ 1.1beta3 was used to display 3D protein structures. The Orbitrap Elite mass spectrometer was operated using the Thermo Xcalibur software version 2.2 SP1.48. For the analysis of MS data, MaxQuant version 1.5.3.30 was used for analysing MS datasets and Perseus version 1.6.2.1 was used for subsequent statistical data analysis. Thermo Xcalibur Qual Browser version 3.0.63, RawMeat version 2.1 and Preview version 3.2.0 were used for the quality control of MS data.

2.2 Methods

2.2.1 Cell biological methods

2.2.1.1 Preparation of *A. thaliana* protoplasts

Protoplasts were prepared from an Arabidopsis (Col-0) root cell suspension culture in the group of Dr. Erich Kombrink, MPIPZ Cologne. At day 4 after passaging to fresh B5

culture medium, roughly 40 mL of the culture were collected by centrifugation (5 min, 2000 rpm). Afterwards, the cells were washed with 25 mL of sterile 240 mM $CaCl_2$ (5 min, 2000 rpm). To digest cell walls, the root cells were incubated overnight (o/N) at 26 °C in the dark on a rotary shaker (20 rpm) with 60-70 mL of protoplast enzyme solution. The next day, the protoplasts were collected by centrifugation (2 min, 2000 rpm), followed by a washing step with 25 mL of sterile 240 mM $CaCl_2$ (2 min, 1500 rpm) prior to resuspension in B5 culture medium to a final volume of about 15 mL. To further purify and concentrate the protoplasts, floating was used (5 min, 1000 rpm) and the obtained protoplast layer was carefully collected in a fresh tube. Protoplasts were either directly used for chemical *in situ* labelling (2.2.3.3.2) or aliquots of protoplasts were stored at -80 °C until use for *in vitro* labelling of extracts (2.2.3.3.3).

2.2.1.2 Preparation of competent *E. coli* cells

As *E. coli* does not harbour a natural competence for the uptake of free DNA from their surroundings, it needs to be made competent to enable subsequent transformation with a construct.

2.2.1.2.1 Preparation of chemically competent TOP10 cells

Chemically competent TOP10 *E. coli* cells were prepared in variation to Hanahan *et al*.[223] by Pierre Stegemann, University of Duisburg-Essen. In brief, seed stocks were first prepared by streaking out *E. coli* TOP10 cells onto a super optimal broth (SOB)-agar plate and incubation o/N at 23 °C. A single colony was picked and used to inoculate 2 mL of fresh SOB medium prior to o/N incubation at 23 °C while gently shaking. Sterile glycerol was added to the culture to a final concentration of 15% (w/v) and 1 mL aliquots of were directly flash-frozen in liquid nitrogen and stored at -80 °C.

To prepare chemically competent cells, 250 mL of fresh SOB medium were inoculated with 1 mL of seed stock and grown at 20 °C and 200 rpm for about 16 h until an optical density at a wavelength of 600 nm (OD_{600}) of ca. 0.3 was reached. Afterwards, the cells were collected by centrifugation (3000 rpm, 10 min, 4 °C) and the supernatant was carefully removed. The cell pellet was resuspended in 80 mL of ice-cold CCMB80 buffer and the cells were incubated on ice for 20 min prior to collection of the cells by centrifugation (3000 rpm, 10 min, 4 °C). Next, the supernatant was removed and the cells were resuspended in 10 mL of ice-cold CCMB80 buffer. The OD_{600} of a mixture

of 200 µL SOB and 50 µL of the resuspended cells was determined and ice-cold CCMB80 buffer was added to the resuspended cells until an OD_{600} of 1.0-1.5 of the mixture of 200 µL SOB and 50 µL of the resuspended cells was reached. 50 µL aliquots of chemically competent bacteria were directly flash-frozen in liquid nitrogen and stored at -80 °C until use for heat shock transformation (2.2.1.3.1).

2.2.1.2.2 Preparation of electrocompetent BL21 (DE3) cells

E. coli BL21 (DE3) cells were streaked out onto an N-Z-Amine (NZA) agar plate and incubated o/N at 37 °C. A single colony was picked and used to inoculate 7.5 mL fresh NZA medium to obtain a pre-culture via o/N incubation at 37 °C while shaking at 200 rpm. The pre-culture was used to inoculate 200 mL fresh NZA medium to an OD_{600} of 0.1. The culture was grown at 30 °C and 200 rpm for about 3 h until an OD_{600} of ca. 0.5 was reached. Afterwards, the culture was cooled on ice for 30 min and the cells were collected by centrifugation (4000 rpm, 30 min, 4 °C). The supernatant was removed and the cell pellet was washed successively by resuspension in ice-cold sterile Milli-Q water for four times (4000 rpm, 20 min, 4 °C). Lastly, the obtained cell pellet was taken up in 3.5 mL 7% (v/v) dimethyl sulfoxide (DMSO; in sterile H_2O). 50 µL aliquots of electrocompetent bacteria were directly flash-frozen in liquid nitrogen and stored at -80 °C until use for transformation by electroporation (2.2.1.3.2).

2.2.1.3 Transformation of competent *E. coli* cells

The transformation of electrocompetent cells is a process in which a cloned plasmid is passively taken up through the cell wall.

2.2.1.3.1 Heat shock transformation

50 µL aliquots of flash-frozen chemically competent *E. coli* Top10 cells (2.2.1.2.1) were thawed on ice and 10 µL of each digested PCR product (2.2.2.2) or 5 µL of the digested PCR product after clean-up (2.2.2.4), if applicable, were pipetted to a separate aliquot of the cells. The cells were mixed carefully and incubated with the plasmids on ice for 20-30 min. To perform the heat shock, the cells were placed at 42 °C for 45 sec prior to another incubation on ice for 2 min. Next, the cells were taken up in 950 µL fresh NZA medium and incubated in a thermomixer at 37 °C for 1 h shaking at 700-850 rpm. To obtain single colonies carrying the plasmids encoding for the mutant forms of

AtEH7, 10 µL, 100 µL and 890 µL of the transformed cells were each streaked out onto selective NZA agar plates (200 µg mL^{-1} ampicillin) and the dried plates were incubated o/N at 37 °C. Single colonies were used to inoculate 10 mL of selective NZA medium (200 µg mL^{-1} ampicillin). The inoculated cultures were grown o/N shaking at 200 rpm and used for plasmid preparation (2.2.2.5) to identify positive clones by sequencing (2.2.2.6) as well as for the preparation of bacterial stocks (2.2.1.4).

2.2.1.3.2 Electroporation

50 µL aliquots of flash-frozen electrocompetent *E. coli* BL21 (DE3) cells (2.2.1.2.2) were thawed on ice and 0.5 µL (around 120-385 ng DNA) of the *eh7*::pET-59-DEST plasmid encoding WT AtEH7 and the plasmids *eh7(C111A)*::pET-59-DEST, *eh7(C152A)*::pET-59-DEST and *eh7(C186A)*::pET-59-DEST encoding for the single-mutant forms of AtEH7 were added to a separate aliquot of the cells. The cells were mixed carefully and incubated with the plasmid for 2 min on ice before they were transferred into pre-cooled electroporation cuvettes. A voltage of 1800 V was applied to the cells using the electroporator, resulting in a discharge time constant of about 4-6 ms for a successful transformation. The cells were directly taken up in 900 µL fresh NZA medium and incubated in the thermomixer at 37 °C for 1 h shaking at 500 rpm. To obtain single colonies carrying the plasmids encoding for the WT and single-mutant forms of AtEH7, the transformed cells were each streaked out onto selective NZA agar plates (200 µg mL^{-1} ampicillin) and the dried plates were incubated o/N at 37 °C. Single colonies were used to inoculate 10 mL of selective NZA medium (200 µg mL^{-1} ampicillin). The inoculated cultures were grown o/N shaking at 200 rpm and used for the preparation of bacterial stocks (2.2.1.4) that were utilised for the expression of recombinant WT or mutant AtEH7 (2.2.1.5).

2.2.1.4 Preparation of bacterial stocks

To prepare bacterial glycerol stocks of previously transformed *E. coli* Top10 or BL21 (DE3) cells (2.2.1.3.1 and 2.2.1.3.2) carrying the plasmid *eh7*::pET-59-DEST, *eh7(C111A)*::pET-59-DEST, *eh7(C152A)*::pET-59-DEST or *eh7(C186A)*::pET-59-DEST, 1 mL 50 % (w/v) sterile glycerol and 1 mL of a saturated *E. coli* o/N culture in NZA medium (200 µg mL^{-1} ampicillin) were mixed and frozen at -80 °C.

2.2.1.5 Expression of recombinant AtEH7

For the expression of recombinant WT or single-mutant AtEH7, 20 mL fresh NZA medium (200 µg mL^{-1} ampicillin) were inoculated with a clone of *E. coli* BL21 (DE3) transformed with either *eh7*::pET-59-DEST, *eh7(C111A)*::pET-59-DEST, *eh7(C152A)*::pET-59-DEST or *eh7(C186A)*::pET-59-DEST from a glycerol stock. The pre-cultures were incubated o/N at 37 °C while shaking at 200 rpm. The next morning, 1 L fresh NZA medium (200 µg mL^{-1} ampicillin) was inoculated with the pre-culture to an OD_{600} of 0.05. The inoculated expression culture was then incubated in a shaker at 30 °C and 150 rpm for about 3 h until an OD_{600} of 0.5-0.6 (log-phase) was reached. Next, the protein expression of recombinant AtEH7 was induced by adding isopropyl β-D-thiogalactopyranoside (IPTG) to a final concentration of 0.5 mM and the culture was incubated for another 4 h at 18 °C shaking at 150 rpm. Bacteria were harvested from the induced cultures by centrifugation (20 min, 5000 × g, 4 °C), the pellets were flash-frozen in liquid nitrogen and stored at -80 °C until protein extraction (2.2.1.6.1) and purification of recombinant AtEH7 (2.2.3.1) was done. The successful expression of recombinant AtEH7 was confirmed by polyacrylamide gel electrophoresis (PAGE) (2.2.3.6) and subsequent colloidal Coomassie staining (2.2.3.9).

2.2.1.6 Cell disruption and protein extraction

2.2.1.6.1 Disruption of *E. coli* cells

To extract recombinant AtEH7 obtained after IPTG-induced protein expression (2.2.1.5), *E. coli* cells were disrupted by high-pressure homogenization using the French pressure cell press.

Prior to the cell disruption, cell pellets from a 1 L *E. coli* culture were resuspended in LEW lysis buffer supplemented with 1× cOmplete™ Mini ethylenediaminetetraacetic acid (EDTA)-free Protease Inhibitor Cocktail, filled up to a total volume of 15-20 mL and kept on ice. The cell suspension was transferred into the cooled cylinder unit of the French Press and passed through the needle valve using an internal pressure of about 1000-1500 Psi. This step was conducted with a total of seven iterations.

After disruption of *E. coli* cells, the crude cell extract was cleared by centrifugation (45-60 min 14000 rpm, 4 °C) to separate the soluble proteins from the cell debris. The

obtained lysates were transferred into new tubes prior to purification of recombinant AtEH7 (2.2.3.1).

2.2.1.6.2 Disruption of human cancer cells

Human cancer cells were disrupted by sonication using the Bioruptor after *in situ* labelling (2.2.3.3.1). To this end, cell pellets were taken up in 50 µL 1× phosphate-buffered saline (PBS) supplemented with 1× cOmplete™ Mini EDTA-free Protease Inhibitor Cocktail (gel analysis) or 1 mL 1× PBS supplemented with 1× MS-SAFE Protease and Phosphatase Inhibitor (affinity enrichment) and the Bioruptor was used at high voltage for 15 min with a cycle of 1 min pulse and 30 sec pause (10 cycles) to break up cells.

Afterwards, the extract was cleared by centrifugation (1 h, 14000 rpm, 4 °C) to separate the soluble proteins from the cell debris and the supernatant was transferred into a fresh tube. The protein concentration of the obtained lysates was determined by a modified Bradford assay (2.2.3.2) before the lysates were directly submitted to a 'click' reaction (2.2.3.5).

2.2.1.6.3 Disruption of *A. thaliana* plant material

To prepare a protein extract from *A. thaliana* Col-0 protoplasts, cell pellets were taken up in an appropriate volume of 1× PBS. Pellets obtained after *in situ* labelling of protoplasts (2.2.3.3.2) were taken up in 50 µL 1× PBS (gel analysis) or 500 µL 1× PBS supplemented with 1× MS-SAFE Protease and Phosphatase Inhibitor (affinity enrichment). For the preparation of protoplast extracts designated for *in vitro* labelling (2.2.3.3.3), each pellet (2.2.1.1) was taken up in 200-250 µL 1× PBS. The resuspended cells were directly sonicated using the Bioruptor at high voltage for 15 min with a cycle of 1 min pulse and 30 sec pause (10 cycles) to break up cells.

Leaves from 4-week-old *A. thaliana* Col-0 plants and 2-week-old *A. thaliana* Col-0 or *eh3-2* seedlings grown on half strength Murashige and Skoog basal medium were grinded in liquid nitrogen using a precooled mortar (placed on ice) and pestle until a fine dried powder remained which was aliquoted into precooled 1.5 mL tubes (about half filled). For the preparation of protein extracts designated for *in vitro* labelling (2.2.3.3.3), the plant powder was taken up in an appropriate volume of 1× PBS. The

powder from leaves was taken up in 500 µL 1× PBS. The powder from seedlings was taken up in 150-350 µL 1× PBS (gel analysis) or 500 µL 1× PBS (affinity enrichment) either without (OBD) or supplemented with 1× MS-SAFE Protease and Phosphatase Inhibitor (IGD) per tube. The suspended plant powder was grinded again using a pestle and cordless pestle motor until the mix looked homogenous and sonicated with the Bioruptor using the previously described settings.

Afterwards, the extracts were cleared by centrifugation (20-30 min, 14000 rpm, 4 °C) to separate the proteins from the cell debris and the supernatant was transferred into a fresh tube. If necessary, the extract was centrifuged again (5 min, 14000 rpm, 4 °C) to obtain a clear lysate. The protein concentration of the lysates was determined by a modified Bradford assay (2.2.3.2) before the lysates were directly submitted to a chemical labelling (2.2.3.3.3) or 'click' reaction (2.2.3.5).

2.2.2 Molecular biological methods

2.2.2.1 Determination of DNA concentrations

The determination of DNA concentrations was done photo-spectrometrically using the micro volume settings of the UV-visible (UV/Vis)-spectrophotometer for double-stranded DNA which measures the absorption of a sample at a wavelength of 260 nm and determines the purity of a DNA sample by measuring contaminations e.g. with proteins and chemicals like phenols or chaotropic salts.

To this end, the spectrophotometer was first calibrated with 1-2 µL of the solvent used for dissolution of the DNA (being either Redissolving Buffer TRIS from the NucleoBond® Xtra Plus kit or Elution Buffer AE from the NucleoSpin® Plasmid kit). Then, 1-2 µL of the isolated plasmid DNA (2.2.2.5) were applied onto the lens for the concentration determination at 260 nm. The purity of the sample is given by the two ratios of the wavelengths 260/280 nm and 260/230 nm.

2.2.2.2 Site-directed mutagenesis of AtEH7 by PCR

Site-directed mutagenesis of AtEH7 was used to introduce single point mutations of cysteine residues to alanines through amplification of the *eh7*::pET-59-DEST plasmid by PCR using suitably modified gene specific primers. For the PCR reactions to

generate the plasmids coding for mutant C111A, C152A and C186A AtEH7, the following reaction mix was prepared:

5 µL PfuUltra HF reaction buffer (10×)
1 µL deoxyribonucleotide triphosphate (dNTP) mix (10 mM each)
1.25 µL forward primer (10 µM)
1.25 µL reverse primer (10 µM)
1 µL DNA polymerase PfuUltra HF (2.5 U μL^{-1})
± 1.25 µL DMSO (100%)
Fill up to 45 µL with sterile nuclease-free water
5 µL plasmid DNA (10 ng μL^{-1})

As template DNA, 50 ng of the *eh7*::pET-59-DEST plasmid was added to the PCR mix, resulting in a total sample volume of 50 µL per reaction. As a negative control, a reaction mix lacking DNA polymerase and reaction buffer but containing all three primer pairs used for site-directed mutagenesis (Tab. 6) was pipetted. The PCR samples were then amplified in the thermocycler by applying the following PCR program:

2‘	98 °C	
30‘‘	95 °C	18-25 cycles
30‘‘	55 °C	
9‘	72 °C	
∞	4 °C	

Directly after the PCR reaction 1 µL *Dpn*I (20 U μL^{-1}) was added per PCR sample followed by an incubation for 1 h at 37 °C. The digested PCR products were analysed by agarose gel electrophoresis (2.2.2.3) to confirm the successful DNA amplification. Prior to the subsequent heat shock transformation of *E. coli* (2.2.1.3.1) with the three mutant constructs *eh7(C111A)*::pET-59-DEST, *eh7(C152A)*::pET-59-DEST or *eh7(C186A)*::pET-59-DEST, a clean-up of the digested PCR product (2.2.2.4) was performed, if necessary.

2.2.2.3 Agarose gel electrophoresis for analysing DNA

During the agarose gel electrophoresis, negatively charged DNA fragments are separated according to their size in a sieve-like matrix after applying voltage to the DNA.

For the electrophoretic separation of amplified DNA, a 1% agarose gel was prepared. To this end, 1 g of agarose was dissolved in 100 mL 1× tris-borate-EDTA (TBE) buffer, supplemented with 2 µL HD Green for the detection of DNA under UV-light and poured into the electrophoresis device. For electrophoresis, 1× TBE buffer was used as running buffer. Before loading on the gel, 10-20 µL of the digested PCR products (2.2.2.2) were mixed with an appropriate volume of 6× DNA loading dye. To determine the size of analysed DNA fragments, 5 µL of a 1 kb DNA ladder were additionally loaded on the gel. To separate the DNA fragments electrophoretically, a constant voltage of 100 V was applied for 1 h. After electrophoresis, the gel was documented using a gel documentation system.

2.2.2.4 Clean-up of PCR products

The clean-up of PCR products (2.2.2.2) prior to heat shock transformation of *E. coli* (2.2.1.3.1) was done using the NucleoSpin® Gel and PCR Clean-up kit manufactured by Macherey-Nagel following the manufacturer's instructions for PCR clean-up (01/2012, Rev. 04), if necessary. As advised, the sample volume was adjusted to 100 µL with sterile nuclease-free water prior to sample loading onto the column. Deviating from the protocol, the binding of the DNA to the silica membrane was performed twice by re-loading of the flow-through. Washing of the silica membrane was done twice as recommended. A two-step elution was used to release the DNA from the silica membrane as suggested for larger fragments. To this end, the membrane was incubated twice with15 µL of preheated Buffer NE for 5 min at 70 °C, followed by a first centrifugation step at low speed (30-50 × g, 1 min, room temperature (RT)) and second centrifugation step at higher speed (11000 × g, 1 min, RT).

2.2.2.5 Plasmid preparation from *E. coli*

The preparation of the plasmids *eh7(C111A)*::pET-59-DEST, *eh7(C152A)*::pET-59-DEST and *eh7(C186A)*::pET-59-DEST carrying the mutant *eh7* gene from *E. coli*

TOP10 cultures (2.2.1.3.1) was performed using the NucleoSpin® Plasmid kit for *E. coli* cultures with a volume of up to 10 mL or the NucleoBond® Xtra Plus kit for larger culture volumes, both manufactured by Macherey-Nagel.

For the plasmid preparation with the NucleoSpin® Plasmid kit, the protocol for the isolation of low-copy plasmids, P1 constructs, or cosmids (11/2012, Rev. 08) was used following the manufacturer's instructions. 9 mL of a saturated *E. coli* culture were utilised as starting material. As recommended, the silica membrane was washed with Buffer AW, without preheating to 50 °C. In alteration to the protocol, the elution step was performed twice, each time using 30 µL Buffer AE that was preheated to 70 °C. This was done in order to increase the yield of the isolated plasmid DNA.

For the plasmid preparation with the NucleoBond® Xtra Plus kit, the protocol for low-copy plasmid purification (Midi) (03/2012, Rev. 10) was followed using 100 mL of a saturated *E. coli* culture. The lysate was not cleared prior to loading onto the equilibrated NucleoBond® Xtra Column Filter. As recommended, the Buffer ELU was preheated to 50 °C prior to the elution of plasmid DNA. The NucleoBond® Xtra eluates were concentrated and desalted by using a NucleoBond® Finalizer. Elution of the plasmid DNA was achieved by passing 200 µL of Redissolving Buffer TRIS through the NucleoBond® Finalizer.

After the plasmid was prepared from *E. coli*, the DNA concentration was determined photo-spectrometrically (2.2.2.1) and plasmid DNA of selected clones was submitted to a sequence analysis (2.2.2.6).

2.2.2.6 Sequence analysis

The sequence analysis of selected clones obtained after site-directed mutagenesis (2.2.2.2) and plasmid preparation from *E. coli* (2.2.2.5) was performed by DNA sequencing based on the chain termination method according to Sanger[224] to check for the introduction of the desired point mutations of cysteines to alanines (C111A, C152A and C186A).

To this end, 50 µL plasmid DNA with a concentration of 100 ng μL^{-1} were sent to the company Microsynth Seqlab (Göttingen, Germany) for analysis together with 100 µL of the self-constructed sequencing primers (10 µM; Tab. 7). The self-constructed

sequencing primers bind within the *eh7* gene (see Appendix 6) and allow sequencing on both DNA strands. Their design took the length of the *eh7* gene into consideration as the Sanger sequencing runs have a typical length with a maximum of about 1000 bp[225]. To cover the full length of the *eh7* sequence, the gene was additionally sequenced using the T7 primer for the forward sequencing reaction and the T7term primer for the reverse reaction, both provided by the company (Tab. 7).

The analysis of the obtained sequencing data was done using the software SeqMan Pro™. Based on these results, a positive clone was selected per construct for the transformation of *E. coli* (2.2.1.3.2) and expression of recombinant single-mutant C111A, C152A and C186A AtEH7 (2.2.1.5).

2.2.3 Protein biochemical methods

2.2.3.1 Purification of recombinant AtEH7

2.2.3.1.1 Preparation and regeneration of IMAC columns

Immobilised metal affinity chromatography (IMAC) columns were prepared by packing an empty gravity flow column with an integrated filter frit with 1 g of a Ni(II)-iminodiacetic acid (Ni-IDA) resin, resulting in a column bed volume of 2 mL. The packed resin was equilibrated with five bed volumes of LEW buffer and stored at 4 °C.

After use, the columns were first washed with two bed volumes of 6 M guanidine hydrochloride (GuHCl) in 0.2 M acetic acid followed by five bed volumes of Milli-Q water. Next, three bed volumes of 0.5 M NaOH were passed over the column followed by five bed volumes of Milli-Q water. In the subsequent step, the column was washed with five bed volumes of ethanol absolute followed by five bed volumes of Milli-Q water. Then, five bed volumes of 100 mM EDTA pH 8.0 were passed over the column followed by five bed volumes of Milli-Q water. For recharging of the columns, five bed volumes of 100 mM $NiSO_4$ were passed over the resin followed by 10 bed volumes of Milli-Q water. Lastly, the resin was washed with two bed volumes of 20% ethanol and the regenerated columns were stored in the same solvent at 4 °C until use (2.2.3.1.2).

2.2.3.1.2 Purification of His-tagged proteins

Recombinant His-tagged WT or single-mutant AtEH7 was purified from *E. coli* protein extracts (2.2.1.6.1) by gravity-flow column chromatography using a separate

prepacked column (2.2.3.1.1) for each of the different AtEH7 proteins. The resin was first washed using 10 bed volumes of Milli-Q water to remove any residual ethanol and subsequently equilibrated by passing 10 bed volumes of LEW lysis buffer over the column. The lysate was passed twice over the resin to enable binding of recombinant AtEH7. Elution of the bound proteins from the column was done ten times with 2 mL IMAC200 elution buffer. All fractions containing recombinant AtEH7 as confirmed by PAGE (2.2.3.6) and subsequent colloidal Coomassie staining (2.2.3.9) were combined and concentrated to around 3-4 mL using Vivaspin® 15R columns (molecular weight cut-off in daltons (MWCO) 10000; 3000 × g, 4 °C) prior to size-exclusion chromatography (2.2.3.1.3).

2.2.3.1.3 Size-exclusion chromatography

After purification of recombinant WT and single-mutant AtEH7 by IMAC (2.2.3.1.2), the enzymes were further purified using size-exclusion chromatography (SEC). To this end, an ÄKTA FPLC chromatography system coupled to a Frac-920 fraction collector was used. Separation of the samples was performed on an equilibrated Superdex™ 75 PG Hiload 16/60 column with a flow rate of 0.5-0.8 mL min^{-1} IMAC200 elution buffer. Prior to sample loading, the concentrated protein solution was centrifuged (10 min, 15000 rpm, 4 °C) to remove any insoluble particles that would clog the chromatography system.

All fractions containing recombinant AtEH7 as confirmed by PAGE (2.2.3.6) and colloidal Coomassie staining (2.2.3.9) were combined and concentrated to around 1 mL using Vivaspin® 15R columns (MWCO 10000; 3000 × g, 4 °C). Prior to use in spike-in labelling experiments (2.2.3.3.3) or enzyme assays (2.2.3.10), recombinant AtEH7 was freshly dialysed against IMAC5 buffer for at least 2 h at 4 °C using Slide-A-Lyzer™ MINI devices (MWCO 3500 or 10000) and the protein concentration of the dialysed enzymes was determined by a modified Bradford assay (2.2.3.2).

2.2.3.2 Protein concentration determination according to Bradford

For the determination of the concentration of protein extracts (2.2.1.6) or purified recombinant AtEH7 (2.2.3.1.3), a modified Bradford assay[226] using the Roti®-Nanoquant system was performed following the manufacturer's instructions. This

assay is based on determination of the ratio between protein-bound and unbound (i.e. solvent) Coomassie.

To determine protein concentrations, adequate amounts of the protein extracts or purified AtEH7 were utilised (usually around 2-10 µL) and filled up to a final volume of 200 µL with MS-grade ultrapure water. Two different dilutions were prepared from each sample with unknown protein concentration. 800 µL of the 1x Roti®-Nanoquant solution were added and the samples were vortexed well. After a short incubation time of 5-10 min, the absorption of all samples was measured at wavelengths of 450 nm and 590 nm using a multimode microplate reader and the quotient of the absorbance at 590 nm/450 nm was determined to compare the ratios of bound (absorbance maxima at 590 nm) to unbound (absorbance maxima at 450 nm) Coomassie. With the help of a bovine serum albumin (BSA) standard curve, these quotients were used to determine the average protein concentration of a protein sample.

To generate a BSA standard curve, 200 µL BSA solutions with concentrations ranging from 0-100 µg mL^{-1} were each mixed with 800 µL 1× Roti®-Nanoquant solution. The quotient of the absorbance at 590 nm/450 nm was determined, plotted against the respective BSA concentration and fitting of the data was done using linear regression.

2.2.3.3 Chemical labelling reactions

A chemical labelling enables the visualisation and identification of the target proteins of a chemical probe within a complex proteome (see 1.2). All chemical probes and competitors used for chemical labelling were dissolved in DMSO.

2.2.3.3.1 *In situ* labelling of HeLa cells

HeLa cells were cultured in Dulbecco's Modified Eagle's Medium (DMEM) supplemented with 10% fetal calf serum (FCS) and 1% Penicillin/Streptomycin (Pen/Strep) by incubation at 37 °C under a 5% CO_2 atmosphere. Only cells with a maximum of 17 passages were used for the experiments. For labelling of cells followed by gel analysis, around 0.9×10^6 cells were seeded per well of a 6-well plate in a volume of 3 mL fresh DMEM ca. 17 h prior to the experiment. For labelling of cells followed by affinity enrichment of target enzymes, cells were seeded in 150 x 20 mm dishes in a volume of 15 mL fresh DMEM and grown to semi-confluency prior to the experiment,

whereby two plates were used per treatment. Immediately before the labelling reaction, the old medium was exchanged for fresh DMEM prewarmed to 37 °C. The competitor, being either **Ner**, afatinib or gefitinib, was directly added into the medium to obtain the desired concentrations as indicated for the respective experiment (0.1% DMSO) and the cells were incubated for 1 h under culturing conditions. DMSO was added to all samples that were not preincubated with a competitor at an equal concentration. After preincubation with the competitor, **≡Ner** was added directly into the medium to obtain the respective probe concentration as indicated (0.1% DMSO per well of a 6-well plate, 0.01% DMSO per 15 cm dish) and the cells were further incubated for a time period of 4 h under culturing conditions. No-probe control samples were treated with DMSO at an equal concentration instead of **≡Ner**.

After the labelling reaction, cells were harvested from the plates. To this end, the old medium was collected in a separate centrifuge tube for each sample and the cells were washed with Dulbecco's PBS (DPBS) prewarmed to 37 °C (3 mL per well of a 6-well plate, 10 mL per 15 cm dish). The DPBS was collected in the same tube as the old medium and the adherent cells were detached by trypsination with 0.05% Trypsin-EDTA, prewarmed to 37 °C, for 5-10 min under culturing conditions (1 mL per well of a 6-well plate, 3 mL per 15 cm dish). Then, the trypsinised cells were taken up in fresh DMEM supplemented with FCS (to inactivate trypsin) and Pen/Strep (3 mL per well of a 6-well plate, 7 mL per 15 cm dish). The cells were pipetted up and down to completely wash them off from the plate and transferred into the respective tubes containing the retained culture medium and DPBS. The cells were collected by centrifugation (5 min, 250 × g, RT), the supernatant was removed and the cell pellets were washed twice with the same volume of prewarmed DPBS as used to wash the plates (5 min, 250 × g, RT). Cells from the same treatment were pooled during the washing step, if applicable. The obtained cell pellets were resuspended in 1 mL prewarmed DPBS and the cell suspensions were transferred into a 1.5 mL tube. The cells were centrifuged once again (5 min, 250 × g, RT) and the supernatant was removed. Cell pellets were flash-frozen in liquid nitrogen and stored at -80 °C until the labelled cells were disrupted (2.2.1.6.2), the protein concentration of the extract was determined by a modified Bradford assay (2.2.3.2) and the extract was submitted to a ‘click’ reaction (2.2.3.5) prior to direct analysis on gel (2.2.3.6) or affinity enrichment of labelled target enzymes (2.2.4.1).

2.2.3.3.2 *In situ* labelling of *A. thaliana* protoplasts

For *in situ* labelling of Arabidopsis protoplasts (2.2.1.1), a 1 mL root cell culture containing 1×10^7 (gel analysis) or 5×10^7 (affinity enrichment) cells was incubated with 1 µM or 10 µM **≡Ner,** as indicated, for 3 h at RT while gently shaking. If applicable, a preincubation with **Ner** was done at a final concentration of 10 µM for 1°h at RT while gently shaking. Prior to collecting the labelled protoplasts by centrifugation (10 min, 2000 rpm), the root cell culture was diluted with 9 mL 240 mM $CaCl_2$. After the supernatant was removed, the protoplast pellets were flash-frozen in liquid nitrogen and stored at -80 °C until the labelled cells were disrupted (2.2.1.6.3), the protein concentration of the extract was determined by a modified Bradford assay (2.2.3.2) and the extract was submitted to a 'click' reaction (2.2.3.5) prior to direct analysis on gel (2.2.3.6) or affinity enrichment of labelled target enzymes (2.2.4.1).

2.2.3.3.3 *In vitro* labelling of *A. thaliana* protein extracts

Arabidopsis protoplast, seedling or leaf extracts were prepared as described (2.2.1.6.3). All *in vitro* labelling reactions were carried out in 1× PBS. For basic labelling reactions with 1 µM or 10 µM **≡Ner** or 10 µM **≡Ctrl1** or **≡Ctrl2** for 1 h at RT, after or without preincubation with the indicated competitors at indicated concentrations for 30 min at RT, 50 µg (gel analysis) or 1-2 mg (affinity enrichment) of total protein as determined by a modified Bradford assay (2.2.3.2) was used. The labelling reactions were usually carried out in a final volume of 50 µL (gel analysis) or 1 mL (affinity enrichment), yielding a final protein concentration of about 1-2 µg mL^{-1}. For spike-in experiments, protoplast extract (50 µg) was spiked with indicated amounts of purified recombinant WT or single-mutant AtEH7 (2.2.3.1.3) prior to incubation with 10 µM **≡Ner** for 1 h at RT either with or without preincubation with 100 µM **Ner** for 30 min at RT. All labelling reactions of spiked samples were likewise carried out in a final volume of 50 µL.

Following the labelling reaction, all samples were submitted to a 'click' reaction (2.2.3.5). Samples from spike-in experiments with AtEH7 were subjected to a methanol-chloroform precipitation (2.2.3.4) before the 'click' reaction was performed.

2.2.3.4 Methanol-chloroform protein precipitation

A methanol-chloroform precipitation of labelled protein samples from spike-in experiments with AtEH7 (2.2.3.3.3) was conducted according to Wessel and Flügge[227] to remove the Cu^{2+}-complexing imidazole prior to the 'click' reaction (2.2.3.5).

To this end, the samples were mixed with a 4× sample volume of methanol absolute, vortexed and centrifuged shortly (30 sec, 9000 × g). Next, an equal sample volume of chloroform was added and the samples were vortexed and centrifuged (30 sec, 9000 × g) again. To achieve phase separation, a 3× sample volume of MS-grade ultrapure water was added to the samples, the samples were vortexed vigorously and centrifuged (1 min, 9000 × g) again. The upper aqueous phase was discarded and a 3× sample volume of methanol absolute was added before the samples were mixed at low speed and the proteins were collected by centrifugation (2 min, 9000 × g). Afterwards, the supernatant was discarded and the protein pellet was air-dried for ca. 5 min. The protein pellet was take up in 46 µL 0.5% (w/v) sodium dodecyl sulfate (SDS) in 1× PBS and the samples were sonicated for 5-10 min in an ultrasonic bath at 37 °C and vortexed vigorously to dissolve the proteins.

2.2.3.5 Cu(I)-catalysed 'click' reaction

A CuAAC between a terminal alkyne and an azide was carried out to enable detection and visualisation as well as affinity enrichment of labelled target proteins.

For samples derived from an *in situ* labelling with **≡Ner** (2.2.3.3.1 and 2.2.3.3.2), 50 µg (gel analysis) or 1-2 mg (affinity enrichment) total protein of the crude extract (2.2.1.6.2 and 2.2.1.6.3) as determined by a modified Bradford assay (2.2.3.2) were subjected to a 'click' reaction that was usually carried out in a final volume of 50 µL (gel analysis) or 1 mL (affinity enrichment), yielding a final protein concentration of about 1-2 µg mL^{-1} in 1× PBS. *In vitro* labelled samples (2.2.3.3.3) were processed directly as described in the following. For the 'click' reaction, the protein extract was successively mixed with final concentrations of either 10 µM Cy3-N_3 (gel analysis) or 10 µM TAMRA-biotin-N_3 (affinity purification) in DMSO, 100 µM TBTA in 4:1 DMSO:*tert*-butyl alcohol, 2 mM TCEP and 2 mM $CuSO_4$ in the given order and the preparations were subsequently incubated for 1 h at RT in the dark.

After the ‘click’ reaction, the samples were prepared for direct analysis by PAGE (2.2.3.6) and fluorescence imaging (2.2.3.7) or were subjected to an affinity enrichment of target proteins using avidin beads (2.2.4.1).

2.2.3.6 Polyacrylamide gel electrophoresis

Separation of proteins by PAGE according to their molecular weight (MW) was performed using 11% bis(2-hydroxyethyl)amino-tris(hydroxymethyl)methane (Bis-Tris)-polyacrylamide resolving gels without stacking gel. Prior to loading of ca. 10-15 µg protein on the Bis-Tris gel, the samples were mixed with a ¼ equivalent of 4× lithium dodecyl sulfate (LDS) gel-loading dye supplemented with 100 mM Dithiothreitol (DTT), incubated at 70 °C for 15 min while shaking and centrifuged shortly. For size prediction of protein bands, 7 µL (14-pocket gel) or 10 µL (10-pocket gel) of the pre-stained Spectra™ Multicolor Broad Range protein ladder were in addition loaded on the gel. Gels were run at a constant voltage of 120 V for 1.5 h using 1× 3-(*N*-morpholino)propanesulfonic acid (MOPS) buffer. After protein separation, sample analysis was done by fluorescence imaging (2.2.3.7) and Coomassie brilliant blue staining (2.2.3.9) or Western blot analysis and immunodetection (2.2.3.8).

2.2.3.7 Fluorescence imaging

In this work, fluorophores were used as reporter tags in ‘click’ chemistry (2.2.3.5) to enable the visualisation of labelled target proteins. These fluorophores were detected using fluorescence imaging. To this end, the fluorophore was excited with light of an excitation wavelength specific to each fluorophore, which was emitted by a laser, and the light emission of the fluorophore was detected.

The fluorescence detection of either Cy3 or TAMRA was done using the Typhoon FLA9000 laser scanner with the Cy3-DIGE (difference gel electrophoresis) settings (green laser λem = 532 nm; BPG1 band pass green filter 560-580 nm). The photomultiplier tube was adjusted according to the fluorescence intensity and the picture was scanned with a resolution of 50-100 microns.

2.2.3.8 Western blot analysis and immunodetection

Following the chemical labelling (2.2.3.3.3), 'click' reaction (2.2.3.5) and separation by PAGE (2.2.3.6), proteins were transferred onto a membrane to enable the visualisation of recombinantly expressed AtEH7 by N-terminal His-tag detection.

Prior to the Western blot, the Immobilon®-P polyvinylidene fluoride (PVDF) membrane was first activated in methanol absolute for 5 min and the filter paper, sponges and blotting cassette were equilibrated in blotting buffer. The gel and the transfer membrane were assembled in a gel cassette between two layers of filter paper and a sponge on both sides and the gel cassette was placed in a tank blotting chamber filled with blotting buffer. After the transfer of proteins onto the membrane at a constant voltage of 110 V for 50-60 min, the membrane was washed thrice with 20 mL TBS-Tween (TBS-T) for 10 min. Subsequently the membrane was blocked with 25 mL 3% BSA (w/v) in TBS-T o/N at 4 °C while rotating to occupy free binding sites on the membrane, thereby preventing unspecific binding of the antibody. The membrane was next incubated with 5 µL of a 6× His-tag monoclonal antibody horseradish peroxidase (HRP)-conjugate which was directly added into the blocking solution (1:5000) for 1-2 h at RT while rotating. Subsequently, the membrane was washed with 20 mL TBS-T twice for 10 min and four times for 5 min before the antibody was detected by enhanced chemiluminescence (ECL). For this purpose, the SuperSignal® West Pico Chemiluminescent Substrate and the SuperSignal® West Femto Maximum Sensitivity Substrate were used. The working solutions for both substrates were prepared by mixing equal volumes of the luminol-containing enhancer solution and the peroxide buffer supplied with each of the substrates. Afterwards, the working solutions of the SuperSignal® West Pico Chemiluminescent Substrate and the SuperSignal® West Femto Maximum Sensitivity Substrate were mixed in a ratio of 4:1.The final ECL substrate mix was dispersed on the membrane and the ECL signal was detected using the Amersham™ Imager 600.

2.2.3.9 Colloidal Coomassie brilliant blue staining

A Coomassie solution containing Coomassie Brilliant Blue G-250 or R-250 as a dye is used for the staining of proteins on a polyacrylamide gel subsequent to separation by gel electrophoresis[228]. Colloidal Coomassie staining was first described by Neuhoff *et*

al.[229]. In the original protocol, the Coomassie brilliant blue staining solution additionally contained 8% ammonium sulfate to form the colloidal dye particles and 20% methanol, shifting the equilibrium towards the dispersed form of the dye. Only in its dispersed form, the dye can diffuse into the gel, allowing for low-background staining of proteins with high sensitivity within a short time.

After separation of proteins by PAGE (2.2.3.6), the gel was shortly washed with Milli-Q water and incubated o/N (about 16-24 h) with the colloidal Coomassie stain. The next day, the stained gel was shortly washed with Milli-Q water. To detect the protein bands on the gel, unbound Coomassie was removed from the gel by destaining in either Milli-Q water or a solution of 10% acetic acid for at least 2 h. The destained gel was digitised using a gel documentation system.

2.2.3.10 Enzyme assays with AtEH7

Enzyme assays with WT or single-mutant AtEH7 were carried out in a 96-well plate format by measuring the increase in absorbance over time that is caused from the cleavage of the cleaved epoxide substrate (2*S*,3*S*)-*trans*-3-Phenyl-2-oxiranylmethyl 4-nitrophenyl carbonate (S-NEPC), thereby reflecting AtEH7 activity. This assay was set up with the help of Jenny Bormann, University of Duisburg-Essen. All enzymatic reactions were carried out in 50 mM Tris-(hydroxymethyl)-aminomethane Tris, pH 8.0 in a total reaction volume of 100 µL. Only reactions where the activity of WT AtEH7 was confirmed were additionally carried out in 50 mM Tris, pH 7.0. Recombinant AtEH7 (2.2.3.1.3) was used at the indicated concentrations based on a modified Bradford assay (2.2.3.2). Buffer controls lacking AtEH7 but containing an equal volume of IMAC5 buffer were likewise prepared for each single assay condition additionally. For enzyme kinetic measurements, the enzymatic reaction was started with the addition of the substrate to a final concentration of 100 µM and the absorbance at 405 nm was measured every 20 sec for a time period of 20 min at 25 °C using a multimode microplate reader. To assess the effect of **Ner** and **≡Ner** on the activity of recombinant WT or single-mutant AtEH7, a preincubation with final concentrations of either 0.5% DMSO, 10 µM **Ner** or 10 µM **≡Ner** was done for 10 min at RT prior to the addition of the substrate.

The same assay format was used to assess the concentration-dependent inhibition of WT AtEH7 for the determination of compound-specific IC_{50} values. To this end, 100 nM WT AtEH7 was preincubated with a two-fold concentration series of **Ner**, gefitinib or pelitinib for 10 min at RT. The absorbance of the substrate was measured 60 sec after the addition to the reaction mix using the previous settings and the remaining AtEH7 activity was determined compared to the respective DMSO controls.

2.2.4 Mass spectrometry-based analysis

2.2.4.1 Affinity enrichment of labelled proteins

To clean-up samples prior to the affinity enrichment of probe-labelled (2.2.3.3) proteins, a protein precipitation with methanol was performed on the samples to remove salts and unbound biotin-containing tag from the 'click' reaction (2.2.3.5) that would occupy free avidin binding sites. Thereto, the samples were mixed with a 4× sample volume of methanol absolute (in 5 mL tubes) and vortexed vigorously. After an incubation at -20 °C (1.5 h-o/N), the precipitated proteins were collected by centrifugation (10 min, 14000 rpm). The supernatant was discarded, the obtained protein pellet was washed with 500 µL methanol absolute (10 min, 14000 rpm), air-dried for ca. 5 min and dissolved in 1 mL 1% (w/v) SDS. To aid the protein solvation, the pellet was grinded with a pestle and subsequently incubated at 37 °C for 10-30 min shaking at 1000 rpm. For samples designated for an OBD, undissolved particles were additionally removed by centrifugation (5 min, 37 °C, 14000 rpm). The protein solution was transferred into a 15 mL centrifuge tube and diluted to a final volume of 8.5 mL using 1× PBS (ca. 0.1% SDS) before the equivalent of 100 µL Pierce™ avidin agarose bead mix (50:50 slurry, 50 µL bed volume) was added to the solution. The avidin beads were equilibrated beforehand by washing twice with 1× PBS for 5 min shaking at 1250 rpm and collecting the beads by centrifugation (1 min, 3000 × g) before use. The protein solution was incubated with the beads for 1 h at RT while gently rotating. Thereafter, the beads were collected by centrifugation (5 min, 400 × g) and the supernatant was discarded. Subsequently, the beads were washed 5× with 1% (w/v) SDS for 10 min at RT while gently rotating and collected by centrifugation (5 min, 400 × g). For samples designated for an IGD, the incubation of the proteins with the beads and the following washing steps were carried out in the dark. Prior to

further treatment, the beads were transferred into 1.5 mL protein LoBind tubes, collected by centrifugation (1min, 3000 × g) and the remaining liquid was aspirated.

Samples designated for an IGD (2.2.4.2.1) were processed directly. Samples designated for an OBD (2.2.4.2.2) were additionally washed 4× with MS-grade ultrapure water for 5 min at RT while shaking at 1250 rpm, collected by centrifugation (1 min, 3000 × g) and all remaining liquid was aspirated.

2.2.4.2 Protein digestion

2.2.4.2.1 In-gel digestion

For an IGD of proteins enriched with **≡Ner**, the captured proteins were first released from the avidin agarose beads (2.2.4.1). To this end, the beads were mixed with 35 µL 4× LDS gel-loading dye supplemented with 100 mM DTT and incubated at 90 °C for 20 min while shaking. The beads were subsequently collected by centrifugation (1 min, 3000 × g) and 30 µL of the supernatant were loaded on a gel, followed by sample separation using PAGE (2.2.3.6). For the separation of proteins on a long gel, the procedure was modified accordingly: 12 µL of the Spectra™ Multicolor Broad Range Protein Ladder were loaded on the gel and the gels were run at a constant voltage of 220 V for 2 h 45 min or of 55 V o/N (ca. 16 h) in the dark prior to analysis by fluorescence imaging (2.2.3.7). Protein bands were cut out from the gel using a scalpel based on a full-size print out of the fluorescence scan and cut into small pieces that were collected in a 1.5 mL protein LoBind tube.

First, the gel pieces were washed two times with 500 µL MS-grade ultrapure water for 15 min shaking at 1500 rpm followed by washing twice with 500 µL 100 mM ammonium bicarbonate (ABC) using the same conditions. The reduction of disulphide bonds was achieved by adding 200 µL of a 10 mM TCEP solution (in 100 mM ABC) and subsequent incubation of the gel pieces for 30 min at 62 °C while shaking at 1000 rpm. Next, the TCEP solution was discarded and the proteins were alkylated with 200 µL of a 55 mM solution of iodoacetamide (IAM) (in 100 mM ABC) for 30 min at RT in the dark while shaking at 1000 rpm. Then, the gel pieces were washed three times with 500 µL of a mixture of 100% acetonitrile (ACN)/100 mM ABC (1:1) for 15 min shaking at 1500 rpm followed by incubation with 50-100 µL of 100% ACN for 5-10 min shaking at 1000 rpm. After the ACN was removed, the gel cubes were completely dried

for 10 min at 45 °C using a vacuum concentrator operated in the vacuum-aqueous mode with the brake function set ON. For IGD, the dried gel pieces were rehydrated by adding 20 µL of a 10 ng µL^{-1} trypsin solution (200 ng) that was prepared from a 100 ng µL^{-1} trypsin stock solution in trypsin resuspension buffer (Promega) by 1:10 dilution with 25 mM ABC. Subsequently, the gel pieces were completely covered with 25 mM ABC (150 µL) and incubated o/N (ca.16 h) at 37 °C while shaking at 1000 rpm. The peptide-containing supernatant was then collected in a fresh 1.5 mL protein LoBind tube, the gel pieces were incubated with 100-150 µL 5% formic acid (FA) (v/v) for 15 min at RT while shaking at 1500 rpm and the supernatant was combined with the recovered digestion mix in the fresh tube to end the enzymatic digestion. Finally, the gel pieces were washed three times with decreasing volumes of ACN (100 µL, 70 µL and 50 µL) for 15 min shaking at 1500 rpm. Each of the supernatants of these washing steps was combined with the recovered digestion mix of the respective samples and the liquid of all samples was evaporated in the vacuum concentrator using the previously described settings until the samples were completely dry (ca. 3-5 h prior to desalting of the samples (2.2.4.3), the peptides were redissolved in 100 µL StageTip-solution A (STSA) by sonication for 10 min in an ultrasonic bath and vigorous shaking for 5 min.

2.2.4.2.2 On-bead digestion

For an OBD of enriched proteins, avidin agarose beads (2.2.4.1; 50 µL bed vol.) were taken up in 100 µL 0.8 M urea (in 50 mM ABC). To reduce disulphide bonds, DTT (in 50 mM ABC) was added to a final concentration of 10 mM. The beads were subsequently incubated for 1 h at RT shaking at 1500 rpm. For the alkylation of cysteine residues, IAM (in 50 mM ABC) was added to a final concentration of 25 mM, followed by an incubation for 1 h at RT shaking at 1500 rpm in the dark. To quench the alkylation reaction and thereby prevent the alkylation of trypsin, an equimolar amount of DTT was added to the reaction, resulting in a final concentration of 35 mM DTT, and the samples were incubated for 10 min at RT while shaking at 1500 rpm. Bead-bound proteins were digested o/N (ca.16 h) at 37 °C shaking at 1250 rpm after the addition of 10 µL of a 100 ng µL^{-1} solution of trypsin (Thermo Scientific) in 50 mM acetic acid to the beads. The next day, beads were collected by centrifugation (5 min, 3000 × g) and 95 µL of the peptide-containing supernatant was transferred into a fresh 1.5 mL protein LoBind tube containing 5 µL of pure FA. Then, the beads were washed with 50 µL

1% (v/v) FA by shaking at 1500 rpm at RT for 15 min, collected again by centrifugation (5 min, 3000 × g) and the supernatant was combined with the supernatant of the respective sample in the fresh tube. Prior to desalting of the peptide samples (2.2.4.3), these were passed over self-prepared 200 µL tips containing two layers of a 1.2 µm poresize GF/C glass microfiber filter to remove any remaining beads that would clog the C18 membrane during the desalting step. The tips were first equilibrated with 100 µL GF/C equilibration buffer (3 min, 50 × g) using a tip adapter for 96-well plates. In the last step, the samples were loaded onto the tips and centrifuged until the samples had passed through the filter tip completely (50 × g). Beads clogging the tip above the filter were carefully resuspended using a gel-loading tip.

2.2.4.3 Desalting of peptide samples

For desalting of peptide samples prior to LC-MS/MS, self-made 200 µL C18-StageTips[230] made up of two layers of an octadecyl silica membrane were used.

The C18 membrane was first activated by adding 50 µL of methanol on top of the white plug in the StageTips. Next, the tips were centrifuged in a suitable adapter for 1.5 mL tubes or for 96-well plates (2 min, 600 × g). Then, the tips were equilibrated with 50 µL of StageTip-solution B (STSB) (2 min, 600 × g), followed by equilibration with 50 µL of STSA (3 min, 800 × g). Afterwards the peptide sample was loaded onto the equilibrated StageTips. For desalting of peptide samples obtained from an IGD (2.2.4.2.1) or an OBD (2.2.4.2.2), the complete sample was loaded onto the StageTips (unknown amount of peptides). Then, the tips were centrifuged until all liquid has passed through the tips (800 × g). The flow-through was reapplied and passed through the C18-membrane once again. Next, the membrane was washed once with 100 µL STSA or twice by passing 50 µL of STSA over the StageTips, followed by 25 µL of STSA (800 × g). The peptides were eluted from the membrane by pipetting 25-50 µL STSB to the StageTips and centrifuging the tips (2 min, 600 × g). This elution step was repeated once again. The eluted peptide samples were evaporated in a vacuum concentrator at 45 °C operated in the vacuum-aqueous mode with the brake function set ON until all liquid was removed (1-3 h) and the dried peptide samples were stored at -20 °C until direct analysis by MS. For LC-MS/MS analysis (2.2.4.4), peptides were resuspended in 10 µL 0.1 % (v/v) FA. Peptides eluted into 1.5 mL protein LoBind tubes were dissolved by sonication for 10 min in an ultrasonic bath and vigorous shaking for

5 min. Peptides eluted into a 96-well plate were dissolved by incubation in a thermomixer for 30 min shaking at 1350 rpm. Subsequently. Peptides were transferred into a skirted 96-well PCR-plate compatible with the autosampler of the mass spectrometer.

2.2.4.4 LC-MS/MS analysis

Peptide samples (2.2.4.3) were analysed by LC-MS/MS on an Orbitrap Elite[231] mass spectrometer coupled to an EASY-nLC 1000 LC system. The LC was operated in the one-column mode using a fused silica capillary (75 µm × 21-40 cm) with an integrated PicoFrit emitter, packed in-house with Reprosil-Pur 120 C18-AQ 1.9 µm resin, as the analytical column. A column oven encasing the analytical column was attached to a nanospray flex ion source. During data acquisition, the temperature of the column oven was set to 45 °C or 50 °C. As mobile phases for the LC system, solvent A (0.1% (v/v) FA in water) and solvent B (0.1% (v/v) FA in ACN) were used (prepared from UPLC grade solvents). During loading of the peptides (7 µL) onto the analytical column, the maximum flow rate was adjusted to not exceed the set pressure limit of 980 bar (usually around 0.6-1.0 µL min^{-1}). Peptides originating from an IGD were separated on the analytical column by running a 70 min gradient (gradient: start with 7% B; gradient 7-35% B for 60 min; gradient 35-80% B for 5 min and 80% B for 5 min). For the separation of peptides originating from an OBD, the gradient was extended to 140 min (gradient: start with 7% B; gradient 7-35% B for 120 min; gradient 35-80% B for 10 min and 80% B for 10 min). Both gradients were run with a flow of 300 nL min^{-1}. The Orbitrap Elite mass spectrometer was operated in the positive ion mode using the Thermo Xcalibur software (version 2.2 SP1.48). Peptides were ionised by ESI with a spray voltage (ionization potential) of 1.8 kV. Precursor ions were scanned in the Orbitrap mass analyser (FT-MS) at a resolution of 60000 FWHM at *m/z* 400 (MS^1). The mass range for precursor ion scanning was set to 300-1800 *m/z* and the use of the internal lock mass option (polysiloxane: 445.120025 *m/z*)[232] was activated. To enable peptide sequencing and identification, precursor ions were subsequently fragmented into product ions by using CID with a normalised collision energy of 35%. Only peptide ions with a charge state > 1 were allowed for fragmentation. Data dependent acquisition was used for recording of product ion spectra in the ion trap with a variable scan range and a rapid scan rate (MS^2). A repetitive cycle consisting of a full precursor ion scan (1.0-3.0×10^6 ions or 50 ms) followed by 12 product ion scans (1.0×10^4 ions

or 80 ms; 1 micro scan) for peptide samples from IGDs or 15 product ion scans (1.0×10^4 ions or 60 ms; 4 micro scans) for peptide samples from OBDs was used for the analysis of peptides. For the generation of product ion spectra, only the peptides with the highest intensity in the full scan (threshold of 500 counts) were selected (Top^n method). For the acquisition of MS^2 spectra, a dynamic exclusion of precursor ions was used with a repeat count of one. The *m/z* of an ion was put into an exclusion list consisting of a maximum of 500 members for 120 s after its MS/MS has been acquired. Moreover, preview mode for the FT-MS, monoisotopic precursor selection, charge state screening and ion injection time prediction were enabled during data acquisition. Acquired RAW data was subjected to further data analysis (2.2.5.1 and 2.2.5.2).

2.2.5 Computer-based analysis

2.2.5.1 MaxQuant search for quantification of mass spectrometric RAW data

The software MaxQuant with the implemented search engine Andromeda[233] was used to perform protein identification and quantification of LC-MS/MS RAW data (2.2.4.4). The raw files of each sample from one experimental setup previously analysed by MS were loaded into the software tool. Non-fractionated samples collectively received a unique experiment name. LFQ with a built-in normalisation and a minimum ratio count of 2 was activated as a group-specific parameter (MaxLFQ algorithm)[99]. Match between runs with a maximum match time window of 0.7 min and an alignment time window of 20 min was switched on as a global parameter to enable retention time alignment between different LC-MS/MS runs, thereby allowing for the transfer of MS/MS identifications from one MS run to the next. All other settings were kept as default (MaxQuant version 1.5.3.30). In brief, ‘Trypsin/P’ was set as digestion enzyme for a specific search with a maximum of 2 missed cleavages that were allowed. Moreover, the default settings allowed for the oxidation of methionine residues (16 Da) and the acetylation of the protein N-terminus (42 Da) as dynamic modifications as well as the alkylation of cysteine residues (57 Da) as a static modification for the Andromeda searches. ‘Orbitrap’ was selected as the instrument type for Andromeda searches with a precursor mass tolerance of ±20 ppm (first search) and ±4.5 ppm (main search), while the MS/MS match tolerance was set to ±0.5 Da. Based on a target-decoy approach, the peptide spectrum match false discovery rate (FDR) and the protein FDR were set to 0.01. The minimal length of peptides was 7 amino acids

with a maximal peptide mass of 4600 Da. Protein quantification was based on unique and razor peptides. Unmodified peptides or peptides with dynamic modifications with a minimum score of 40 were allowed for quantification.

RAW spectra were searched against the UniProt *Homo sapiens* (UP000005640_9606.fasta; 74416 entries) or the UniProt *Arabidopsis thaliana* (strain cv. Columbia) (UP000006548_3702.fasta; 39381 entries) database, accordingly. A contaminants database (as implemented in MaxQuant, 245 sequences) containing known MS contaminants was included by default for all searches to estimate the level of contamination. Evaluation of data generated by MaxQuant was done using Perseus (2.2.5.2).

2.2.5.2 Statistical analysis with Perseus

Perseus[234] is a software package for the analysis and filtering of proteomics data generated as an output of the software MaxQuant. During the analysis with MaxQuant (2.2.5.1), a proteinGroups.txt file is generated. This file was uploaded into the Perseus (version 1.6.2.1) workspace and the MS/MS counts (IGD) or LFQ intensities (OBD) for all samples were added to the Perseus matrix as main columns. First, the rows of the matrix were filtered based on categorical columns to remove proteins groups that were only identified by peptides with a modification site, proteins that were hits found in the reverse database and proteins that are potential contaminants (proteins introduced during the sample preparation). Full data for all IGD experiments was exported after these initial filtering steps and can be found in the appendix (Appendix 7-9, Tab. 17-19). Only protein groups with a minimum number of 2 MS/MS counts in total were reported.

For samples resulting from an IGD after labelling with **≡Ner** in HeLa cell culture, no further filtering of data was done. The spectral counts for the detected human pan-HER kinase targets of **Ner** were reported in Fig. 14. For samples resulting from an IGD after labelling with **≡Ner** in Arabidopsis, protein groups were further filtered to only keep proteins in the matrix that fall into a MW range of 25-50 kDa. Moreover, only protein groups with a number of spectral counts < 1 for DMSO as well as **Ner**-pretreated samples and a number of spectral counts > 2 for noncompetition **≡Ner**-labelled

samples were kept to facilitate the identification of putative probe targets. All remaining protein groups were reported in the respective figures (Fig. 16 and Fig. 18).

For samples resulting from an OBD after labelling of Arabidopsis seedling extract with **≡Ner**, categorical groups were first defined to combine all biological replicates per condition, thereby allowing for the comparison of normalised protein group quantities between different treatment groups. This relative quantification was based only on the LFQ intensities calculated by MaxQuant. In the next step, LFQ intensities were transformed to the log_2-scale to facilitate data interpretation. To determine the log_2-fold enrichment of protein groups by **≡Ner** or the inactive control probes **≡Ctrl1** and **≡Ctrl2** compared to the DMSO control, only those protein groups that were detected for all four biological replicates of the respective noncompetition probe-labelled samples were kept for further analysis by filtering of rows based on valid values. Missing LFQ intensities were imputed from a normal distribution (width 0.3, down shift 1.8) prior to quantification to allow statistical analysis. The log_2-fold enrichment of protein groups with either of the employed probes was calculated based on the mean LFQ intensities compared to the DMSO control. All protein groups with a positive fold enrichment were reported (Fig. 20a-c; Appendix 10, Tab. 20-22) and kept for further analysis. Moreover, the effects of a pretreatment with **Ner** on the enrichment of protein groups with **≡Ner** or **≡Ctrl1** and **≡Ctrl2** were examined. To this end, the fold change in protein abundance between noncompetition and **Ner**-pretreated probe-labelled samples as well as the statistical significance thereof was assessed using a two-sided Student's *t*-test (permutation-based FDR: 0.05, S0: 0). To visualise the results of the *t*-test, a volcano plot where the log_2-fold change between noncompetition and **Ner**-pretreated probe-labelled samples is plotted against the -log p-value was generated (Fig. 20d-f). All proteins with a > two-fold reduction in their abundance and a p-value < 0.05 were considered as secondary hits, whereas a p-value < 0.01 indicates primary hits. Full data obtained from the *t*-test is reported in the appendix (Appendix 11, Tab. 23-25).

All MS datasets that were generated and analysed during this work have been deposited to the ProteomeXchange Consortium[235] via the PRIDE[236] partner repository with the dataset identifier PXD019640.

2.2.5.3 Generation of a homology model of AtEH7

SWISS-MODEL homology modelling[237-242] was used to model the protein structure of AtEH7. This work was done with the help of Geronimo Heilmann, University of Duisburg-Essen. For the search against the SWISS-MODEL template library (2016-07-20) by the BLAST[243] and HHblits[244] algorithms, the amino acid sequence of AtEH7 was used (UniProt ID: O81299, At4g02340 protein/T14p8.15). The highest sequence similarity to AtEH7 (0.48) was found for StEH1, an EH from *Solanum tuberosum* (potato, UniProt ID: Q41415, PDB code: 4Y9S[245], 2.0 Å resolution) which was subsequently used to build the structure model. The model was computed by the modelling engine ProMod3 which performs target-template alignment and QMean[246,247] was used to assess the quality of the model.

PyMOL™ (1.1beta3)[248] was used to display the modelled structure. Active site residues of AtEH7 were annotated based on the corresponding Pfam[249] annotations whereas further amino acid residues involved in the reaction mechanism (1.6) were annotated based on a sequence alignment with stEH1[196]. Cysteine residues were additionally displayed in the modelled structure.

2.2.5.4 Sequence homology comparison

The T-coffee web server[250,251] version-11.00.d625267 was used to generate a multiple sequence alignment (MSA) of AtEH7 with other EHs from *A. thaliana* or *Nicotiana benthamiana* (*N. benthamiana*). All EH sequences were retrieved from UniProtKB[252]. Colouring of amino acid residues based on their conservation scale was done by sequence analysis of the MSA output file with the program BOXSHADE, whereby the fraction of sequences that must agree for shading was set to 0.5.

2.2.5.5 Analysis of AtEH7 sequence conservation scale

The ConSurf web server[253-255] was used to assess the evolutionary conservation scale for each amino acid position within the sequence of AtEH7. For this analysis, the phylogenetic relations between a target sequence and other homologous sequences are evaluated. The server was used with sequence only (ConSeq[256] method), as no protein structure was provided for the search. The MSA was generated by ConSurf using the default settings. In brief, the search against the UniRef90 protein database

was done using HMMER as homologue search algorithm with 1 iteration and an E-value cut-off of 0.0001. Homologues for ConSurf analyses were selected automatically. By default, 150 sequences were selected that sample the list of homologues of AtEH7, with a maximal identity between sequences of 95% and a minimal identity for homologues of 35%. MAFFT-L-INS-i was selected as alignment method to build the MSA. The Bayesian method was used to calculate the rate of evolution at each site in the MSA and the best-fit model was selected as the evolutionary substitution model.

3. Results

3.1 Ner acts as an SA signalling agonist in Arabidopsis

Preliminary experiments for this work were performed at the MPIPZ Cologne by Dr. Vivek Halder. The SA signalling pathway is involved in various plant physiological processes and, most importantly, mediates resistance to pathogen infections (1.3). Though this pathway has been intensively studied over the past decades, a complete understanding of the underlying molecular mechanisms and proteins involved in SA signalling, i. e. direct interactors of SA or indirect interactors that impact on SA levels, is still lacking. Especially the role of kinases in SA signalling remains obscure. Signalling pathways in most cases are mediated through a myriad of different (protein) kinases. This also holds true for the signalling network orchestrating plant innate immunity which includes further pathogen-associated pathways[257]. One example, amongst others, is the perception of the pathogen-secreted bacterial elicitor flagellin which involves a receptor-like kinase[258] and additional mitogen-activated protein (MAP) kinases[259] to finally induce the transcription of defence genes. However, such an involvement of a kinase signalling cascade in signal perception has not yet been demonstrated for SA signalling.

To possibly identify novel kinases that are involved in SA signalling, a focused chemical library comprising 89 kinase inhibitors (Appendix 12, Tab. 26) was screened in Arabidopsis using a HT reporter plant-based *in situ* assay with SA-responsive *PR1p::GUS* seedlings (Fig. 11)[260]. In these seedlings, an enhanced release of SA leads to the induction of the *PR-1* promoter and thus to the transcription of the *GUS* reporter gene which is under the control of this promoter. GUS is able to cleave 4-methylumbelliferyl-β-D-glucuronide (4-MUG), which is added as an exogenous substrate, into 4-methylumbelliferone (4-MU), whose fluorescent emission can be monitored to quantify GUS activity that is positively correlated to the level of released SA (Fig. 11a). To facilitate the evaluation of screening hits, GUS activity was normalised to the solvent control (DMSO) and converted into a Z-score to set a threshold for statistical evaluation (Fig. 11b). Five compounds were detected as primary hits with a Z-score ≥ 1.5, i. e. they showed a 1.5-fold higher activity than the negative control (DMSO). These were, in addition to the positive control SA (Cpd 90),

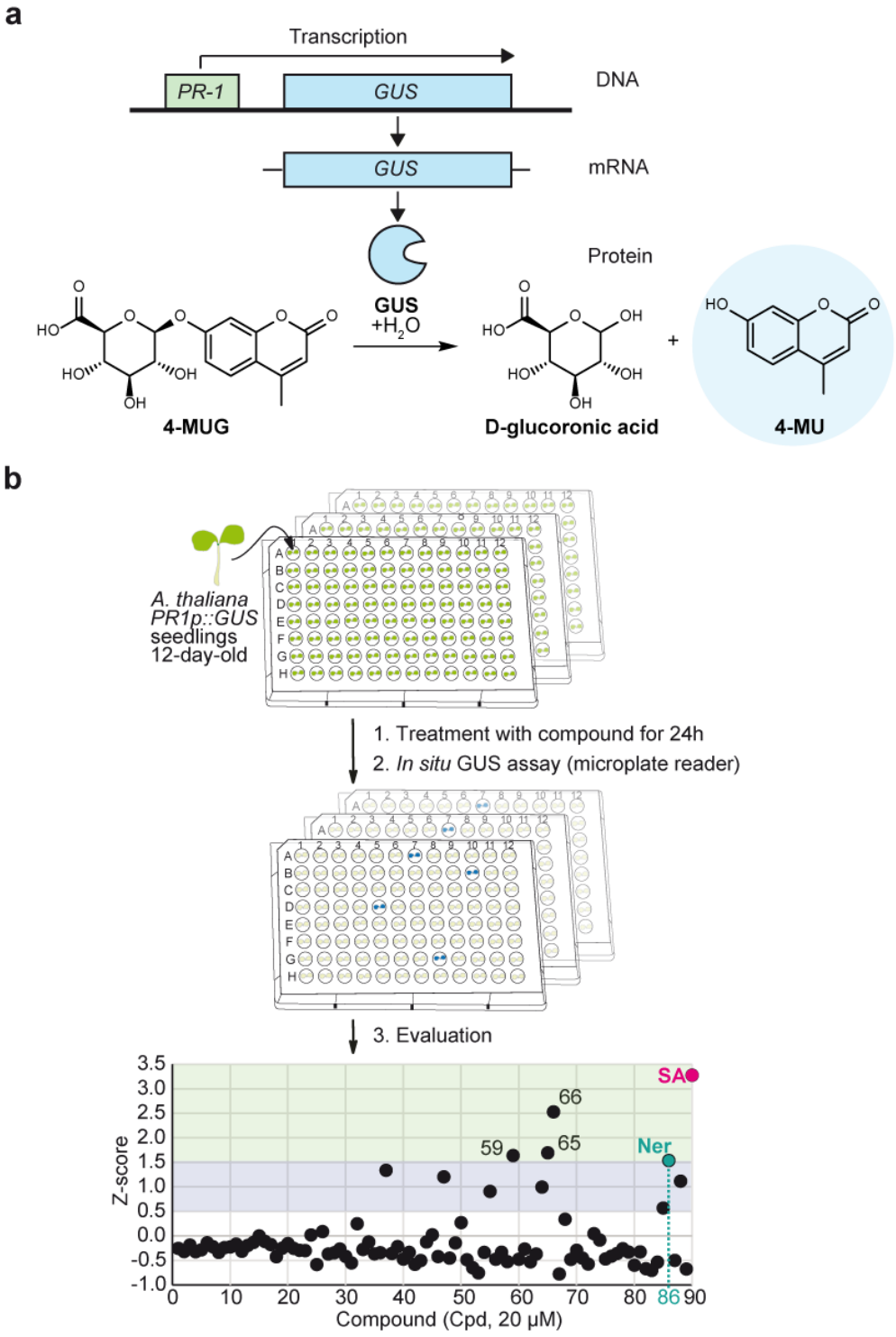

Fig. 11 Kinase inhibitor screen for SA agonists in Arabidopsis. (a) In *PR1p::GUS* seedlings, the *GUS* reporter gene, which is under the control of the SA-inducible *PR-1* promotor, is expressed upon release of SA. GUS then cleaves the exogenous substrate 4-MUG into fluorescent 4-MU. (b) A 89-membered chemical library of kinase inhibitors was screened in 12-day-old Arabidopsis *PR1p::GUS* seedlings to assess the ability for each compound to induce the release of SA. Preincubation of the seedlings with the respective compounds was done at a final concentration of 20 µM for 24 h. SA agonists were identified through the detection of *in situ* GUS activity. For compound evaluation, GUS activity was converted into a Z-score. Compounds with a Z-score ≥ 0.5 and < 1.5 were considered moderately active hits. Compounds with a threshold ≥ 1.5 were considered primary hits and are indicated in the figure accordingly.

genistein (Cpd 59), BAY 11-7082 (Cpd 65), 5,6-dichloro-1-β-(D)-ribofuranosyl benzimidazole (DRB; Cpd 66) and **Ner** (Cpd 86). Six additional compounds were detected as moderately active hits with a Z-score ≥ 0.5 and < 1.5. All remaining compounds showed a Z-score < 0.5. Among the primary hits, genistein, BAY 11-7082 and DRB (see Appendix 5, Fig. 37) were all ruled out for follow-up studies. Genistein[261] and DRB[262] are known inhibitors of DNA replication processes whereas BAY 11-7082[263] possesses broad-spectrum kinase inhibitory activity. Compounds that inhibit fundamental cellular processes like DNA replication or those that exert broad-spectrum activity make further characterisation steps challenging. Moreover, genistein is a plant-derived isoflavonoid endogenous to Arabidopsis[264] and is therefore less interesting to study in the context of SA signalling. **Ner**, on the other hand, was selected for further studies as it is a selective and irreversible pan-HER TKI in humans and was never evaluated *in planta* before. In addition, the two structurally related compounds gefitinib (Cpd 85) and pelitinib (Cpd 88), which both likewise act as TKIs in humans, were detected as moderately active hits (see Appendix 5, Fig. 37). Pelitinib (EKB-569), like **Ner**, is a 4-anilino-3-cyanoquinoline-based irreversible pan-HER inhibitor[115,265], while gefitinib (ZD1839, Iressa™) is a reversible and selective EGFR inhibitor[115,266]. These facts provided **Ner** as an interesting starting point for further studies regarding the identification of novel proteins involved in SA signalling.

3.2 Chemical synthesis of ≡Ner

To ease the identification of the molecular targets of **Ner** in Arabidopsis, an alkyne-functionalised version of **Ner**, **≡Ner**, was synthesised by Dr. Jan Krahn and Sarah Resch at the University of Duisburg-Essen. To this end, a propargyl moiety was chemically introduced to replace one of the two *N*-methyl residues of **Ner** in a multistep sequence. In the first step, the alkyne-modified linker was synthesised. In the second step, the amino butenoate moiety of **Ner** was hydrolysed through a selective acid catalysis and in the last step, the alkyne-modified linker was coupled to **Ner** (Appendix 13, Fig. 38).This derivative is suitable for the use as a two-step chemical probe as it allows to exploit the Michael system of **Ner** for covalent binding to target enzymes, whereas the introduced ligation handle aids the target identification process. Such two-step probes can be used for the chemical labelling of protein extracts *in vitro* as well as of whole cells *in vivo*. In the second step, they can be modified with a suitable

tag for in-gel visualisation as well as affinity enrichment of target proteins using ‘click’ chemistry.

3.3 Evaluation of ≡Ner in HeLa cell culture

With **≡Ner** at hand, first experiments were carried out in human cell culture to proof the functional integrity of the probe, since the chemical manipulation of a drug, such as the introduction of an alkyne moiety, may cause an alternating activity. To this end, HeLa cells were labelled *in situ* with a ten-fold dilution series of **≡Ner** either with or without preincubation with 10 µM **Ner** (Fig. 12).

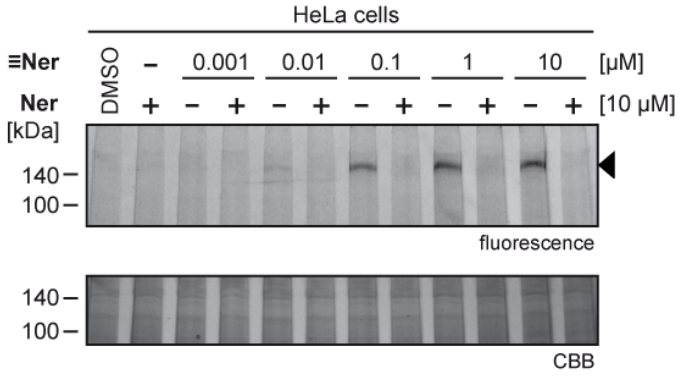

Fig. 12 *In situ* labelling of HeLa cells with ≡Ner. Competitive *in situ* labelling of HeLa cells with **≡Ner** visualised by fluorescence detection. A ten-fold dilution series of **≡Ner** was used for labelling. Preincubation with **Ner** was done at a final concentration of 10 µM. *In situ* labelling (2.2.3.3.1), cell disruption (2.2.1.6.2), protein concentration determination (2.2.3.2) and ‘click’ reaction (2.2.3.5) were performed as described in the methods section. For the sample separation by gel electrophoresis (2.2.3.6), 15 µL of the samples (ca. 11 µg protein) and 7 µL of protein ladder were loaded on an 11 % Bis-Tris gel. The fluorescence of the fluorophore Cy3 ($\lambda_{ex.}$ = ~550 nm excitation, $\lambda_{em.}$ = ~570 nm emission) was detected using the Cy3-DIGE settings (green laser $\lambda_{em.}$ = 532 nm, BPG1 band pass green filter 560-580 nm) of the laser scanner (2.2.3.7). Equal loading of the gel was confirmed by staining with a colloidal Coomassie solution (2.2.3.9).

With increasing concentrations of **≡Ner**, a labelled protein band at a MW of more than 140 kDa became visible. A concentration of 10 nM **≡Ner** was found to be sufficient to obtain weak labelling, whereas a concentration of 1 µM **≡Ner** already yielded complete labelling. After preincubation with **Ner**, this signal was completely abolished in all samples that were labelled with **≡Ner**, even at equimolar concentrations of the probe and the competitor. This pinpoints that **≡Ner** indeed is a functional version of **Ner** and that both compounds bind to the same 140 kDa human target(s) in HeLa cell culture.

To examine if the obtained protein band indeed resulted from the labelling of at least one of the human HER receptor TK targets of **Ner**, the irreversible pan-HER TKI

afatinib (BIBW2992, Gilotrif™) which inhibits EGFR, HER2 and HER4 at low nanomolar concentrations[267,268] and the previously introduced TKI gefitinib (see Appendix 5, Fig. 37) were utilised alongside **Ner** in a ten-fold dilution series for a competitive *in situ* labelling of HeLa cells with 0.5 µM **≡Ner** (Fig. 13).

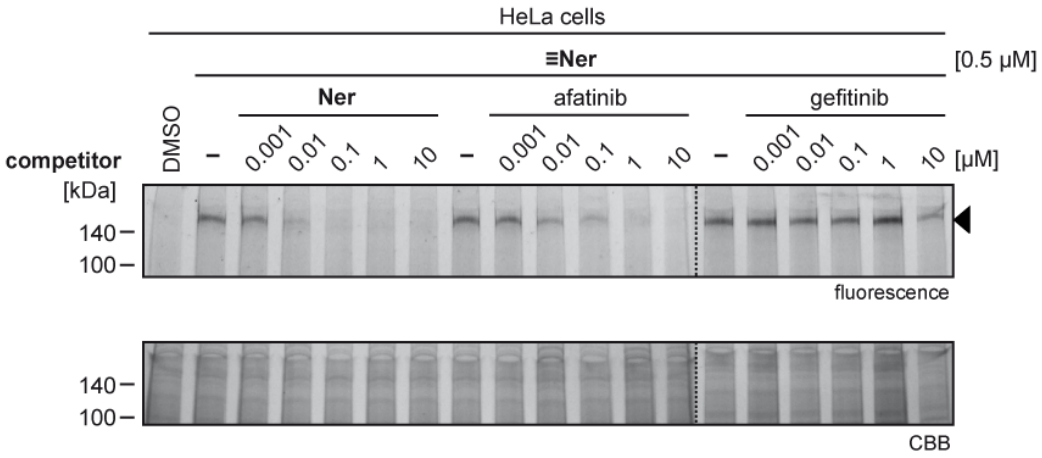

Fig. 13 Effect of other HER-targeted TKIs on the *in situ* labelling of HeLa cells with ≡Ner. Competitive *in situ* labelling of HeLa cells with **≡Ner** visualised by fluorescence detection. A final probe concentration of 0.5 µM **≡Ner** was used. A ten-fold dilution series of **Ner**, afatinib and gefitinib was used for preincubation. *In situ* labelling (2.2.3.3.1), cell disruption (2.2.1.6.2), protein concentration determination (2.2.3.2) and 'click' reaction (2.2.3.5) were performed as described in the methods section. For the sample separation by gel electrophoresis (2.2.3.6), 15 µL of the samples (ca. 11 µg protein) and 7 µL of protein ladder were loaded on an 11 % Bis-Tris gel. The fluorescence of the fluorophore Cy3 ($\lambda_{ex.}$ = ~550 nm excitation, $\lambda_{em.}$ = ~570 nm emission) was detected using the Cy3-DIGE settings (green laser $\lambda_{em.}$ = 532 nm, BPG1 band pass green filter 560-580 nm) of the laser scanner (2.2.3.7). Equal loading of the gel was confirmed by staining with a colloidal Coomassie solution (2.2.3.9).

Like **Ner**, the covalently-binding TKI afatinib was able to reduce the labelling of the protein band obtained with 0.5 µM **≡Ner** at concentrations down to 10 nM. However, the labelling with **≡Ner** was completely abolished at concentrations of 100 nM **Ner** and above, while a ten-fold higher concentration of afatinib was required for complete competition of the labelling with **≡Ner**. The reversible TKI gefitinib was found to be less potent in competing **≡Ner**-labelling. A preincubation with 10 µM gefitinib only resulted in a slight reduction of the labelling intensity obtained with **≡Ner**, whereas a preincubation with lower concentrations of gefitinib had no visible effect on the labelling intensity of **≡Ner**. Since pretreatment with afatinib and gefitinib resulted in a reduction of the labelling intensity with **≡Ner**, it is likely that **≡Ner** indeed labels the human HER kinase EGFR. The labelling of further HER receptor TKs with **≡Ner** is likewise conceivable, since preincubation with **Ner** and afatinib, which both target the same HER kinases, similarly reduced the labelling intensity of **≡Ner** and moreover had an

additional effect to the preincubation with gefitinib, which can not necessarily be explained only by the reversible binding mode of gefitinib.

To validate that the band pattern observed with **≡Ner** stemmed from the labelling of human HER receptor TKs and to precisely determine which of these HER kinases were targeted, **≡Ner** was applied in a pulldown experiment. Thus, HeLa cells were labelled *in situ* with 0.5 µM **≡Ner** either without or after preincubation with 10 µM **Ner** and the extracted proteins were submitted to a 'click' reaction with a trifunctional TAMRA-N_3-biotin tag that served the affinity enrichment of **≡Ner**-labelled proteins using avidin-agarose beads. Enriched proteins were analysed directly on gel, the labelled protein band at a MW of above 140 kDa was cut out and was next subjected to an IGD with trypsin. The obtained peptide mix was subsequently analysed by LC/MS-MS (Fig. 14).

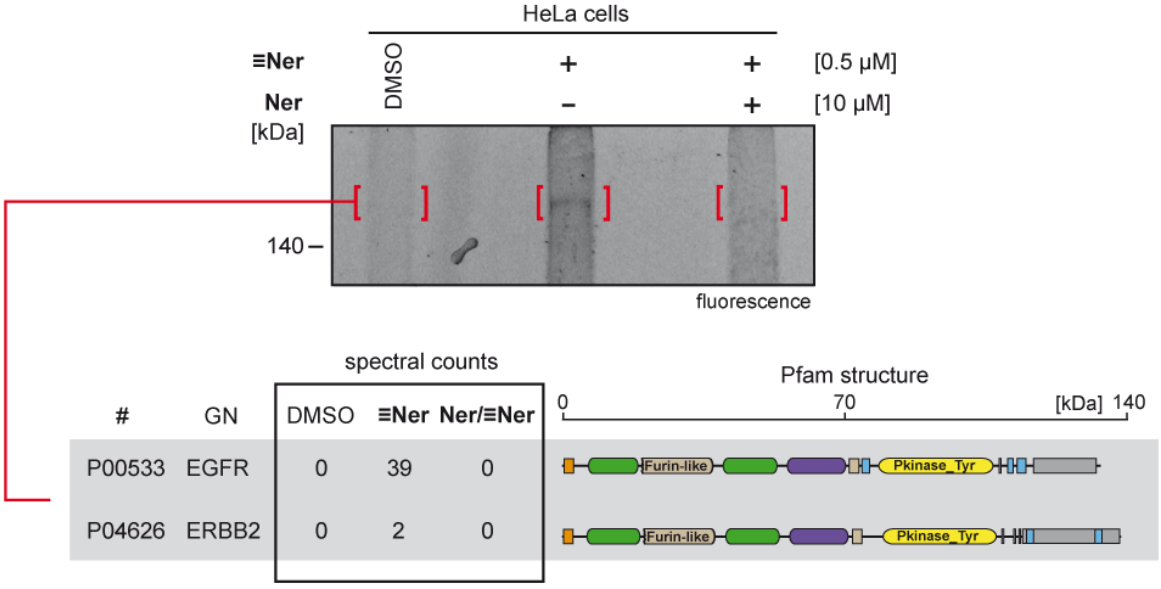

Fig. 14 Target identification of ≡Ner by i*n situ* labelling of HeLa cells. Competitive *in situ* labelling of HeLa cells with **≡Ner** visualised by fluorescence detection. A final probe concentration of 0.5 µM **≡Ner** was used. Preincubation with **Ner** was done at a final concentration of 10 µM. *In situ* labelling (2.2.3.3.1), cell disruption (2.2.1.6.2), protein concentration determination (2.2.3.2), 'click' reaction (2.2.3.5), and affinity enrichment (2.2.4.1) were performed as described in the methods section. For the sample separation by gel electrophoresis (2.2.3.6 and 2.2.4.2.1), 30 µL of the samples (unknown amount of protein) and 12 µL of protein ladder were loaded on a long 11 % Bis-Tris gel. The fluorescence of the fluorophore TAMRA ($\lambda_{ex.}$ = ~546 nm excitation, $\lambda_{em.}$ = ~565 nm emission) was detected using the Cy3-DIGE settings (green laser $\lambda_{em.}$ = 532 nm, BPG1 band pass green filter 560-580 nm) of the laser scanner (2.2.3.7). Sample preparation of the gel bands (marked in red brackets) by IGD (2.2.4.2.12.2.4.2) and desalting of peptide samples (2.2.4.3) were performed prior to LC/MS-MS based analysis (2.2.4.4), database search (2.2.5.1) and statistical evaluation (2.2.5.2). Spectral counts for the HER receptor TKs that were detected in this analysis are indicated for each measured sample, along with the UniProt ID (#), the gene name (GN), and the corresponding Pfam structure.

EGFR (134 kDa; canonical protein) which has an apparent MW of approximately 170 kDa in its native glycosylated form[269,270] as well as HER2 (ErbB2, 138 kDa; canonical protein) with an apparent MW of ca. 185 kDa for the glycoprotein[271] were both detected as target proteins of **≡Ner** based on database search and statistical evaluation of MS data. This matched with the position of the labelled protein band on the gel. EGFR was detected predominantly over HER2 which was only detected with two spectral counts. Even though HeLa is a HER2-negative cell line[272], this was surprising given the fact that **Ner** was developed as a TKI that is more potent for HER2 than for EGFR (see 1.2). HER4 (147 kDa; canonical protein), a protein of ca.180 kDa in its mature form[273], was not detected in this analysis. Preincubation with **Ner** led to a complete absence of the target proteins in the analysed sample, as was likewise observed for the DMSO control sample. A complete list of detected proteins after initial filtering to remove irrelevant protein groups (2.2.5.2) can be found in the appendix (Appendix 7, Tab. 17). Based on these results, **≡Ner** was found to be a fully functional version of **Ner** for the detection of the human HER receptor protein TKs. Hence, **≡Ner** was considered a suitable chemical probe for the investigation of the molecular targets of **Ner** in *A. thaliana*.

3.4 Target identification of Ner in *A. thaliana*

After the functional integrity of **≡Ner** was proven in human HeLa cells, this probe was applied to identify the molecular targets of **Ner** in *A. thaliana*. For the initial labelling experiments, protoplasts were chosen as they are well suited for *in situ* labelling. An *in situ* labelling of intact cells is advantageous over an *in vitro* labelling of protein extracts due to the far more native conditions as well as a reduced off-target labelling, a well-known general effect in chemical proteomics experiments[38,56]. Even though two-step chemical labelling of intact seedlings has previously been reported[274], seedlings however are complex multicellular organisms whose cells are encased by a cell wall, which can hamper the *in situ* labelling. Therefore, protoplasts were considered the optimal model system to initially evaluate **Ner** in Arabidopsis as they are cultivatable, unicellular entities with an enzymatically degraded cell wall[275]. To this end, an *in situ* labelling of protoplasts from an Arabidopsis root cell culture with 1 µM or 10 µM **≡Ner** either with or without preincubation with 10 µM **Ner** was performed (Fig. 15).

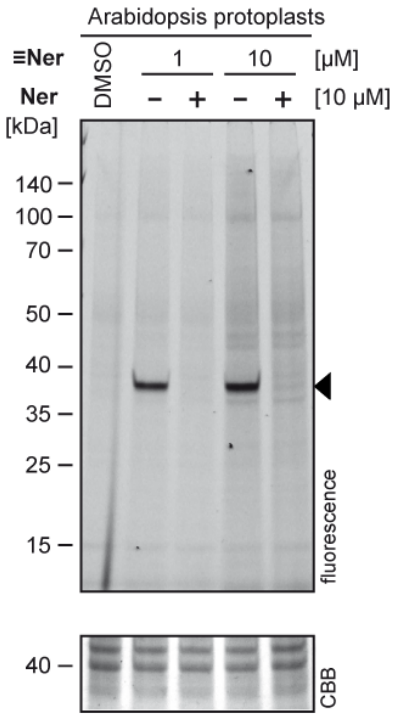

Fig. 15 *In situ* labelling of *A. thaliana* protoplasts with ≡Ner. Competitive *in situ* labelling of *A. thaliana* root protoplasts with **≡Ner** visualised by fluorescence detection. A final probe concentration of 1 µM or 10 µM **≡Ner** was used. Preincubation with **Ner** was done at a final concentration of 10 µM. *In situ* labelling (2.2.3.3.2), cell disruption (2.2.1.6.3), protein concentration determination (2.2.3.2) and 'click' reaction (2.2.3.5) were performed as described in the methods section. For the sample separation by gel electrophoresis (2.2.3.6), 15 µL of the samples (ca. 11 µg protein) and 7 µL of protein ladder were loaded on an 11 % Bis-Tris gel. The fluorescence of the fluorophore Cy3 ($\lambda_{ex.}$ = ~550 nm excitation, $\lambda_{em.}$ = ~570 nm emission) was detected using the Cy3-DIGE settings (green laser $\lambda_{em.}$ = 532 nm, BPG1 band pass green filter 560-580 nm) of the laser scanner (2.2.3.7). Equal loading of the gel was confirmed by staining with a colloidal Coomassie solution (2.2.3.9).

The *in situ* labelling of *A. thaliana* protoplasts with 1 µM or 10 µM **≡Ner** resulted in the presence of a single intense protein band at a MW of about 35-40 kDa, whereas only weak background labelling was obtained. The strong labelling of the 35-40 kDa band was completely abolished by pretreatment with 10 µM **Ner** prior to labelling with **≡Ner**. This complete inhibition of the labelling with **≡Ner** by **Ner** indicates that the labelled protein is a direct and specific molecular target of **Ner** and does not result from off-target labelling with **≡Ner**.

In the next step, the protein target of **Ner** in Arabidopsis that corresponded to the observed 35-40 kDa band was identified. To determine whether the target of **Ner** belongs to the protein kinases comprising 381 soluble kinases and 561 membrane-associated receptor kinases in Arabidopsis[276] or whether the target protein belongs to a different class of enzymes, the *in situ* labelling of *A. thaliana* protoplasts with 1 µM **≡Ner** and preincubation with 10 µM **Ner** was repeated using a larger number of cells.

Following the 'click' reaction with TAMRA-N_3-biotin and the affinity enrichment of **≡Ner**-labelled proteins using avidin-agarose beads, proteins were analysed directly on gel. The labelled protein band was excised from the gel, subjected to an IGD with trypsin and an MS-based analysis of the peptides was performed subsequently (Fig. 16).

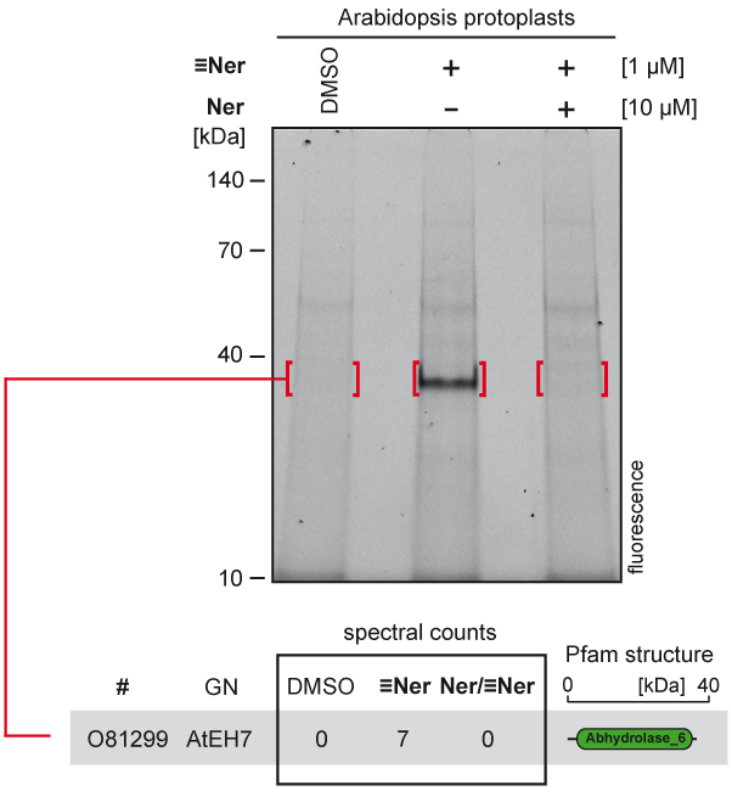

Fig. 16 Target identification of ≡Ner by *in situ* labelling of *A. thaliana* protoplasts. Competitive *in situ* labelling of *A. thaliana* protoplasts with **≡Ner** visualised by fluorescence detection. A final probe concentration of 1 µM **≡Ner** was used. Preincubation with **Ner** was done at a final concentration of 10 µM. *In situ* labelling (2.2.3.3.2), cell disruption (2.2.1.6.3), protein concentration determination (2.2.3.2), 'click' reaction (2.2.3.5), and affinity enrichment (2.2.4.1) were performed as described in the methods section. For the sample separation by gel electrophoresis (2.2.3.6 and 2.2.4.2.1.), 30 µL of the samples (unknown amount of protein) and 7 µL of protein ladder were loaded on an 11 % Bis-Tris gel. The fluorescence of the fluorophore TAMRA ($\lambda_{ex.}$ = ~546 nm excitation, $\lambda_{em.}$ = ~565 nm emission) was detected using the Cy3-DIGE settings (green laser $\lambda_{em.}$ = 532 nm, BPG1 band pass green filter 560-580 nm) of the laser scanner (2.2.3.7). Sample preparation of the gel bands (marked in red brackets) by IGD (2.2.4.2.1) and desalting of peptide samples (2.2.4.3) were performed prior to LC/MS-MS based analysis (2.2.4.4), database search (2.2.5.1) and statistical evaluation (2.2.5.2). Spectral counts for the hit that was detected in this analysis are indicated for each measured sample, along with the UniProt ID (#), the gene name (GN), and the corresponding Pfam structure.

Surprisingly, the LC-MS/MS-based analysis revealed *A. thaliana* epoxide hydrolase 7 (AtEH7, At4g02340; 37 kDa) as the only potential direct molecular target of **≡Ner** and thus **Ner** instead of a kinase. AtEH7 is a sEH that was confirmed to be localised in the peroxisomes of a plant cell by Reumann *et al*. using 2D gel-based MS and fluorescence microscopy employing an enhanced yellow fluorescent protein (EYFP)

fusion construct as well as by Eubel *et al*. using 1D and 2D gel-based analysis in combination with LC-MS [277,278]. Further hits were neglected as potential **Ner**-targets by the filtering criteria applied (2.2.5.2). A complete list reporting all identified hits remaining after the initial filtering to remove irrelevant protein groups can be found in the appendix (Appendix 8, Tab. 18).

As **Ner** was originally identified from the initial screen for SA agonists in Arabidopsis seedlings, it was further tested if AtEH7 could additionally be identified as a potential target of **Ner** in these young plants. For this purpose, the *in vitro* labelling of Arabidopsis protein extracts originating from protoplasts, seedlings and leaves with 1 µM or 10 µM **≡Ner** either without or after preincubation with 10 µM **Ner** was first evaluated (Fig. 17).

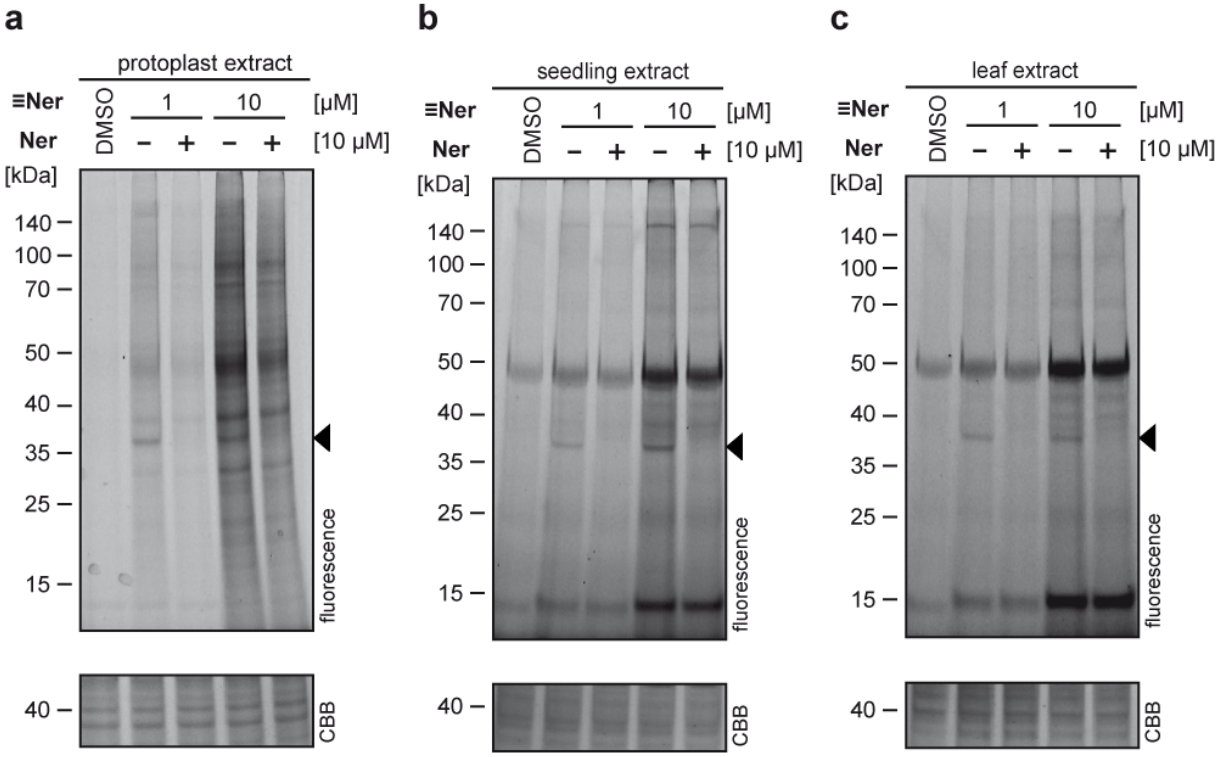

Fig. 17 *In vitro* labelling of *A. thaliana* Col-0 extracts with ≡Ner. Competitive *in vitro* labelling of *A. thaliana* Col-0 protoplast (a), seedling (b) and leaf (c) extract with **≡Ner** visualised by fluorescence detection. A final probe concentration of 1 µM or 10 µM **≡Ner** was used. Preincubation with **Ner** was done at a final concentration of 10 µM. Disruption of Arabidopsis plant material (2.2.1.6.3), protein concentration determination (2.2.3.2), labelling of protein extracts (2.2.3.3.3) and 'click' reaction (2.2.3.5) were performed as described in the methods section. For the sample separation by gel electrophoresis (2.2.3.6), 15-20 µL of the samples (ca. 10-14 µg protein) and 7 µL of protein ladder were loaded on an 11 % Bis-Tris gel. The fluorescence of the fluorophore Cy3 ($\lambda_{ex.}$ = ~550 nm excitation, $\lambda_{em.}$ = ~570 nm emission) was detected using the Cy3-DIGE settings (green laser $\lambda_{em.}$ = 532 nm, BPG1 band pass green filter 560-580 nm) of the laser scanner (2.2.3.7). Equal loading of the gel was confirmed by staining with a colloidal Coomassie solution (2.2.3.9).

As observed for the *in situ* labelling of Arabidopsis protoplasts, the *in vitro* labelling of protoplast extract with 1 µM or 10 µM **≡Ner** resulted in the presence of a protein band at a MW of about 37 kDa that was completely abolished by the pretreatment with 10 µM **Ner** (Fig. 17a). Though, the labelling of protoplast extract led to higher background labelling, especially for the labelling with 10 µM **≡Ner**, which was not competable with **Ner**. Similar to the labelling of protoplast extract, the labelling of seedling (Fig. 17b) and leaf extracts (Fig. 17c) likewise resulted in the presence of a competable band at a MW of about 37 kDa. Indeed, the non-competable off-target labelling with **≡Ner** was even stronger for these green plant materials as it was presumably mainly resulting from the labelling of the small and large chains of ribulose-1,5-bisphosphate carboxylase (RuBisCO). RuBisCO is a highly abundant protein in the photosynthetic cells of the green plant material and was furthermore suggested to be even the most abundant protein in the (terrestrial) world as reviewed by Ellis[279]. This statement was critically illuminated by Raven in his review, but it was still considered valid that RuBisCO is the most abundant protein on land and, probably, in marine biota[280]. The large chain of RuBisCO (rbcL; 53 kDa) is encoded in the plastid genome while the small chains (RBCS-1A, RBCS-1B, RBCS-2B and RBCS-3B; 20.2-20.3 kDa) are encoded in the nuclear genome, synthesised in the cytosol and imported into the chloroplast where the transit peptide (5.5 kDa) is cleaved off of the precursor to yield the mature protein[281-284]. Since the expression of rbcL in the nongreen plastids of root cells is suppressed at the transcription level, the prevalence of RuBisCO is restricted to the chloroplasts of green plant material[285].

As the 37 kDa protein band matching the size of AtEH7 was likewise obtained for the *in vitro* labelling of plant extracts with **≡Ner**, the identification of the target enzyme was repeated with Arabidopsis seedlings. To this end, seedling extract was labelled with 10 µM **≡Ner** without or after preincubation with 10 µM **Ner**. As described for the *in situ* labelling of Arabidopsis protoplasts, the 37 kDa band was cut out from the gel and the peptide mix obtained after an IGD with trypsin was analysed by LC-MS/MS (Fig. 18). As anticipated, AtEH7 was repeatedly identified as the top hit by MS data analysis based on spectral counts. In addition to AtEH7, AtATPC1 (At4g04640; 40.9 kDa) and AtADK1/AtADK2 (At3g09820/At5g03300; 37.8 kDa) remained as further potential targets of **≡Ner** after the filtering criteria (2.2.5.2) were applied to the data. A complete

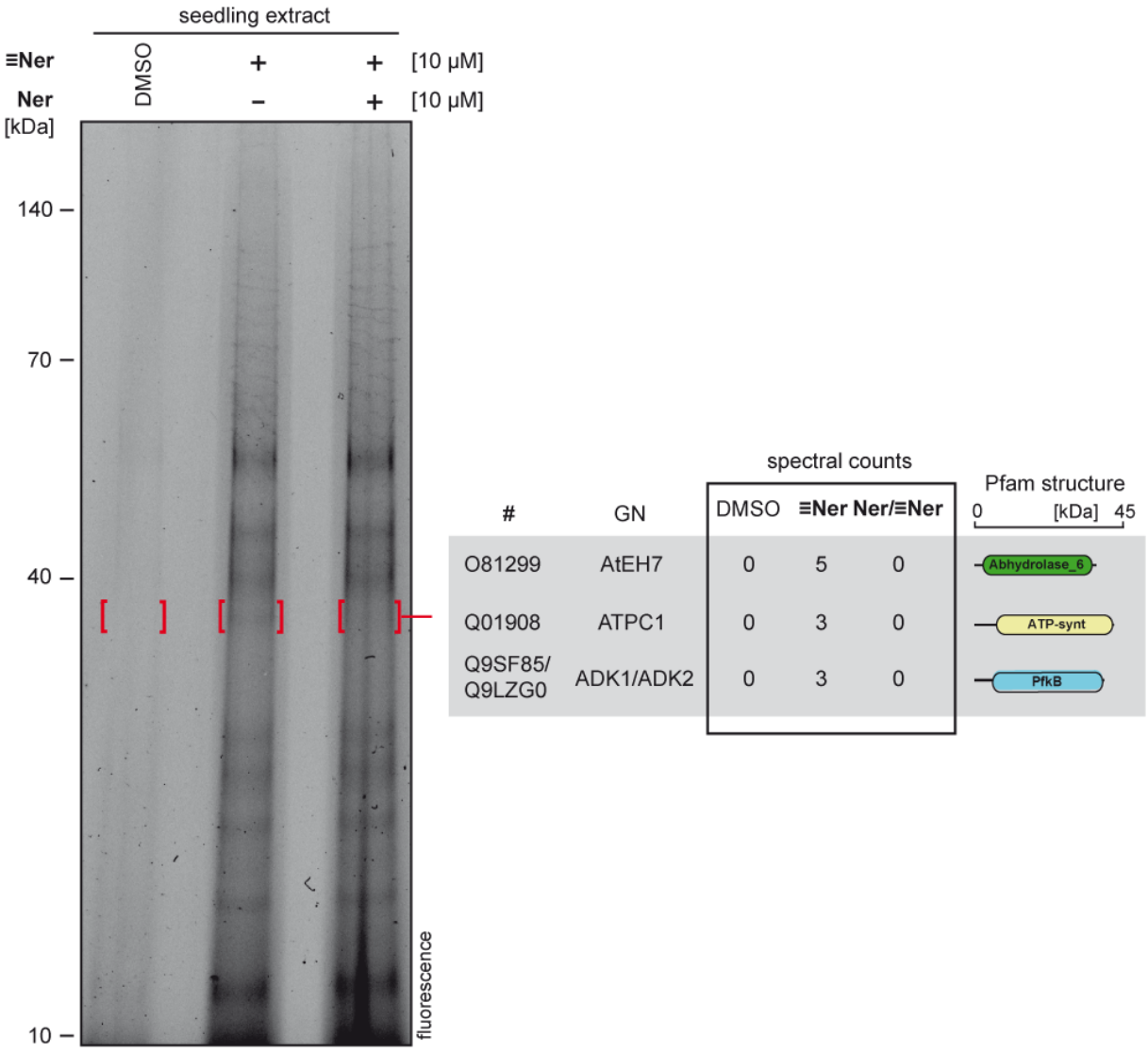

Fig. 18 Target identification of ≡Ner by *in vitro* labelling of *A. thaliana* seedling extract. Competitive *in vitro* labelling of *A. thaliana* seedling extract with **≡Ner** visualised by fluorescence detection. A final probe concentration of 10 µM **≡Ner** was used. Preincubation with **Ner** was done at a final concentration of 10 µM. Disruption of Arabidopsis plant material (2.2.1.6.3), protein concentration determination (2.2.3.2), labelling of protein extract (2.2.3.3.3), 'click' reaction (2.2.3.5) and affinity enrichment (2.2.4.1) were performed as described in the methods section. For the sample separation by gel electrophoresis (2.2.3.6 and 2.2.4.2.1), 30 µL of the samples (unknown amount of protein) and 12 µL of protein ladder were loaded on a long 11 % Bis-Tris gel. The fluorescence of the fluorophore TAMRA ($\lambda_{ex.}$ = ~546 nm excitation, $\lambda_{em.}$ = ~565 nm emission) was detected using the Cy3-DIGE settings (green laser $\lambda_{em.}$ = 532 nm, BPG1 band pass green filter 560-580 nm) of the laser scanner (2.2.3.7). Sample preparation of the gel bands (marked in red brackets) by IGD (2.2.4.2.1) and desalting of peptide samples (2.2.4.32.2.4.3) were performed prior to LC/MS-MS based analysis (2.2.4.4), database search (2.2.5.1) and statistical evaluation (2.2.5.2). Spectral counts for the hits that were detected in this analysis are indicated for each measured sample, along with the UniProt ID (#), the gene name (GN), and the corresponding Pfam structure.

list of all identified hits remaining after the initial filtering to remove irrelevant protein groups can be found in the appendix (Appendix 9, Tab. 19). AtATPC1 encodes for the gamma subunit of Arabidopsis chloroplast ATP synthase, a key enzyme in photosynthesis, together with AtATPC2[286]. AtADK1/AtADK2 encode for adenosine

kinase 1/2 that both show a high sequence similarity to each other[287] and therefore could not be differentiated based on the peptides identified by LC-MS/MS. Both enzymes have been quite well studied and are therefore known to be involved in energy production. Thus, they have not yet been linked with playing a role in SA signaling. However, AtATPC1 as well as AtADK1/AtADK2, although the latter functioning as a kinase, albeit not as a protein kinase, were rejected from further analysis on their potential contributions to the SA phenotype. AtADK1/AtADK2 was additionally identified in the unlabelled DMSO and **Ner**-pretreated control samples in the *in situ* labelling experiment with Arabidopsis protoplasts which was critical for ruling out this target. AtATPC1 was not detected in the previous *in situ* labelling experiment with protoplasts, most likely, because this protein is located in chloroplasts[286], which are absent in root cells, as already described earlier. Since a strong labelling of the 37 kDa protein band with **≡Ner** was formerly observed for the *in situ* experiment with root cell protoplasts, AtATPC1 was additionally excluded as a potential target candidate of **Ner** provoking the observed SA phenotype. Consequently, AtEH7 rather than a kinase unexpectedly remained the only putative major target of **≡Ner** and thus **Ner** that was effectively identified from both independent LC-MS/MS-based analyses of the 37 kDa protein band after IGD in Arabidopsis.

Indeed, the analysis of the 37 kDa protein band alone is not sufficient to cover the full (off-) target repertoire of **≡Ner** in Arabidopsis. To more accurately determine the compounds selectivity or the lack thereof, a global analysis of all enzymes covalently targeted by **≡Ner** and **Ner** in *A thaliana* was performed. This analysis was done in seedlings as these were used for the SA activator screen and showed a higher background labelling on gel aside from the specific 37 kDa band. In addition to **≡Ner**, two structurally related control probes were included in this experiment to check for indirect effects of **Ner** that could have led to the observed SA phenotype through *PR-1* induction, such as depletion of intracellular redox regulators like S-nitrosoglutathione which is involved in maintaining homeostasis between the monomeric and oligomeric state of NPR1 as it facilitates NPR1 oligomerisation, thereby counteracting the role of thioredoxins in reducing intermolecular disulphide bonds in oligomerised NPR1[161]. These control probes are **≡Ctrl1**, the electrophilic linker with the alkyne tag of **≡Ner** and **≡Ctrl2**, **≡Ctrl1** coupled to 6-aminoquinoline, which is structurally more closely related to **≡Ner**. Both control probes were synthesised by Sarah Resch, University of

Duisburg Essen (Appendix 13, Fig. 38). Such indirect effects, however, were not expected to be responsible for the activation of *PR-1* induction in the reporter plant-based assay with SA-responsive *PR1p::GUS* seedlings, since the employed chemical library contains many strongly electrophilic compounds, such as members of the tyrphostins containing α,β-unsaturated amide electrophiles, i.e. Michael acceptors (e. g. Cpd 14 or Cpd 25), or potentially reactive compounds like GF 109203X (Cpd 31), which did not provoke induction of *PR-1* expression in the screen for SA activators.

Prior to the LC-MS/MS-based target analysis, these control probes were confirmed to be functionally inactive in labelling the 37 kDa band. To this end, **≡Ctrl1** and **≡Ctrl2** were applied to Arabidopsis Col-0 seedling extract *in vitro* at a final concentration of 10 µM alongside with 10 µM **≡Ner** either without or after preincubation with 10 µM **Ner** to check for their labelling capabilities (Fig. 19).

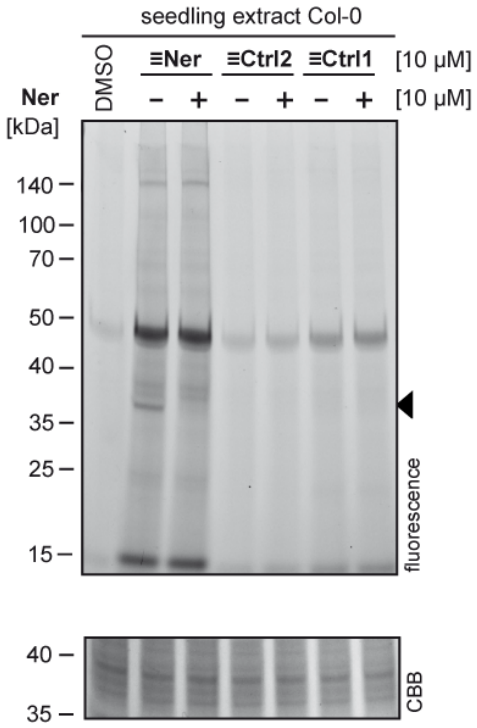

Fig. 19 Evaluation of the control probes ≡Ctrl1 and ≡Ctrl2 in Arabidopsis. Competitive *in vitro* labelling of *A. thaliana* Col-0 seedling extract with **≡Ner**, **≡Ctrl1** and **≡Ctrl2** visualised by fluorescence detection. A final probe concentration of 10 µM **≡Ner**, **≡Ctrl1** or **≡Ctrl2** was used for the labelling. Preincubation with **Ner** was done at a final concentration of 10 µM. Disruption of Arabidopsis plant material (2.2.1.6.3), protein concentration determination (2.2.3.2), labelling of protein extract (2.2.3.3.3) and 'click' reaction (2.2.3.5) were performed as described in the methods section. For the sample separation by gel electrophoresis (2.2.3.6), 20 µL of the samples (ca. 15 µg protein) and 7 µL of protein ladder were loaded on an 11 % Bis-Tris gel. The fluorescence of the fluorophore Cy3 ($\lambda_{ex.}$ = ~550 nm excitation, $\lambda_{em.}$ = ~570 nm emission) was detected using the Cy3-DIGE settings (green laser $\lambda_{em.}$ = 532 nm, BPG1 band pass green filter 560-580 nm) of the laser scanner (2.2.3.7). Equal loading of the gel was confirmed by staining with a colloidal Coomassie solution (2.2.3.9).

In contrast to **≡Ner**, **≡Ctrl1** and **≡Ctrl2** did not label the 37 kDa band previously identified as AtEH7. Moreover, no signals other than those resulting from the labelling of RuBisCO were detectable for the two control probes. For **≡Ctrl1**, the intensity of the signal for RuBisCO was comparable with the signal obtained for the DMSO control, meaning that this control probe did not show any additional labelling to the background signal probably resulting from unspecific attachment of the fluorescent 'click' tag to abundant proteins during the 'click' reaction[56]. In case of **≡Ctrl2**, the signal was a bit more intense than for the no-probe control, but less intense than for **≡Ner**. Since both control probes did not show specific labelling, a preincubation with **Ner** therefore also had no observable effect. Consequently, **≡Ctrl1** as well as **≡Ctrl2** were confirmed to be functionally inactive in labelling the 37 kDa band and therefore allow to control for indirect effects which may stem from the binding of **Ner** to unspecific target proteins, resulting in the induction of *PR-1* expression.

After the control probes were found to be functionally inactive and therefore suitable for the evaluation of unspecific **Ner** targets, they were introduced alongside **≡Ner** for the global analysis of probe targets to determine the selectivity of these probes. To this end, seedling extract was labelled with 10 µM **≡Ner**, **≡Ctrl1** or **≡Ctrl2** either with or without preincubation with 10 µM **Ner**. Afterwards, all samples were 'clicked' with TAMRA-N_3-biotin and probe-labelled proteins were affinity-enriched using avidin-agarose beads. All captured proteins were directly digested on-bead with trypsin and the obtained peptide mix was analysed by LC-MS/MS (Fig. 20). After the filtering of the initial data (2.2.5.2), 236 different protein groups remained in total that were detected in all four replicates of noncompetition **≡Ner**-labelled samples. Of these, 188 protein groups were found to be enriched compared to the DMSO control (Fig. 20a; Appendix 10, Tab. 20). Those comprise 98 primary hits with a fold enrichment > 2. Repeating this analysis for **≡Ctrl1** and **≡Ctrl2**, 164 and 174 different protein groups, respectively, remained in total that were detected in all four replicates of noncompetition probe-labelled samples after the filtering of the initial data. Of these, 149 protein groups comprising 10 primary hits were found to be enriched compared to the DMSO control for **≡Ctrl1** (Fig. 20b; Appendix 10, Tab. 21) whereas 135 protein groups comprising 13 primary hits were found to be enriched compared to the DMSO control for **≡Ctrl2** (Fig. 20c; Appendix 10, Tab. 22). The low number of primary hits enriched with **≡Ctrl1**

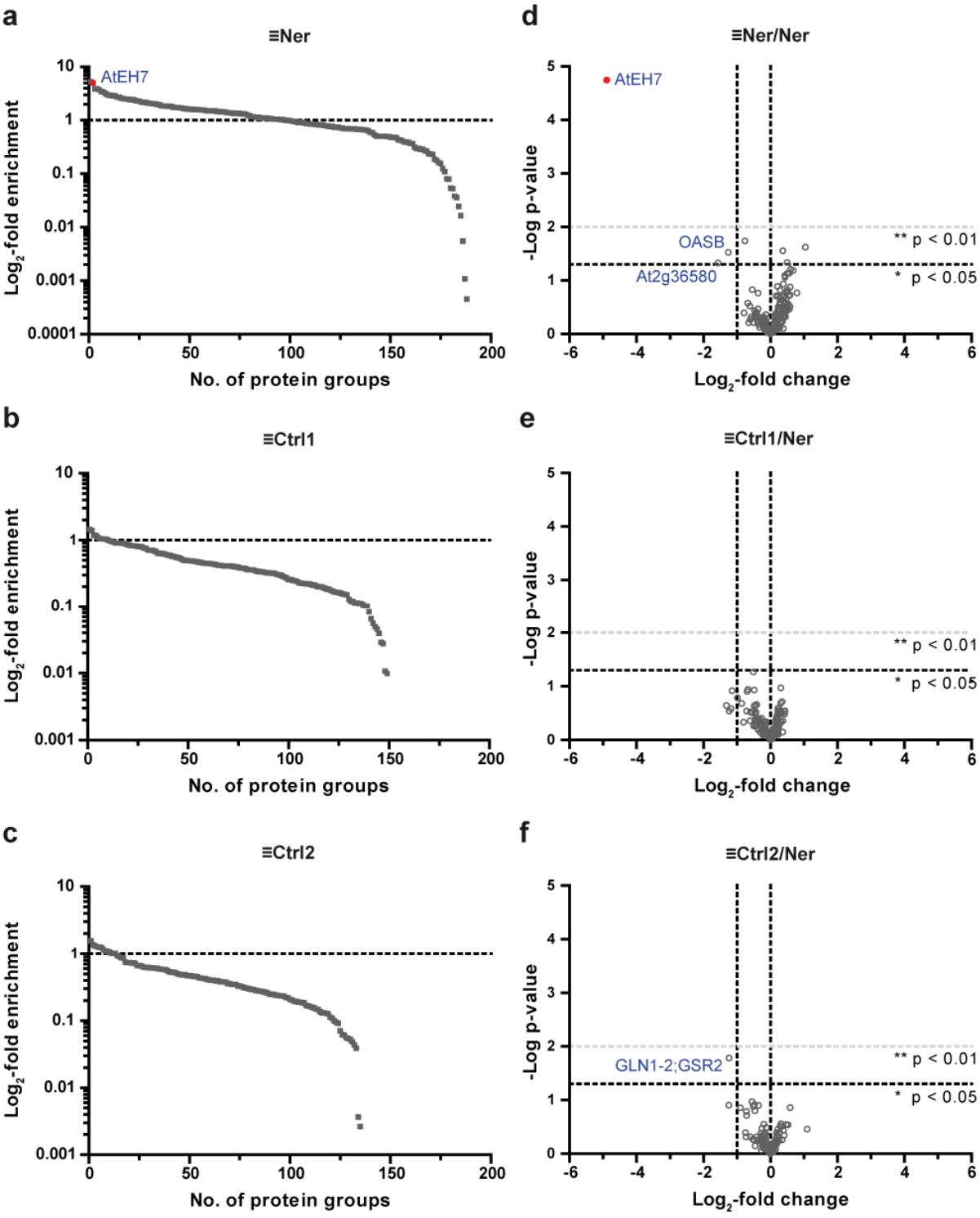

Fig. 20 Proteomics analysis of global ≡Ner, ≡Ctrl1 and ≡Ctrl2 targets in Arabidopsis. Logarithmic plot of all protein groups that were enriched with (a) **≡Ner,** (b) **≡Ctrl1** or (c) **≡Ctrl2** compared to the DMSO control against their corresponding log_2-fold enrichment factor. Proteins with a fold enrichment > 2 that lay above the dotted line were considered primary hits. (d-f) Volcano plot showing the log_2-fold change in protein abundance against the -log p-value between noncompetition **≡Ner-, ≡Ctrl1**- or **≡Ctrl2**-enriched proteins and **Ner**-preincubated **≡Ner-, ≡Ctrl1**- or **≡Ctrl2**-enriched proteins. Statistical significance was calculated based on a two-sample Student's *t*-test. For proteins with a statistical significant (p-value < 0.05) fold reduction in their abundance after **Ner**-pretreatment of > 2, gene names are indicated. Each treatment group comprised four biological replicates.

and **≡Ctrl2** in contrast to **≡Ner** indicates that both control probes possessed a lower reactivity than **≡Ner**, as already indicated by the labelling experiment with Arabidopsis seedlings where only RuBisCO was visibly targeted by **≡Ctrl1** and **≡Ctrl2** (Fig. 19). This suggests that the enrichment of protein groups among the group of samples labelled with these two probes merely resulted from unspecific attachment of the corresponding proteins to the beads during the affinity enrichment step.

To further enable the differentiation between the specific and off-targets of **≡Ner** among the cohort of the 188 **≡Ner**-enriched proteins groups, a volcano plot comparing the group of noncompetition **≡Ner**-labelled samples with the group of **Ner**-preincubated **≡Ner**-labelled samples was generated. Specific targets of **Ner** were expected to be less abundant in the group of **Ner**-preincubated **≡Ner**-labelled samples, in contrast to off-targets of **≡Ner** which were not expected to be affected by a pretreatment with **Ner**. Targets were considered as potentially specific if they were significantly ($p < 0.05$) found to pass the threshold of being more than two-fold less abundant after preincubation with **Ner**. Out of the 188 **≡Ner**-enriched protein groups, only 3 protein groups showed a fold reduction > 2 in their abundance after **Ner**-pretreatment, which all passed the significance threshold (Fig. 20d; Appendix 11, Tab. 23). To examine whether these three protein groups were specific for **Ner** or could be considered as unspecific target proteins, the same analysis was repeated for the two control probes **≡Ctrl1** and **≡Ctrl2**. Out of the 149 protein groups enriched with **≡Ctrl1**, 4 protein groups showed a fold reduction > 2 in their abundance after **Ner**-pretreatment (Fig. 20e; Appendix 11, Tab. 24). However, none of these four underrepresented protein groups passed the significance threshold. Out of the 135 protein groups enriched with **≡Ctrl2**, 2 protein groups showed a fold reduction > 2 in their abundance after **Ner**-pretreatment (Fig. 20f; Appendix 11, Tab. 25). Here, one out of these two underrepresented protein groups passed the significance threshold. Since this protein group was however not shared among the significantly underrepresented hits detected for **Ner**-preincubated **≡Ner**-labelled samples, **Ner** was not considered to induce *PR-1* expression through binding to unspecific target proteins.

To more precisely investigate the protein targets specific to **≡Ner** and **Ner**, all protein groups that were exclusively enriched with **≡Ner** were further investigated. Thereto, the cohort of protein groups enriched with this probe was compared to the cohorts of protein groups enriched with the two control probes **≡Ctrl1** and **≡Ctrl2** (Fig. 21).

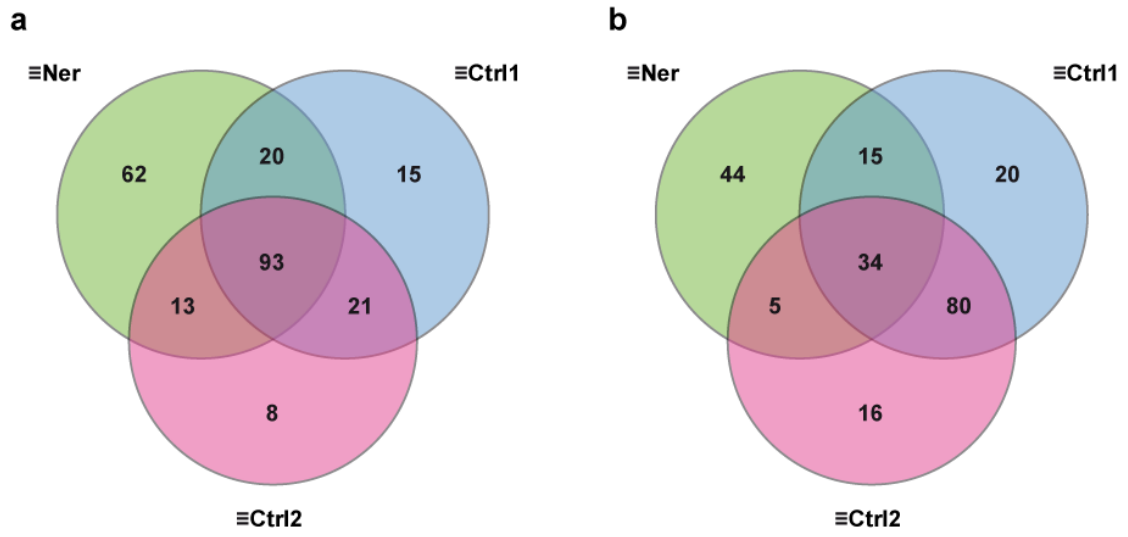

Fig. 21 Numeric Venn diagram comparing the protein groups enriched with the different probes. (a) Comparison among all protein groups enriched with **≡Ner** (188) and the two control probes **≡Ctrl1** (149) and **≡Ctrl2** (135) compared to the DMSO-control. (b) Comparison among the primary protein groups enriched with **≡Ner** (fold enrichment > 2; 98) and all protein groups enriched with **≡Ctrl1** and **≡Ctrl2** compared to the DMSO-control.

Out of the total of 188 protein groups enriched with **≡Ner** compared to the DMSO control, 62 protein groups were exclusive to **≡Ner** when compared with all protein groups enriched with each of the two control probes **≡Ctrl1** and **≡Ctrl2** compared to the DMSO control (Fig. 21a). Among the 98 primary hits, about half, i.e. 44 protein groups, were exclusive to **≡Ner** compared to all protein groups enriched with **≡Ctrl1** and **≡Ctrl2** (Fig. 21b). A complete list of all primary protein groups exclusive to **≡Ner** is reported in the following table (Tab. 12). Among the hits exclusive to **≡Ner**, AtAOR, a chloroplastic NADPH-dependent alkenal/one oxidoreductase (At1g23740; 41 kDa) showed the highest $\log_2$-fold enrichment of 5.2, directly followed by AtEH7 with the second highest $\log_2$-fold enrichment of 5.0. However, when having a look at the unprocessed data (available via the PRIDE repository, see 2.2.5.2) before the imputation of missing values was done, AtAOR was additionally detected in two out of four of the DMSO-control samples, albeit with a $\log_2$-fold lower LFQ intensity of ca. 5.9 over the mean LFQ intensities for both groups. AtEH7, by contrast, was completely absent in all DMSO control samples. Therefore, the lower fold enrichment with **≡Ner** for AtEH7 than for AtAOR stems from the imputation of missing LFQ intensities from the normal distribution, which was necessary to allow for the statistical evaluation of the MS data. Hence, despite the higher $\log_2$-fold enrichment for AtAOR with respect to the processed data, AtEH7 was considered the top enzyme target by fold enrichment exclusive to **≡Ner** in Arabidopsis.

Tab. 12 Primary protein groups exclusively enriched with ≡Ner. Overview about all primary protein groups exclusively enriched with **≡Ner** compared to the DMSO control and their respective log_2-fold enrichment factor.

No.	Log_2-fold enrichment	Protein group (gene name)
1	5.24003	AOR
2	5.00996	At4g02340/T14P8.15
3	3.40845	RPS3A; RPS3B; RPS3C
4	2.94608	ADH1
5	2.8719	MDAR2
6	2.69674	CAD4
7	2.53802	UGE1
8	2.50495	GLYR1
9	2.49673	RPL40A; RPL40B; RPS27AA; RPS27AB; RPS27AC; RUB1; RUB2; UBQ3; UBQ4; UBQ9; UBQ10; UBQ11; UBQ12; UBQ13; UBQ14
10	2.45050	ADK2
11	2.42660	At5g28840
12	2.42014	MCD7.8; At4g26390
13	2.29147	rpl22
14	2.19112	ELF5A-2
15	2.19016	SDH
16	2.06828	SUR1
17	1.99068	GPX1
18	1.96359	ACP4
19	1.87916	At3g52990
20	1.83799	VEP1
21	1.83001	SSU1; MFL8.15
22	1.82734	HSP70-3
23	1.75652	PED1
24	1.73191	DHAR3
25	1.72034	LTA2
26	1.70241	ALAAT1
27	1.65048	RPS23A; RPS23B
28	1.62811	CBBY
29	1.61844	UGD2
30	1.61409	GRF6
31	1.50701	MTHFR2
32	1.48628	PRXIIB; TPX1
33	1.46625	HACL
34	1.45478	At3g02730
35	1.33258	rps11
36	1.22061	At2g36580
37	1.16848	PDH2
38	1.16149	RPS10A; RPS10C; At4g25740
39	1.14989	rps12-A
40	1.11031	RPL4D; At5g02870
41	1.08406	OASA1
42	1.05204	FPS1

43	1.03512	rpl14
44	1.00940	RPL5

To further elucidate which of the hits that are exclusive to **≡Ner** are also specific for **Ner** and do not result from off-target labelling, the protein groups that were significantly underrepresented ($p < 0.05$; fold change > 2) within the group of **Ner**-preincubated **≡Ner**-labelled samples compared to the group of noncompetition **≡Ner**-labelled samples was examined (Fig. 20d). This analysis confirmed AtAOR, the top hit by fold enrichment, as an off-target of **≡Ner** as it was not detected within the group of potentially specific **Ner** targets only consisting of the three members AtEH7, AtOASB (At2g43750; 41.7 kDa) and At2g36580 (57.5 kDa). All other primary hits exclusively enriched with **≡Ner** were likewise excluded as specific **Ner** targets and were therefore off-targets of **≡Ner**. Among the small group of potentially specific **Ner** targets, AtEH7 unambiguously showed the highest log_2-fold change of -4.9 after **Ner**-preincubation with the most significant -log p-value of 4.7 (Fig. 20d; Appendix 11, Tab. 23). AtOASB, a chloroplastic/chromoplastic cysteine synthase and At2g36580, a pyruvate kinase showed log_2-fold enrichments of 3.7 and 1.2 with **≡Ner** compared to the DMSO control (Fig. 20a; Appendix 10, Tab. 20). After preincubation with **Ner**, the log_2-fold changes were -1.3 and -1.6, respectively, with a p-value just above the significance level ($p < 0.05$; Fig. 20d; Appendix 11, Tab. 23). AtOASB was however excluded as a specific target of **Ne**r since it was not found among the hits exclusively enriched with **≡Ner**. Indeed, when having a look at the unprocessed data, AtOASB was detected in almost all samples of this analysis, including the DMSO control as well as **≡Ctrl1** and **≡Ctrl2** labelled samples, where a preincubation with **Ner** had no significant effect on the abundance of AtOASB in the samples. Even though the mean LFQ intensity was the highest for **≡Ner**-labelled samples, AtOASB was not considered as a target specific to **≡Ner** and **Ner**. At2g36580, although being exclusively enriched with **≡Ner**, was however similarly detected in one replicate each of **Ner**-pretreated samples labelled with **≡Ctrl1** and **≡Ctrl2** when having a look at the unprocessed data and therefore was likewise not a target specific to **≡Ner** and **Ner**. AtEH7, in contrast, was exclusively detected in noncompetition **≡Ner**-labelled samples and was therefore confirmed as the only global target specific to **Ner** and **≡Ner** in Arabidopsis.

To sum up the results obtained from this experiment, **Ner** was not only excluded to induce *PR-1* expression through covalent binding to an unspecific protein target, but

AtEH7 was furthermore confirmed as the only putative specific and covalent global protein target of **Ner**. AtEH7 therefore potentially contributes to the observed SA phenotype through the induction of *PR-1* expression. Since the preceding analyses only covered the identification of covalent interaction partners of **≡Ner**, it is however not excluded that **Ner** potentially influences other target proteins through binding via non-covalent interactions which were not subject of analysis in the present work.

3.5 Validation of AtEH7 as a direct target of Ner in *A. thaliana*

After all previous analyses revealed AtEH7 as the only putative specific target protein of **≡Ner** and **Ner**, AtEH7 was validated as a direct target of **Ner** in *A. thaliana*. To this end, a comparative *in vitro* labelling of seedling extracts from Col-0 and AtEH7-deficient *eh3-2* knock-out plants was performed with 1 µM or 10 µM **≡Ner** either after or without preincubation with 10 µM **Ner** (Fig. 22).

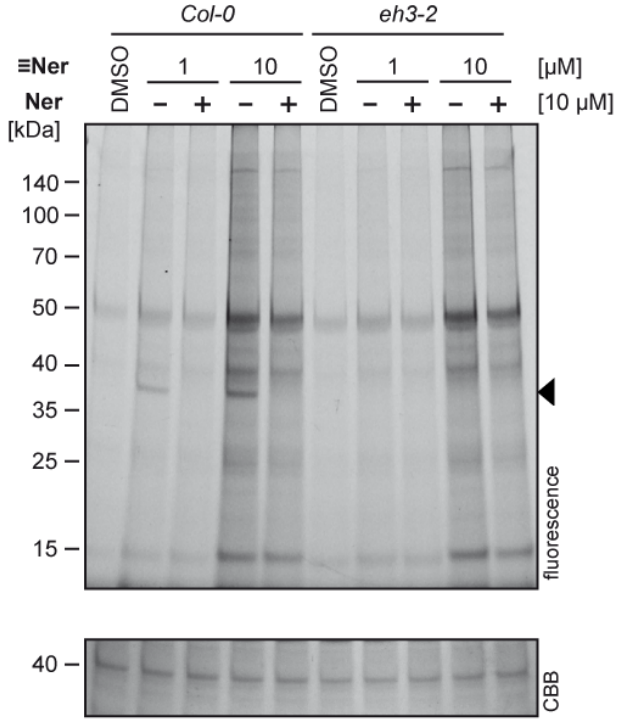

Fig. 22 *In vitro* labelling of *A. thaliana* Col-0 and *eh3-2* seedling extract with ≡Ner. Competitive *in vitro* labelling of *A. thaliana* Col-0 and *eh3-2* seedling extract with **≡Ner** visualised by fluorescence detection. A final probe concentration of 1 µM or 10 µM **≡Ner** was used. Preincubation with **Ner** was done at a final concentration of 10 µM. Disruption of Arabidopsis plant material (2.2.1.6.3), protein concentration determination (2.2.3.2), labelling of protein extract (2.2.3.3.3) and 'click' reaction (2.2.3.5) were performed as described in the methods section. For the sample separation by gel electrophoresis (2.2.3.6), 20 µL of the samples (ca. 14 µg protein) and 7 µL of protein ladder were loaded on an 11 % Bis-Tris gel. The fluorescence of the fluorophore Cy3 ($\lambda_{ex.}$ = 550 nm excitation, $\lambda_{em.}$ = ~570 nm emission) was detected using the Cy3-DIGE settings (green laser $\lambda_{em.}$ = 532 nm, BPG1 band pass green filter 560-580 nm) of the laser scanner (2.2.3.7). Equal loading of the gel was confirmed by staining with a colloidal Coomassie solution (2.2.3.9).

The *in vitro* labelling of *A. thaliana* Col-0 seedling extract with 1 µM and 10 µM **≡Ner** again resulted in the presence of a protein band at a MW of about 37 kDa which is absent in the samples pretreated with 10 µM **Ner**. This protein band matches the size of AtEH7. In the *in vitro* labelling of AtEH7-deficient *eh3-2* Arabidopsis seedling extract with 1 µM or 10 µM **≡Ner** this protein band was completely absent, indicating that AtEH7 indeed is a direct target of **≡Ner** and thus **Ner**. A preincubation with 10 µM **Ner** therefore had no visible effect on the labelling with the probe.

To further validate AtEH7 as a direct target of **Ner**, WT AtEH7 was recombinantly produced in *E. coli* (Fig. 23). To this end, *E.coli* BL21 (DE3) was transformed with the *eh7*::pET-59-DEST plasmid and the expression of recombinant AtEH7 was induced with IPTG. Recombinant WT AtEH7 was extracted by cell disruption and purified by IMAC (Fig. 23a) and SEC (Fig. 23b+c). The purified recombinant enzyme was first employed in a chemical labelling experiment with **≡Ner** to evaluate if recombinant WT AtEH7 is likewise targeted by **Ner** as is the endogenous protein. To this end, different amounts of WT AtEH7 ranging from 1-10 µg were spiked to 50 µg of Arabidopsis protoplast extract. In addition, the purified enzyme as well as the protoplast extract were solely labelled with 10 µM **≡Ner**. Labelling for all conditions was done either with or without preincubation with 100 µM **Ner** (Fig. 24). As already observed in former experiments, the labelling of the protoplast extract without the addition of recombinant AtEH7 with **≡Ner** resulted in the presence of a protein band at a MW of about 37 kDa, resembling the size of endogenous AtEH7, which was abolished after pretreatment with **Ner**. The labelling of purified recombinant AtEH7 with **≡Ner** resulted in the presence of a protein band of a MW of about 50 kDa, matching the size of the recombinant protein with a MW of 51.9 kDa. A pretreatment with **Ner** likewise led to an abolishment of the labelled band. Since the 52 kDa band was not visible for the no-probe control containing the pure enzyme nor for the sample preincubated with **Ner**, the band in the labelled noncompetition sample results from specific labelling of AtEH7 with **≡Ner**, and not from the sole abundance of the recombinant protein in the sample or from unspecific labelling of this abundant protein. For the labelling of spike-in samples with **≡Ner**, both protein bands at a MW of 37 kDa and 52 kDa were visible and competable by a pretreatment with **Ner**. The intensity of both bands was increasing with higher concentrations of recombinant WT AtEH7 spiked to the protoplast extract,

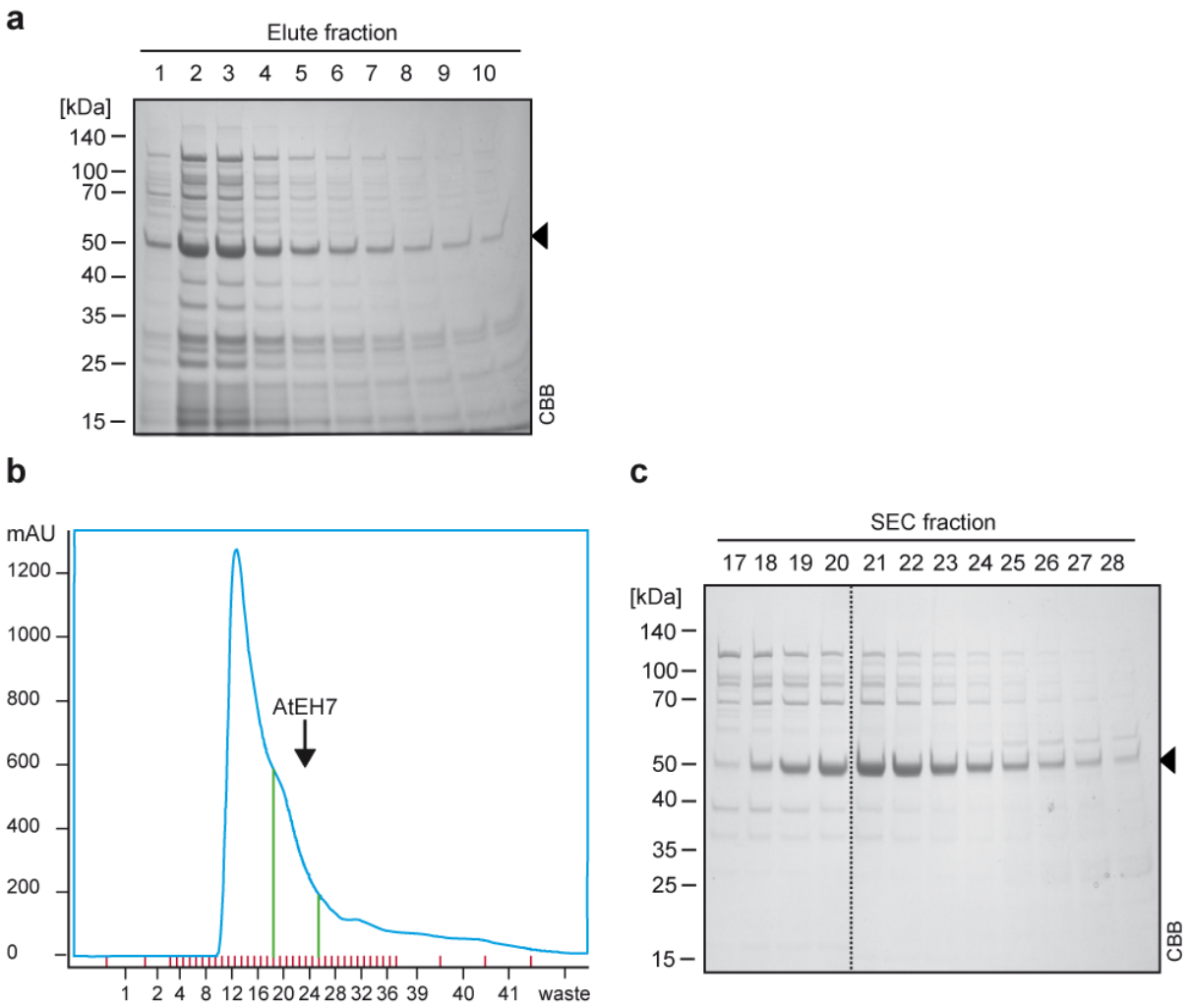

Fig. 23 Purification of recombinant WT AtEH7. (a) Recombinant WT AtEH7 which was produced in (2.2.1.5) and extracted from *E. coli* (2.2.1.6.1) was purified by IMAC using a NI-IDA resin (2.2.3.1.2). Eluted fractions were analysed by gel electrophoresis (2.2.3.6) and subsequent staining with a colloidal Coomassie solution (2.2.3.9). AtEH7 was confirmed to be present on gel and fractions containing AtEH7 were combined. (b) SEC (2.2.3.1.3) of the pooled AtEH7 elution on a Superdex™ column using IMAC200 buffer as eluent. (c) SEC fractions were analysed by gel electrophoresis and colloidal Coomassie staining and fractions containing large amounts of AtEH7 were combined (as indicated in (b)) to yield the final enzyme purification that was utilised in chemical labelling experiments (2.2.3.3.3) as well as in enzyme assays (2.2.3.10). Representative data.

with the upper 52 kDa band being much more intense than the lower 37 kDa band. For the spike-in of 5 µg and 10 µg of recombinant AtEH7 to Arabidopsis protoplast extract, another protein band at a MW of about 40 kDa that was competable by pretreatment with **Ner** was visible. Surprisingly, the labelling intensity of the 52 kDa band was much higher for the sample spiked with 10 µg of recombinant WT AtEH7 than the labelling intensity observed for the same amount of purified enzyme solely. The exact position of recombinant WT AtEH7 on the gel was confirmed by Western blot analysis. An α-His HRP-conjugated antibody targeted against the N-terminal His-tag configuration of

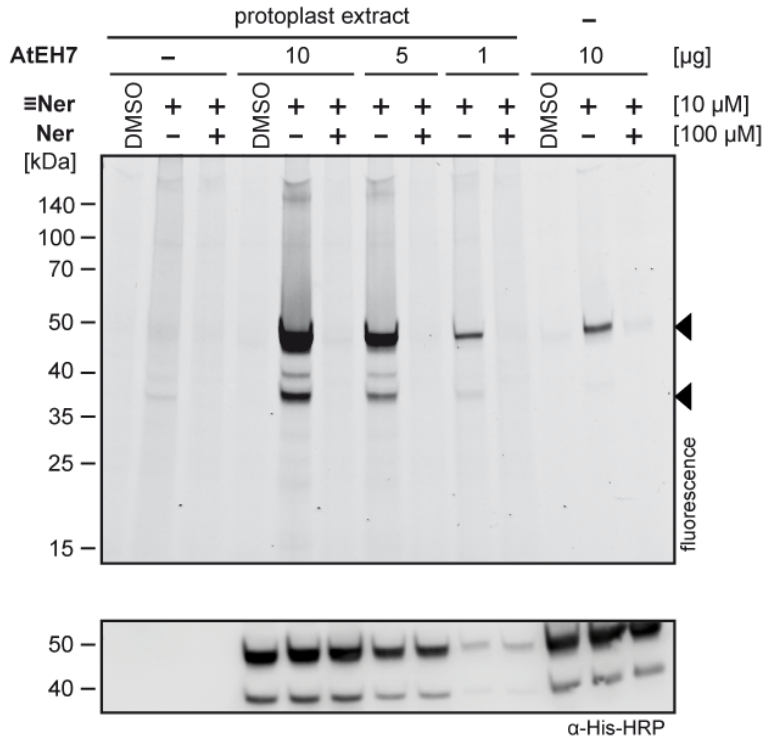

Fig. 24 Labelling of recombinant WT AtEH7. Competitive *in vitro* labelling of Arabidopsis protoplast extract, recombinant WT AtEH7 spiked to Arabidopsis protoplast extract and purified AtEH7 with **≡Ner** visualised by fluorescence detection. Different amounts of AtEH7 ranging from 1-10 µg were spiked to 50 µg Arabidopsis protoplast extract whereas 10 µg of purified AtEH7 and 50 µg of protoplast extract alone were additionally utilised for the labelling. A final probe concentration of 10 µM **≡Ner** was used. Preincubation with **Ner** was done at a final concentration of 100 µM. Expression and purification of recombinant WT AtEH7 (2.2.1.5, 2.2.1.6.1 and 2.2.3.1), disruption of Arabidopsis plant material (2.2.1.6.3), protein concentration determination (2.2.3.2), *in vitro* labelling (2.2.3.3.3), methanol-chloroform precipitation (2.2.3.4) and 'click' reaction (2.2.3.5) were performed as described in the methods section. For the sample separation by gel electrophoresis (2.2.3.6), 13.3 µL of the samples (10 µg of total protein from Arabidopsis chloroplasts, 2 µg of recombinant WT AtEH7 at max) and 7 µL of protein ladder were loaded on an 11 % Bis-Tris gel. The fluorescence of the fluorophore Cy3 ($\lambda_{ex.}$ = ~550 nm excitation, $\lambda_{em.}$ = ~570 nm emission) was detected using Cy3-DIGE settings (green laser $\lambda_{em.}$ = 532 nm, BPG1 band pass green filter 560-580 nm) of the laser scanner (2.2.3.7). The position of recombinant AtEH7 on the gel was confirmed by Western blotting using an α-His HRP-conjugated antibody (2.2.3.8).

recombinant AtEH7 that is suitable for chemiluminescent immunodetection after electrophoretic sample separation and fluorescence detection was used. The immunohistochemical His-tag detection however additionally revealed that a His-tagged species of about the size of endogenous AtEH7 was present in all samples containing the purified enzyme for an unascertained reason. It is therefore likely that the strong labelling of the 37 kDa band observed for the spike-in samples does not solely result from the labelling of endogenous AtEH7, but was actually caused by the additive labelling of the additional His-tagged species present in the samples. Yet, these results clearly demonstrate that recombinant WT AtEH7 is equally targeted by

≡Ner and **Ner** as is the endogenous protein and therefore is suitable for further *in vitro* studies with **Ner**.

Next, the purified enzyme was employed in an enzyme kinetics assay. Before examining the effects of **Ner** on AtEH7 activity, the recombinant enzyme was first confirmed to be active. The conducted EH assay was based on the increase in absorbance upon the cleavage of the epoxide substrate S-NEPC into UV-quantifiable *para*-nitrophenol and a cyclic carbonate (Fig. 25a) and was set up with the help of Jenny Bormann, University of Duisburg-Essen. S-NEPC has been developed as a substrate for cytosolic EHs to easily monitor their activity spectrophotometrically. In addition to the epoxide functional group, this substrate carries a carbonate that upon hydrolysis of the epoxide undergoes a cyclisation resulting in the release of *para*-nitrophenol[288]. *para*-nitrophenol is a stable chromogenic substrate with an absorption maximum at a wavelength of 405 nm which is often employed as a product in enzymatic assays due to its facile detectability[289].

To initially test whether this assay platform was suitable to assess the activity of recombinant WT AtEH7, the assay was performed at pH 7.0 and pH 8.0 using different concentrations of the protein (Fig. 25b+c). The enzyme kinetics assay showed that the absorbance at 405 nm was increasing over time for all tested enzymatic reactions until a plateau was reached. This increase in absorbance was correlated with the employed AtEH7 concentration, thereby proving the established enzyme assay to be functional and the recombinant WT AtEH7 to be active. At a pH of 7.0 (Fig. 25b), the slope of the initial increase in absorbance at 405 nm was lower for all tested concentrations of AtEH7, compared to the slope of the initial increase in absorbance at 405 nm for all reactions containing the same amount of AtEH7 carried out at pH 8.0 (Fig. 25c). The higher activity of AtEH7 at pH 8.0 was particularly observed when larger amounts of AtEH7 were employed to catalyse the enzymatic reaction. A pH of 8.0 is close to the physiological pH of 8.4±0.3 that was measured in the alkaline Arabidopsis peroxisomes where AtEH7 is located[290]. However, the solubility of **Ner** in aqueous solution is generally low but increases at lower pH and is best below pH 5.0[291]. Due to this aspect, the activity of AtEH7 was also determined at a slightly lower pH value of 7.0 to partly compromise the solubility issue that causes **Ner** to precipitate when applied at higher concentrations. But since the activity of recombinant WT AtEH7 was

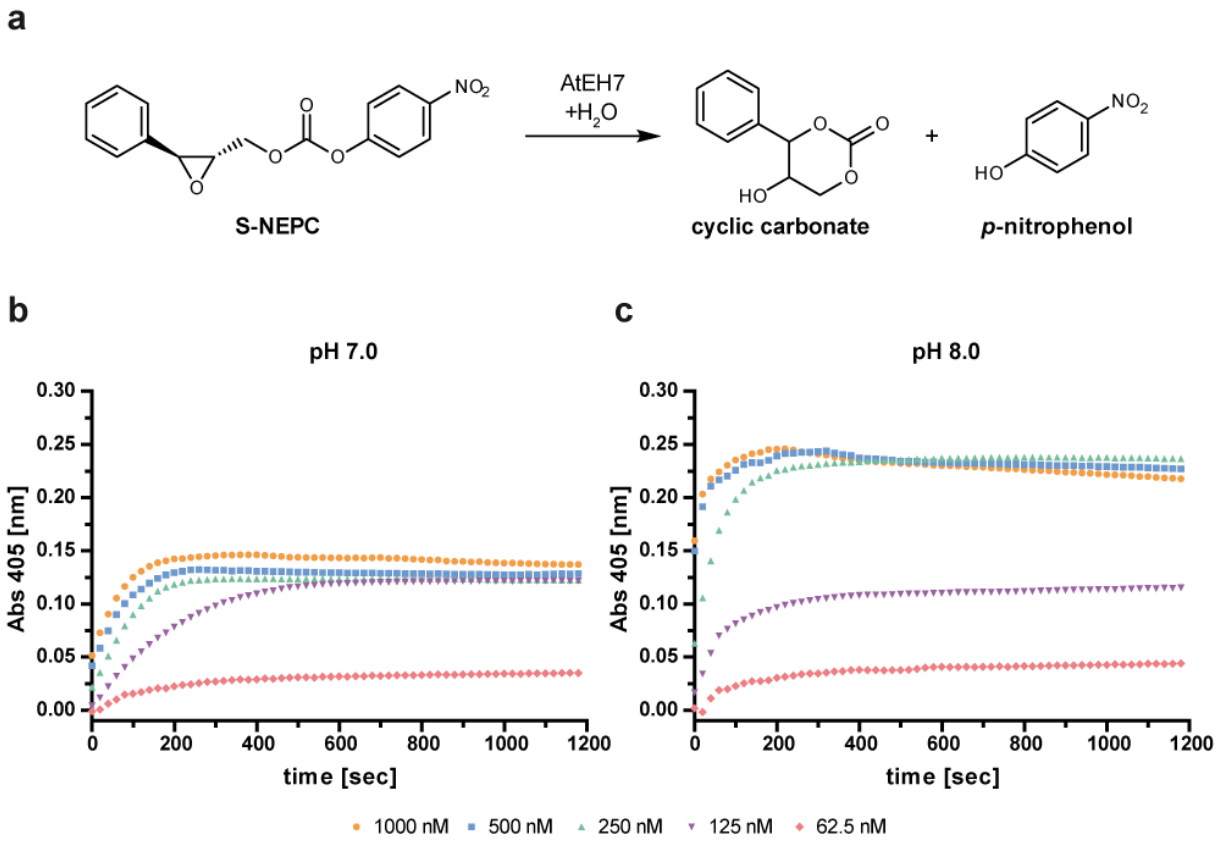

Fig. 25 Verification of recombinant WT AtEH7 activity. (a) The implemented enzyme assay was based on the cleavage of the epoxide substrate S-NEPC by AtEH7, resulting in the presence of UV-quantifiable *para*-nitrophenol which has its absorbance maximum at a wavelengths of 405 nm alongside with a cyclic carbonate. The increase in the absorbance at 405 nm is therefore positively correlated to the activity of recombinant AtEH7. The activity of recombinant WT AtEH7 was assayed in (b) Tris pH 7.0 or (c) Tris pH 8.0 buffer using an enzyme kinetics assay (2.2.3.10). WT AtEH7 was employed at a two-fold concentration range from 62.5-1000 nM. Upon addition of the epoxide substrate, the absorbance at 405 nm was monitored over time for a total of 20 min. Values (net absorbance) represent the mean values of two technical replicates.

considerably lower at a pH value of 7.0 than at a pH value of 8.0 and hence larger amounts of enzyme would be needed to perform the reaction, all subsequent enzymatic assays with AtEH7 were carried out at a pH value of 8.0.

After the activity of recombinant WT AtEH7 was confirmed and the effect of the pH on the activity was assessed, the influence of **Ner** on AtEH7 activity was determined. For this purpose, 100 nM WT AtEH7 was preincubated with a two-fold concentration series of **Ner** for 10 min prior to measuring the absorbance at 405 nm after the addition of the epoxide substrate to the reaction mix using the previously established assay platform. The remaining enzymatic activity was calculated compared to the DMSO control. In addition to **Ner**, the two structurally related TKIs pelitinib and gefitinib that were identified as moderately active screening hits from the initial screen for SA agonists were included in this assay (Fig. 26).

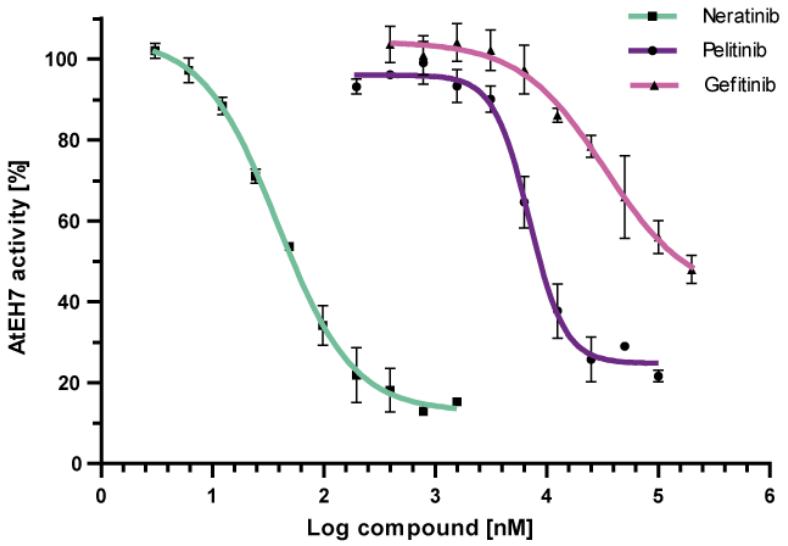

Fig. 26 Concentration-dependent inhibition of recombinant WT AtEH7. The activity of recombinant WT AtEH7 was assessed at pH 8.0 using the previously introduced enzyme assay (2.2.3.10). WT AtEH7 at a concentration of 100 nM was preincubated with a two-fold concentration series of either **Ner**, pelitinib or gefitinib for 10 minutes. The absorbance at a wavelength of 450 nm was measured 60 sec after the addition of the epoxide substrate to the reaction. The remaining enzymatic activity of AtEH7 was determined compared to the DMSO-control. Values represent the mean values (± SD) of three technical replicates.

Ner as well as pelitinib and gefitinib were all found to inhibit the enzymatic activity of WT AtEH7 in the conducted enzyme assay. However, the inhibitory potency of the reversible EGRF inhibitor gefitinib is comparatively low with an IC_{50} value of 33.4 µM (95% confidence interval (CI): 19.9-56.2 µM). The irreversible pan-HER inhibitor pelitinib was slightly more potent in reducing WT AtEH7 activity than gefitinib, with an IC_{50} value of 7.0 µM (95% CI: 6.2-7.8 µM). **Ner**, in contrast, was a potent inhibitor of WT AtEH7 activity with an IC_{50} value of 38.6 nM (95% CI: 33.7-44.2 nM). Although **Ner** was a potent inhibitor of AtEH7, a residual enzymatic activity of about 10-15% was still observed when the plateau of **Ner** inhibition compared to the DMSO control was reached. A similar phenomenon was observed for AtEH7 inhibition with pelitinib, for which a residual enzymatic activity of 20-25% was detected. With regard to gefitinib, it could not be ascertained whether such a plateau of residual enzymatic activity would likewise be obtained, as gefitinib could not be assayed at the required concentrations. Irrespective of the residual enzymatic activity, AtEH7 was indeed confirmed as a direct target of **Ner**, acting as a nanomolar inhibitor of AtEH7. Moreover, pelitinib and gefitinib were further identified as inhibitors of AtEH7, but with a considerably lower inhibitory potency. This result was in accordance with the result of the initial screen for SA activators (3.1), where the Z-score for gefitinib was below the Z-score of pelitinib and well below the Z-score of the primary hit **Ner**. It is therefore reasonable to assume that

all three TKIs act as SA activators through inhibition of AtEH7 and that their different inhibitory potency is due to structural differences, especially for gefitinib (with the lowest potency and Z-score), which is a reversible TKI, while pelitinib and **Ner** both possess a covalent mode of binding.

Furthermore, the inhibitory potency of **Ner** in reducing AtEH7 labelling with **≡Ner** was determined on-gel. To this end, Arabidopsis protoplast extract was preincubated with a two-fold dilution series of **Ner** prior to the labelling with 1 µM **≡Ner** (Fig. 27).

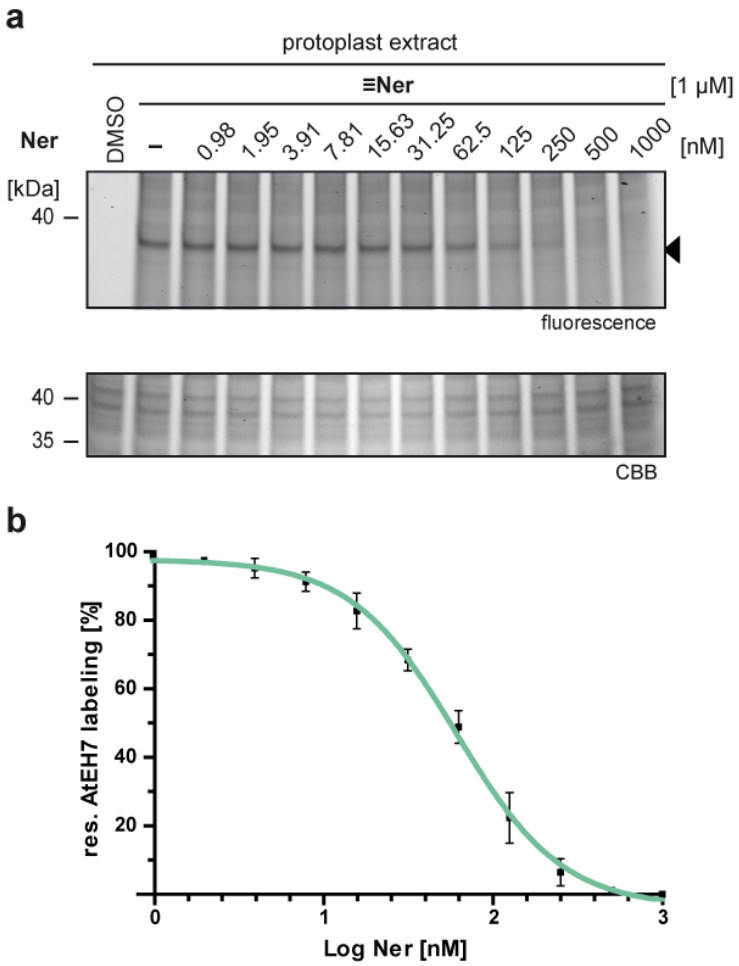

Fig. 27 Concentration-dependent inhibition of AtEH7 labelling with ≡Ner. (a) Concentration-dependent competitive *in vitro* labelling of *A. thaliana* protoplast extract with **≡Ner** visualised by fluorescence detection (representative gel). A final probe concentration of 1 µM **≡Ner** was used. Preincubation with **Ner** was done using a two-fold concentration series. Disruption of Arabidopsis plant material (2.2.1.6.3), protein concentration determination (2.2.3.2), labelling of protein extract (2.2.3.3.3) and 'click' reaction (2.2.3.5) were performed as described in the methods section. For the sample separation by gel electrophoresis (2.2.3.6), 20 µL of the samples (ca. 15 µg protein) and 7 µL of protein ladder were loaded on an 11 % Bis-Tris gel. The fluorescence of the fluorophore Cy3 ($\lambda_{ex.}$ = ~550 nm excitation, $\lambda_{em.}$ = ~570 nm emission) was detected using the Cy3-DIGE settings (green laser $\lambda_{em.}$ = 532 nm, BPG1 band pass green filter 560-580 nm) of the laser scanner (2.2.3.7). Equal loading of the gel was confirmed by staining with a colloidal Coomassie solution (2.2.3.9). (b) Plot of the residual AtEH7 labelling with **≡Ner** after preincubation with the indicated concentration of **Ner** compared to the noncompetition **≡Ner**-labelled control. Values represent the mean values (± SD) of three technical replicates.

A concentration-dependent inhibition of the labelling of the 37 kDa band resembling AtEH7 with **≡Ner** by **Ner** was visible (Fig. 27a). The labelling intensity of this band was quantified for each labelled lane of the gel (excluding the DMSO control sample) using FIJI. To plot the residual AtEH7 labelling with **≡Ner** after preincubation with the different concentrations of **Ner**, the labelling intensity of the 37 kDa band of all labelled samples was compared with the intensity of the same band in the control sample without preincubation with **Ner** (Fig. 27b). **Ner** was found to inhibit **≡Ner**-labelling with an IC_{50} of 60.6 nM (95% CI: 54.1-67.9 nM). This value falls into about the same nanomolar range as the IC_{50} that was determined for **Ner** regarding the inhibition of 100 nM recombinant WT AtEH7.

Finally, the effect of other phenotypic screening hits that were identified from the initial screen for SA agonists on the labelling of AtEH7 with **≡Ner** was investigated. This was performed in order to evaluate whether other active compounds may have likewise triggered *PR-1* induction and thus *GUS* transcription via inhibition of AtEH7 during the screen, as was observed for **Ner**. To this end, all primary hits with a Z-score ≥ 1.5 (except for SA itself), namely genistein, BAY 11-7082 and DRB as well as the moderately active hits with structural similarity to **Ner**, i. e. gefitinib and pelitinib, were applied in a competitive labelling approach (see Appendix 5, Fig. 37). For this experiment, Arabidopsis protoplast extract was preincubated with 10 µM of all test compounds prior to labelling with 1 µM **≡Ner** (Fig. 28). A preincubation with genistein (Cpd 59), BAY 11-7082 (Cpd 65), DRB (Cpd 66) and gefitinib (Cpd 85) had no visible effect on the labelling intensity of AtEH7 with **≡Ner**. Pelitinib (Cpd 88), in contrast, led to a reduction of the labelling intensity of AtEH7 with **≡Ner**. However, the signal was not completely abolished as observed for **Ner**. This data is coherent with the IC_{50} values of **Ner**, pelitinib and gefitinib as determined from the inhibition of recombinant WT AtEH7 which indicates that **Ner** is more than 100 times more potent in inhibiting AtEH7 activity than pelitinib and nearly 1000 times more potent as gefitinib. Therefore, it is likely that the structurally closely related irreversible TKI pelitinib and the reversible TKI gefitinib display the same mode-of-action in inducing *PR-1* expression through inhibition of AtEH7. The structurally unrelated compounds, however, are likely to activate SA signalling via a differential pathway as they did not visually impact on AtEH7 labelling with **≡Ner**.

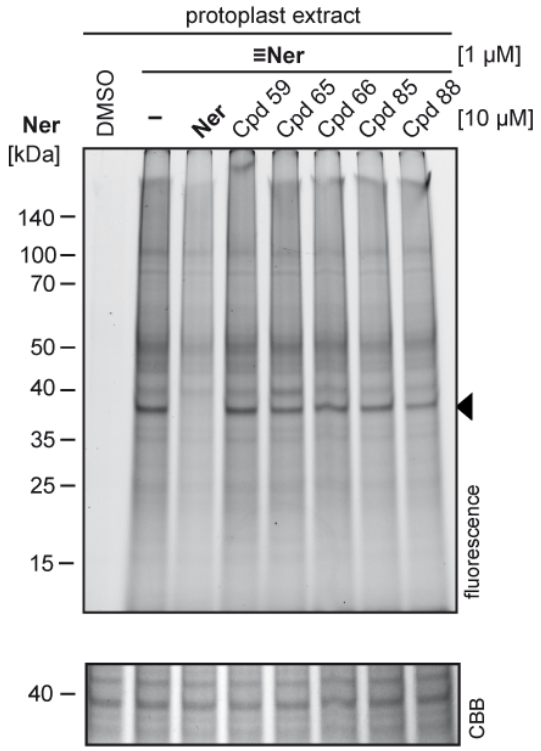

Fig. 28 Influence of other phenotypic screening hits on AtEH7 labelling with ≡Ner. Competitive *in vitro* labelling of *A. thaliana* protoplast extract with **≡Ner** employing further phenotypic screening hits visualised by fluorescence detection. A final probe concentration of 1 µM **≡Ner** was used. Preincubation with the different hits from the screen for SA signalling agonists was done at a final concentration of 10 µM. Disruption of Arabidopsis plant material (2.2.1.6.3), protein concentration determination (2.2.3.2), labelling of protein extract (2.2.3.3.3) and 'click' reaction (2.2.3.5) were performed as described in the methods section.. For the sample separation by gel electrophoresis (2.2.3.6), 20 µL of the samples (ca. 15 µg protein) and 7 µL of protein ladder were loaded on an 11 % Bis-Tris gel. The fluorescence of the fluorophore Cy3 ($\lambda_{ex.}$ = ~550 nm excitation, $\lambda_{em.}$ = ~570 nm emission) was detected using the Cy3-DIGE settings (green laser $\lambda_{em.}$ = 532 nm, BPG1 band pass green filter 560-580 nm) of the laser scanner (2.2.3.7). Equal loading of the gel was confirmed by staining with a colloidal Coomassie solution (2.2.3.9).

3.6 Identification of the Ner binding site of AtEH7

After AtEH7 was successfully identified and confirmed as a specific and covalent molecular target of **Ner** in Arabidopsis, the precise binding site of **Ner** to AtEH7 was determined in the next steps. Since **Ner** targets a conserved cysteine residue within the ATP binding pocket of its human HER kinase target enzymes (1.2), it was first examined whether **Ner** binds to one of the three cysteine residues present in the protein sequence of AtEH7, which are C111, C152 and C186. To address this question, a pretreatment of Arabidopsis seedling extract with the common cysteine alkylating agent IAM at a final concentration of 10 mM in direct comparison with a pretreatment with 10 µM **Ner** prior to *in vitro* labelling with 1 µM or 10 µM **≡Ner** was initially performed (Fig. 29).

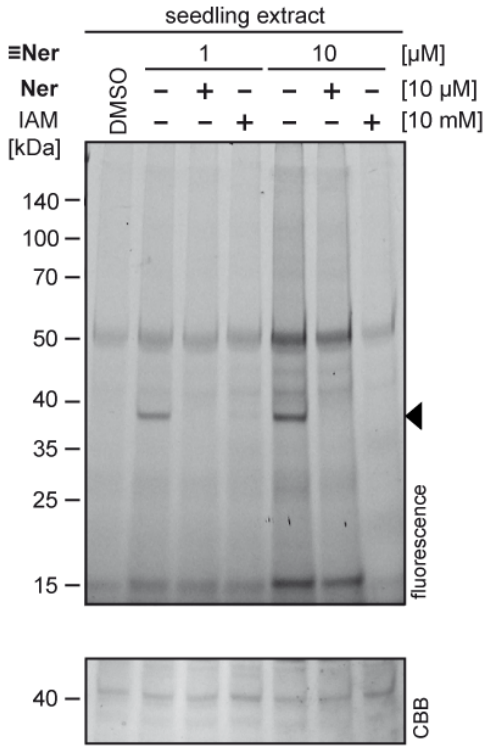

Fig. 29 *In vitro* labelling of *A. thaliana* Col-0 seedlings with ≡Ner and preincubation with IAM. Competitive *in vitro* labelling of *A. thaliana* Col-0 seedling extract to assess the impact of IAM on AtEH7 labelling with **≡Ner** visualised by fluorescence detection. A final probe concentration of 1 µM or 10 µM **≡Ner** was used. Preincubation was done using a final concentration of 10 µM **Ner** or 10 mM IAM. Disruption of Arabidopsis plant material (2.2.1.6.3), protein concentration determination (2.2.3.2), labelling of protein extract (2.2.3.3.3) and 'click' reaction (2.2.3.5) were performed as described in the methods section. For the sample separation by gel electrophoresis (2.2.3.6), 20 µL of the samples (ca. 14 µg protein) and 7 µL of protein ladder were loaded on an 11 % Bis-Tris gel. The fluorescence of the fluorophore Cy3 ($\lambda_{ex.}$ = ~550 nm excitation, $\lambda_{em.}$ = ~570 nm emission) was detected using the Cy3-DIGE settings (green laser $\lambda_{em.}$ = 532 nm, BPG1 band pass green filter 560-580 nm) of the laser scanner (2.2.3.7). Equal loading of the gel was confirmed by staining with a colloidal Coomassie solution (2.2.3.9).

As observed for the pretreatment with **Ner**, a pretreatment with IAM prior to the labelling of Arabidopsis seedling extract with **≡Ner** resulted in the abolishment of the AtEH7 protein band at a MW of 37 kDa. The inhibition of AtEH7 labelling by IAM implicates that **≡Ner** and thus **Ner** target a free cysteine residue of AtEH7. Though, IAM was previously described to show offsite mono- and dialkylation of various other amino acid residues, i. e. serine, threonine, glutamic acid, aspartic acid, lysine, histidine and tyrosine[292]. Furthermore, reactivity of Michael acceptor-based targeted covalent small molecule inhibitors towards lysine as well as histidine residues has been shown[293,294] and reactivity of **Ner** towards a lysine residue of human serum albumin has been particularly described[291]. Hence, it is also possible, albeit highly improbable, that **Ner** possesses off-cysteine reactivity on AtEH7 in Arabidopsis since offsite alkylation with IAM occurs to a far lesser extent than alkylation of cysteine residues. A

study by Hains and Robinson found that off-site alkylation of glutamic acid, the most common off-target amino acid for alkylation with IAM, occurs only at a rate of up to 0.2%[295]. Thus, the observed abolishment of the labelling of AtEH7 with **≡Ner** after pretreatment with IAM very likely resulted from **≡Ner** targeting one of the three cysteine residues of AtEH7.

To check whether **Ner** actually inhibits AtEH7 through binding to any of the three cysteine residues present in the amino acid sequence and, if so, which cysteine residue is precisely targeted, PCR-based site-directed mutagenesis[296-298] was used to generate the AtEH7 single mutants C111A, C152A and C186A, in which one of the cysteine residues was replaced by an alanine for each mutant (Fig. 30). An alanine-scanning is common in site-directed mutagenesis, as alanine is a non-bulky and unreactive amino acid with a reduced side chain retaining the β-carbon which does not alter the secondary structure of the protein[299].

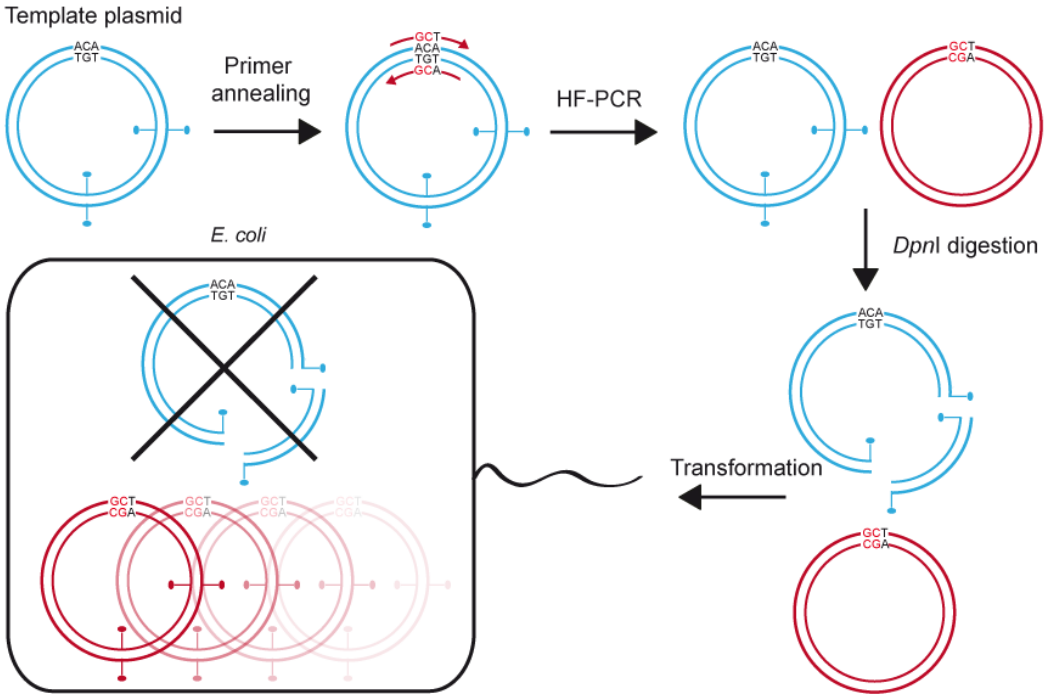

Fig. 30 Site-directed mutagenesis by PCR. Schematic representation of the high-fidelity (HF) PCR-based site-directed mutagenesis (2.2.2.2) strategy to generate the three AtEH3 mutants C111A, C152A and C186A. A methylated template plasmid isolated from *E. coli* was amplified using a set of specifically designed primers that carry the desired point mutations and introduced them into the DNA sequence of the gene which is encoded in the plasmid using a HF DNA-polymerase. The product of the PCR reaction was subsequently digested with *Dpn*I, followed by agarose gel-based analysis (2.2.2.3). The digestion of the PCR product with *Dpn*I resulted in a degradation of the methylated template plasmid DNA while the unmethylated amplified DNA stayed intact. Hence, after transformation of *E.coli* with the PCR product (2.2.1.3.1), only the intact plasmid could be amplified. After plasmid preparation from *E. coli* (2.2.2.5), the introduction of the desired mutations was confirmed by sequencing (2.2.2.6). Adapted from Ahmadiankia, 2013[300].

The successful amplification of the DNA using the designed primer pairs was confirmed using agarose gel electrophoresis (Appendix 14, Fig. 39) and the effective introduction of the point mutations that resulted in the replacement of cysteines by alanines was confirmed by DNA sequencing of selected clones. As previously described for the WT form of recombinant AtEH7 (see 3.5, Fig. 23), the C111A, C152A and C186A mutant AtEH7 proteins were expressed in *E. coli*, extracted by cell disruption and further purified by IMAC and subsequent SEC (Appendix 15, Fig. 40). The purified recombinant enzymes were first subjected to a chemical labelling experiment with **≡Ner** to test whether the C111A, C152A and C186A mutant forms of AtEH7 were also targeted by **Ner**. For this purpose, 50 µg of Arabidopsis protoplast extract was spiked with 10 µg of the WT and mutant forms of recombinant AtEH7 prior to the labelling with 10 µM **≡Ner** without or after preincubation with 100 µM **Ner** (Fig. 31). A control lane showing the labelling of the pure protoplast extract lacking spiked AtEH7 with **≡Ner** can be found on a control gel in the appendix (Appendix 16, Fig. 41). This sample was prepared together with the spike-in samples. Here, the labelling of the 37 kDa band resembling endogenous AtEH7 was observable. For the labelling of Arabidopsis protoplast extract spiked with recombinant WT AtEH7 with **≡Ner**, two protein bands were visible. The lower protein band matched the size of endogenous AtEH7 with a MW of 37 kDa. The upper protein band matched the size of recombinant AtEH7 with a MW of 51.9 kDa which was confirmed to be present by Western blot analysis against the His-tag configuration of recombinant AtEH7 using an α-His HRP-conjugated antibody and subsequent chemiluminescent immunodetection which followed the electrophoretic sample separation and fluorescence detection. A preincubation with 100 µM **Ner** led to the abolishment of both protein bands, indicating that these bands both stemmed from the specific labelling of AtEH7. Protein bands of the same MW were additionally present for the protoplast extract spiked with mutant C111A or C152A AtEH7. These were equally competable by a preincubation with **Ner**, demonstrating that Cys111 and Cys152 of AtEH7 are not targeted by **≡Ner** and **Ner**. On the contrary, both protein bands were completely absent in protoplast extract spiked with mutant C186A AtEH7. A preincubation with **Ner** therefore had no additional effect. The absence of the 52 kDa band in the noncompetition **≡Ner**-labelled sample indicates that **Ner** binds to AtEH7 via a covalent modification of Cys186. However, the absence of the 37 kDa in this sample might be explained by the phenomenon already

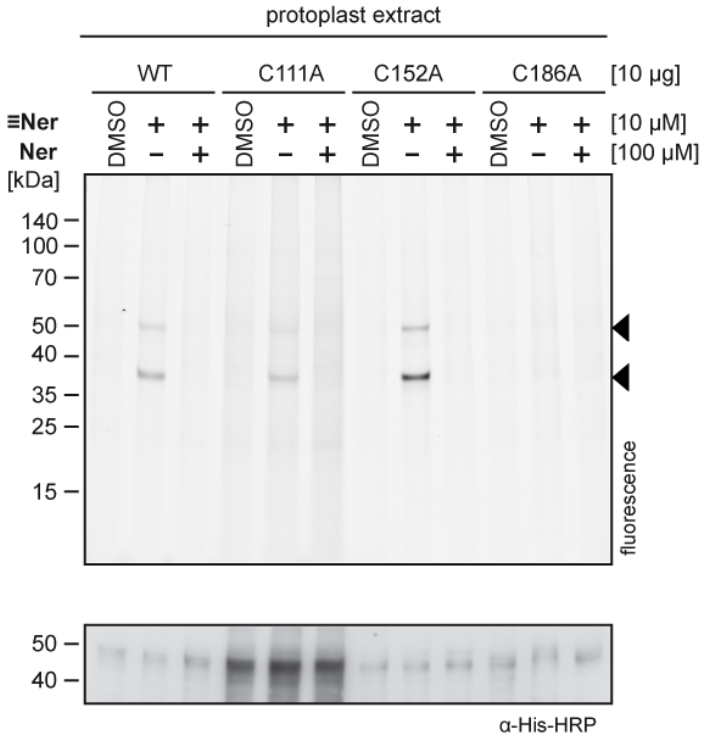

Fig. 31 Labelling of recombinant WT and mutant AtEH7. Competitive *in vitro* labelling of recombinant WT and mutant AtEH7 spiked to an Arabidopsis protoplast extract with **≡Ner** visualised by fluorescence detection. 10 µg of WT or mutant AtEH7 was spiked to 50 µg Arabidopsis protoplast extract. A final probe concentration of 10 µM **≡Ner** was used. Preincubation with **Ner** was done at a final concentration of 100 µM. Expression and purification of recombinant WT and mutant AtEH7 (2.2.1.5, 2.2.1.6.1 and 2.2.3.1), disruption of Arabidopsis plant material (2.2.1.6.3), protein concentration determination (2.2.3.2), *in vitro* labelling (2.2.3.3.3), methanol-chloroform precipitation (2.2.3.4) and 'click' reaction (2.2.3.5) were performed as described in the methods section. For the sample separation by gel electrophoresis (2.2.3.6), ca. 5-15 µg of total protein from Arabidopsis chloroplasts as well as 1-3 µg of recombinant AtEH7 and 7 µL of protein ladder were loaded on an 11 % Bis-Tris gel. The fluorescence of the fluorophore Cy3 ($\lambda_{ex.}$ = ~550 nm excitation, $\lambda_{em.}$ = ~570 nm emission) was detected using Cy3-DIGE settings (green laser $\lambda_{em.}$ = 532 nm, BPG1 band pass green filter 560-580 nm) of the laser scanner (2.2.3.7). The position of recombinant AtEH7 on the gel was confirmed by Western blotting using an α-His HRP-conjugated antibody (2.2.3.8).

observed for the labelling of recombinant WT AtEH7, i.e. that a His-tagged species present within the recombinant enzyme purification and matching the size of endogenous AtEH7 was mainly responsible for the strong labelling observed at a MW of 37 kDa (see Fig. 24). Although such a species could not be detected on the Western blot in this spike-in experiment in addition to the 52 kDa band matching full-size recombinant WT and mutant AtEH7, the presence of this species is not completely excluded. Here, after immunodetection, the protein band of full-size recombinant AtEH7 itself showed a much lower intensity compared to the spike-in experiment with WT AtEH7 only, probably resulting from higher impurities of the enzyme purifications. Taking the low intensity of the 52 kDa band into account, it is possible that the amount of the 37 kDa species loaded on the gel was not sufficient for immunodetection under

the chosen experimental settings, as this species was detected with a considerably lower intensity for the spike-in experiment with recombinant WT AtEH7 than the 52 kDa band. Yet, these results clearly indicate that **Ner**, in Arabidopsis, possesses a similar mode-of-binding via covalent targeting of a cysteine residue as in human and that the precise residue modified by **≡Ner** and **Ner** is Cys186.

The purified recombinant WT and mutant AtEH7 enzymes were subsequently utilised in the previously introduced kinetic enzyme assay to assess the effect of **Ner** and **≡Ner** on their activity. To this end, the activity of mutant AtEH7 was proved first and the optimal enzyme concentration of the WT and mutant enzymes for the subsequent studies was determined (Fig. 32). As previously observed for WT AtEH7 (Fig. 25), the enzyme kinetics assay with the WT as well as with all three mutant forms of the enzyme equally showed an increase in the absorbance at 405 nm over time until a plateau was reached (Fig. 32a-d). The increase in absorbance was correlated with the employed AtEH7 concentration and resulted from the cleavage of the epoxide substrate S-NEPC, releasing the UV-quantifiable *para*-nitrophenol. Thus, recombinant mutant C111A, C152A as well as C186A AtEH7 were proven to be functionally active forms of the enzyme, even though they showed differential specific activities, and are therefore suitable for the assessment of changes in their activity upon compound treatment.

After the activity of the WT and mutant AtEH7 proteins was confirmed, the effect of a pretreatment with 10 µM **Ner** or **≡Ner** on their activity was examined and the remaining enzymatic activity was calculated (Fig. 33). The enzyme kinetics assay with WT AtEH7 (Fig. 33a) reconfirmed the inhibitory potency of **Ner** on AtEH7 activity, which had already been shown before (Fig. 26). A preincubation with 10 µM **Ner** led to a significant reduction of the enzymatic activity of about 67.5% compared to the DMSO control ($p < 0.0001$; Fig. 33e), as monitored by a slower increase in the absorbance at 405 nm due to a reduced cleavage rate of the epoxide substrate S-NEPC. Similar to a preincubation of WT AtEH7 with **Ner**, the preincubation with **≡Ner** resulted into a significantly reduced enzymatic activity of about 62.4% compared to the DMSO control ($p < 0.0001$; Fig. 33e). In addition, the preincubation of the C111A and C152A mutant forms of AtEH7 with **Ner** or **≡Ner** (Fig. 33b+c) likewise led to a significant reduction of the enzymatic activity of about 53.8% and 61.8% for **Ner** as well as 43.1% and 75.4% for **≡Ner**, respectively, compared to the DMSO control (all $p < 0.0001$; Fig. 33e). The

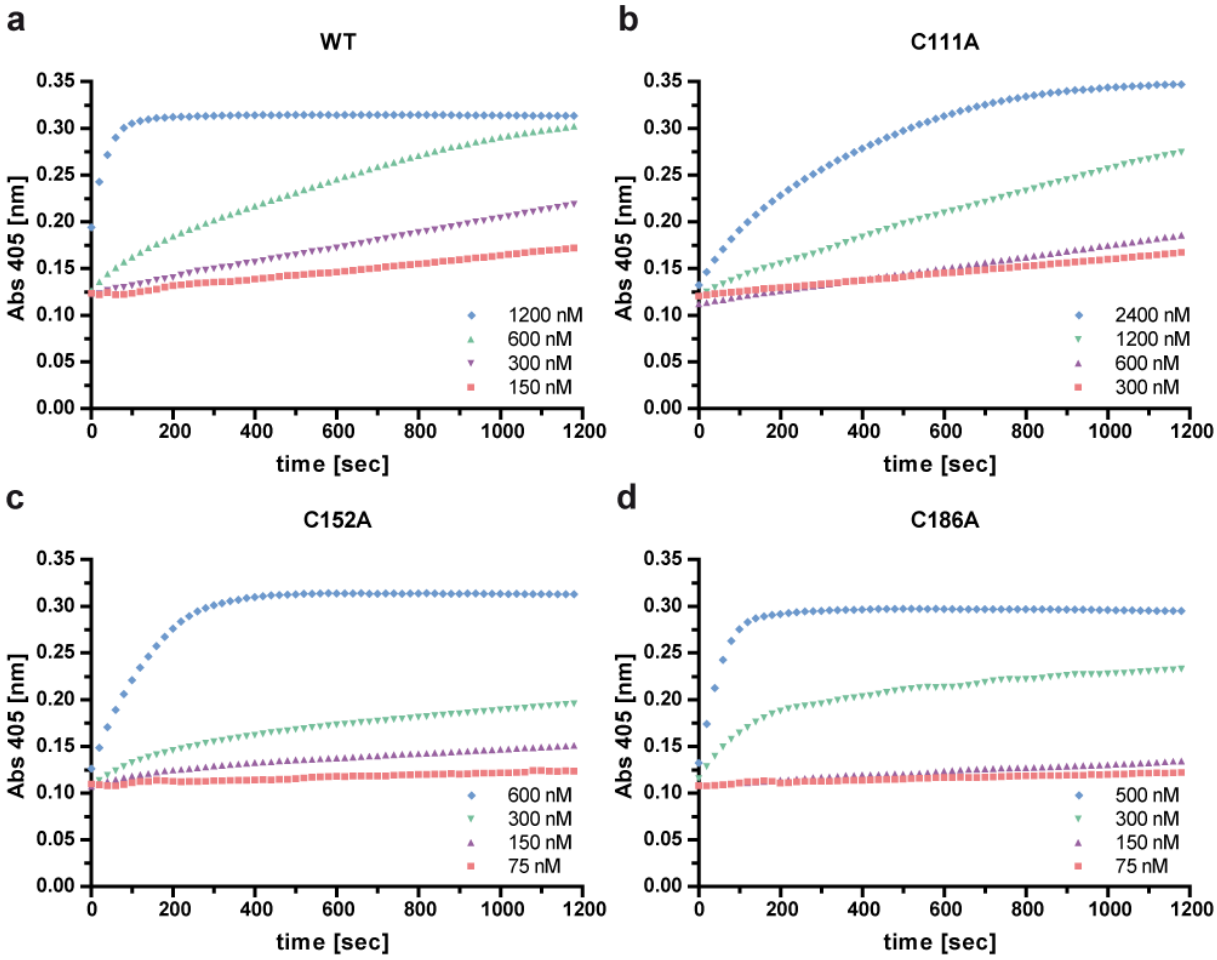

Fig. 32 Verification of recombinant mutant AtEH7 activity. (a-d)The activity of recombinant mutant C111A, C152A and C186A AtEH7 was assayed alongside WT AtEH7 at pH 8.0 using the previously introduced enzyme kinetics assay (2.2.3.10) where the turnover of the epoxide substrate S-NEPC into UV-quantifiable *para*-nitrophenol by AtEH7 was monitored over time. WT and mutant AtEH7 was employed at different concentrations as indicated in the respective figures. Upon addition of the epoxide substrate, the absorbance at 405 nm was monitored over time for a total of 20 min. Values represent the mean values of two technical replicates.

activity of C186A mutant AtEH7, on the other hand, was not significantly ($p \geq 0.05$) affected by a preincubation of the enzyme with either **Ner** or **≡Ner** (Fig. 33d). Compared to the DMSO control, an activity of 98.7% after pretreatment with **Ner** ($p = 0.7504$) and of 86.7% after pretreatment with **≡Ner** ($p = 0.0747$) was still retained (Fig. 33e), indicating that both compounds did not bind to the C186A mutant and thus confirming that **Ner** inhibits AtEH7 through binding to Cys186. However, the relative decrease in AtEH7 activity after **Ner**- and **≡Ner**-pretreatment was not directly comparable between the individual forms of the enzyme and the reported values only account for the respective assay conditions, as varying concentrations of the enzymes had to be used due to the differential specific activity of the enzymes. Yet, the activity

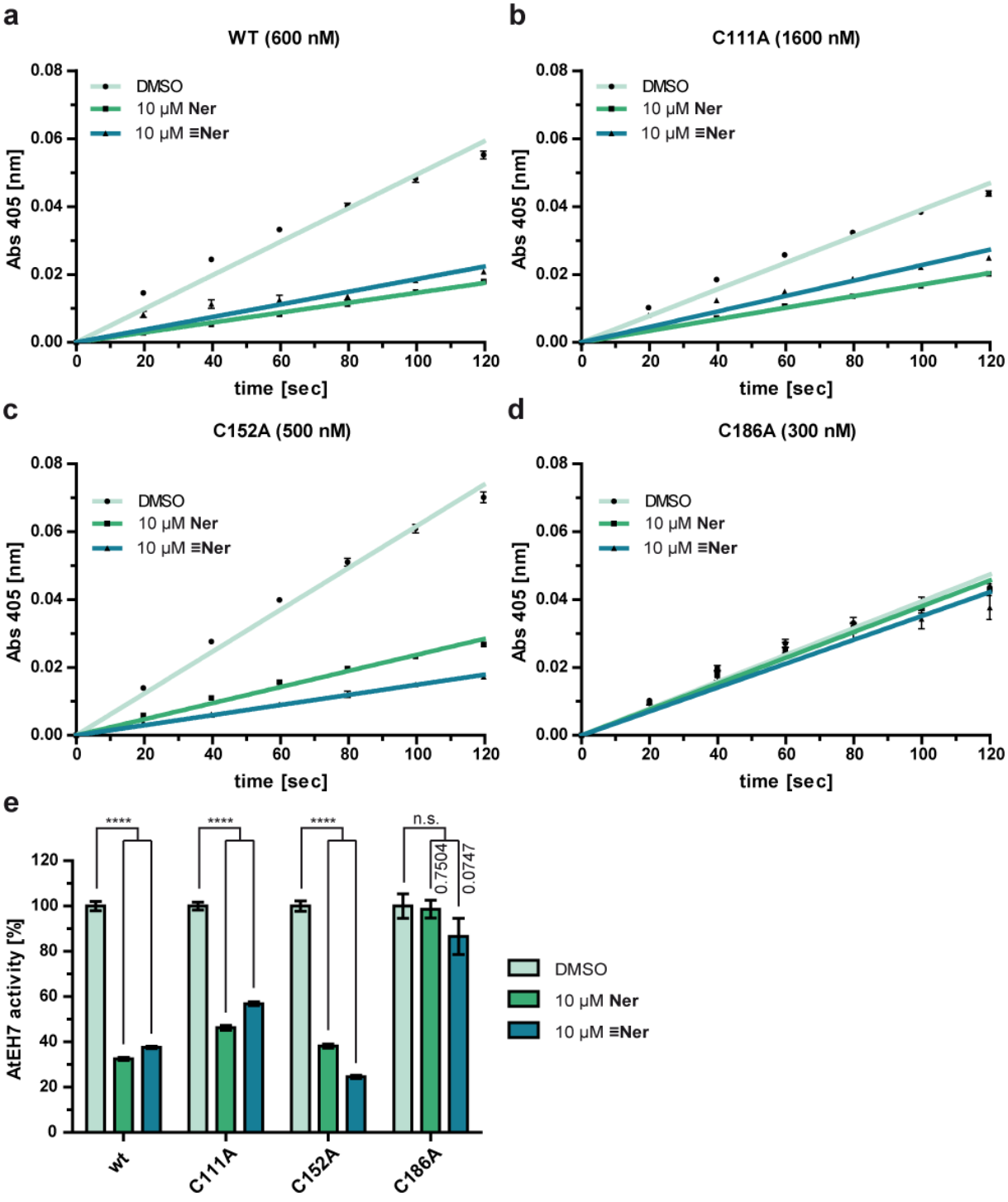

Fig. 33 Enzyme kinetics studies of mutant AtEH7 activity. (a-d) Enzymatic activity of WT and mutant C111A, C152A and C186A AtEH7 was determined at pH 8.0 using the previously introduced enzyme kinetics assay (2.2.3.10) where the turnover of the epoxide substrate S-NEPC into UV-quantifiable *para*-nitrophenol by AtEH7 was monitored over time. Indicated amounts of recombinant WT and mutant AtEH7 were pretreated with either 10 µM **Ner**, 10 µM **≡Ner** or DMSO for 10 min prior to the addition of the substrate to start the enzymatic reaction. Substrate turnover in the linear range (R^2 >0.9 for all data points per treatment) measured at a wavelength of 405 nm is shown. Values (net absorbance t_n subtracted by initial absorbance t_0) represent the mean values (± SD) of three technical replicates. (e) The remaining activity of **Ner**- and **≡Ner**-pretreated WT and mutant AtEH7 at 120 sec after the addition of the substrate was normalised to the respective DMSO control and statistical significance for a reduction in AtEH7 activity was assessed using an unpaired two-tailed *t*-test (**** $p < 0.0001$, n.s. = not significant).

of WT, C111A and C152A AtEH7 was significantly reduced after **Ner**-and **≡Ner**-pretreatment compared to the respective DMSO controls, while the activity of C186A AtEH7 was not significantly altered by pretreatment with either of the two compounds even though the lowest amount of the purified enzyme had to be employed for this mutant. Thus, all experimental data suggests that **Ner** binds to a free cysteine residue, i.e. Cys186, of AtEH7 in Arabidopsis and therefore possesses a similar mode of binding as is known for its human target enzymes.

Since **Ner** is expected to bind to Cys186 of AtEH7 based on the previous data, this residue was further confirmed as the binding site of **Ner** using bioinformatics analyses. The ConSurf server is a web tool that makes use of the phylogenetic relations between a target sequence and other homologous sequences to evaluate the evolutionary conservation scale for each amino acid position within the sequence of a protein (2.2.5.5; Fig. 34).

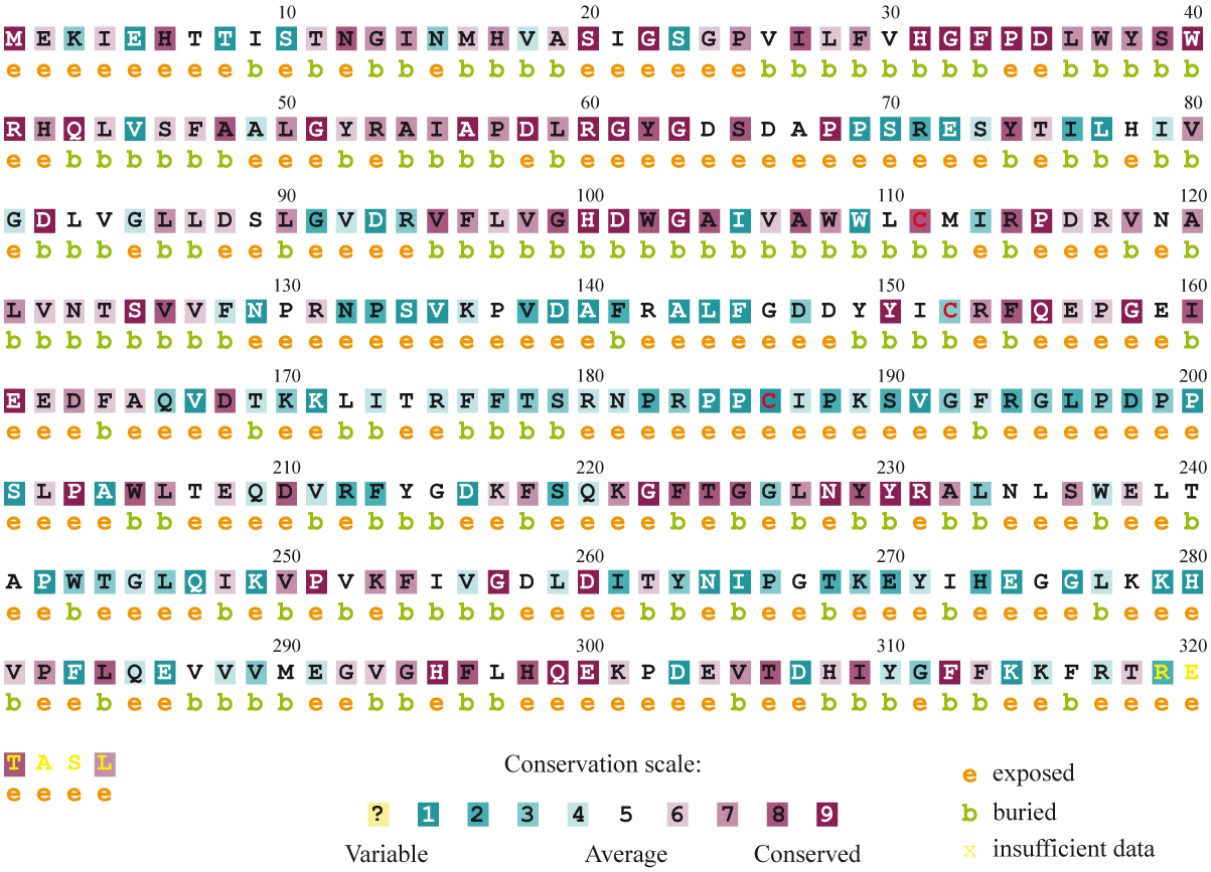

Fig. 34 AtEH7 sequence features. The sequence of AtEH7 was analysed using the ConSurf web server (2.2.5.5) to determine the evolutionary conservation scale of each amino acid position based on phylogenetic relations with 150 other homologous sequences. In addition to the amino acid conservation scale, the analysis gives further information about the surface exposure of each amino acid.

For AtEH7, the sequence analysis showed that Cys186 is not conserved among homologous sequences as this amino acid position is very variable with a conservation scale of only 1. Cys152 had a higher conservation scale of 3, rendering this amino acid position still variable. Cys111, on the contrary, displayed a considerably higher conservation scale of 8, rendering this amino acid position very conserved. Furthermore, the sequence analysis of AtEH7 with ConSurf also proposed the solvent exposure for each amino acid position. While Cys111 and Cys152 were buried inside the protein, Cys186 was positioned within a region of exposed amino acid residues. Thus, Cys186 was the only cysteine residue of AtEH7 predicted to be surface exposed. This result supports the previous finding that Cys186 is the binding site of **Ner** to AtEH7.

In addition to the phylogenetic analysis with ConSurf, a homology model for AtEH7 based on the published structure of the potato sEH StEH1 was generated with the help of Geronimo Heilmann, University of Duisburg-Essen using SWISS-MODEL (2.2.5.3; Fig. 35).

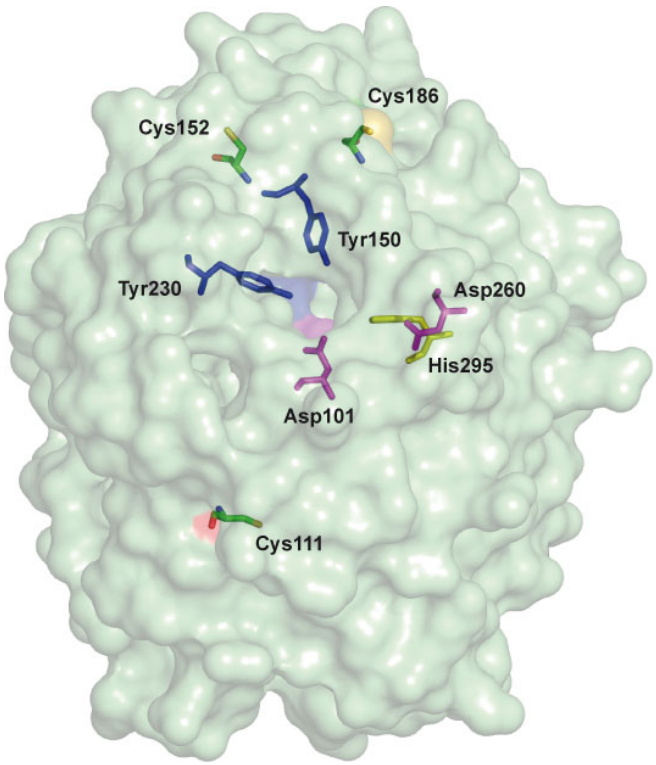

Fig. 35 AtEH7 structure homology model. The 3D structure of AtEH7 was modelled based on the structure of the potato sEH StEH1 (2.2.5.3). The active site residues of the enzyme comprising Asp101, Tyr230 and His295 as well as Tyr150 and Asp260 which additionally play a role for the reaction mechanism of the EH are highlighted at the centre of the structure. The three cysteine residues Cys111, Cys152 and Cys186 that are present in the Sequence of AtEH7 were coloured by element as they are considered to be potential binding sites of **Ner**.

The structure homology model showed that AtEH7 is a typical representative of the sEHs with the Asp101/His295/Asp260 residues most likely forming the catalytic triad at the active site of the enzyme. The two tyrosine residues Tyr150 and Tyr230, which are positioned within the lid domain, presumably hydrogen bond to the oxygen of the epoxide functional group, thereby positioning the epoxide substrate at the active centre. This homology model further supported the insights gained from the ConSurf analysis being that Cys111 and Cys152 are not exposed to the surface of the protein, while Cys186 is surface exposed. Here, the amino acid side chain of Cys186 with the nucleophilic sulfhydryl group was protruding to the outside. Therefore, Cys186 is not involved in intramolecular disulphide bridge formation and is thus freely accessible for **Ner**. Thus, the bioinformatical analyses further confirmed Cys186 as the binding site of AtEH7 for **Ner**.

4. Discussion and Outlook

SA plays a major role as a plant hormone in signalling, mediating diverse important physiological processes as well as plant defence mechanisms upon a pathogen attack, resulting in plant immunity. Due to its important role in maintaining the physical integrity of a plant, SA signalling has been intensively studied over the past decades. However, a complete understanding of this important signalling pathway and the proteins involved therein is still lacking. Especially the role of kinases, a class of enzymes that play an important role in signal transduction in a wide variety of signalling pathways, including those involved in the response to a pathogen infection, is unknown. Consequently, the identification of new SA-binding proteins or proteins effecting SA levels is being promoted by various studies involving HT screening methodologies.

The present work is based on preliminary experiments obtained from a HT forward chemical genetics screen of a comprehensive kinase inhibitor library employing SA-responsive *PR1p::GUS A.thaliana* seedlings for the identification of SA signalling agonists (Fig. 11). During that work, the irreversible pan-HER TKI **Ner**, which is approved for the treatment of early-stage as well as advanced or metastatic HER2-positive breast cancer, was identified to promote the release of SA in Arabidopsis. To determine the direct molecular targets of **Ner** in Arabidopsis and thereby presumably identify new proteins involved in SA signalling, chemoproteomics was used. To this end, an alkyne-tagged **Ner** derivative (**≡Ner**) was employed as a chemical probe for target labelling and affinity enrichment that allowed for the subsequent target identification using MS-based proteomics.

4.1 ≡Ner is a functional version of Ner

Since structural modifications of bioactive small molecules such as the introduction of an alkyne handle can dramatically alter a compounds activity (see 1.1.1), **≡Ner** was first confirmed to be fully functional in labelling the human target enzymes of **Ner** in HeLa cell culture. Indeed, the labelling with **≡Ner** resulted in the presence of a protein band corresponding to the size of the HER kinases, which was not only competable with **Ner** (Fig. 12), but also with the TKIs afatinib and gefitinib (Fig. 13) and which could be identified as EGFR/HER2 by MS-based chemoproteomics analysis (Fig. 14). With

a functional **Ner**-derived probe at hand, the target enzymes of **Ner** in Arabidopsis were further investigated in the present work.

4.2 AtEH7 is a direct target of Ner in Arabidopsis

Initial labelling experiments with **≡Ner** in Arabidopsis using intact root protoplasts (Fig. 15) or protein extract from different tissues (Fig. 17) all revealed the presence of a single protein band at a MW of about 37 kDa. Subsequent submission of the labelled protein band to an IDG followed by MS-based analysis led to the unexpected identification of a sEH, i.e. AtEH7 (named after the most recent nomenclature as found in Pineau *et al*.[188]), which is localised in the plant peroxisomes, as a putative direct molecular target of **≡Ner** and hence **Ner** in *A. thaliana*, instead of a kinase (Fig. 16 and Fig. 18). Further putative targets that were identified from the labelling of seedling extract with **≡Ner** could be rejected due to different criteria for exclusion. The selectivity of **≡Ner** and **Ner** for AtEH7 was demonstrated by an OBD after labelling of Arabidopsis seedling extract (Fig. 20) which included the two structurally related control probes **≡Ctrl1**, the electrophilic linker of **≡Ner** and **≡Ctrl2**, the **≡Ctrl1** moiety linked to 6-aminoquinoline (Fig. 38). Both probes were shown to be functionally inactive in labelling the 37 kDa band (Fig. 19) and therefore allowed for the analysis of indirect effects of **Ner** by analysing the global target enzyme repertoire of all probes under evaluation. Due to the selectivity of **Ner** for AtEH7 as the only potential covalent target, this EH is suggested to play a role in SA signalling. The identification of non-covalent binding partners of **Ner** that may have contributed to the observed SA phenotype through the induction of *PR-1* expression was however not covered by the conducted experiments.

AtEH7 was on the one hand confirmed as a direct molecular target of **Ner** by using chemical labelling of AtEH7-deficient *eh3-2* Arabidopsis seedlings (named after the previous nomenclature as in Cassin-Ross *et al*.[301]) in direct comparison with Col-0 seedlings (Fig. 22). On the other hand, recombinant WT AtEH7 expressed in and purified from *E.coli* BL21 (DE3) (Fig. 23) was used in a spike-in experiment for chemical labelling with **≡Ner** (Fig. 24) and was additionally employed in an enzyme assay with **Ner** after the EH activity of the purified enzyme was confirmed (Fig. 25). **Ner** was found to inhibit the activity of recombinant AtEH7 with an IC_{50} of 38.6 nM

(Fig. 26). Moreover, the IC_{50} of **Ner** for the inhibition of AtEH7 labelling was determined to be 60.6 nM (Fig. 27), which falls into about the same nanomolar range as the IC_{50} observed for the inhibition of AtEH7 activity. These experiments thus likewise confirmed AtEH7 as a direct molecular target of **Ner** in Arabidopsis. Furthermore, the two structurally related compounds pelitinib and gefitinib that were identified as moderately active hits from the initial screen for SA agonists additionally showed inhibition of AtEH7 in the enzyme assay, but with considerably higher IC_{50} values of 7.0 µM and 33.4 µM, respectively (Fig. 26). This finding suggests that all three TKIs, that share EGFR as a common target in human, coherently act as SA agonists based on a similar mode of action via targeting AtEH7. However, it cannot be excluded that pelitinib and gefitinib might have further targets in Arabidopsis. The other primary active screening hits besides **Ner** however seem to enhance the release of SA via other modes of action, as they did not visibly impact on the labelling of AtEH7 with **≡Ner** (Fig. 28).

Many kinase inhibitors are known to target not only a single kinase, but rather inhibit several different specific or unspecific off-target enzymes. A large-scale study by Davis *et al*. on the selectivity of kinase inhibitors investigated the activity of a broad panel of kinase inhibitors, including **Ner**, on a selection of different kinases from different subfamilies comprising about 80% of the human catalytically active kinome. The results from this study indicate that most of the tested kinase inhibitors showed a poor selectivity for their dedicated targets, not only within the subfamily of their target(s), but also within other kinase subfamilies[127]. Another comprehensive study by Lanning *et al*. has for example investigated the off-target effects of PF-6274484[302], a covalent EGFR inhibitor such as **Ner**, in human cell culture using chemoproteomics, which allowed the investigation of other targets beyond kinases. This study showed that the specific off-targets of PF-6274484 indeed almost exclusively comprise other kinases or other enzymes containing active site or conserved functional cysteines[303]. It was therefore even more surprising that **Ner**, in Arabidopsis, neither inhibits a kinase nor another ATP-binding protein, but rather solely targets an EH with high selectivity, as cases in which a kinase inhibitor targets an EH have only scarcely been described[304]. However, EHs are not only exceptional targets of kinase inhibitors, but have also rarely been described as targets of chemical probes. Such an example is the use of a biotinylated

version of the electrophilic metabolite 15-deoxy-Δ-prostaglandin J2 which was found to target rat sEH through covalent modification of a catalytically inactive cysteine residue in close proximity to the EH active site using MS-based proteomics[305]. In any case, the present work underlines the versatility of chemical probes in the often challenging identification and confirmation steps when studying the target enzymes of small molecule inhibitors that were for example identified from a phenotypic screen[306,307]. Combining chemoproteomics with chemical genetics thus allows to reliably unravel both, the direct target enzymes as well as the off-targets of small molecule inhibitors, even if these are completely unpredictable and imply a novel biological mechanism. This rapid approach is equally applicable to fully differentiated, multicellular organisms like plants[308], as has been reiterated in this work. In addition, especially the potential of cysteine-directed covalent inhibitors in addressing different enzyme classes and their employment in the design of new chemical probes has once again been demonstrated[309].

4.3 Ner binds to Cys186 of AtEH7

After the discovery and confirmation of AtEH7 as a target enzyme of **Ner**, the precise binding site of **Ner** in AtEH7 was further determined in this work. Since **Ner** binds to a conserved cysteine residue located within the ATP-binding pocket of its human HER-receptor targets, it was first assessed whether **Ner** possesses a similar mode of covalent binding via targeting a free and chemically reactive cysteine residue of AtEH7, i. e. a reduced cysteine residue with a free thiol not being involved in the formation of a disulphide bridge in the native state of the protein. To this end, the effect of an alkylation of free cysteine residues with IAM on the labelling with **≡Ner** was studied, indicating that **Ner** indeed targets one of the three cysteine residues present in the sequence of AtEH7 (Fig. 29). In order to ascertain to which of the cysteine residues **Ner** exactly binds, the three AtEH7 single mutants C111A, C152A and C186A were generated using site-directed mutagenesis. The recombinant mutant AtEH7 proteins expressed in and purified from *E.coli* BL21 (DE3) (Fig. 40) were used in a spike-in experiment for a chemical labelling with **≡Ner** (Fig. 31) as well as for an enzyme kinetics assay with **≡Ner** and **Ner** (Fig. 33) upon confirmation of their activity (Fig. 32), as previously described for recombinant WT AtEH7. These experiments consistently

showed that **Ner** binds to Cys186 of AtEH7, as the C186A mutant was neither labelled with **≡Ner**, nor did **≡Ner** or **Ner** significantly impact on the activity of this mutant. The confirmation of Cys186 as the binding site of **Ner** in AtEH7 was further supported through bioinformatics analyses that demonstrated the low conservation scale of this residue among homologous sequences and the probable exposition of Cys186 on the cell surface, with the nucleophilic sulfhydryl group positioned towards the surrounding (Fig. 34 and Fig. 35). Cys111 and Cys152, on the contrary, were suggested to be more conserved residues that are additionally buried inside the protein and thus are not solvent accessible.

In Arabidopsis, seven gene loci coding for different EHs are known. These are, in accordance with Pineau *et al.*, AtEH1 (At3g05600.1), AtEH2 (At2g26750.1), AtEH3 (At2g26740.1), AtEH4 (At4g15955.3), AtEH5 (At4g15960.1), AtEH6 (At3g51000.1) and AtEH7 (At4g02340.1)[188]. All seven Arabidopsis EHs contain an α/β-hydrolase fold as confirmed by InterPro (release 77.0) analysis[310]. From an evolutionary point of view, AtEH6 early diverged from the other Arabidopsis EHs and is therefore more distantly related to them. Phylogenetic analysis among EHs from embryophyta showed that AtEH6 belongs to a clade containing EHs from mono- and dicotyledones that probably arose from a common ancestor of seed plants, while the other Arabidopsis EHs, which are more closely related to each other, belong to a clade of EHs from dicotyledones. The further diversification into different EH isoforms in angiosperms probably occurred in response to the higher complexity of their reproduction mechanisms[188]. Up till now, very little is known about the functions of the different isoforms of EHs in Arabidopsis, as in general holds true for the quite scarcely investigated plant EHs[187]. AtEH1 and AtEH3 are the best studied EHs in Arabidopsis, both of which were investigated in a dedicated publication. AtEH1, a cytosolic EH, was described to be involved in the synthesis of poly-hydroxylated cutin monomers through hydrolysis of epoxide-containing C18 fatty acids[188]. Cutin monomers, together with other components, build up the plant cuticle, the outer layer of the plant, which functions as an important physical barrier against environmental influences such as desiccation, bacterial and fungal pathogen attacks or insect herbivores[311,312]. Expression of AtEH3 transcripts is known to be slightly enhanced upon water deprivation as well as strongly enhanced upon exposure to the plant hormone auxin. It was thus postulated that AtEH3 might

function in detoxification of metabolites resulting from the auxin treatment or in the synthesis of cutin monomers, as was later proven for AtEH1, due to the enhanced expression in response to drought stress[216]. Though, the precise function of AtEH3 has not yet been confirmed. Additional reports on Arabidopsis EHs have only been made in the course of more comprehensive screens conducted in Arabidopsis. AtEH2 was identified from a mutant screen to potentially play a role in plant resistance to heavy metals[313]. AtEH3 was furthermore found to be induced upon treatment with methyl vinyl ketone[314]. For AtEH4, AtEH5 and AtEH6, no dedicated function or phenotype have been reported so far. However, AtEH4 was reported to be a probable endoplasmic reticulum (ER) protein, as ER localisation was elucidated using a green fluorescent protein (GFP) fusion construct[278] while the expression of AtEH6 was for example found to be enhanced in developing siliques compared with seedlings using a microarray analysis, as was additionally observed for AtEH1[315]. Peroxisomal-localised AtEH7 (see 3.4) has previously been described to be potentially involved in β-oxidation of fatty acids. In the underlying study, AtEH7, here referred to as EH3, was found to possibly play a role in 2,4-dichlorophenoxybutyric acid (2,4-DB) metabolism and to presumably affect the catabolism of 12-oxo-phytodienoic acid (OPDA). The experiments were carried out using two AtEH7-deficient Arabidopsis mutant lines, the knock-down mutant *eh3-1* and the knock-out mutant *eh3-2*, which was also employed in this work[301].

Even though the different Arabidopsis EH isoforms have been ascribed different functions based on the little information available, their sequences are highly homologous to each other owing to their close phylogenetic relation, as the homology comparison shows (Appendix 17, Fig. 42). Despite their high sequence similarity, Cys186, the binding site of **Ner**, is exclusive to AtEH7. Cys111 and Cys152, both of which were ruled out as potential binding sites of **Ner**, are conserved among all seven Arabidopsis EHs, respectively all Arabidopsis EHs except for the most distantly related AtEH6 which lacks a cysteine residue in alignment with Cys152 of AtEH7. The exclusivity of Cys186 for AtEH7 further strengthens the binding site identification studies employing **≡Ner** and **Ner** and additionally supports the identification of AtEH7 as the sole EH target of **Ner** in Arabidopsis based on the chemoproteomics studies with **≡Ner**. An analysis of the amino acid surface accessibility using NetSurfP-2.0[316]

shows that the other Arabidopsis EHs not only lack a cysteine in homology to Cys186, but do not contain a cysteine residue that is predicted to be exposed and therefore solvent accessible, except for AtEH5, which contains a single cysteine residue predicted to be exposed. This residue (Cys5) is however located at the N-terminus and is thus expected to be cleaved off as shown by MitoFates[317] analysis, since AtEH5 is putatively localised in the mitochondrion. The lack of a cysteine residue that is targetable by **Ner** in the other Arabidopsis EHs hence further fosters the afore-mentioned studies on target and binding site identification.

Beyond that, the present data showed that the labelling of recombinant WT AtEH7 with **≡Ner** was enhanced in the background of the protoplast proteome compared with the labelling of the purified enzyme. The binding of **Ner** to AtEH7 is very likely analogously affected. Since binding of **Ner** to AtEH7 is based on a Michael addition with the sulfhydryl group of Cys186, one possibility for this observation is that this residue is not present in its reduced form, e.g. through oxidative cysteine modification including protein aggregation, which may occur during the protein expression and purification steps or during protein storage[318,319], thereby preventing efficient binding of **Ner** to this residue. However, this modification appears to be reversed in the presence of the lysate. In order to minimise such oxidative damage, the use of a reductant as an additive to the buffer could be advantageous[320] and thus enhance the binding of **≡Ner** and **Ner** to AtEH7 in the absence of the Arabidopsis proteome. Though under reductive conditions, Cu-catalysed oxidation has been described to occur during IMAC[321] and Fenton-type metal-catalysed oxidation reactions have additionally been observed in the presence of other trace metals like Ni(II), which is more regularly used for IMAC, and atmospheric oxygen as the oxidising agent, albeit to a lesser extent than with Cu(II)[322]. The addition of a metal chelator to the buffer could thus be additionally beneficial to prevent oxidative cysteine modification in theory, but this in turn negatively affects the protein purification by IMAC. Hence, optimising a buffer for protein purification and storage is often a more complicated process[320]. Besides, it is possible that the binding of **≡Ner** to AtEH7 via Cys186 is generally more complex than anticipated. In this case, it would thus be possible that additional cofactors or binding partners assist the labelling of AtEH7 with **≡Ner** or that AtEH7 or **≡Ner** undergo metabolisation in the lysate. In human, **Ner** is supposed to be a substrate of CYP3A,

a member of the cytochrome P450 superfamily[323]. Indeed, in a study by Aljakouch *et al*., **Ner** was shown to be metabolised in human cancer cells using label-free Raman microspectroscopy and the respective metabolites of **Ner** were identified by LC-MS. In all the proposed structures of these metabolites, the amino butenoate moiety of **Ner** is hydrolysed, which results in a loss of the α,β-unsaturated carbonyl electrophile[324]. Hence, if **Ner** was similarly metabolised in Arabidopsis, this would rather prevent the binding to AtEH7, than enhancing it, rendering the further options more conceivable. If the binding of **≡Ner** and **Ner** to AtEH7 is actually prevented by oxidative cysteine modification or relies on such a more complex mechanism, this probably also affects the inhibitory potency of **Ner** as determined by the enzyme assay with recombinant WT AtEH7, which could thus be even higher.

The modelled position of Cys186 on the cell surface is not in close proximity to the active site of AtEH7, suggesting that **Ner** inhibits AtEH7 activity through binding to an allosteric pocket. This would implicate that AtEH7 activity is rather inhibited through a conformational change of the enzyme than by directly blocking the entrance to the active site for the physiological substrates of the enzyme. However, it was observed that neither **Ner**, nor pelitinib or gefitinib did inhibit AtEH7 activity completely. The dose-response-curve showed that at high inhibitor concentrations when the endpoint of the sigmoidal curve was reached, AtEH7 still exhibited a remaining activity in comparison to the DMSO-treated control, which was not further decreased when applying higher concentrations of the inhibitor. In this respect, two possible reasons are conceivable. On the one hand, it would be feasible that **Ner** and the structurally related TKIs belong to the class of partial AtEH7 inhibitors. This could be investigated by assessing the enzyme kinetics of AtEH7 inhibition, whereby partial inhibition can be determined by plotting fractional velocity against the reciprocal inhibitor concentration[325]. On the other hand, it is also possible that the low solubility of the inhibitors prevented that high inhibitor concentrations were indeed achieved in the assay. This might be plausible in light of the fact that **Ner** is poorly soluble in aqueous solution, especially at a pH above 5.0 (see 3.5).

It remains however unknown whether Cys186 also plays a physiological role in the regulation of the activity of AtEH7. The concept of redox regulation of cysteine residues

has gained increasing attention as an important mechanism in biology in recent years and regulatory cysteines that are not located at the active site of an enzyme are known as molecular switches that regulate the function of an enzyme[326,327]. Such redox switches have been for example described for different kinases as reviewed by Klomsiri *et al*. and thus play a role in cell signalling processes. Changes in their redox status can either act inhibitory or activating and often regulate protein function in co-occurrence with phosphorylation/dephosphorylation events[327]. However, little is known about the regulation of EH activity in general, and, in particular, there is a lack of knowledge about the potential role of functional cysteines, which especially accounts for the regulation of plant EHs. Although the redox regulation of the rat sEH by the electrophilic metabolite 15-deoxy-Δ-prostaglandin J2 through covalent modification of a catalytically inactive cysteine residue has been reported, as mentioned earlier[305] and phosphorylation was proposed to regulate the activity of leukotriene A_4 hydrolase[328], such examples where EH activity is regulated on the protein level have rarely been described in mammals. The regulation of EH activity rather seems to mostly occur on the transcript level and a variety of distinct inducers for the expression of the different types of EHs has been identified[329-333]. In accordance, the lifetime of mammalian sEHs, which was found to be remarkably low, even at physiological temperatures, has been suggested to be associated with *in vivo* regulation of EHs. Plant sEHs from cress and potato, by contrast, showed considerably longer lifetimes under the same conditions[215]. A regulation of plant EH activity on the protein level is therefore even more conceivable and could be subject to further evaluation. Especially the role of Cys186 in regulating the function of AtEH7 could be worthwhile to study, as redox regulation of EH activity in the oxidising environment of the peroxisomes would present an interesting concept of regulation.

4.4 AtEH7 is linked to plant immunity

Even though plant EHs have been frequently described to be involved in mediating stress response and host defence, which also holds true for AtEH3 and AtEH1, respectively, a potential role for an EH in modulating SA signalling, a key pathway in plant immunity, has not been described in *A. thaliana*, nor in any other plant species before. This study indeed has proven the SA agonist **Ner** as a potent inhibitor of AtEH7,

and therefore directly links EH activity with *PR-1* expression and thus SA signalling for the first time. However, the connection between a peroxisomal EH and plant immunity has previously been established. A study by Wijekoon *et al*. has revealed an involvement of the two EHs NbEH2.1 and NbEH2.2 from *N. benthamiana*, which are predicted to be localised in the plant peroxisomes, in pathogen resistance, as their expression was enhanced upon pathogen challenge. Moreover, virus-induced gene silencing of NbEH2.1 led to a time-delayed appearance of plant lesions after treatment with the fungal pathogen *Colletotrichum destructivum*, while the infection with the further fungal or bacterial pathogens tested was not affected. Due to this finding, NbEH2.1 was hypothesised to play a role in the synthesis of cutin monomers[334]. This assumption was additionally supported by the broad substrate susceptibility of NbEH2.1 for a variety of different fatty acid epoxides produced from oleic acid, *cis*-11-eicosenoic acid, linoleic acid or 9(*S*)-hydroperoxy-10(*E*),12(*Z*)-octadecadienoic acid[335]. Surprisingly, a homology comparison of AtEH7 with these two EHs from *N. benthamiana* shows that AtEH7 is highly homologous to NbEH2.1 (61% identity) as well as to NbEH2.2 (60% identity). Indeed, all three cysteine residues of AtEH7 including Cys186 are conserved among the three protein sequences (Appendix 18, Fig. 43). It would therefore be interesting to investigate whether **Ner** likewise targets NbEH2.1 as well as NbEH2.2 and, if so, whether the inhibition of either one of these two enzymes produces a similar SA phenotype as has been observed for the inhibition of AtEH7. In such a case, this would suggest that these enzymes from two different plant species belonging to distinct plant families exert a homologous function that is linked with plant immunity. By supposing the connection between AtEH7 inhibition and *PR-1* induction, the present work thus highlights the important role of EHs in plant immunity, despite their more popular function in lipid metabolism.

Not only have peroxisomal EHs been previously attributed to plant immunity, but an association between the peroxisomes and plant signalling has furthermore been already ascertained. This does not solely cover a linkage with the production of fatty acid-derived signalling molecules but additionally with plant hormone signalling, including SA signalling. Both, C16 as well as C18 fatty acids and their derivatives have been either directly or indirectly associated with plant defence and thus participate in plant immunity. Indirect functions include their roles as signalling molecules that induce

plant defence responses or their involvement in building up cutin monomers. On the other hand, fatty acids can directly function as antimicrobial compounds[336]. Degradation of fatty acids occurs mainly in the peroxisomes, which are well known as an 'oxidative' compartment. Indeed in plants, the peroxisomes are the only place where β-oxidation, the primary route of fatty acid catabolism, takes place[337,338]. As being the site of oxidative fatty acid degradation, the peroxisomes are involved in lipid metabolism and thus in cellular signalling[339]. In the course of oxidative fatty acid breakdown, an important class of fatty acid-derived metabolites, i.e. oxygenated lipids, the so called oxylipins, are produced[340,341]. Oxylipins can be either enzymatically or non-enzymatically obtained from polyunsaturated fatty acids and several of these oxylipins likewise play an essential role as signalling molecules[342,343]. In plants, oxylipins, which have been described to possess a variety of different physiological functions including plant defence against pathogen infections, are mainly produced from polyunsaturated C18 fatty acids via the lipoxygenase (LOX) pathway. Here, LOXs transform fatty acids such as linoleic acid (18:2) or linolenic acid (18:3) into hydroperoxide intermediates, which serve as substrates for various downstream processing enzymes that produce a multitude of different classes of oxylipins. These include the peroxygenases, which produce epoxides as well as epoxy alcohols from hydroperoxides, some of which are known as endogenous substrates of plant EHs (see 1.4) [341,344]. Prominent examples for oxylipins are the jasmonates, which comprise the phytohormone JA and its methyl derivatives as well as the JA precursor OPDA and the JA amino acid conjugate jasmonoyl-*L*-isoleucine (JA-Ile) which are all biologically active compounds[343,345,346]. JA functions as a signalling component mainly in response to abiotic stress, wounding, as for example induced by insect herbivores, and necrotic fungal pathogens[346]. Thus, the relevance of oxylipins for JA signalling is obvious, while a role of (oxygenated) lipids in SA signalling seems to not have been described before.

Apart from fatty acids, not only the precursors of the plant hormone and oxylipin JA, but additionally the precursors of the phytohormones auxin and SA were likewise demonstrated to undergo β-oxidation in the peroxisomes as reviewed by Kao *et al*. (Fig. 36)[347]. In addition to the main route of SA biosynthesis from chorismate via isochorismate following the ICS pathway in the plant chloroplasts (see 1.3), the PAL

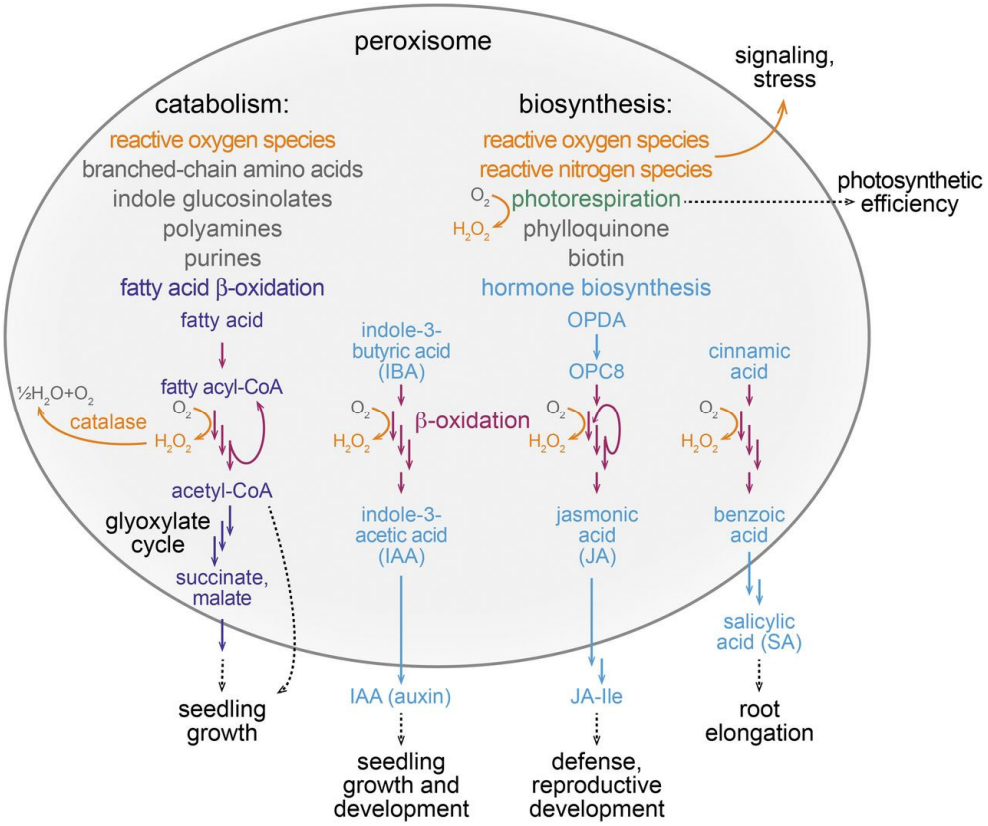

Fig. 36 β-oxidation in the plant peroxisome. In the plant peroxisome, diverse catabolic as well as biosynthetic processes take place. For some of these processes, β-oxidation plays a major role. On the one hand, lipid droplet-derived fatty acids are imported into the peroxisomes where they undergo degradative β-oxidation for energy production. On the other hand, in the course of phytohormone biosynthesis, indole-3-butyric acid (IBA), OPDA-derived 3-oxo-2-(2′-pentenyl)-cyclopentane-1-octanoic acid (OPC8) and *trans*-cinnamic acid, the precursors of auxin, JA and SA, respectively, likewise undergo β-oxidation in the peroxisome. Taken from Kao *et al*., 2018[347]. Copyright (2018) American Society of Plant Biologists.

pathway includes the transformation of chorismate into benzoic acid as the direct precursor of SA. Here, L-phenylalanine as an intermediate product of this pathway is converted into *trans*-cinnamic acid in the plant cytosol[348]. *trans*-cinnamic acid, probably as a coenzyme A (CoA) ester, is next imported into the plant peroxisome where benzoyl-CoA is produced from cinnamoyl-CoA acid through β-oxidation as has been confirmed for Arabidopsis[347,349]. Benzoic acid is next derived from benzoyl-CoA and released into the cytosol where SA is synthesised[347,350].

Besides being the place where the precursors of the phytohormones SA and JA are produced, the peroxisomes furthermore represent a site of plant hormone crosstalk[347]. Crosstalk between SA and JA signalling is well known in the regulation of plant defence mechanisms in response to attacks of biotrophic or necrotrophic pathogens as well as

in response to herbivory[351]. Indeed, the two phytohormones SA and JA have been reported to act both antagonistically as well as synergistically, while most reports focus on the antagonistic nature of SA-JA crosstalk which has been primarily studied in the context of wounding[340]. In the majority of cases described, this antagonism was based on the suppressive role of SA on JA signalling, in particular on JA biosynthesis and JA-dependent induction of proteinase inhibitor genes[340,351]. JA biosynthesis for example is directly controlled through SA-mediated suppression of *LOX2* and *allene oxide synthase* gene expression as well as through SA-mediated inhibition of catalase 2 activity[352-354]. Despite these findings, there is additional evidence that the suppression of the JA biosynthesis pathway by SA is not necessary for the antagonistic effect of SA on the expression of JA-responsive marker genes like *PDF1.2* and *VSP2,* which leads to a downregulation of JA signalling[355]. Certainly, cytosolic NPR1 as an important key player in SA-JA crosstalk has been found to be required for this antagonistic effect of SA on JA signalling while it was further suggested that SA-mediated redox changes based on increased levels in glutathione play a role in JA signalling decrement[352,356]. However, the kinetics of SA and JA signalling regulation are highly dynamic[356] and thus not only the control of JA signalling by SA is known. On the contrary, a case where the inhibition of JA production as well as of the accumulation of wound-inducible gene transcripts led to an increase in SA levels upon wounding has additionally been reported in *Nicotiana tabacum*[357]. This illustrates how tightly SA signalling and JA signalling are interrelated with each other and makes it even more difficult to elucidate how inhibition of AtEH7 activity could possibly induce SA signalling through the release of SA, causing the induction of *PR-1* expression.

Furthermore, not only a connection between the SA signalling pathway and the plant peroxisomes has already been established, but also the role of sEHs in modulation of signalling molecules, like those derived from polyunsaturated fatty acids that play a role in inflammation as part of the innate immune response and thus immunity, has been intensively studied in human before[358,359]. Here, epoxyeicosatrienoic acids (EETs) produced from arachidonic acid via the cytochrome P450 pathway, which act mainly anti-inflammatory, are hydrolysed to their corresponding dihydroxy-eicosatrienoic acids (DHETs) by sEH. As a result of this important role, sEH has become a target enzyme for the treatment of inflammatory diseases since its inhibition

keeps up the level of anti-inflammatory EETs[359]. But not only mammals have been a subject of study with respect to the role of EH activity in immunity and signalling. The inhibition of a mammalian sEH homologue in the midgut of female mosquitos by AUDA has for example been shown to induce antibacterial responses, leading to a local reduction of the bacterial load and thus identified epoxy fatty acids from host blood as regulators of immune response[360].

In conclusion, the results presented in this work clearly highlight the versatility of chemical probes for chemoproteomics-based target identification studies of small molecule inhibitors. Here, **Ner**, which induced *PR-1* expression and thus SA signalling in *PR1p::GUS* Arabidopsis seedlings, was proven a nanomolar allosteric inhibitor of peroxisomal-localised AtEH7 which covalently targets a surface exposed cysteine residue, i.e. Cys186. Based on these results it was proposed that inhibition of AtEH7 led to an induction of SA signalling, suggesting a role for AtEH7 in plant immunity. In turn, these results give rise to further investigations. Although the concept of plant hormones regulating EH levels is known[212], as has been shown for methyl jasmonate[220] as well as auxin[216] and ethylene[361], the activation of the SA signalling pathway through inhibition of an EH would represent a new way of regulation that needs to be further explored. First, the biological role of AtEH7 and consequently how its inhibition could lead to induction of SA signalling is completely unknown. On the one hand, it is possible that AtEH7 is either directly involved in SA signalling or indirectly by modulating those components that are directly involved therein. On the other hand, it is also well conceivable that the induction of the SA signalling pathway was caused by perturbation of the JA signalling cascade. Plant signalling is highly complex and integrated and the crosstalk of these two signalling pathways is well described. This option would thus imply that AtEH7 functions in JA signalling instead of SA signalling. In fact, JA signalling is even more closely associated with the peroxisomes as they house the final steps of JA biosynthesis[346,347]. Moreover, the proposed role of AtEH7 in the catabolism of the JA precursor OPDA and thus its potential involvement in β-oxidation further supports the possibility that AtEH7 is actually functioning in JA signalling rather than in modulating SA signalling. For instance, it would thus be beneficial to monitor the levels of OPDA and other jasmonates in Arabidopsis Col-0 and *eh3-2* mutant plants after treatment with **Ner** to confirm the involvement of AtEH7

in OPDA catabolism, thereby gaining deeper insight into the putative role of AtEH7 in JA signalling. Furthermore, testing the effect of **Ner** on the OPDA-inducible Arabidopsis jasmonate reporter line *VSP1::GUS*[362], could give an idea about the direct impact of **Ner** on the JA signalling cascade. Second, the physiological epoxide substrate of AtEH7 is so far unknown and therefore it is uncertain where this substrate acts and what its specific function is. Albeit, it appears to be a modulator of plant immunity, which under normal conditions is steadily turned over into its diol form, while inhibition of AtEH7 leads to accumulation of the epoxide form. This substrate can either be directly involved in plant defence signalling or contribute to plant immunity through being involved in the synthesis of cutin monomers. Since, it has been proposed that AtEH7 homologues are exclusive to plant species belonging to the Brassicaceae family[277], which comprises oilseed plants that are particularly rich in lipid droplets mainly storing neutral lipids, i.e. fatty acid-containing triaglycerols and sterol esters[363], this concept of SA signalling activation through inhibition of an EH does apparently not seem to be common among the plant kingdom. This is however contrasted by the fact that AtEH7 shows a high sequence identity with NbEH2.1 as well as NbEH2.2 from the Solanaceae species *N. benthamiana*, which play a role in plant immunity and share a cysteine residue in homology with **Ner**-targeted Cys186 in Arabidopsis AtEH7. Thus it is possible that such a regulatory mechanism could actually still be more widespread among the plant kingdom, giving rise to further investigations into this direction.

5. References

1 Ong, S. E. *et al.* Identifying the proteins to which small-molecule probes and drugs bind in cells. *P Natl Acad Sci USA* **106**, 4617-4622 (2009).

2 Lomenick, B., Olsen, R. W. & Huang, J. Identification of direct protein targets of small molecules. *ACS Chem Biol* **6**, 34-46 (2011).

3 Schenone, M., Dancik, V., Wagner, B. K. & Clemons, P. A. Target identification and mechanism of action in chemical biology and drug discovery. *Nat Chem Biol* **9**, 232-240 (2013).

4 Serrano, M., Kombrink, E. & Meesters, C. Considerations for designing chemical screening strategies in plant biology. *Frontiers in Plant Science* **6**, 131 (2015).

5 Dejonghe, W. & Russinova, E. Plant Chemical Genetics: From Phenotype-Based Screens to Synthetic Biology. *Plant Physiology* **174**, 5-20 (2017).

6 Bantscheff, M. & Drewes, G. Chemoproteomic approaches to drug target identification and drug profiling. *Bioorgan Med Chem* **20**, 1973-1978 (2012).

7 Moellering, R. E. & Cravatt, B. F. How Chemoproteomics Can Enable Drug Discovery and Development. *Chemistry & Biology* **19**, 11-22 (2012).

8 Liu, Y., Patricelli, M. P. & Cravatt, B. F. Activity-based protein profiling: the serine hydrolases. *Proc Natl Acad Sci U S A* **96**, 14694-14699 (1999).

9 Cravatt, B. F., Wright, A. T. & Kozarich, J. W. Activity-based protein profiling: from enzyme chemistry to proteomic chemistry. *Annu Rev Biochem* **77**, 383-414 (2008).

10 Ostrowski, K. & Barnard, E. A. Application of isotopically labelled specific inhibitors as a method in enzyme cytochemistry. *Exp Cell Res* **25**, 465-468 (1961).

11 Fenteany, G. *et al.* Inhibition of proteasome activities and subunit-specific amino-terminal threonine modification by lactacystin. *Science* **268**, 726-731 (1995).

12 Shi, G. P., Munger, J. S., Meara, J. P., Rich, D. H. & Chapman, H. A. Molecular cloning and expression of human alveolar macrophage cathepsin S, an elastinolytic cysteine protease. *J Biol Chem* **267**, 7258-7262 (1992).

13 Bernstein, K. E., Welsh, S. L. & Inman, J. K. A deeply recessed active site in angiotensin-converting enzyme is indicated from the binding characteristics of biotin-spacer-inhibitor reagents. *Biochem Biophys Res Commun* **167**, 310-316 (1990).

14 Steven, F. S., Griffin, M. M., Williams, L. A., Clarke, N. W. & Maier, H. Labelling of tumour cells with a biotinylated inhibitor of a cell surface protease. *J Enzyme Inhib* **4**, 337-346 (1991).

15 Sin, N. *et al.* The anti-angiogenic agent fumagillin covalently binds and inhibits the methionine aminopeptidase, MetAP-2. *Proc Natl Acad Sci U S A* **94**, 6099-6103 (1997).

16 Bogyo, M. *et al.* Covalent modification of the active site threonine of proteasomal beta subunits and the Escherichia coli homolog HslV by a new class of inhibitors. *Proc Natl Acad Sci U S A* **94**, 6629-6634 (1997).

17 Bogyo, M., Verhelst, S., Bellingard-Dubouchaud, V., Toba, S. & Greenbaum, D. Selective targeting of lysosomal cysteine proteases with radiolabeled electrophilic substrate analogs. *Chem Biol* **7**, 27-38 (2000).

18 Greenbaum, D., Medzihradszky, K. F., Burlingame, A. & Bogyo, M. Epoxide electrophiles as activity-dependent cysteine protease profiling and discovery tools. *Chem Biol* **7**, 569-581 (2000).

19 Kato, D. *et al.* Activity-based probes that target diverse cysteine protease families. *Nat Chem Biol* **1**, 33-38 (2005).

20 Ratcliffe, S. J., Yi, T. & Khandekar, S. S. Synthesis and characterization of 5'-p-fluorosulfonylbenzoyl-2' (or 3')-(biotinyl)adenosine as an activity-based probe for protein kinases. *J Biomol Screen* **12**, 126-132 (2007).

21 Patricelli, M. P. *et al.* Functional interrogation of the kinome using nucleotide acyl phosphates. *Biochemistry* **46**, 350-358 (2007).

22 Yee, M. C., Fas, S. C., Stohlmeyer, M. M., Wandless, T. J. & Cimprich, K. A. A cell-permeable, activity-based probe for protein and lipid kinases. *J Biol Chem* **280**, 29053-29059 (2005).

23 Zhao, Q. *et al.* Broad-Spectrum Kinase Profiling in Live Cells with Lysine-Targeted Sulfonyl Fluoride Probes. *J Am Chem Soc* **139**, 680-685 (2017).

24 Shreder, K. R. *et al.* Design and synthesis of AX7574: a microcystin-derived, fluorescent probe for serine/threonine phosphatases. *Bioconjug Chem* **15**, 790-798 (2004).

25 Lo, L. C. *et al.* Design and synthesis of class-selective activity probes for protein tyrosine phosphatases. *J Proteome Res* **1**, 35-40 (2002).

26 Kumar, S. *et al.* Activity-based probes for protein tyrosine phosphatases. *Proc Natl Acad Sci U S A* **101**, 7943-7948 (2004).

27 Kalesh, K. A. *et al.* Peptide-based activity-based probes (ABPs) for target-specific profiling of protein tyrosine phosphatases (PTPs). *Chem Commun (Camb)* **46**, 589-591 (2010).

28 Sieber, S. A., Niessen, S., Hoover, H. S. & Cravatt, B. F. Proteomic profiling of metalloprotease activities with cocktails of active-site probes. *Nat Chem Biol* **2**, 274-281 (2006).

29 Saghatelian, A., Jessani, N., Joseph, A., Humphrey, M. & Cravatt, B. F. Activity-based probes for the proteomic profiling of metalloproteases. *Proc Natl Acad Sci U S A* **101**, 10000-10005 (2004).

30 Chan, E. W., Chattopadhaya, S., Panicker, R. C., Huang, X. & Yao, S. Q. Developing photoactive affinity probes for proteomic profiling: hydroxamate-based probes for metalloproteases. *J Am Chem Soc* **126**, 14435-14446 (2004).

31 Salisbury, C. M. & Cravatt, B. F. Activity-based probes for proteomic profiling of histone deacetylase complexes. *Proc Natl Acad Sci U S A* **104**, 1171-1176 (2007).

32 Vocadlo, D. J. & Bertozzi, C. R. A strategy for functional proteomic analysis of glycosidase activity from cell lysates. *Angew Chem Int Ed Engl* **43**, 5338-5342 (2004).

33 Witte, M. D. *et al.* Ultrasensitive in situ visualization of active glucocerebrosidase molecules. *Nat Chem Biol* **6**, 907-913 (2010).

34 Schröder, S. P. *et al.* Towards broad spectrum activity-based glycosidase probes: synthesis and evaluation of deoxygenated cyclophellitol aziridines. *Chem Commun (Camb)* **53**, 12528-12531 (2017).

35 Fonović, M. & Bogyo, M. Activity-based probes as a tool for functional proteomic analysis of proteases. *Expert Rev Proteomic* **5**, 721-730 (2008).

36 Hong, B. K., Dong, T. & Lei, X. G. Recent advances in target identification by natural product based chemical probes. *Sci China Chem* **59**, 1088-1092 (2016).

37 Gerry, C. J. & Schreiber, S. L. Chemical probes and drug leads from advances in synthetic planning and methodology. *Nat Rev Drug Discov* **17**, 333-352 (2018).

38 Wright, M. H. & Sieber, S. A. Chemical proteomics approaches for identifying the cellular targets of natural products. *Nat Prod Rep* **33**, 681-708 (2016).

39 Xu, J. Q., Li, X. Q., Ding, K. & Li, Z. Q. Applications of Activity-Based Protein Profiling (ABPP) and Bioimaging in Drug Discovery. *Chem-Asian J* **15**, 34-41 (2020).

40 Verhelst, S. H. & Bogyo, M. Chemical proteomics applied to target identification and drug discovery. *Biotechniques* **38**, 175-177 (2005).

41 van Kasteren, S. I., Florea, B. I. & Overkleeft, H. S. Activity-Based Protein Profiling: From Chemical Novelty to Biomedical Stalwart. *Methods Mol Biol* **1491**, 1-8 (2017).

42 Geurink, P. P., Prely, L. M., van der Marel, G. A., Bischoff, R. & Overkleeft, H. S. Photoaffinity labeling in activity-based protein profiling. *Top Curr Chem* **324**, 85-113 (2012).

43 Singh, A., Thornton, E. R. & Westheimer, F. H. The photolysis of diazoacetylchymotrypsin. *J Biol Chem* **237**, 3006-3008 (1962).

44 Wang, S. *et al.* Advanced Activity-Based Protein Profiling Application Strategies for Drug Development. *Front Pharmacol* **9**, 353 (2018).

45 Mackinnon, A. L. & Taunton, J. Target Identification by Diazirine Photo-Cross-linking and Click Chemistry. *Curr Protoc Chem Biol* **1**, 55-73 (2009).

46 Fleet, G. W. J., Porter, R. R. & Knowles, J. R. Affinity Labelling of Antibodies with Aryl Nitrene as Reactive Group. *Nature* **224**, 511-512 (1969).

47 Smith, R. A. G. & Knowles, J. R. Aryldiazirines - Potential Reagents for Photolabeling of Biological Receptor Sites. *Journal of the American Chemical Society* **95**, 5072-5073 (1973).

48 Galardy, R. E., Craig, L. C. & Printz, M. P. Benzophenone triplet: a new photochemical probe of biological ligand-receptor interactions. *Nat New Biol* **242**, 127-128 (1973).

49 Coleman, J. E. Zinc enzymes. *Curr Opin Chem Biol* **2**, 222-234 (1998).

50 Jeffery, D. A. & Bogyo, M. Chemical proteomics and its application to drug discovery. *Curr Opin Biotechnol* **14**, 87-95 (2003).

51 Yang, Y., Fonović, M. & Verhelst, S. H. Cleavable Linkers in Chemical Proteomics Applications. *Methods Mol Biol* **1491**, 185-203 (2017).

52 van Swieten, P. F. *et al.* Development of an isotope-coded activity-based probe for the quantitative profiling of cysteine proteases. *Bioorg Med Chem Lett* **14**, 3131-3134 (2004).

53 Adam, G. C., Sorensen, E. J. & Cravatt, B. F. Trifunctional chemical probes for the consolidated detection and identification of enzyme activities from complex proteomes. *Molecular & Cellular Proteomics* **1**, 828-835 (2002).

54 Speers, A. E., Adam, G. C. & Cravatt, B. F. Activity-based protein profiling in vivo using a copper(I)-catalyzed azide-alkyne [3+2] cycloaddition. *Journal of the American Chemical Society* **125**, 4686-4687 (2003).

55 Yang, Y. L., Hahne, H., Kuster, B. & Verhelst, S. H. L. A Simple and Effective Cleavable Linker for Chemical Proteomics Applications. *Molecular & Cellular Proteomics* **12**, 237-244 (2013).

56 Speers, A. E. & Cravatt, B. F. Profiling enzyme activities in vivo using click chemistry methods. *Chemistry & Biology* **11**, 535-546 (2004).

57 Huisgen, R. 1,3-Dipolar Cycloadditions. Past and Future. *Angew Chem Int Edit* **2**, 565-632 (1963).

58 Bock, V. D., Hiemstra, H. & van Maarseveen, J. H. Cu-I-catalyzed alkyne-azide "click" cycloadditions from a mechanistic and synthetic perspective. *Eur J Org Chem* **2006**, 51-68 (2006).

59 Rostovtsev, V. V., Green, L. G., Fokin, V. V. & Sharpless, K. B. A stepwise Huisgen cycloaddition process: Copper(I)-catalyzed regioselective "ligation" of azides and terminal alkynes. *Angew Chem Int Edit* **41**, 2596-2599 (2002).

60 Haldón, E., Nicasio, M. C. & Pérez, P. J. Copper-catalysed azide-alkyne cycloadditions (CuAAC): an update. *Org Biomol Chem* **13**, 9528-9550 (2015).

61 Chan, T. R., Hilgraf, R., Sharpless, K. B. & Fokin, V. V. Polytriazoles as copper(I)-stabilizing ligands in catalysis. *Organic Letters* **6**, 2853-2855 (2004).

62 Bevilacqua, V. *et al.* Copper-chelating azides for efficient click conjugation reactions in complex media. *Angew Chem Int Ed Engl* **53**, 5872-5876 (2014).

63 Baskin, J. M. *et al.* Copper-free click chemistry for dynamic in vivo imaging. *Proc Natl Acad Sci U S A* **104**, 16793-16797 (2007).

64 Zweerink, S. *et al.* Activity-based protein profiling as a robust method for enzyme identification and screening in extremophilic Archaea. *Nat Commun* **8**, 15352 (2017).

65 Morimoto, K. & van der Hoorn, R. A. L. The Increasing Impact of Activity-Based Protein Profiling in Plant Science. *Plant Cell Physiol* **57**, 446-461 (2016).

66 Arastu-Kapur, S. *et al.* Identification of proteases that regulate erythrocyte rupture by the malaria parasite Plasmodium falciparum. *Nat Chem Biol* **4**, 203-213 (2008).

67 Stolze, S. C. *et al.* The Antimalarial Natural Product Symplostatin 4 Is a Nanomolar Inhibitor of the Food Vacuole Falcipains. *Chemistry & Biology* **19**, 1546-1555 (2012).

68 Staub, I. & Sieber, S. A. beta-lactams as selective chemical probes for the in vivo labeling of bacterial enzymes involved in cell wall biosynthesis, antibiotic resistance, and virulence. *Journal of the American Chemical Society* **130**, 13400-13409 (2008).

69 Niphakis, M. J. & Cravatt, B. F. Enzyme Inhibitor Discovery by Activity-Based Protein Profiling. *Annual Review of Biochemistry, Vol 83* **83**, 341-377 (2014).

70 van Esbroeck, A. C. M. *et al.* Activity-based protein profiling reveals off-target proteins of the FAAH inhibitor BIA 10-2474. *Science* **356**, 1084-1087 (2017).

71 Clegg, M. A., Tomkinson, N. C. O., Prinjha, R. K. & Humphreys, P. G. Small molecules and their role in effective preclinical target validation. *Future Med Chem* **9**, 1579-1582 (2017).

72 Evans, G. A. Designer science and the "omic" revolution. *Nature Biotechnology* **18**, 127-127 (2000).

73 de Hoog, C. L. & Mann, M. Proteomics. *Annu Rev Genom Hum G* **5**, 267-293 (2004).

74 Drewes, G. & Knapp, S. Chemoproteomics and Chemical Probes for Target Discovery. *Trends Biotechnol* **36**, 1275-1286 (2018).

75 Aebersold, R. & Mann, M. Mass spectrometry-based proteomics. *Nature* **422**, 198-207 (2003).

76 Sharma, K. S. Mass spectrometry-The early years. *Int J Mass Spectrom* **349**, 3-8 (2013).

77 Goldstein, E. Ueber eine noch nicht untersuchte Strahlungsform an der Kathode inducirter Entladungen. *Annalen der Physik* **300**, 38-48 (1898).

78 Dempster, A. J. A new method of positive ray analysis. *Phys Rev* **11**, 316-325 (1918).

79 Biemann, K., Gapp, F. & Seibl, J. Application of Mass Spectrometry to Structure Problems .1. Amino Acid Sequence in Peptides. *Journal of the American Chemical Society* **81**, 2274-2275 (1959).

80 Paul, W. & Steinwedel, H. Ein Neues Massenspektrometer Ohne Magnetfeld. *Z Naturforsch A* **8**, 448-450 (1953).

81 Futrell, J. H. & Miller, C. D. Tandem Mass Spectrometer for Study of Ion-Molecule Reactions. *Rev Sci Instrum* **37**, 1521-1526 (1966).

82 Comisaro.Mb & Marshall, A. G. Frequency-Sweep Fourier-Transform Ion-Cyclotron Resonance Spectroscopy. *Chem Phys Lett* **26**, 489-490 (1974).

83 Fenn, J. B., Mann, M., Meng, C. K., Wong, S. F. & Whitehouse, C. M. Electrospray ionization for mass spectrometry of large biomolecules. *Science* **246**, 64-71 (1989).

84 Makarov, A. Electrostatic axially harmonic orbital trapping: A high-performance technique of mass analysis. *Analytical Chemistry* **72**, 1156-1162 (2000).

85 Yates, J. R., Ruse, C. I. & Nakorchevsky, A. Proteomics by Mass Spectrometry: Approaches, Advances, and Applications. *Annu Rev Biomed Eng* **11**, 49-79 (2009).

86 Mørtz, E. *et al.* Sequence tag identification of intact proteins by matching tanden mass spectral data against sequence data bases. *Proc Natl Acad Sci U S A* **93**, 8264-8267 (1996).

87 Horn, D. M., Zubarev, R. A. & McLafferty, F. W. Automated de novo sequencing of proteins by tandem high-resolution mass spectrometry. *Proc Natl Acad Sci U S A* **97**, 10313-10317 (2000).

88 Zhang, Y. Y., Fonslow, B. R., Shan, B., Baek, M. C. & Yates, J. R. Protein Analysis by Shotgun/Bottom-up Proteomics. *Chem Rev* **113**, 2343-2394 (2013).

89 Han, X. M., Aslanian, A. & Yates, J. R. Mass spectrometry for proteomics. *Curr Opin Chem Biol* **12**, 483-490 (2008).

90 Cupp-Sutton, K. A. & Wu, S. High-throughput quantitative top-down proteomics. *Mol Omics* **16**, 91-99 (2020).

91 Doerr, A. Mass spectrometry-based targeted proteomics. *Nature Methods* **10**, 23-23 (2013).

92 Ong, S. E. & Mann, M. Mass spectrometry-based proteomics turns quantitative. *Nat Chem Biol* **1**, 252-262 (2005).

93 Zhang, H. & Ge, Y. Comprehensive Analysis of Protein Modifications by Top-Down Mass Spectrometry. *Circ-Cardiovasc Gene* **4**, 711 (2011).

94 Zhang, Z. R., Wu, S., Stenoien, D. L. & Paša-Tolić, L. High-Throughput Proteomics. *Annu Rev Anal Chem* **7**, 427-454 (2014).

95 Speers, A. E. & Cravatt, B. F. A tandem orthogonal proteolysis strategy for high-content chemical proteomics. *Journal of the American Chemical Society* **127**, 10018-10019 (2005).

96 Shevchenko, A., Tomas, H., Havlis, J., Olsen, J. V. & Mann, M. In-gel digestion for mass spectrometric characterization of proteins and proteomes. *Nat Protoc* **1**, 2856-2860 (2006).

97 Fonović, M., Verhelst, S. H. L., Sorum, M. T. & Bogyo, M. Proteomics evaluation of chemically cleavable activity-based probes. *Molecular & Cellular Proteomics* **6**, 1761-1770 (2007).

98 Speicher, K. D., Kolbas, O., Harper, S. & Speicher, D. W. Systematic analysis of peptide recoveries from in-gel digestions for protein identifications in proteome studies. *J Biomol Tech* **11**, 74-86 (2000).

99 Cox, J. *et al.* Accurate proteome-wide label-free quantification by delayed normalization and maximal peptide ratio extraction, termed MaxLFQ. *Mol Cell Proteomics* **13**, 2513-2526 (2014).

100 Zhu, W. H., Smith, J. W. & Huang, C. M. Mass Spectrometry-Based Label-Free Quantitative Proteomics. *J Biomed Biotechnol*, 840518 (2010).

101 Ong, S. E. *et al.* Stable isotope labeling by amino acids in cell culture, SILAC, as a simple and accurate approach to expression proteomics. *Molecular & Cellular Proteomics* **1**, 376-386 (2002).

102 Gygi, S. P. *et al.* Quantitative analysis of complex protein mixtures using isotope-coded affinity tags. *Nature Biotechnology* **17**, 994-999 (1999).

103 Thompson, A. *et al.* Tandem mass tags: A novel quantification strategy for comparative analysis of complex protein mixtures by MS/MS. *Analytical Chemistry* **75**, 1895-1904 (2003).

104 Ross, P. L. *et al.* Multiplexed protein quantitation in Saccharomyces cerevisiae using amine-reactive isobaric tagging reagents. *Molecular & Cellular Proteomics* **3**, 1154-1169 (2004).

105 Kleifeld, O. *et al.* Identifying and quantifying proteolytic events and the natural N terminome by terminal amine isotopic labeling of substrates. *Nat Protoc* **6**, 1578-1611 (2011).

106 Gerber, S. A., Rush, J., Stemman, O., Kirschner, M. W. & Gygi, S. P. Absolute quantification of proteins and phosphoproteins from cell lysates by tandem MS. *P Natl Acad Sci USA* **100**, 6940-6945 (2003).

107 Parker, C. E., Mocanu, V., Mocanu, M., Dicheva, N. & Warren, M. R. Mass Spectrometry for Post-Translational Modifications. In *Neuroproteomics*. (ed O. Alzate), Chapter 6 (CRC Press/Taylor & Francis, Boca Raton (FL), 2010).

108 Leitner, A. Cross-linking and other structural proteomics techniques: how chemistry is enabling mass spectrometry applications in structural biology. *Chem Sci* **7**, 4792-4803 (2016).

109 Rabindran, S. K. *et al.* Antitumor activity of HKI-272, an orally active, irreversible inhibitor of the HER-2 tyrosine kinase. *Cancer Res* **64**, 3958-3965 (2004).

110 Deeks, E. D. Neratinib: First Global Approval. *Drugs* **77**, 1695-1704 (2017).

111 Finlay, M. R. V. & Ward, R. A. Small Molecule Inhibitors of the Epidermal Growth Factor Receptor. In *Cancer II*. (ed Michael J. Waring), 39-39 (Springer International Publishing, 2018).

112 Rabindran, S. K. Antitumor activity of HER-2 inhibitors. *Cancer Lett* **227**, 9-23 (2005).

113 Michael, A. Ueber die Addition von Natriumacetessig-und Natriummalonsäureäthern zu den Aethern ungesättigter Säuren. *Journal für Praktische Chemie* **35**, 349-356 (1887).

114 Tsou, H. R. *et al.* Optimization of 6,7-disubstituted-4-(arylamino)quinoline-3-carbonitriles as orally active, irreversible inhibitors of human epidermal growth factor receptor-2 kinase activity. *J Med Chem* **48**, 1107-1131 (2005).

115 Wissner, A. & Mansour, T. S. The development of HKI-272 and related compounds for the treatment of cancer. *Arch Pharm (Weinheim)* **341**, 465-477 (2008).

116 Karachaliou, N., Fernandez-Bruno, M., Bracht, J. W. P. & Rosell, R. EGFR first- and second-generation TKIs-there is still place for them in EGFR-mutant NSCLC patients. *Transl Cancer Res* **8**, S23-S47 (2019).

117 Chmielecki, J. *et al.* EGFR-Mutant Lung Adenocarcinomas Treated First-Line with the Novel EGFR Inhibitor, XL647, Can Subsequently Retain Moderate Sensitivity to Erlotinib. *J Thorac Oncol* **7**, 434-442 (2012).

118 Sequist, L. V. Second-generation epidermal growth factor receptor tyrosine kinase inhibitors in non-small cell lung cancer. *Oncologist* **12**, 325-330 (2007).

119 Pao, W. *et al.* Acquired resistance of lung adenocarcinomas to gefitinib or erlotinib is associated with a second mutation in the EGFR kinase domain. *Plos Med* **2**, 225-235 (2005).

120 Yu, H. A. *et al.* Analysis of Tumor Specimens at the Time of Acquired Resistance to EGFR-TKI Therapy in 155 Patients with EGFR-Mutant Lung Cancers. *Clin Cancer Res* **19**, 2240-2247 (2013).

121 Berman, H. M. *et al.* The Protein Data Bank. *Nucleic Acids Res* **28**, 235-242 (2000).

122 Yun, C. H. *et al.* The T790M mutation in EGFR kinase causes drug resistance by increasing the affinity for ATP. *Proc Natl Acad Sci U S A* **105**, 2070-2075 (2008).

123 Sjin, R. T. T. *et al.* In Vitro and In Vivo Characterization of Irreversible Mutant-Selective EGFR Inhibitors That Are Wild-Type Sparing. *Mol Cancer Ther* **13**, 1468-1479 (2014).

124 Chew, W., Cheal, G. K. & Lunetta, J. F. Methods of synthesizing substituted 3-cyanoquinolines and intermediates thereof. International Patent No. WO2006127207 (2006).

125 Gu, N. *et al.* The Wittig-Horner reaction for the synthesis of neratinib. *Res Chem Intermediat* **39**, 3105-3110 (2013).

126 Hossam, M., Lasheen, D. S. & Abouzid, K. A. Covalent EGFR Inhibitors: Binding Mechanisms, Synthetic Approaches, and Clinical Profiles. *Arch Pharm (Weinheim)* **349**, 573-593 (2016).

127 Davis, M. I. *et al.* Comprehensive analysis of kinase inhibitor selectivity. *Nature Biotechnology* **29**, 1046-1051 (2011).

128 Ross, J. S. *et al.* The HER-2 receptor and breast cancer: ten years of targeted anti-HER-2 therapy and personalized medicine. *Oncologist* **14**, 320-368 (2009).

129 Iqbal, N. & Iqbal, N. Human Epidermal Growth Factor Receptor 2 (HER2) in Cancers: Overexpression and Therapeutic Implications. *Mol Biol Int* **2014**, 852748 (2014).

130 Yan, M. *et al.* HER2 expression status in diverse cancers: review of results from 37,992 patients. *Cancer Metast Rev* **34**, 157-164 (2015).

131 Slamon, D. J. *et al.* Human-Breast Cancer - Correlation of Relapse and Survival with Amplification of the Her-2 Neu Oncogene. *Science* **235**, 177-182 (1987).

132 Klapper, L. N. *et al.* The ErbB-2/HER2 oncoprotein of human carcinomas may function solely as a shared coreceptor for multiple stroma-derived growth factors. *P Natl Acad Sci USA* **96**, 4995-5000 (1999).

133 Tzahar, E. *et al.* A hierarchical network of interreceptor interactions determines signal transduction by neu differentiation factor/neuregulin and epidermal growth factor. *Molecular and Cellular Biology* **16**, 5276-5287 (1996).

134 Pollock, N. I. & Grandis, J. R. HER2 as a Therapeutic Target in Head and Neck Squamous Cell Carcinoma. *Clin Cancer Res* **21**, 526-533 (2015).

135 Richard, S. *et al.* Pertuzumab and trastuzumab: the rationale way to synergy. *An Acad Bras Cienc* **88**, 565-577 (2016).

136 Collins, D. M. *et al.* Preclinical Characteristics of the Irreversible Pan-HER Kinase Inhibitor Neratinib Compared with Lapatinib: Implications for the Treatment of HER2-Positive and HER2-Mutated Breast Cancer. *Cancers* **11** (2019).

137 Sánchez-Martín, M. & Pandiella, A. Differential action of small molecule HER kinase inhibitors on receptor heterodimerization: Therapeutic implications. *Int J Cancer* **131**, 244-252 (2012).

138 Guy, P. M., Platko, J. V., Cantley, L. C., Cerione, R. A. & Carraway, K. L., 3rd. Insect cell-expressed p180erbB3 possesses an impaired tyrosine kinase activity. *Proc Natl Acad Sci U S A* **91**, 8132-8136 (1994).

139 Food and Drug Administration. FDA approves neratinib for extended adjuvant treatment of early stage HER2-positive breast cancer. https://www.fda.gov/drugs/resources-information-approved-drugs/fda-approves-neratinib-extended-adjuvant-treatment-early-stage-her2-positive-breast-cancer. Accessed 17 March 2020, 19:07.

140 European Medicines Agency. Refusal of the marketing authorisation for Nerlynx (neratinib). https://www.ema.europa.eu/en/documents/smop-initial/questions-answers-refusal-marketing-authorisation-nerlynx-neratinib_en.pdf. Accessed 17 March 2020, 19:38.

141 Chan, A. *et al.* Neratinib after trastuzumab-based adjuvant therapy in patients with HER2-positive breast cancer (ExteNET): a multicentre, randomised, double-blind, placebo-controlled, phase 3 trial. *Lancet Oncol* **17**, 367-377 (2016).

142 European Medicines Agency. Positive opinion on the marketing authorisation for Nerlynx (neratinib). https://www.ema.europa.eu/en/documents/smop-initial/questions-answers-positive-opinion-marketing-authorisation-nerlynx-neratinib_en.pdf. Accessed 17 March 2020, 19:39.

143 European Medicines Agency. Nerlynx. https://www.ema.europa.eu/en/medicines/human/EPAR/nerlynx. Accessed 17 March 2020, 19:25.

144 Food and Drug Administration. FDA approves neratinib for metastatic HER2-positive breast cancer. https://www.fda.gov/drugs/resources-information-approved-drugs/fda-approves-neratinib-metastatic-her2-positive-breast-cancer. Accessed 17 March 2020, 19:12.

145 Saura, C. *et al.* Neratinib plus capecitabine versus lapatinib plus capecitabine in patients with HER2+metastatic breast cancer previously treated with >= 2 HER2-directed regimens: Findings from the multinational, randomized, phase III NALA trial. *Journal of Clinical Oncology* **37**, 1002-1002 (2019).

146 Seyfferth, C. & Tsuda, K. Salicylic acid signal transduction: the initiation of biosynthesis, perception and transcriptional reprogramming. *Front Plant Sci* **5**, 697 (2014).

147 Wildermuth, M. C., Dewdney, J., Wu, G. & Ausubel, F. M. Isochorismate synthase is required to synthesize salicylic acid for plant defence. *Nature* **414**, 562-565 (2001).

148 Dempsey, D. A., Vlot, A. C., Wildermuth, M. C. & Klessig, D. F. Salicylic Acid biosynthesis and metabolism. *Arabidopsis Book* **9**, e0156 (2011).

149 Kumar, D. Salicylic acid signaling in disease resistance. *Plant Sci* **228**, 127-134 (2014).

150 Dean, J. V., Shah, R. P. & Mohammed, L. A. Formation and vacuolar localization of salicylic acid glucose conjugates in soybean cell suspension cultures. *Physiol Plantarum* **118**, 328-336 (2003).

151 Dean, J. V. & Delaney, S. P. Metabolism of salicylic acid in wild-type, ugt74f1 and ugt74f2 glucosyltransferase mutants of Arabidopsis thaliana. *Physiol Plant* **132**, 417-425 (2008).

152 Hennig, J., Malamy, J., Grynkiewicz, G., Indulski, J. & Klessig, D. F. Interconversion of the salicylic acid signal and its glucoside in tobacco. *Plant J* **4**, 593-600 (1993).

153 Seo, S., Ishizuka, K. & Ohashi, Y. Induction of Salicylic-Acid Beta-Glucosidase in Tobacco-Leaves by Exogenous Salicylic-Acid. *Plant Cell Physiol* **36**, 447-453 (1995).

154 Shulaev, V., Silverman, P. & Raskin, I. Airborne signalling by methyl salicylate in plant pathogen resistance. *Nature* **385**, 718-721 (1997).

155 Ross, J. R., Nam, K. H., D'Auria, J. C. & Pichersky, E. S-Adenosyl-L-methionine:salicylic acid carboxyl methyltransferase, an enzyme involved in floral scent production and plant defense, represents a new class of plant methyltransferases. *Arch Biochem Biophys* **367**, 9-16 (1999).

156 Forouhar, F. *et al.* Structural and biochemical studies identify tobacco SABP2 as a methyl salicylate esterase and implicate it in plant innate immunity. *P Natl Acad Sci USA* **102**, 1773-1778 (2005).

157 Costet, L. *et al.* Relationship between localized acquired resistance (LAR) and the hypersensitive response (HR): HR is necessary for LAR to occur and salicylic acid is not sufficient to trigger LAR. *Mol Plant Microbe In* **12**, 655-662 (1999).

158 Park, S. W., Kaimoyo, E., Kumar, D., Mosher, S. & Klessig, D. F. Methyl salicylate is a critical mobile signal for plant systemic acquired resistance. *Science* **318**, 113-116 (2007).

159 Cao, H., Glazebrook, J., Clarke, J. D., Volko, S. & Dong, X. N. The Arabidopsis NPR1 gene that controls systemic acquired resistance encodes a novel protein containing ankyrin repeats. *Cell* **88**, 57-63 (1997).

160 Mou, Z., Fan, W. H. & Dong, X. N. Inducers of plant systemic acquired resistance regulate NPR1 function through redox changes. *Cell* **113**, 935-944 (2003).

161 Tada, Y. *et al.* Plant immunity requires conformational charges of NPR1 via S-nitrosylation and thioredoxins. *Science* **321**, 952-956 (2008).

162 Kinkema, M., Fan, W. H. & Dong, X. N. Nuclear localization of NPR1 is required for activation of PR gene expression. *Plant Cell* **12**, 2339-2350 (2000).

163 Jin, H. *et al.* Salicylic acid-induced transcriptional reprogramming by the HAC-NPR1-TGA histone acetyltransferase complex in Arabidopsis. *Nucleic Acids Res* **46**, 11712-11725 (2018).

164 Lebel, E. *et al.* Functional analysis of regulatory sequences controlling PR-1 gene expression in Arabidopsis. *Plant J* **16**, 223-233 (1998).

165 Zhang, Y. L., Fan, W. H., Kinkema, M., Li, X. & Dong, X. N. Interaction of NPR1 with basic leucine zipper protein transcription factors that bind sequences required for salicylic acid induction of the PR-1 gene. *P Natl Acad Sci USA* **96**, 6523-6528 (1999).

166 Després, C., DeLong, C., Glaze, S., Liu, E. & Fobert, P. R. The arabidopsis NPR1/NIM1 protein enhances the DNA binding activity of a subgroup of the TGA family of bZIP transcription factors. *Plant Cell* **12**, 279-290 (2000).

167 Zhou, J. M. *et al.* NPR1 differentially interacts with members of the TGA/OBF family of transcription factors that bind an element of the PR-1 gene required for induction by salicylic acid. *Mol Plant Microbe In* **13**, 191-202 (2000).

168 Fan, W. H. & Dong, X. N. In vivo interaction between NPR1 and transcription factor TGA2 leads to salicylic acid-mediated gene activation in Arabidopsis. *Plant Cell* **14**, 1377-1389 (2002).

169 Després, C. *et al.* The Arabidopsis NPR1 disease resistance protein is a novel cofactor that confers redox regulation of DNA binding activity to the basic domain/leucine zipper transcription factor TGA1. *Plant Cell* **15**, 2181-2191 (2003).

170 Rochon, A., Boyle, P., Wignes, T., Fobert, P. R. & Després, C. The coactivator function of Arabidopsis NPR1 requires the core of its BTB/POZ domain and the oxidation of C-terminal cysteines. *Plant Cell* **18**, 3670-3685 (2006).

171 Wang, D., Amornsiripanitch, N. & Dong, X. N. A genomic approach to identify regulatory nodes in the transcriptional network of systemic acquired resistance in plants. *Plos Pathog* **2**, 1042-1050 (2006).

172 Pape, S., Thurow, C. & Gatz, C. The Arabidopsis PR-1 promoter contains multiple integration sites for the coactivator NPR1 and the repressor SNI1. *Plant Physiol* **154**, 1805-1818 (2010).

173 Saleh, A. *et al.* Posttranslational Modifications of the Master Transcriptional Regulator NPR1 Enable Dynamic but Tight Control of Plant Immune Responses. *Cell Host Microbe* **18**, 169-182 (2015).

174 Spoel, S. H. *et al.* Proteasome-Mediated Turnover of the Transcription Coactivator NPR1 Plays Dual Roles in Regulating Plant Immunity. *Cell* **137**, 860-872 (2009).

175 Fu, Z. Q. *et al.* NPR3 and NPR4 are receptors for the immune signal salicylic acid in plants. *Nature* **486**, 228-232 (2012).

176 Skelly, M. J., Furniss, J. J., Grey, H., Wong, K. W. & Spoel, S. H. Dynamic ubiquitination determines transcriptional activity of the plant immune coactivator NPR1. *Elife* **8**, e47005 (2019).

177 Cao, H., Li, X. & Dong, X. N. Generation of broad-spectrum disease resistance by overexpression of an essential regulatory gene in systemic acquired resistance. *P Natl Acad Sci USA* **95**, 6531-6536 (1998).

178 Kachroo, P., Yoshioka, K., Shah, J., Dooner, H. K. & Klessig, D. F. Resistance to turnip crinkle virus in Arabidopsis is regulated by two host genes and is salicylic acid dependent but NPR1, ethylene, and jasmonate independent. *Plant Cell* **12**, 677-690 (2000).

179 Wong, C. E., Carson, R. A. J. & Carr, J. P. Chemically induced virus resistance in Arabidopsis thaliana is independent of pathogenesis-related protein expression and the NPR1 gene. *Mol Plant Microbe In* **15**, 75-81 (2002).

180 Mandal, B. *et al.* Biological and molecular analyses of the acibenzolar-S-methyl-induced systemic acquired resistance in flue-cured tobacco against Tomato spotted wilt virus. *Phytopathology* **98**, 196-204 (2008).

181 Pieterse, C. M. J., Van der Does, D., Zamioudis, C., Leon-Reyes, A. & Van Wees, S. C. M. Hormonal Modulation of Plant Immunity. *Annu Rev Cell Dev Bi* **28**, 489-521 (2012).

182 Lu, H., Greenberg, J. T. & Holuigue, L. Editorial: Salicylic Acid Signaling Networks. *Frontiers in Plant Science* **7**, 238 (2016).

183 Manohar, M. *et al.* Identification of multiple salicylic acid-binding proteins using two high throughput screens. *Frontiers in Plant Science* **5**, 777 (2015).

184 Ding, Y. Z., Shaholli, D. & Mou, Z. L. A large-scale genetic screen for mutants with altered salicylic acid accumulation in Arabidopsis. *Frontiers in Plant Science* **5**, 763 (2015).

185 Oesch, F. Mammalian epoxide hydrases: inducible enzymes catalysing the inactivation of carcinogenic and cytotoxic metabolites derived from aromatic and olefinic compounds. *Xenobiotica* **3**, 305-340 (1973).

186 Morisseau, C. & Hammock, B. D. Epoxide hydrolases: Mechanisms, inhibitor designs, and biological roles. *Annu Rev Pharmacol* **45**, 311-333 (2005).

187 Morisseau, C. Role of epoxide hydrolases in lipid metabolism. *Biochimie* **95**, 91-95 (2013).

188 Pineau, E. *et al.* Arabidopsis thaliana EPOXIDE HYDROLASE1 (AtEH1) is a cytosolic epoxide hydrolase involved in the synthesis of poly-hydroxylated cutin monomers. *New Phytol* **215**, 173-186 (2017).

189 Parker, R. E. & Isaacs, N. S. Mechanisms of Epoxide Reactions. *Chem Rev* **59**, 737-799 (1959).

190 Arand, M., Cronin, A., Oesch, F., Mowbray, S. L. & Jones, T. A. The telltale structures of epoxide hydrolases. *Drug Metab Rev* **35**, 365-383 (2003).

191 Decker, M., Arand, M. & Cronin, A. Mammalian epoxide hydrolases in xenobiotic metabolism and signalling. *Arch Toxicol* **83**, 297-318 (2009).

192 Fretland, A. J. & Omiecinski, C. J. Epoxide hydrolases: biochemistry and molecular biology. *Chem-Biol Interact* **129**, 41-59 (2000).

193 Hammock, B. D., Grant, D. & Storms, D. Epoxide hydrolases. In *Comprehensive Toxicology*. Vol. 3 Biotransformation (ed F.P. Guengerich), Ch. 18, 283-305 (Pergamon Press, Oxford, 1997).

194 Wojtasek, H. & Prestwich, G. D. An insect juvenile hormone-specific epoxide hydrolase is related to vertebrate microsomal epoxide hydrolases. *Biochem Bioph Res Co* **220**, 323-329 (1996).

195 Zou, J. Y. *et al.* Structure of Aspergillus niger epoxide hydrolase at 1.8 angstrom resolution: implications for the structure and function of the mammalian microsomal class of epoxide hydrolases. *Structure* **8**, 111-122 (2000).

196 Elfström, L. T. & Widersten, M. Catalysis of potato epoxide hydrolase, StEH1. *Biochem J* **390**, 633-640 (2005).

197 Barth, S., Fischer, M., Schmid, R. D. & Pleiss, J. Sequence and structure of epoxide hydrolases: A systematic analysis. *Proteins* **55**, 846-855 (2004).

198 Arand, M. *et al.* Sequence Similarity of Mammalian Epoxide Hydrolases to the Bacterial Haloalkane Dehalogenase and Other Related Proteins - Implication for the Potential Catalytic Mechanism of Enzymatic Epoxide Hydrolysis. *Febs Letters* **338**, 251-256 (1994).

199 Ollis, D. L. *et al.* The Alpha/Beta-Hydrolase Fold. *Protein Eng* **5**, 197-211 (1992).

200 Holmquist, M. Alpha/Beta-Hydrolase Fold Enzymes: Structures, Functions and Mechanisms. *Curr Protein Pept Sc* **1**, 209-235 (2000).

201 Armstrong, R. N. & Cassidy, C. S. New structural and chemical insight into the catalytic mechanism of epoxide hydrolases. *Drug Metab Rev* **32**, 327-338 (2000).

202 Hopmann, K. H. & Himo, F. Theoretical study of the full reaction mechanism of human soluble epoxide hydrolase. *Chem-Eur J* **12**, 6898-6909 (2006).

203 Hopmann, K. H. & Himo, F. Insights into the reaction mechanism of soluble epoxide hydrolase from theoretical active site mutants. *J Phys Chem B* **110**, 21299-21310 (2006).

204 Serrano-Hervás, E., Garcia-Borràs, M. & Osuna, S. Exploring the origins of selectivity in soluble epoxide hydrolase from Bacillus megaterium. *Org Biomol Chem* **15**, 8827-8835 (2017).

205 Laughlin, L. T., Tzeng, H. F., Lin, S. & Armstrong, R. N. Mechanism of microsomal epoxide hydrolase. Semifunctional site-specific mutants affecting the alkylation half-reaction. *Biochemistry* **37**, 2897-2904 (1998).

206 Tzeng, H. F., Laughlin, L. T., Lin, S. & Armstrong, R. N. The catalytic mechanism of microsomal epoxide hydrolase involves reversible formation and rate-limiting hydrolysis of the alkyl-enzyme intermediate. *Journal of the American Chemical Society* **118**, 9436-9437 (1996).

207 Blée, E. & Schuber, F. Regio- and enantioselectivity of soybean fatty acid epoxide hydrolase. *J Biol Chem* **267**, 11881-11887 (1992).

208 Mowbray, S. L., Elfström, L. T., Ahlgren, K. M., Andersson, C. E. & Widersten, M. X-ray structure of potato epoxide hydrolase sheds light on substrate specificity in plant enzymes. *Protein Sci* **15**, 1628-1637 (2006).

209 Blée, E. & Schuber, F. Occurrence of Fatty-Acid Epoxide Hydrolases in Soybean (Glycine-Max) - Purification and Characterization of the Soluble Form. *Biochem J* **282**, 711-714 (1992).

210 Pinot, F. *et al.* Epoxide hydrolase activities in the microsomes and the soluble fraction from Vicia sativa seedlings. *Plant Physiol Bioch* **35**, 103-110 (1997).

211 Sauveplane, V. *et al.* Arabidopsis thaliana CYP77A4 is the first cytochrome P450 able to catalyze the epoxidation of free fatty acids in plants. *Febs J* **276**, 719-735 (2009).

212 Newman, J. W., Morisseau, C. & Hammock, B. D. Epoxide hydrolases: their roles and interactions with lipid metabolism. *Prog Lipid Res* **44**, 1-51 (2005).

213 Stark, A., Houshmand, H., Sandberg, M. & Meijer, J. Characterization of the Activity of Fatty-Acid Epoxide Hydrolase in Seeds of Castor Bean (Ricinus-Communis L) - Presence of Epoxide Hydrolases in Glyoxysomes and Cytosol. *Planta* **197**, 84-88 (1995).

214 Summerer, S. *et al.* Stereochemical features of the hydrolysis of 9,10-epoxystearic acid catalysed by plant and mammalian epoxide hydrolases. *Biochem J* **366**, 471-480 (2002).

215 Morisseau, C. *et al.* Cress and potato soluble epoxide hydrolases: Purification, biochemical characterization, and comparison to mammalian enzymes. *Archives of Biochemistry and Biophysics* **378**, 321-332 (2000).

216 Kiyosue, T. *et al.* Characterization of an Arabidopsis Cdna for a Soluble Epoxide Hydrolase Gene That Is Inducible by Auxin and Water-Stress. *Plant J* **6**, 259-269 (1994).

217 Blée, E. & Schuber, F. Biosynthesis of Cutin Monomers - Involvement of a Lipoxygenase Peroxygenase Pathway. *Plant J* **4**, 113-123 (1993).

218 Guo, A., Durner, J. & Klessig, D. F. Characterization of a tobacco epoxide hydrolase gene induced during the resistance response to TMV. *Plant J* **15**, 647-656 (1998).

219 Pinot, F. *et al.* omega-hydroxylation of epoxy- and hydroxy-fatty acids by CYP94A1: possible involvement in plant defence. *Biochem Soc T* **28**, 867-870 (2000).

220 Stapleton, A. *et al.* Cloning and Expression of Soluble Epoxide Hydrolase from Potato. *Plant J* **6**, 251-258 (1994).

221 Studier, F. W. & Moffatt, B. A. Use of Bacteriophage-T7 Rna-Polymerase to Direct Selective High-Level Expression of Cloned Genes. *J Mol Biol* **189**, 113-130 (1986).

222 Hanahan, D. Techniques for transformation of E. coli. In *DNA cloning: a practical approach*. Vol. 1 (ed D.M. Glover), 109 (IRL Press, Oxford, 1985).

223 Hanahan, D., Jessee, J. & Bloom, F. R. Plasmid Transformation of Escherichia-Coli and Other Bacteria. *Method Enzymol* **204**, 63-113 (1991).

224 Sanger, F., Nicklen, S. & Coulson, A. R. DNA sequencing with chain-terminating inhibitors. *Proc Natl Acad Sci U S A* **74**, 5463-5467 (1977).

225 Hill, J. T. *et al.* Poly Peak Parser: Method and Software for Identification of Unknown Indels Using Sanger Sequencing of Polymerase Chain Reaction Products. *Dev Dynam* **243**, 1632-1636 (2014).

226 Bradford, M. M. A rapid and sensitive method for the quantitation of microgram quantities of protein utilizing the principle of protein-dye binding. *Anal Biochem* **72**, 248-254 (1976).

227 Wessel, D. & Flügge, U. I. A Method for the Quantitative Recovery of Protein in Dilute-Solution in the Presence of Detergents and Lipids. *Anal Biochem* **138**, 141-143 (1984).

228 Fazekas de St Groth, S., Webster, R. G. & Datyner, A. Two new staining procedures for quantitative estimation of proteins on electrophoretic strips. *Biochim Biophys Acta* **71**, 377-391 (1963).

229 Neuhoff, V., Arold, N., Taube, D. & Ehrhardt, W. Improved Staining of Proteins in Polyacrylamide Gels Including Isoelectric-Focusing Gels with Clear Background at Nanogram Sensitivity Using Coomassie Brilliant Blue G-250 and R-250. *Electrophoresis* **9**, 255-262 (1988).

230 Rappsilber, J., Mann, M. & Ishihama, Y. Protocol for micro-purification, enrichment, pre-fractionation and storage of peptides for proteomics using StageTips. *Nat Protoc* **2**, 1896-1906 (2007).

231 Michalski, A. *et al.* Ultra high resolution linear ion trap Orbitrap mass spectrometer (Orbitrap Elite) facilitates top down LC MS/MS and versatile peptide fragmentation modes. *Mol Cell Proteomics* **11**, O111.013698 (2012).

232 Olsen, J. V. *et al.* Parts per million mass accuracy on an Orbitrap mass spectrometer via lock mass injection into a C-trap. *Mol Cell Proteomics* **4**, 2010-2021 (2005).

233 Cox, J. *et al.* Andromeda: a peptide search engine integrated into the MaxQuant environment. *J Proteome Res* **10**, 1794-1805 (2011).

234 Tyanova, S. *et al.* The Perseus computational platform for comprehensive analysis of (prote)omics data. *Nat Methods* **13**, 731-740 (2016).

235 Deutsch, E. W. *et al.* The ProteomeXchange consortium in 2020: enabling 'big data' approaches in proteomics. *Nucleic Acids Res* **48**, D1145-D1152 (2020).

236 Perez-Riverol, Y. *et al.* The PRIDE database and related tools and resources in 2019: improving support for quantification data. *Nucleic Acids Res* **47**, D442-D450 (2019).

237 Arnold, K., Bordoli, L., Kopp, J. & Schwede, T. The SWISS-MODEL workspace: a web-based environment for protein structure homology modelling. *Bioinformatics* **22**, 195-201 (2006).

238 Guex, N., Peitsch, M. C. & Schwede, T. Automated comparative protein structure modeling with SWISS-MODEL and Swiss-PdbViewer: A historical perspective. *Electrophoresis* **30**, S162-S173 (2009).

239 Biasini, M. *et al.* SWISS-MODEL: modelling protein tertiary and quaternary structure using evolutionary information. *Nucleic Acids Res* **42**, W252-W258 (2014).

240 Bertoni, M., Kiefer, F., Biasini, M., Bordoli, L. & Schwede, T. Modeling protein quaternary structure of homo- and hetero-oligomers beyond binary interactions by homology. *Sci Rep-Uk* **7** (2017).

241 Bienert, S. *et al.* The SWISS-MODEL Repository-new features and functionality. *Nucleic Acids Res* **45**, D313-D319 (2017).

242 Waterhouse, A. *et al.* SWISS-MODEL: homology modelling of protein structures and complexes. *Nucleic Acids Res* **46**, W296-W303 (2018).

243 Camacho, C. *et al.* BLAST plus : architecture and applications. *Bmc Bioinformatics* **10** (2009).

244 Remmert, M., Biegert, A., Hauser, A. & Soding, J. HHblits: lightning-fast iterative protein sequence searching by HMM-HMM alignment. *Nature Methods* **9**, 173-175 (2012).

245 Amrein, B. A. *et al.* Expanding the Catalytic Triad in Epoxide Hydrolases and Related Enzymes. *ACS Catal* **5**, 5702-5713 (2015).

246 Benkert, P., Biasini, M. & Schwede, T. Toward the estimation of the absolute quality of individual protein structure models. *Bioinformatics* **27**, 343-350 (2011).

247 Studer, G. *et al.* QMEANDisCo-distance constraints applied on model quality estimation. *Bioinformatics* **36**, 1765-1771 (2020).

248 The PyMOL Molecular Graphics System, Version 1.1beta3, Schrödinger, LLC.

249 Finn, R. D. *et al.* The Pfam protein families database: towards a more sustainable future. *Nucleic Acids Res* **44**, D279-D285 (2016).

250 Notredame, C., Higgins, D. G. & Heringa, J. T-Coffee: A novel method for fast and accurate multiple sequence alignment. *J Mol Biol* **302**, 205-217 (2000).

251 Tommaso, P. *et al.* T-Coffee: a web server for the multiple sequence alignment of protein and RNA sequences using structural information and homology extension. *Nucleic Acids Res* **39**, W13-W17 (2011).

252 The UniProt Consortium. UniProt: the universal protein knowledgebase. *Nucleic Acids Res* **46**, 2699 (2018).

253 Ashkenazy, H., Erez, E., Martz, E., Pupko, T. & Ben-Tal, N. ConSurf 2010: calculating evolutionary conservation in sequence and structure of proteins and nucleic acids. *Nucleic Acids Res* **38**, W529-W533 (2010).

254 Celniker, G. *et al.* ConSurf: Using Evolutionary Data to Raise Testable Hypotheses about Protein Function. *Isr J Chem* **53**, 199-206 (2013).

255 Ashkenazy, H. *et al.* ConSurf 2016: an improved methodology to estimate and visualize evolutionary conservation in macromolecules. *Nucleic Acids Res* **44**, W344-W350 (2016).

256 Berezin, C. *et al.* ConSeq: the identification of functionally and structurally important residues in protein sequences. *Bioinformatics* **20**, 1322-1324 (2004).

257 Tena, G., Boudsocq, M. & Sheen, J. Protein kinase signaling networks in plant innate immunity. *Curr Opin Plant Biol* **14**, 519-529 (2011).

258 Gómez-Gómez, L. & Boller, T. FLS2: An LRR receptor-like kinase involved in the perception of the bacterial elicitor flagellin in Arabidopsis. *Mol Cell* **5**, 1003-1011 (2000).

259 Asai, T. *et al.* MAP kinase signalling cascade in Arabidopsis innate immunity. *Nature* **415**, 977-983 (2002).

260 Halder, V. & Kombrink, E. Facile high-throughput forward chemical genetic screening by in situ monitoring of glucuronidase-based reporter gene expression in Arabidopsis thaliana. *Front Plant Sci* **6**, 13 (2015).

261 Zhou, N. J. *et al.* Genistein Inhibition of Topoisomerase II alpha Expression Participated by Sp1 and Sp3 in HeLa Cell. *Int J Mol Sci* **10**, 3255-3268 (2009).

262 Chodosh, L. A., Fire, A., Samuels, M. & Sharp, P. A. 5,6-Dichloro-1-Beta-D-Ribofuranosylbenzimidazole Inhibits Transcription Elongation by Rna Polymerase-Ii Invitro. *Journal of Biological Chemistry* **264**, 2250-2257 (1989).

263 Lee, J., Rhee, M. H., Kim, E. & Cho, J. Y. BAY 11-7082 Is a Broad-Spectrum Inhibitor with Anti-Inflammatory Activity against Multiple Targets. *Mediat Inflamm* (2012).

264 Lapcik, O. *et al.* Isoflavonoids are present in Arabidopsis thaliana despite the absence of any homologue to known isoflavonoid synthases. *Plant Physiol Bioch* **44**, 106-114 (2006).

265 Torrance, C. J. *et al.* Combinatorial chemoprevention of intestinal neoplasia. *Nature Medicine* **6**, 1024-1028 (2000).

266 Barker, A. J. *et al.* Studies leading to the identification of ZD1839 (Iressa (TM)): An orally active, selective epidermal growth factor receptor tyrosine kinase inhibitor targeted to the treatment of cancer. *Bioorganic & Medicinal Chemistry Letters* **11**, 1911-1914 (2001).

267 Li, D. *et al.* BIBW2992, an irreversible EGFR/HER2 inhibitor highly effective in preclinical lung cancer models. *Oncogene* **27**, 4702-4711 (2008).

268 Solca, F. *et al.* Target Binding Properties and Cellular Activity of Afatinib (BIBW 2992), an Irreversible ErbB Family Blocker. *J Pharmacol Exp Ther* **343**, 342-350 (2012).

269 King, L. E., Carpenter, G. & Cohen, S. Characterization by Electrophoresis of Epidermal Growth-Factor Stimulated Phosphorylation Using a-431 Membranes. *Biochemistry* **19**, 1524-1528 (1980).

270 Wang, X. Q., Sun, P., O'Gorman, M., Tai, T. D. & Paller, A. S. Epidermal growth factor receptor glycosylation is required for ganglioside GM3 binding and GM3-mediated suppresion of activation. *Glycobiology* **11**, 515-522 (2001).

271 Akiyama, T., Sudo, C., Ogawara, H., Toyoshima, K. & Yamamoto, T. The Product of the Human C-Erbb-2 Gene - a 185-Kilodalton Glycoprotein with Tyrosine Kinase-Activity. *Science* **232**, 1644-1646 (1986).

272 Oh, D. Y. *et al.* HER2 as a novel therapeutic target for cervical cancer. *Oncotarget* **6**, 36219-36230 (2015).

273 Plowman, G. D. *et al.* Ligand-specific activation of HER4/p180erbB4, a fourth member of the epidermal growth factor receptor family. *Proc Natl Acad Sci U S A* **90**, 1746-1750 (1993).

274 Kaschani, F. *et al.* Minitags for small molecules: detecting targets of reactive small molecules in living plant tissues using 'click chemistry'. *Plant J* **57**, 373-385 (2009).

275 Fowke, L. C. & Constabel, F. Plant Protoplasts: An Experimental System for Cell Biologists. In *Plant Cell Culture in Crop Improvement*. (eds S. K. Sen & Kenneth L. Giles), 185-200 (Springer US, 1983).

276 Zulawski, M., Schulze, G., Braginets, R., Hartmann, S. & Schulze, W. X. The Arabidopsis Kinome: phylogeny and evolutionary insights into functional diversification. *Bmc Genomics* **15** (2014).

277 Reumann, S. *et al.* Proteome analysis of Arabidopsis leaf peroxisomes reveals novel targeting peptides, metabolic pathways, and defense mechanisms. *Plant Cell* **19**, 3170-3193 (2007).

278 Eubel, H. *et al.* Novel Proteins, Putative Membrane Transporters, and an Integrated Metabolic Network Are Revealed by Quantitative Proteomic Analysis of Arabidopsis Cell Culture Peroxisomes. *Plant Physiology* **148**, 1809-1829 (2008).

279 Ellis, R. J. The most abundant protein in the world. *Trends Biochem Sci* **4**, 241-244 (1979).

280 Raven, J. A. Rubisco: still the most abundant protein of Earth? *New Phytol* **198**, 1-3 (2013).

281 Kung, S. Tobacco fraction 1 protein: a unique genetic marker. *Science* **191**, 429-434 (1976).

282 Highfield, P. E. & Ellis, R. J. Synthesis and transport of the small subunit of chloroplast ribulose bisphosphate carboxylase. *Nature* **271**, 420-424 (1978).

283 Robinson, C. & Ellis, R. J. Transport of Proteins into Chloroplasts - the Precursor of Small Subunit of Ribulose Bisphosphate Carboxylase Is Processed to the Mature Size in 2 Steps. *Eur J Biochem* **142**, 343-346 (1984).

284 Krebbers, E., Seurinck, J., Herdies, L., Cashmore, A. R. & Timko, M. P. Four genes in two diverged subfamilies encode the ribulose-1,5-bisphosphate carboxylase small subunit polypeptides of Arabidopsis thaliana. *Plant Mol Biol* **11**, 745-759 (1988).

285 Isono, K., Niwa, Y., Satoh, K. & Kobayashi, H. Evidence for transcriptional regulation of plastid photosynthesis genes in Arabidopsis thaliana roots. *Plant Physiology* **114**, 623-630 (1997).

286 Inohara, N. *et al.* Two genes, atpC1 and atpC2, for the gamma subunit of Arabidopsis thaliana chloroplast ATP synthase. *J Biol Chem* **266**, 7333-7338 (1991).

287 Moffatt, B. A. *et al.* Adenosine kinase of Arabidopsis. Kinetic properties and gene expression. *Plant Physiol* **124**, 1775-1785 (2000).

288 Dietze, E. C., Kuwano, E. & Hammock, B. D. Spectrophotometric Substrates for Cytosolic Epoxide Hydrolase. *Anal Biochem* **216**, 176-187 (1994).

289 Bowers, G. N., Mccomb, R. B., Christensen, R. G. & Schaffer, R. High-Purity 4-Nitrophenol - Purification, Characterization, and Specifications for Use as a Spectrophotometric Reference Material. *Clin Chem* **26**, 724-729 (1980).

290 Shen, J. B. *et al.* Organelle pH in the Arabidopsis Endomembrane System. *Mol Plant* **6**, 1419-1437 (2013).

291 European Medicines Agency. Nerlynx - Assessment report. https://www.ema.europa.eu/en/documents/assessment-report/nerlynx-epar-public-assessment-report_en.pdf. Accessed 19 April 2020, 10:19.

292 Müller, T. & Winter, D. Systematic Evaluation of Protein Reduction and Alkylation Reveals Massive Unspecific Side Effects by Iodine-containing Reagents. *Mol Cell Proteomics* **16**, 1173-1187 (2017).

293 Pettinger, J. *et al.* An Irreversible Inhibitor of HSP72 that Unexpectedly Targets Lysine-56. *Angew Chem Int Edit* **56**, 3536-3540 (2017).

294 Jakob, C. G. *et al.* Novel Modes of Inhibition of Wild-Type Isocitrate Dehydrogenase 1 (IDH1): Direct Covalent Modification of His315. *Journal of Medicinal Chemistry* **61**, 6647-6657 (2018).

295 Hains, P. G. & Robinson, P. J. The Impact of Commonly Used Alkylating Agents on Artifactual Peptide Modification. *Journal of Proteome Research* **16**, 3443-3447 (2017).

296 Hemsley, A., Arnheim, N., Toney, M. D., Cortopassi, G. & Galas, D. J. A Simple Method for Site-Directed Mutagenesis Using the Polymerase Chain-Reaction. *Nucleic Acids Res* **17**, 6545-6551 (1989).

297 Picard, V., Ersdalbadju, E., Lu, A. Q. & Bock, S. C. A Rapid and Efficient One-Tube Pcr-Based Mutagenesis Technique Using Pfu DNA-Polymerase. *Nucleic Acids Res* **22**, 2587-2591 (1994).

298 Weiner, M. P. *et al.* Site-Directed Mutagenesis of Double-Stranded DNA by the Polymerase Chain-Reaction. *Gene* **151**, 119-123 (1994).

299 Cunningham, B. C. & Wells, J. A. High-Resolution Epitope Mapping of Hgh-Receptor Interactions by Alanine-Scanning Mutagenesis. *Science* **244**, 1081-1085 (1989).

300 Ahmadiankia, N., Neshati, V., Neshati, Z., Swildens, J. & de Vries, A. A. F. Generation of Helper Plasmids Encoding Mutant Adeno-associated Virus Type

2 Capsid Proteins with Increased Resistance against Proteasomal Degradation. *Iran J Basic Med Sci* **16**, 813-821 (2013).

301 Cassin-Ross, G. & Hu, J. P. Systematic Phenotypic Screen of Arabidopsis Peroxisomal Mutants Identifies Proteins Involved in beta-Oxidation. *Plant Physiology* **166**, 1546-1559 (2014).

302 Schwartz, P. A. *et al.* Covalent EGFR inhibitor analysis reveals importance of reversible interactions to potency and mechanisms of drug resistance. *P Natl Acad Sci USA* **111**, 173-178 (2014).

303 Lanning, B. R. *et al.* A road map to evaluate the proteome-wide selectivity of covalent kinase inhibitors. *Nat Chem Biol* **10**, 760-767 (2014).

304 Liu, J. Y. *et al.* Sorafenib has soluble epoxide hydrolase inhibitory activity, which contributes to its effect profile in vivo. *Mol Cancer Ther* **8**, 2193-2203 (2009).

305 Charles, R. L. *et al.* Redox Regulation of Soluble Epoxide Hydrolase by 15-Deoxy-Delta-Prostaglandin J(2) Controls Coronary Hypoxic Vasodilation. *Circ Res* **108**, 324-334 (2011).

306 Evans, M. J., Saghatelian, A., Sorensen, E. J. & Cravatt, B. F. Target discovery in small-molecule cell-based screens by in situ proteome reactivity profiling. *Nature Biotechnology* **23**, 1303-1307 (2005).

307 Hall, C. I. *et al.* Chemical genetic screen identifies Toxoplasma DJ-1 as a regulator of parasite secretion, attachment, and invasion. *P Natl Acad Sci USA* **108**, 10568-10573 (2011).

308 Dejonghe, W. & Russinova, E. Target identification strategies in plant chemical biology. *Frontiers in Plant Science* **5**, 352 (2014).

309 Hoch, D. G., Abegg, D. & Adibekian, A. Cysteine-reactive probes and their use in chemical proteomics. *Chem Commun* **54**, 4501-4512 (2018).

310 Mitchell, A. L. *et al.* InterPro in 2019: improving coverage, classification and access to protein sequence annotations. *Nucleic Acids Res* **47**, D351-D360 (2019).

311 Ziv, C., Zhao, Z. Z., Gao, Y. G. & Xia, Y. Multifunctional Roles of Plant Cuticle During Plant-Pathogen Interactions. *Frontiers in Plant Science* **9**, 1088 (2018).

312 Blanc, C. *et al.* The Cuticle Mutant eca2 Modifies Plant Defense Responses to Biotrophic and Necrotrophic Pathogens and Herbivory Insects. *Mol Plant Microbe In* **31**, 344-355 (2018).

313 Sanz-Fernández, M. *et al.* Screening Arabidopsis mutants in genes useful for phytoremediation. *J Hazard Mater* **335**, 143-151 (2017).

314 Weber, H., Chetelat, A., Reymond, P. & Farmer, E. E. Selective and powerful stress gene expression in Arabidopsis in response to malondialdehyde. *Plant J* **37**, 877-888 (2004).

315 Moire, L., Rezzonico, E., Goepfert, S. & Poirier, Y. Impact of unusual fatty acid synthesis on futile cycling through beta-oxidation and on gene expression in transgenic plants(1[w]). *Plant Physiology* **134**, 432-442 (2004).

316 Klausen, M. S. *et al.* NetSurfP-2.0: Improved prediction of protein structural features by integrated deep learning. *Proteins* **87**, 520-527 (2019).

317 Fukasawa, Y. *et al.* MitoFates: Improved Prediction of Mitochondrial Targeting Sequences and Their Cleavage Sites. *Molecular & Cellular Proteomics* **14**, 1113-1126 (2015).

318 Konz, J. O., King, J. & Cooney, C. L. Effects of oxygen on recombinant protein expression. *Biotechnol Progr* **14**, 393-409 (1998).

319 Torosantucci, R., Schöneich, C. & Jiskoot, W. Oxidation of Therapeutic Proteins and Peptides: Structural and Biological Consequences. *Pharm Res-Dordr* **31**, 541-553 (2014).

320 Bondos, S. E. & Bicknell, A. Detection and prevention of protein aggregation before, during, and after purification. *Anal Biochem* **316**, 223-231 (2003).

321 Krishnamurthy, R., Madurawe, R. D., Bush, K. D. & Lumpkin, J. A. Conditions Promoting Metal-Catalyzed Oxidations during Immobilized Cu-Iminodiacetic Acid Metal Affinity-Chromatography. *Biotechnol Progr* **11**, 643-650 (1995).

322 Bridgewater, J. D., Lim, J. & Vachet, R. W. Transition metal-peptide binding studied by metal-catalyzed oxidation reactions and mass spectrometry. *Analytical Chemistry* **78**, 2432-2438 (2006).

323 Abbas, R., Hug, B. A., Leister, C., Burns, J. & Sonnichsen, D. Pharmacokinetics of oral neratinib during co-administration of ketoconazole in healthy subjects. *Brit J Clin Pharmaco* **71**, 522-527 (2011).

324 Aljakouch, K. *et al.* Raman Microspectroscopic Evidence for the Metabolism of a Tyrosine Kinase Inhibitor, Neratinib, in Cancer Cells. *Angew Chem Int Edit* **57**, 7250-7254 (2018).

325 Whiteley, C. G. Enzyme kinetics: partial and complete non-competitive inhibition. *Biochem Educ* **27**, 15-18 (1999).

326 Parvez, S., Long, M. J. C., Poganik, J. R. & Aye, Y. Redox Signaling by Reactive Electrophiles and Oxidants. *Chem Rev* **118**, 8798-8888 (2018).

327 Klomsiri, C., Karplus, P. A. & Poole, L. B. Cysteine-Based Redox Switches in Enzymes. *Antioxid Redox Sign* **14**, 1065-1077 (2011).

328 Rybina, I. V., Liu, H., Gor, Y. & Feinmark, S. J. Regulation of leukotriene A4 hydrolase activity in endothelial cells by phosphorylation. *J Biol Chem* **272**, 31865-31871 (1997).

329 Seidegård, J. & Depierre, J. W. Microsomal Epoxide Hydrolase Properties, Regulation and Function. *Biochimica Et Biophysica Acta* **695**, 251-270 (1983).

330 Hammock, B. D. & Ota, K. Differential Induction of Cytosolic Epoxide Hydrolase, Microsomal Epoxide Hydrolase, and Glutathione S-Transferase Activities. *Toxicol Appl Pharm* **71**, 254-265 (1983).

331 Sheehan, J. E., Pitot, H. C. & Kasper, C. B. Transcriptional Regulation and Localization of the Tissue-Specific Induction of Epoxide Hydrolase by Lead Acetate in Rat-Kidney. *Journal of Biological Chemistry* **266**, 5122-5127 (1991).

332 Kim, S. G. Transcriptional Regulation of Rat Microsomal Epoxide Hydrolase Gene by Imidazole Antimycotic Agents. *Mol Pharmacol* **42**, 273-279 (1992).

333 Harris, T. R. & Hammock, B. D. Soluble epoxide hydrolase: Gene structure, expression and deletion. *Gene* **526**, 61-74 (2013).

334 Wijekoon, C. P., Goodwin, P. H., Valliani, M. & Hsiang, T. The role of a putative peroxisomal-targeted epoxide hydrolase of Nicotiana benthamiana in interactions with Colletotrichum destructivum, C. orbiculare or Pseudomonas syringae pv. tabaci. *Plant Science* **181**, 177-187 (2011).

335 Huang, F. C. & Schwab, W. Molecular characterization of NbEH1 and NbEH2, two epoxide hydrolases from Nicotiana benthamiana. *Phytochemistry* **90**, 6-15 (2013).

336 Kachroo, A. & Kachroo, P. Fatty Acid-Derived Signals in Plant Defense. *Annu Rev Phytopathol* **47**, 153-176 (2009).

337 Kindl, H. Fatty-Acid Degradation in Plant Peroxisomes - Function and Biosynthesis of the Enzymes Involved. *Biochimie* **75**, 225-230 (1993).

338 Poirier, Y., Antonenkov, V. D., Glumoff, T. & Hiltunen, J. K. Peroxisomal beta-oxidation - A metabolic pathway with multiple functions. *Bba-Mol Cell Res* **1763**, 1413-1426 (2006).

339 Lodhi, I. J. & Semenkovich, C. F. Peroxisomes: A Nexus for Lipid Metabolism and Cellular Signaling. *Cell Metab* **19**, 380-392 (2014).

340 Creelman, R. A. & Mulpuri, R. The oxylipin pathway in Arabidopsis. *Arabidopsis Book* **1**, e0012 (2002).

341 Blée, E. Impact of phyto-oxylipins in plant defense. *Trends Plant Sci* **7**, 315-321 (2002).

342 Genva, M. *et al.* New insights into the biosynthesis of esterified oxylipins and their involvement in plant defense and developmental mechanisms. *Phytochem Rev* **18**, 343-358 (2019).

343 Eckardt, N. A. Oxylipin signaling in plant stress responses. *The Plant Cell* **20**, 495-497 (2008).

344 Blée, E. Phytooxylipins and plant defense reactions. *Prog Lipid Res* **37**, 33-72 (1998).

345 Dave, A. & Graham, I. A. Oxylipin signaling: a distinct role for the jasmonic acid precursor cis-(+)-12-oxo-phytodienoic acid (cis-OPDA). *Frontiers in Plant Science* **3**, 42 (2012).

346 Turner, J. G., Ellis, C. & Devoto, A. The jasmonate signal pathway. *Plant Cell* **14**, S153-S164 (2002).

347 Kao, Y. T., Gonzalez, K. L. & Bartel, B. Peroxisome Function, Biogenesis, and Dynamics in Plants. *Plant Physiology* **176**, 162-177 (2018).

348 Lefevere, H., Bauters, L. & Gheysen, G. Salicylic Acid Biosynthesis in Plants. *Front Plant Sci* **11**, 338 (2020).

349 Bussell, J. D., Reichelt, M., Wiszniewski, A. A. G., Gershenzon, J. & Smith, S. M. Peroxisomal ATP-Binding Cassette Transporter COMATOSE and the Multifunctional Protein ABNORMAL INFLORESCENCE MERISTEM Are Required for the Production of Benzoylated Metabolites in Arabidopsis Seeds. *Plant Physiology* **164**, 48-54 (2014).

350 Yalpani, N., León, J., Lawton, M. A. & Raskin, I. Pathway of Salicylic-Acid Biosynthesis in Healthy and Virus-Inoculated Tobacco. *Plant Physiology* **103**, 315-321 (1993).

351 Thaler, J. S., Humphrey, P. T. & Whiteman, N. K. Evolution of jasmonate and salicylate signal crosstalk. *Trends Plant Sci* **17**, 260-270 (2012).

352 Spoel, S. H. *et al.* NPR1 modulates cross-talk between salicylate- and jasmonate-dependent defense pathways through a novel function in the cytosol. *Plant Cell* **15**, 760-770 (2003).

353 Yuan, H. M., Liu, W. C. & Lu, Y. T. CATALASE2 Coordinates SA-Mediated Repression of Both Auxin Accumulation and JA Biosynthesis in Plant Defenses. *Cell Host Microbe* **21**, 143-155 (2017).

354 Harms, K., Ramirez, I. & Peña-Cortés, H. Inhibition of wound-induced accumulation of allene oxide synthase transcripts in flax leaves by aspirin and salicylic acid. *Plant Physiology* **118**, 1057-1065 (1998).

355 Leon-Reyes, A. *et al.* Salicylate-mediated suppression of jasmonate-responsive gene expression in Arabidopsis is targeted downstream of the jasmonate biosynthesis pathway. *Planta* **232**, 1423-1432 (2010).

356 Koornneef, A. *et al.* Kinetics of salicylate-mediated suppression of jasmonate signaling reveal a role for redox modulation. *Plant Physiology* **147**, 1358-1368 (2008).

357 Seo, S. *et al.* Tobacco Map Kinase - a Possible Mediator in Wound Signal-Transduction Pathways. *Science* **270**, 1988-1992 (1995).

358 Calder, P. C. Polyunsaturated fatty acids, inflammation, and immunity. *Lipids* **36**, 1007-1024 (2001).

359 Morisseau, C. & Hammock, B. D. Impact of Soluble Epoxide Hydrolase and Epoxyeicosanoids on Human Health. *Annual Review of Pharmacology and Toxicology, Vol 53, 2013* **53**, 37-58 (2013).

360 Xu, J. W. *et al.* Ingestion of the epoxide hydrolase inhibitor AUDA modulates immune responses of the mosquito, Culex quinquefasciatus during blood feeding. *Insect Biochem Molec* **76**, 62-69 (2016).

361 Arahira, M., Nong, V. H., Udaka, K. & Fukazawa, C. Purification, molecular cloning and ethylene-inducible expression of a soluble-type epoxide hydrolase from soybean (Glycine max [L.] Merr.). *Eur J Biochem* **267**, 2649-2657 (2000).

362 Guerineau, F., Benjdia, M. & Zhou, D. X. A jasmonate-responsive element within the A-thaliana vsp1 promoter. *J Exp Bot* **54**, 1153-1162 (2003).

363 Pyc, M. *et al.* Turning Over a New Leaf in Lipid Droplet Biology. *Trends Plant Sci* **22**, 596-609 (2017).

Appendix

Appendix 1: Chemicals

Tab. 13 List of chemicals. All chemicals used in this work are reported together with their respective supplier.

Chemical	Supplier
(2*S*,3*S*)-*trans*-3-Phenyl-2-oxiranylmethyl 4-nitrophenyl carbonate	Sigma-Aldrich (Merck)
2,4-Dichlorophenoxyacetic acid	Sigma-Aldrich (Merck)
3-(*N*-morpholino)propanesulfonic acid (MOPS)	Sigma-Aldrich (Merck)
Acetic acid, glacial	Fisher Chemical (Thermo Fisher Scientific)
Acetic acid, Optima™ LC/MS Grade	Fisher Chemical (Thermo Fisher Scientific)
Acetonitrile (ACN), HiPerSolv CHROMANORM®	VWR Chemicals
ACN, LC-MS Ultra CHROMASOLV®	Honeywell Riedel-de Haën™
Acrylamide/Bisacrylamide solution, 37.5:1, 30%	SERVA
Agar-agar	Merck
Agarose LE	Biozym Scientific GmbH
Ammonium bicarbonate (ABC)	Sigma-Aldrich (Merck)
Ammonium persulfate (APS)	Sigma-Aldrich (Merck)
Ammonium sulfate	Sigma-Aldrich (Merck)
Ampicillin sodium salt	AppliChem
Bis(2-hydroxyethyl)amino-tris(hydroxymethyl)methane (Bis-Tris)	AppliChem
Boric acid	Sigma-Aldrich (Merck)
Calcium chloride dihydrate	Sigma-Aldrich (Merck)
Calcium chloride, anhydrous	Sigma-Aldrich (Merck)
Chloroform	Sigma-Aldrich (Merck)
Coomassie Brilliant Blue G-250 ultrapure	Alfa Aesar (Thermo Fisher Scientific)
Copper(II) sulfate	Sigma-Aldrich (Merck)
Dimethyl sulfoxide (DMSO)	Sigma-Aldrich (Merck)
Disodium hydrogen phosphate	VWR Chemicals
DL-Dithiothreitol (DTT)	Sigma-Aldrich (Merck) Acros Organics (Thermo Fisher Scientific)
EDTA disodium salt dihydrate	VWR Chemicals Carl Roth
Ethanol absolute, for analysis	Fisher Chemical (Thermo Fisher Scientific)
Ethylenediaminetetraacetic acid (EDTA), free acid	VWR Chemicals
Formic acid (FA), Optima™ LC/MS Grade	Fischer Chemical (Thermo Fisher Scientific)
Gamborg's B-5 Basal Medium with Minimal Organics	Sigma-Aldrich

Glycerol, ROTIPURAN	Carl Roth
Glycine	VWR Chemicals
Guanidine hydrochloride (GuHCL)	AppliChem
Hydrochloric acid (HCl), 37%	Carl Roth VWR Chemicals
Imidazole	Sigma-Aldrich (Merck)
Iodoacetamide (IAM)	GE Healthcare Life Sciences (now Cytiva) Acros Organics (Thermo Fisher Scientific)
Isopropyl β-D-thiogalactopyranoside (IPTG), dioxane-free	Thermo Scientific™ (Thermo Fisher Scientific)
Liquid nitrogen	Central chemical storage facilities of the university Duisburg-Essen
Lithium dodecyl sulfate (LDS)	AppliChem
Magnesium chloride hexahydrate	Sigma-Aldrich (Merck)
Magnesium sulfate heptahydrate	Supelco (Merck)
Manganese(II) chloride tetrahydrate	Sigma-Aldrich (Merck)
Methanol, HPLC grade	Fisher Chemical (Thermo Fisher Scientific)
Methanol, LC-MS Ultra CHROMASOLV®	Honeywell Riedel-de Haën™
N,*N*,*N*′,*N*′-Tetramethylethylenediamine (TEMED)	Sigma-Aldrich (Merck)
Nickel(II) sulfate	Sigma-Aldrich (Merck)
Nuclease-free water	VWR Chemicals
N-Z-Amine® AS (NZA)	Millipore (Merck)
ortho-phosphoric acid, 85%	SAFC (Merck)
Potassium acetate	Sigma-Aldrich (Merck)
Potassium chloride	Supelco (Merck)
Potassium dihydrogen phosphate	AppliChem
Sodium chloride	VWR Chemicals
Sodium dihydrogen phosphate	VWR Chemicals
Sodium dodecyl sulfate (SDS)	Carl Roth
Sodium hydroxide	VWR Chemicals
Sucrose	Sigma-Aldrich (Merck)
tert-butyl alcohol	Sigma-Aldrich (Merck)
Tris((1-benzyl-4-triazolyl)methyl)amine (TBTA)	Sigma-Aldrich (Merck)
Tris(2-carboxyethyl)phosphine (TCEP)	Sigma-Aldrich (Merck)
Tris(hydroxymethyl)aminomethane (Tris base)	Sigma-Aldrich (Merck)
Tris-Hydrochloride (Tris HCl)	Millipore (Merck)
Triton® X-100	AppliChem
Tryptone, Bacto™	Gibco™ (Thermo Fisher Scientific)
Tween® 20	AppliChem
Urea, PlusOne™	GE Healthcare Life Sciences (now Cytiva)

Water, MS-grade ultrapure, HiPerSolv CHROMANORM®	VWR Chemicals
Water; LC-MS Ultra CHROMASOLV®	Honeywell Riedel-de Haën™
Yeast extract granulated	Millipore (Merck)

Appendix 2: Consumable material

Tab. 14 List of consumables. All consumable material used in this work is reported together with its respective supplier.

Consumable	Supplier
Centrifuge tubes, 15 mL, 50 mL	Eppendorf Greiner Bio-One VWR Sarstedt
Chromatography paper	VWR
Dispenser tips, Plastibrand® PD-tips, various sizes	Brand
Disposable pestle, 1.5 mL	VWR
Electroporation cuvettes, 1 mm	Biozym Scientific GmbH
Fused silica capillary with integrated PicoFrit emitter, self-pack, OD360/ID75, PF360-75-15-N-5	New Objective
Glass microfiber filters GF/C, 1.2 µM poresize, 0.26 µM thickness	Whatman® (Cytiva)
Glass pasteur pipettes	Brandt
Gravity flow columns, Protino®, 35 mL	Macherey-Nagel
Microplate, 96-well, clear, conical bottom	Eppendorf
Microplate, 96-well, clear, flat bottom	Sarstedt
Needle, Sterican®, various sizes	B. Braun Melsungen AG
Octadecyl (C18) Empore™ silica membrane solid phase extraction disks, 47 mm	Supelco (Merck)
PCR Plate, Thermo-Fast™, 96-well, full-Skirted, low profile, black lettering	Thermo Scientific (Thermo Fisher Scientific)
PCR tubes, 0.2 mL,stripes with flat caps	Biozym Scientific GmbH
Petri dishes, round, 92x16mm	Sarstedt
Pipette tips, 10 µL, 200 µL, 1 mL	STARLAB Eppendorf
Pipette tips, 5 mL, 10 mL	Eppendorf
Pipette tips, Mµlti Flex® for gel loading, 1-200 µL	Carl Roth
Pipette tips, UltraFine™ with filter, 10 µL, 200 µL, 1 mL	VWR
PVDF membrane Immobilon®-P	Millipore (Merck)
Reaction tubes, 0.5 mL, 1.5 mL, 2 mL	Sarstedt Carl Roth
Reaction tubes, protein LoBind, 1.5 mL, 2 mL, 5 mL	Eppendorf
Reprosil-Pur 120 C18-AQ 1.9 µm resin	Dr. Maisch GmbH
Scalpel	Swann-Morton
Screw cap micro tubes, 2 mL	Sarstedt
Sealing mat, for 96 Wells PCR microplates, AxyMats™, silicone	Axygen® (Corning)
Sealing mat, for DWP 96/1000 plates	Eppendorf
Semi-micro cuvettes, 10 mm	Sarstedt

Serological pipettes, 1 mL, 5 mL, 10 mL, 25 mL	Sarstedt
Slide-A-Lyzer™ MINI devices, MWCO 3500 and 10000	Thermo Scientific (Thermo Fisher Scientific)
Sterile filter, 0.2 µM	Sarstedt
Syringe, various sizes	B. Braun Melsungen AG
Tissue culture dish 150×20 mm, TC treated	Sarstedt
Tissue culture dish 60×15 mm, TC treated	Sarstedt
Tissue culture plate, 6-well, TC treated, flat bottom with lid	Sarstedt
Vivaspin® 15R columns, MWCO 10000	Sartorius

Appendix 3: Laboratory equipment

Tab. 15 List of laboratory equipment. All laboratory devices used in this work are reported together with their respective manufacturer and unit type.

Laboratory device	Unit type	Manufacturer
Benchtop centrifuge	5415R, 5424R, 5430R, 5810R	Eppendorf
Bioruptor® Standard Sonication device with 1.5 mL tube holder	UCD-200	Diagenode
Blotting apparatus	Mini Trans-Blot® Cell	Bio-Rad
Centrifuge tip adapter for 96 well plates	200 µL tips	GL Sciences
CO_2-incubator	Galaxy® 170R	New Brunswick Scientific (Eppendorf)
Column oven for nano-ESI	PRSO-V1	Sonation GmbH
Cordless pestle motor	47747-370	VWR
DNA-gelelectrophoresis apparatus	VWRI 700-0034	VWR
Drigalski spatula	45 mm	Glaswarenfabrik Karl Hecht GmbH & Co KG
Electroporator	Eporator	Eppendorf
FPLC chromatography system	ÄKTA	GE Healthcare Life Sciences (now Cytiva)
FPLC fraction collector	Frac-920	GE Healthcare Life Sciences (now Cytiva)
Freezer	LGex 3410 MediLine	Liebherr
FRENCH® Press	FA-078 with FRENCH Pressure cell FA-032	SLM Aminco (Thermo)
Fridge	LKUv 1610 MediLine; LKexv 5400 MediLine	Liebherr
Gel casting chamber	GCC-210	C.B.S. Scientific
Gel documentation system	GEL Slite 'Touch'	Intas
Heating-ThermoMixer	MHR 23	HLC Ditabis
Hemocytometer	Neubauer improved,0.1 mm depth	Carl Roth
Ice flaker	AF103	Scotsman
Imaging system	Amersham™ Imager 600	GE Heathcare
Incubator	IN160plus	Memmert GmbH + Co. KG
Incubator shaker	Innova 42R	New Brunswick Scientific (Eppendorf)
Laboratory peristaltic pump	120S/DV	Watson-Marlow

Laser scanner with MultiStage	Typhoon™ FLA9000	GE Healthcare Life Sciences (now Cytiva)
Light microscope	CK2	Olympus
Magnetic stirrer	C-MAG HS 7; RCT classic	IKA
Micro centrifuge	Sprout® ProFuge 10K	Heathrow Scientific LLC STRATAGENE
Micro scales	ENTRIS224I-1S	Sartorius
Microbiological safety cabinet	Mars Pro 1800 Class II	ScanLaf
Microwave	R-940(IN)	SHARP
Mortar with pestle, porcelain	Mortar with 220 mL/240 mL capacity and pestle with135 mm/150 mm friction surface	VWR Collection
Multimode microplate reader	Spark 10M	Tecan
Needle (for tip preparation)	Kel-F Hub NDL, ga 16, 51 mm, pst3 16 gauge, with Ø 1 mm metal pin as plunger	HAMILTON
Orbital shaker	3019	GFL
Orbitrap mass spectrometer	Orbitrap Elite™ Hybrid Ion Trap Mass Spectrometer with ETD, EASY-nLC 1000 liquid chromatograph, Nanospray Flex™ ion source ES071	Thermo Scientific
pH benchtop meters	inoLab® pH 720	WTW
Pipette controller	pipetus®	Hirschmann
Pipettes	Research® plus PIPETMAN Classic™	Eppendorf Gilson
Pipettes, 8-channel	Research® plus	Eppendorf
Pipettes, electronic	Xplorer®	Eppendorf
Power supply	300V EV261	VWR Consort
Protein-gelelectrophoresis apparatus	MGV-202-U	C.B.S. Scientific
Repeating pipette	Handystep® electronic	BRAND
Roller shaker	SRT9	Stuart
Rotator	SB2	Stuart
Scales	ENTRIS423I-1S LPC-723i	Sartorius VWR
Shaker	Vibrax® VXR basic +VX 2E attachment	IKA
Thermocycler	Mastercycler® nexus gradient; nexus eco; nexus X2e	Eppendorf

Thermomixer	ThermoMixer® C	Eppendorf
Ultra-low temperature freezer	HERAfreeze™ HFU500TV	Thermo Scientific
Ultrapure water system	Milli-Q® Reference with Q-POD® element	Merck-Millipore
Ultrasonic bath	Sonorex RK 102 H	Bandelin
UV/Vis-spectrophotometer	DS-11+	DeNOVIX
Vacuum aspiration system	BioChem-VacuuCenter BVC professional	Vacuubrand
Vacuum concentrator	Concentrator plus with rotor F-45-48-11 and rotor A-2-VC	Eppendorf
Vortexer	VV3	VWR
Water bath	1003	GFL

Appendix 4: Buffers and solutions

Tab. 16 List of buffers and solutions. All buffers and solutions used in this work are reported together with their respective composition.

Buffer or solution	Composition
B5 culture medium	1× B5-salts, 1 mg L^{-1} 2,4-Dichlorophenoxyacetic acid, 0.4 M sucrose; pH 5.7, filter sterilised
Bis-Tris buffer, 1.25 M	131 g Bis-Tris, ca. 40-50 mL 25% HCl, filled up to 500 mL with MS-grade ultrapure water; pH 6.6, filter sterilised
Blotting buffer	1× SDS running buffer, 20% methanol, 70% Milli-Q water
CCMB80 buffer	10 mL of a 1M stock KOAc pH 7.0 (10 mM), 11.8 g $CaCl_2 \cdot 2H_2O$ (80 mM), 4.0 g $MnCl_2 \cdot 4H_2O$ (20 mM), 2.0 g $MgCl_2 \cdot 6H_2O$ (10 mM), 100 mL glycerol (10% (v/v)), filled up to 1 L with Milli-Q water; pH 6.4 (do not adjust pH up), filter sterilised, stored at 4 °C
Colloidal Coomassie Stain	100 g ammonium sulfate, 20 mL 5% (w/v) Coomassie G-250 solution, 30 mL *ortho*-phosphoric acid 85%, 200 mL ethanol, filled up to 1 L with Milli-Q water
GF/C equilibration buffer	1 mL 0.8 M urea in 50 mM ABC, 550 µL 10% FA
IMAC200 buffer	50 mM $NaHPO_4$, 300 mM NaCl, 200 mM imidazole; pH 8.0, filter sterilised
IMAC5 buffer	50 mM $NaHPO_4$, 300 mM NaCl, 5 mM imidazole; pH 8.0, filter sterilised
LDS gel-loading dye, 4x	4 g glycerol (40% (w/v)), 0.682 g Tris base (563 mM), 0.666 g Tris HCl (423 mM), 0.8 g LDS (8% (w/v)), 0.0076 g EDTA-$Na_2 \cdot 2H_2O$ (2 mM), 0.75 mL 1% (w/v) Coomassie G-250 solution (0.075% (w/v)), filled up to 10 mL with MS-grade ultrapure water
LEW buffer	50 mM $NaHPO_4$, 300 mM NaCl; pH 8.0
LEW lysis buffer	50 mM $NaHPO_4$, 300 mM NaCl, 0.1% (w/v) Triton® X-100; pH 8.0
MOPS running buffer, 20x	104.6 g MOPS (1 M), 60.6 g Tris base (1 M), 10 g SDS (2% (w/v)), 2.996 g (20.5 mM) EDTA free acid, filled up to 500 mL with Milli-Q water; pH ~7.7 (not adjusted)
NZA agar	10 g N-Z-Amine, 5 g yeast extract, 10 g NaCl, 15 g Agar, fill up to 1 L with Milli-Q water, autoclaved
NZA medium	10 g N-Z-Amine, 5 g yeast extract, 10 g NaCl, fill up to 1 L with Milli-Q water, autoclaved
PBS, 1×	9.07 g NaCl (155 mM), 0.426 g Na_2HPO_4 (3 mM), 0.144 g KH_2PO_4 (1.06 mM), filled up to 1 L with MS-grade ultrapure water; pH 7.4

Polyacrylamide gel Bis-Tris, 11%	51.33 mL 30% Acrylamide/Bisacrylamide solution, 40.04 mL 1.25 M Bis-Tris buffer, 0.57 mL 10% APS, 0.116 mL TEMED, 48 mL MS-grade ultrapure water
Protoplast enzyme solution	11.67 mg mL^{-1} Cellulase Onozuka R-10 and 2.71 mg mL^{-1} Macerozyme R-10 in 240 mM $CaCl_2$, filter sterilised
SDS running buffer, 10×	30 g Tris base (250 mM), 144 g glycine (1.92 M), 1 g SDS (0.1% (w/v)), filled up to 1 L with Milli-Q water
SOB medium	20 g tryptone, 5 g bacto yeast extract, 0.584 g NaCl, 0.186 g KCl, filled up to 1 L with Milli-Q water; pH 7.5, autoclaved
Sorenson's phosphate buffer ($NaHPO_4$), 1 M	2.5 mL 1 M NaH_2PO_4, 47.5 mL 1 M Na_2HPO_4; pH 8.0 (not adjusted)
STSA	0.5 % FA in MS-grade ultrapure water
STSB	0.5 % FA in 80% ACN/20% MS-grade ultrapure water
TBE buffer, 5x	53.9 g Tris base (445 mM), 27.5 g boric acid (445 mM), 3.72 g EDTA-$Na_2 \cdot 2H_2O$ (10 mM), filled up to 1 L with Milli-Q water; pH 8,0
TBS-T	1× TBS, 0.2% (w/v) Tween® 20
Tris-buffered saline (TBS), 10×	24.2 g Tris base (200 mM), 87.7 g NaCl (1.5 M), filled up to 1 L with Milli-Q water; pH 7.5

Appendix 5: Chemical structures of all kinase inhibitors employed in this work

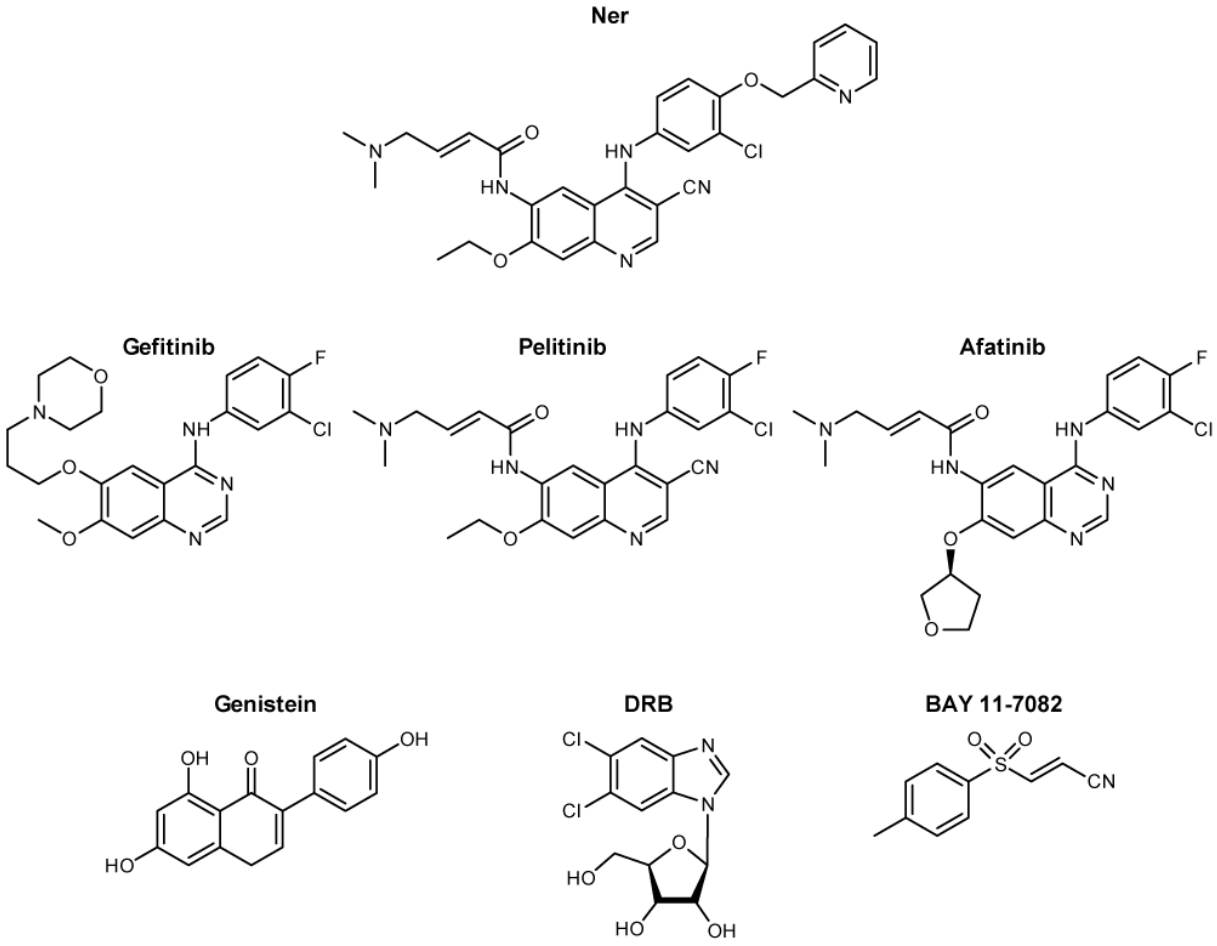

Fig. 37 Chemical structures of all employed kinase inhibitors. Chemical structures of all TKIs as well as of all primary hits identified from the screen for SA agonists that were employed in this work are depicted in direct comparison to the chemical structure of **Ner**.

Appendix 6: Sequence of the *eh7*::pET-59-DEST plasmid

TGGCGAATGGGACGCGCCCTGTAGCGGCGCATTAAGCGCGGCGGGTGTGGTGGTTACGCGCAGCGTGACCGCTAC
ACTTGCCAGCGCCCTAGCGCCCGCTCCTTTCGCTTTCTTCCCTTCCTTTCTCGCCACGTTCGCCGGCTTTCCCCGTC
AAGCTCTAAATCGGGGGCTCCCTTTAGGGTTCCGATTTAGTGCTTTACGGCACCTCGACCCCAAAAAACTTGATTA
GGGTGATGGTTCACGTAGTGGGCCATCGCCCTGATAGACGGTTTTTCGCCCTTTGACGTTGGAGTCCACGTTCTTT
AATAGTGGACTCTTGTTCCAAACTGGAACAACACTCAACCCTATCTCGGTCTATTCTTTTGATTTATAAGGGATT
TTGCCGATTTCGGCCTATTGGTTAAAAAATGAGCTGATTTAACAAAAATTTAACGCGAATTTTAACAAAATATTA
ACGTTTACAATTTCTGGCGGCACGATGGCATGAGATTATCAAAAAGGATCTTCACCTAGATCCTTTTAAATTAAA
AATGAAGTTTTAAATCAATCTAAAGTATATATGAGTAAACTTGGTCTGACAGTTACCAATGCTTAATCAGTGAGG
CACCTATCTCAGCGATCTGTCTATTTCGTTCATCCATAGTTGCCTGACTCCCCGTCGTGTAGATAACTACGATACG
GGAGGGCTTACCATCTGGCCCCAGTGCTGCAATGATACCGCGAGACCCACGCTCACCGGCTCCAGATTTATCAGCA
ATAAACCAGCCAGCCGGAAGGGCCGAGCGCAGAAGTGGTCCTGCAACTTTATCCGCCTCCATCCAGTCTATTAATT
GTTGCCGGGAAGCTAGAGTAAGTAGTTCGCCAGTTAATAGTTTGCGCAACGTTGTTGCCATTGCTACAGGCATCG
TGGTGTCACGCTCGTCGTTTGGTATGGCTTCATTCAGCTCCGGTTCCCAACGATCAAGGCGAGTTACATGATCCCC
CATGTTGTGCAAAAAAGCGGTTAGCTCCTTCGGTCCTCCGATCGTTGTCAGAAGTAAGTTGGCCGCAGTGTTATC
ACTCATGGTTATGGCAGCACTGCATAATTCTCTTACTGTCATGCCATCCGTAAGATGCTTTTCTGTGACTGGTGAG
TACTCAACCAAGTCATTCTGAGAATAGTGTATGCGGCGACCGAGTTGCTCTTGCCCGGCGTCAATACGGGATAAT
ACCGCGCCACATAGCAGAACTTTAAAAGTGCTCATCATTGGAAAACGTTCTTCGGGGCGAAAACTCTCAAGGATC
TTACCGCTGTTGAGATCCAGTTCGATGTAACCCACTCGTGCACCCAACTGATCTTCAGCATCTTTTACTTTCACCA
GCGTTTCTGGGTGAGCAAAAACAGGAAGGCAAAATGCCGCAAAAAAGGGAATAAGGGCGACACGGAAATGTTGA
ATACTCATACTCTTCCTTTTTCAATCATGATTGAAGCATTTATCAGGGTTATTGTCTCATGAGCGGATACATATT
TGAATGTATTTAGAAAAATAAACAAATAGGTCATGACCAAAATCCCTTAACGTGAGTTTTCGTTCCACTGAGCGT
CAGACCCCGTAGAAAAGATCAAAGGATCTTCTTGAGATCCTTTTTTTCTGCGCGTAATCTGCTGCTTGCAAACAA
AAAAACCACCGCTACCAGCGGTGGTTTGTTTGCCGGATCAAGAGCTACCAACTCTTTTTCCGAAGGTAACTGGCTT
CAGCAGAGCGCAGATACCAAATACTGTCCTTCTAGTGTAGCCGTAGTTAGGCCACCACTTCAAGAACTCTGTAGC
ACCGCCTACATACCTCGCTCTGCTAATCCTGTTACCAGTGGCTGCTGCCAGTGGCGATAAGTCGTGTCTTACCGGG
TTGGACTCAAGACGATAGTTACCGGATAAGGCGCAGCGGTCGGGCTGAACGGGGGGTTCGTGCACACAGCCCAGC
TTGGAGCGAACGACCTACACCGAACTGAGATACCTACAGCGTGAGCTATGAGAAAGCGCCACGCTTCCCGAAGGG
AGAAAGGCGGACAGGTATCCGGTAAGCGGCAGGGTCGGAACAGGAGAGCGCACGAGGGAGCTTCCAGGGGGAAAC
GCCTGGTATCTTTATAGTCCTGTCGGGTTTCGCCACCTCTGACTTGAGCGTCGATTTTTGTGATGCTCGTCAGGGG
GGCGGAGCCTATGGAAAAACGCCAGCAACGCGGCCTTTTTACGGTTCCTGGCCTTTTGCTGGCCTTTTGCTCACAT
GTTCTTTCCTGCGTTATCCCCTGATTCTGTGGATAACCGTATTACCGCCTTTGAGTGAGCTGATACCGCTCGCCGC
AGCCGAACGACCGAGCGCAGCGAGTCAGTGAGCGAGGAAGCGGAAGAGCGCCTGATGCGGTATTTTCTCCTTACG
CATCTGTGCGGTATTTCACACCGCATATATGGTGCACTCTCAGTACAATCTGCTCTGATGCCGCATAGTTAAGCCA
GTATACACTCCGCTATCGCTACGTGACTGGGTCATGGCTGCGCCCCGACACCCGCCAACACCCGCTGACGCGCCCT
GACGGGCTTGTCTGCTCCCGGCATCCGCTTACAGACAAGCTGTGACCGTCTCCGGGAGCTGCATGTGTCAGAGGTT
TTCACCGTCATCACCGAAACGCGCGAGGCAGCTGCGGTAAAGCTCATCAGCGTGGTCGTGAAGCGATTCACAGAT
GTCTGCCTGTTCATCCGCGTCCAGCTCGTTGAGTTTCTCCAGAAGCGTTAATGTCTGGCTTCTGATAAAGCGGGCC
ATGTTAAGGGCGGTTTTTTCCTGTTTGGTCACTGATGCCTCCGTGTAAGGGGGATTTCTGTTCATGGGGGTAATG
ATACCGATGAAACGAGAGAGGATGCTCACGATACGGGTTACTGATGATGAACATGCCCGGTTACTGGAACGTTGT
GAGGGTAAACAACTGGCGGTATGGATGCGGCGGGACCAGAGAAAAATCACTCAGGGTCAATGCCAGCGCTTCGTT
AATACAGATGTAGGTGTTCCACAGGGTAGCCAGCAGCATCCTGCGATGCAGATCCGGAACATAATGGTGCAGGGC
GCTGACTTCCGCGTTTCCAGACTTTACGAAACACGGAAACCGAAGACCATTCATGTTGTTGCTCAGGTCGCAGACG
TTTTGCAGCAGCAGTCGCTTCACGTTCGCTCGCGTATCGGTGATTCATTCTGCTAACCAGTAAGGCAACCCCGCCA
GCCTAGCCGGGTCCTCAACGACAGGAGCACGATCATGCTAGTCATGCCCCGCGCCCACCGGAAGGAGCTGACTGGG
TTGAAGGCTCTCAAGGGCATCGGTCGAGATCCCGGTGCCTAATGAGTGAGCTAACTTACATTAATTGCGTTGCGC
TCACTGCCCGCTTTCCAGTCGGGAAACCTGTCGTGCCAGCTGCATTAATGAATCGGCCAACGCGCGGGGAGAGGCG
GTTTGCGTATTGGGCGCCAGGGTGGTTTTTCTTTTCACCAGTGAGACGGGCAACAGCTGATTGCCCTTCACCGCCT
GGCCCTGAGAGAGTTGCAGCAAGCGGTCCACGCTGGTTTGCCCCAGCAGGCGAAAATCCTGTTTGATGGTGGTTA
ACGGCGGGATATAACATGAGCTGTCTTCGGTATCGTCGTATCCCACTACCGAGATGTCCGCACCAACGCGCAGCCC
GGACTCGGTAATGGCGCGCATTGCGCCCAGCGCCATCTGATCGTTGGCAACCAGCATCGCAGTGGGAACGATGCCC
TCATTCAGCATTTGCATGGTTTGTTGAAAACCGGACATGGCACTCCAGTCGCCTTCCCGTTCCGCTATCGGCTGAA

TTTGATTGCGAGTGAGATATTTATGCCAGCCAGCCAGACGCAGACGCGCCGAGACAGAACTTAATGGGCCCGCTA
ACAGCGCGATTTGCTGGTGACCCAATGCGACCAGATGCTCCACGCCCAGTCGCGTACCGTCTTCATGGGAGAAAAT
AATACTGTTGATGGGTGTCTGGTCAGAGACATCAAGAAATAACGCCGGAACATTAGTGCAGGCAGCTTCCACAGC
AATGGCATCCTGGTCATCCAGCGGATAGTTAATGATCAGCCCACTGACGCGTTGCGCGAGAAGATTGTGCACCGCC
GCTTTACAGGCTTCGACGCCGCTTCGTTCTACCATCGACACCACCACGCTGGCACCCAGTTGATCGGCGCGAGATT
TAATCGCCGCGACAATTTGCGACGGCGCGTGCAGGGCCAGACTGGAGGTGGCAACGCCAATCAGCAACGACTGTT
TGCCCGCCAGTTGTTGTGCCACGCGGTTGGGAATGTAATTCAGCTCCGCCATCGCCGCTTCCACTTTTTCCCGCGT
TTTCGCAGAAACGTGGCTGGCCTGGTTCACCACGCGGGAAACGGTCTGATAAGAGACACCGGCATACTCTGCGAC
ATCGTATAACGTTACTGGTTTCACATTCACCACCCTGAATTGACTCTCTTCCGGGCGCTATCATGCCATACCGCGA
AAGGTTTTGCGCCATTCGATGGTGTCCGGGATCTCGACGCTCTCCCTTATGCGACTCCTGCATTAGGAAGCAGCCC
AGTAGTAGGTTGAGGCCGTTGAGCACCGCCGCCGCAAGGAATGGTGCATGCAAGGAGATGGCGCCCAACAGTCCC
CCGGCCACGGGGCCTGCCACCATACCCACGCCGAAACAAGCGCTCATGAGCCCGAAGTGGCGAGCCCGATCTTCCC
CATCGGTGATGTCGGCGATATAGGCGCCAGCAACCGCACCTGTGGCGCCGGTGATGCCGGCCACGATGCGTCCGGC
GTAGAGGATCGAGATCGATCTCGATCCCGCGAAATTAATACGACTCACTATAGGGGAATTGTGAGCGGATAACAA
TTCCCCTCTAGAAATAATTTTGTTTAACTTTAAGAAGGAGATATACCATGGGCAGCAGCCATCATCATCATCATC
ACAGCCATATGGCTAGCGATAAAATTATTCACCTGACTGACGACAGTTTTGACACGGATGTACTCAAAGCGGACG
GGGCGATCCTCGTCGATTTCTGGGCAGAGTGGTGCGGTCCGTGCAAAATGATCGCCCCGATTCTGGATGAAATCG
CTGACGAATATCAGGGCAAACTGACCGTTGCAAAACTGAACATCGATCAAAACCCTGGCACTGCGCCGAAATATG
GCATCCGTGGTATCCCGACTCTGCTGCTGTTCAAAAACGGTGAAGTGGCGGCAACCAAAGTGGGTGCACTGTCTA
AAGGTCAGTTGAAAGAGTTCCTCGACGCTAACCTGGCCCGAGCTCTTGTTCCACGTGGTTCTGTCACAAGTTTGTA
CAAAAAAGCAGGCTTCATGGAGAAGATAGAGCACACGACGATATCTACCAATGGTATTAACATGCATGTGGCTTC
GATTGGTTCAGGTCCAGTGATCCTATTCGTCCATGGCTTTCCCGATCTCTGGTACTCATGGCGTCACCAGCTTGTC
TCTTTCGCTGCCTTAGGTTACCGCGCAATCGCTCCAGATCTTCGAGGATACGGCGATTCCGATGCGCCGCCGTCTC
GTGAATCTTACACCATCCTTCATATCGTCGGAGACCTCGTCGGATTACTGGATTCGCTCGGTGTTGATCGGGTTTT
CCTCGTCGGTCACGATTGGGGAGCAATTGTTGCGTGGTGGCTTTGTATGATCAGGCCTGATCGAGTCAACGCGTT
GGTCAACACTAGCGTTGTGTTTAATCCGAGGAATCCTTCTGTGAAACCTGTTGATGCGTTTAGGGCTTTGTTCGG
CGATGATTACTACATTTGCAGGTTTCAGGAGCCTGGAGAGATCGAAGAGGACTTTGCTCAAGTTGATACAAAAAA
GTTAATAACCAGATTTTTCACTTCGCGTAACCCACGTCCACCTTGCATTCCAAAGTCAGTTGGTTTCAGAGGTTTA
CCTGATCCACCTTCTTTGCCCGCTTGGCTCACCGAACAAGATGTCAGGTTCTACGGAGACAAGTTTAGCCAAAAAG
GCTTCACCGGTGGGCTAAACTACTATCGCGCCCTGAACCTAAGCTGGGAACTAACAGCTCCATGGACCGGTCTACA
AATCAAAGTCCCTGTGAAATTCATAGTGGGTGATCTAGACATAACATACAATATCCCCGGAACAAAGGAATACAT
ACATGAAGGTGGTTTGAAGAAGCACGTACCTTTTCTACAAGAAGTGGTGGTAATGGAAGGTGTAGGTCACTTCCT
CCATCAAGAGAAGCCTGACGAGGTCACTGACCATATCTATGGCTTCTTCAAGAAATTCAGAACCCGCGAAACCGC
ATCCTTGTAGAACCCAGCTTTCTTGTACAAAGTGGTTTCCGCTTGGAGCCACCCGCAGTTCGAAAAGTAAGTGAT
TAACCTAGGCTGCTGCCACCGCTGAGCAATAACTAGCATAACCCCTTGGGGCCTCTAAACGGGTCTTGAGGGGTTT
TTTGCTGAAAGGAGGAACTATATCCGGAT

Appendix 7: Protein groups identified with ≡Ner in HeLa after IGD

Tab. 17 Protein groups identified from the IGD of the *in situ* labelling of HeLa cells with ≡Ner. Complete list of protein groups obtained after initial filtering to remove irrelevant hits (2.2.5.2) that were identified after IGD (2.2.4.2.1) and LC-MS/MS analysis (2.2.4.4) of the samples obtained from the *in situ* labelling of HeLa cells with **≡Ner** (2.2.3.3.1). Protein groups (No.) were sorted by total MS/MS counts across all analysed samples. MS/MS counts for each individual sample, MW, Andromeda score, majority protein IDs (UniProt identifier) and gene names are reported for each protein group.

No.	MS/MS Count DMSO	MS/MS Count ≡Ner	MS/MS Count ≡Ner/ Ner	MW [kDa]	Score	Majority protein IDs (UniProt)	Gene names
1	59	72	38	129.6	323.3	P11498 A0A494C016	PC PC
2	47	64	37	265.6	323.3	Q13085	ACACA
3	22	42	26	280.7	323.3	P21333 Q60FE5 A0A087WWY3	FLNA FLNA FLNA
4	23	3	45	331.8	323.3	P15924	DSP
5	18	30	16	164.9	316.1	P31327	CPS1
6	19	18	20	47.2	269.1	P06733 A0A2R8Y6G6	ENO1 ENO1
7	18	16	13	41.8	235.3	P63261 I3L3I0 I3L1U9 I3L4N8	ACTG1 ACTG1 ACTG1 ACTG1
8	0	39	0	134.3	323.3	P00533 E9PFD7 Q504U8	EGFR EGFR EGFR
9	9	19	6	191.6	202.4	Q00610 A0A087WVQ6	CLTC CLTC
10	10	16	8	18.0	72.0	P62937 F8WE65 C9J5S7	PPIA PPIA PPIA
11	6	16	7	273.4	119.3	P49327 A0A0U1RQF0	FASN FASN
12	9	12	8	57.9	173.7	P14618 B4DNK4 H3BTN5 H3BQ34 H3BR70	PKM PKM PKM PKM PKM
13	8	10	9	67.9	150.9	P29401 A0A0B4J1R6	TKT TKT
14	8	10	8	61.1	110.4	P10809	HSPD1

						E7ESH4	HSPD1
15	8	13	5	50.2	124.5	P68363 Q9BQE3 F5H5D3 Q71U36 F8VVB9 Q6PEY2 A0A1W2PQM2 P0DPH8 P0DPH7	TUBA1B TUBA1C TUBA1C TUBA1A TUBA1B TUBA3E TUBA1C TUBA3D TUBA3C
16	7	8	10	226.5	149.7	P35579	MYH9
17	2	13	9	278.2	95.1	O75369 E7EN95	FLNB FLNB
18	6	10	8	49.7	96.8	P07437 Q5JP53 Q5ST81 Q9BVA1 Q13885	TUBB TUBB TUBB TUBB2B TUBB2A
19	8	9	7	70.9	100.8	P11142 E9PKE3 E9PN89 E9PNE6 P54652	HSPA8 HSPA8 HSPA8 HSPA8 HSPA2
20	10	7	5	38.6	137.8	P07355 H0YKS4 H0YMD0 H0YMU9 H0YN42 H0YMM1 A6NMY6 H0YKZ7 H0YLV6 H0YMT9 H0YKX9 H0YNP5 H0YM50 H0YKL9 H0YMW4	ANXA2 ANXA2 ANXA2 ANXA2 ANXA2 ANXA2 ANXA2P2 ANXA2 ANXA2 ANXA2 ANXA2 ANXA2 ANXA2 ANXA2 ANXA2
21	8	9	4	36.1	68.5	P04406 E7EUT5	GAPDH GAPDH
22	7	7	7	83.3	187.9	P08238	HSP90AB1
23	6	9	6	95.3	55.7	P13639	EEF2
24	9	8	4	50.1	45.9	P68104 Q5VTE0 A0A087WVQ9 Q05639 A0A087WV01 A0A2U3TZH3	EEF1A1 EEF1A1P5 EEF1A1 EEF1A2 EEF1A1 EEF1A2

25	9	5	6	113.8	94.0	Q02413	DSG1
26	6	2	11	81.7	100.0	P14923 C9JTX4 C9J826 C9JK18 C9JKY1	JUP JUP JUP JUP JUP
27	3	9	7	531.8	116.8	Q15149 H0YDN1	PLEC PLEC
28	5	8	5	36.7	55.7	P00338 F5GXY2	LDHA LDHA
29	7	4	4	14.1	52.3	Q6FI13 Q16777	HIST2H2AA3 HIST2H2AC
30	2	9	3	25.8	44.4	P0CG47 P62979 P62987 M0R1V7 J3QS39 Q49A90 J3QTR3 F5H6Q2 F5GYU3 F5H2Z3 F5H265 B4DV12 F5H388 F5H747 F5GXK7 J3QKN0 Q5PY61 Q96C32 P0CG48 J3QSA3 F5GZ39	UBB RPS27A UBA52 UBA52 UBB RPS27A RPS27A UBC UBC UBC UBC UBB UBC UBC UBC UBB UBC UBC UBC UBB UBC
31	4	5	4	57.7	64.8	P04746 P19961 P04745 Q5T085	AMY2A AMY2B AMY1A AMY1A
32	4	4	4	18.5	22.6	P23528 E9PP50 E9PLJ3 E9PS23 E9PQB7 G3V1A4 E9PK25	CFL1 CFL1 CFL1 CFL1 CFL1 CFL1 CFL1
33	2	4	6	170.6	44.7	P07814 V9GYZ6	EPRS1 EPRS1
34	3	5	4	16.6	55.2	P12273	PIP
35	4	6	1	11.7	53.3	P10599	TXN

36	5	2	4	11.3	61.7	P81605	DCD
37	5	3	2	22.1	44.1	Q06830 A0A0A0MSI0 A0A0A0MRQ5	PRDX1 PRDX1 PRDX1
38	2	3	5	70.1	27.1	A0A0G2JIW1 P0DMV9 P0DMV8	HSPA1B HSPA1B HSPA1A
39	0	6	4	189.3	52.2	P46940 A0A0J9YXZ5 H0YLE8	IQGAP1 IQGAP1 IQGAP1
40	5	5	0	53.7	29.5	P08670 B0YJC4	VIM VIM
41	3	4	3	76.6	99.2	P19338 H7BY16	NCL NCL
42	3	3	4	30.8	45.9	P60174	TPI1
43	1	2	6	11.0	75.5	P01040 C9J0E4	CSTA CSTA
44	1	4	4	72.3	46.6	P11021	HSPA5
45	4	2	2	38.7	28.8	P04083 Q5T3N1	ANXA1 ANXA1
46	4	2	2	56.6	44.6	P06576 F8W079 H0YH81	ATP5F1B ATP5F1B ATP5F1B
47	2	2	4	100.0	26.0	Q08554	DSC1
48	1	2	4	16.8	15.7	P63241 I3L397 I3L504 Q6IS14 Q9GZV4 F8WCJ1 C9J7B5 C9J4W5	EIF5A EIF5A EIF5A EIF5AL1 EIF5A2 EIF5A2 EIF5A2 EIF5A2
49	2	2	3	11.8	82.9	P01834	IGKC
50	3	2	2	17.1	18.5	P15531 P22392 E7ERL0 J3KPD9 Q32Q12 O60361	NME1 NME2 NME1 NME1-NME2 NME1-NME2 NME2P1
51	3	2	2	25.0	25.7	P30041	PRDX6
52	0	1	6	15.9	48.9	Q9NZT1	CALML5
53	1	3	2	33.5	24.2	Q01105 P0DME0 A0A0C4DFV9 A0A087X027	SET SETSIP SET SETSIP
54	1	3	2	26.2	9.4	Q9HB71 B2ZWH1	CACYBP CACYBP
55	3	2	1	27.7	68.7	P63104	YWHAZ

						E5RGE1 E5RIR4 E9PD24 E7EVZ2 E7ESK7 E7EX29	YWHAZ YWHAZ YWHAZ YWHAZ YWHAZ YWHAZ
56	1	3	2	243.0	27.3	P27708 F8VPD4	CAD CAD
57	2	2	2	104.9	27.9	O43707 H7C144 F5GXS2	ACTN4 ACTN4 ACTN4
58	1	3	1	80.1	38.4	P05165 A0A1B0GU58 A0A1B0GWI4 A0A1B0GWA1 A0A1B0GUX9	PCCA PCCA PCCA PCCA PCCA
59	2	2	1	36.6	28.9	P07195 A8MW50 A0A3B3IS95 F5H793 C9J7H8	LDHB LDHB *N/A* LDHB LDHB
60	2	2	1	12.2	45.2	P06454 B8ZZQ6 B8ZZA1 B8ZZW7 H7C2N1	PTMA PTMA PTMA PTMA PTMA
61	3	2	0	48.1	13.6	P05783 F8VZY9	KRT18 KRT18
62	1	3	1	74.1	27.0	P02545 Q3BDU5 Q5TCI8	LMNA LMNA LMNA
63	0	0	5	59.8	31.8	P04040	CAT
64	2	2	1	13.2	12.0	P06702	S100A9
65	1	3	1	84.7	31.2	P07900	HSP90AA1
66	1	2	2	37.4	31.3	P22626 A0A087WUI2	HNRNPA2B1 HNRNPA2B1
67	2	2	1	49.8	18.2	P68371 P04350	TUBB4B TUBB4A
68	0	0	5	64.1	53.4	Q5T749	KPRP
69	0	0	5	26.2	41.4	Q5T750	XP32
70	1	3	1	269.8	24.1	Q9Y490	TLN1
71	0	4	0	56.7	22.6	O43175 A0A286YF22 A0A2C9F2M7 A0A286YFM8 A0A286YFL2 A0A286YFA2 A0A286YER3	PHGDH PHGDH PHGDH PHGDH PHGDH PHGDH PHGDH

						A0A286YFC8 A0A286YFB2	PHGDH PHGDH
72	0	0	4	76.6	18.8	Q08188 A0A494C0J7	TGM3 *N/A*
73	2	0	2	13.6	15.3	P0C0S5 Q71UI9 C9J0D1 A0A494C189	H2AZ1 H2AFV H2AZ2 H2AZ1
74	2	1	1	22.8	41.0	P04792 F8WE04	HSPB1 HSPB1
75	1	2	1	34.7	13.0	P05089	ARG1
76	2	2	0	11.7	15.1	P05387 H0YDD8	RPLP2 RPLP2
77	1	2	1	92.5	30.0	P14625 Q96GW1 A0A1W2PRR1	HSP90B1 HSP90B1 HSP90B1
78	0	1	3	27.7	25.2	P31944	CASP14
79	0	4	0	51.0	24.7	P61978 Q5T6W2	HNRNPK HNRNPK
80	0	4	0	141.0	32.0	Q08211	DHX9
81	2	1	0	23.6	6.6	P40429 M0QZU1 A0A096LPE0	RPL13A RPL13A RPL13A
82	1	1	1	16.5	17.7	P61626 F8VV32 A0A0B4J259	LYZ LYZ LYZ
83	3	0	0	14.1	21.9	P0C0S8 Q9BTM1 Q99878 Q96KK5 P20671 A0A0U1RR32 A0A0U1RRH7 Q93077 Q7L7L0 P04908 H0YFX9 P16104 Q8IUE6 A0A3B3IS11	H2AC11 H2AFJ H2AC14 HIST1H2AH H2AC7 hCG_2039566 *N/A* HIST1H2AC HIST3H2A H2AC4 H2AJ H2AX HIST2H2AB *N/A*
84	1	1	1	22.1	6.4	P62081 A0A2R8Y623 B5MCP9	RPS7 RPS7 RPS7
85	1	1	1	16.0	14.5	P68871 F8W6P5 A0A2R8Y7R2 P02042 E9PEW8	HBB HBB HBB HBD HBD

						E9PFT6	HBD
86	2	1	0	46.6	6.8	O75718 C9JP16	CRTAP CRTAP
87	1	1	1	38.4	14.5	Q14103 D6RF44 H0YA96 D6RAF8 H0Y8G5	HNRNPD HNRNPD HNRNPD HNRNPD HNRNPD
88	1	1	1	27.8	18.9	P27348 E9PG15	YWHAQ YWHAQ
89	1	2	0	35.9	6.5	P08758 E9PHT9	ANXA5 ANXA5
90	1	1	1	39.4	12.2	P04075 H3BPS8 H3BQN4 J3KPS3 H3BUH7 H3BR04 H3BU78	ALDOA ALDOA ALDOA ALDOA ALDOA ALDOA ALDOA
91	1	1	1	14.0	7.3	P33778 Q99880 Q93079 Q16778 Q99879 Q99877 Q5QNW6 P58876 O60814 Q8N257 P62807 P23527 P57053 P06899 U3KQK0	HIST1H2BB H2BC13 HIST1H2BH HIST2H2BE H2BC14 H2BC15 HIST2H2BF HIST1H2BD H2BC12 HIST3H2BB H2BC4 HIST1H2BO H2BFS H2BC11 H2BC15
92	1	1	1	44.6	11.5	P00558	PGK1
93	1	1	1	83.3	12.7	P01833	PIGR
94	0	2	1	10.8	15.9	P05109	S100A8
95	1	1	1	23.4	18.6	P09211 A0A087X243 A0A087X2E9 A8MX94	GSTP1 GSTP1 GSTP1 GSTP1
96	1	1	1	71.0	11.2	P17066 P48741	HSPA6 HSPA7
97	1	1	1	50.1	31.3	P26641	EEF1G
98	1	1	1	19.3	18.3	P31025	LCN1
99	1	1	1	22.4	43.1	P37802 X6RJP6	TAGLN2 TAGLN2
100	1	1	1	41.7	23.5	P60709	ACTB

						A0A2R8Y793 P63267 P68133 P62736 P68032	ACTB ACTG2 ACTA1 ACTA2 ACTC1
101	1	1	1	24.2	38.5	P62241 Q5JR95	RPS8 RPS8
102	1	1	1	7.8	14.5	P62857	RPS28
103	1	1	1	5.0	7.8	P63313	TMSB10
104	1	1	1	629.1	12.7	Q09666	AHNAK
105	1	0	2	46.3	13.6	Q96P63	SERPINB12
106	1	1	1	260.7	19.4	Q9UGM3	DMBT1
107	0	2	0	426.7	10.7	P11532 A0A087WV90 E9PDN5 A0A087WTU7 A0A075B6G3	DMD DMD DMD DMD DMD
108	0	0	2	555.7	6.0	P58107 A0A075B730	EPPK1 EPPK1
109	1	1	0	70.9	8.7	Q16881 E2QRB9 E9PIR7 F8W809 A0A087WSW9 A0A182DWI3 A0A087WSY9	TXNRD1 TXNRD1 TXNRD1 TXNRD1 TXNRD1 TXNRD1 TXNRD1
110	1	1	0	31.1	6.6	P29692 E9PMW7 E9PIZ1 E9PPR1 E9PL12 E9PQ49 E9PI39 H0YCK7 E9PK01 A0A087X1X7 E9PRY8	EEF1D EEF1D EEF1D EEF1D EEF1D EEF1D EEF1D EEF1D EEF1D EEF1D EEF1D
111	0	2	0	90.6	12.2	Q00839 A0A1W2PRZ7 A0A1W2PQ74 A0A1W2PQL0 A0A1W2PP34 A0A1W2PPL4 A0A1W2PPH7 Q5RI18 A0A1W2PP35 A0A1X7SBS1 A0A1W2PPS1	HNRNPU HNRNPU HNRNPU HNRNPU HNRNPU HNRNPU HNRNPU HNRNPU HNRNPU HNRNPU HNRNPU

						A0A1W2PQD4	HNRNPU
112	0	2	0	137.9	12.7	P04626 B4DTR1 J3QLU9	ERBB2 ERBB2 ERBB2
113	0	1	1	18.1	10.5	P01591 C9JA05 D6RHJ6 D6RD17	JCHAIN JCHAIN JCHAIN JCHAIN
114	1	1	0	30.3	6.4	D6R9P3 D6RD18 D6RBZ0	HNRNPAB HNRNPAB HNRNPAB
115	0	1	1	29.9	6.2	P61247 D6RGE0 D6RI02 D6RED7 D6RAS7 H0Y8L7 D6RB09 E9PFI5 D6RG13 D6RAT0	RPS3A RPS3A RPS3A RPS3A RPS3A RPS3A RPS3A RPS3A RPS3A RPS3A
116	1	1	0	80.5	12.8	Q96RQ3 G5E9X5 F5GYT8 E9PG35 E9PHF7	MCCC1 MCCC1 MCCC1 MCCC1 MCCC1
117	0	1	1	106.9	14.8	Q14697 F5H6X6 E9PKU7	GANAB GANAB GANAB
118	1	0	1	20.6	10.5	P21291 E9PP21	CSRP1 CSRP1
119	0	1	1	38.7	12.9	P09651 Q32P51 F8VTQ5 F8VZ49 F8W6I7 F8VYN5 F8W646 H0YH80 A0A2R8Y4L2	HNRNPA1 HNRNPA1L2 HNRNPA1 HNRNPA1 HNRNPA1 HNRNPA1 HNRNPA1 HNRNPA1 HNRNPA1P48
120	1	1	0	21.6	6.1	Q07020 F8VUA6 G3V203 H0YHA7 J3QQ67	RPL18 RPL18 RPL18 RPL18 RPL18
121	0	0	2	72.7	11.7	P42357 F8W0V1	HAL HAL
122	1	1	0	73.7	7.2	P38646	HSPA9

						H0YBG6	HSPA9
123	1	0	1	13.5	14.5	H7BZJ3	PDIA3
124	0	0	2	49.4	11.5	Q96QA5 J3KRG2	GSDMA GSDMA
125	0	1	1	15.1	24.7	P07737 K7EJ44	PFN1 PFN1
126	1	0	1	19.9	11.9	Q99497 K7ELW0	PARK7 PARK7
127	1	0	1	53.1	6.9	P52209 K7EMN2 K7EM49 K7EPF6	PGD PGD PGD PGD
128	1	1	0	32.6	12.2	P06748 E5RI98	NPM1 NPM1
129	0	1	1	16.4	7.0	P09228	CST2
130	1	1	0	12.5	7.1	P14174	MIF
131	0	2	0	117.9	6.5	P22314	UBA1
132	0	2	0	76.1	11.3	P23246	SFPQ
133	0	0	2	59.8	12.9	P25705 K7ESA0 K7EQH4 K7EJP1 K7ERX7 K7EK77	ATP5F1A ATP5F1A ATP5F1A ATP5F1A ATP5F1A ATP5F1A
134	0	0	2	15.1	17.3	P47929	LGALS7
135	0	1	1	28.3	11.4	P61981	YWHAG
136	0	0	2	82.9	6.4	Q13835	PKP1
137	0	1	1	52.6	11.9	Q13867 J3KS79 K7ENH5 K7ESE8 J3KSD8 K7ES02	BLMH BLMH BLMH BLMH BLMH BLMH
138	1	1	0	186.5	9.6	Q15058	KIF14
139	0	0	2	68.1	12.4	Q8WVV4	POF1B

Appendix 8: Protein groups identified with ≡Ner in Arabidopsis protoplasts after IGD

Tab. 18 Protein groups identified from the IGD of the *in situ* labelling of Arabidopsis protoplasts with ≡Ner. Complete list of protein groups obtained after initial filtering to remove irrelevant hits (2.2.5.2) that were identified after IGD (2.2.4.2.1) and LC-MS/MS analysis (2.2.4.4) of the samples obtained from the *in situ* labelling of Arabidopsis protoplasts with **≡Ner** (2.2.3.3.2). Protein groups (No.) were sorted by total MS/MS counts across all analysed samples. MS/MS counts for each individual sample, MW, Andromeda score, majority protein IDs (UniProt identifier) and gene names are reported for each protein group.

No.	MS/MS Count DMSO	MS/MS Count ≡Ner	MS/MS Count ≡Ner/ Ner	MW [kDa]	Score	Majority protein IDs (UniProt)	Gene names
1	8	7	11	29.6	323.3	Q42533 F4KE21	BCCP1 CAC1
2	11	4	4	80.5	158.1	Q42523	MCCA
3	6	3	4	35.8	323.3	Q9ZP06 A8MQK3 Q9LKA3	At1g53240 mMDH2 At3g15020
4	4	5	3	49.7	39.1	Q56WH1 B9DHQ0	TUBA3 TUBA5
5	5	4	2	41.8	159.7	P53497 P53494 P0CJ47 P0CJ46	ACT12 ACT4 ACT3 ACT1
6	4	2	3	33.4	219.0	F4HWQ5 F4JJ94 P42644 Q01525 Q96300 P46077 P42643 F4KGV2 F4I1C1 F4KGV5 F4KHY7 F4IP53 F4IP55 P48349 P48348 Q9S9Z8 P48347 Q96299 Q9C5W6	GF14 PHI GRF1 GRF3 GRF2 GRF7 GRF4 GRF1 GRF6 GRF10 GRF6 GRF8 GRF9 GRF9 GRF6 GRF8 GRF11 GRF10 GRF9 GRF12

						P42645	GRF5
7	4	2	3	37.2	132.2	P32962	NIT2
8	4	1	4	70.9	96.7	Q9S9N1	HSP70-5
9	5	2	1	33.9	47.4	F4HQT1 Q9FX54 P25858	GAPC2 GAPC2 GAPC1
10	3	3	2	35.6	112.5	P93819	MDH1
11	3	2	2	35.6	323.3	F4JU04 Q8H121 F4JU03	At4g19880 At4g19880 At4g19880
12	0	7	0	36.7	159.4	O81299	At4g02340/ T14P8.15
13	4	1	1	39.2	22.7	Q38799	PDH2
14	1	3	2	40.3	6.7	Q94AT3	At1g49350
15	4	1	1	38.5	23.7	Q9LF98 Q9SJQ9 B3H6D7	FBA8 FBA6 FBA6
16	2	3	0	35.1	58.2	Q0PGJ6 A0A1P8B1V1	AKR4C9 AKR4C8
17	2	2	1	41.9	154.5	Q9FPF0	DJ1A
18	2	2	1	40.9	29.4	Q9LFW1	RGP2
19	2	1	2	35.3	43.3	Q9SID0 Q9LNE3 Q9LNE4	At2g31390 At1g06030 At1g06020
20	2	0	2	45.7	7.4	A8MRZ7 F4JEL5 F4HV96 F4JEL4 A0A1I9LSZ7 P41377 P41376 Q9CAI7	EIF4A1 EIF4A1 EIF4A-2 EIF4A1 EIF4A1 TIF4A-2 EIF4A1 TIF4A-3
21	2	1	1	32.0	36.0	A0A1P8BAP0 Q9SF85 Q9LZG0	ADK2 ADK1 ADK2
22	2	1	1	21.6	12.2	Q5HZ54 F4IFU5	At2g33510 At2g33510
23	3	1	0	35.6	25.6	Q29Q34	At5g19440
24	2	1	1	36.2	17.1	Q41931	ACO2
25	2	1	1	71.1	12.3	Q9LHA8 F4KCE5 Q9C7X7 O65719 P22953 P22954	HSP70-4 HSC70-1 HSP70-18 HSP70-3 HSP70-1 HSP70-2
26	1	1	1	41.4	9.7	F4HUA0 Q8W4H7 Q8GTY0	At1g07930 A2 A4

						Q0WL56 P0DH99	A3 A1
27	1	1	1	90.6	58.9	F4JFN3 F4JQ55 Q9STX5	HSP90-6 SHD HSP90-7
28	1	1	1	35.7	5.8	O24456	RACK1A
29	1	1	1	80.6	13.1	P27323 P55737 P51818 O03986	HSP90-1 HSP90-2 HSP90-3 HSP90-4
30	1	1	1	75.1	15.4	Q8H1B3	BIP3
31	1	1	1	72.7	7.2	Q8RX28	HDA5
32	1	1	1	88.7	125.0	Q9SIF2	HSP90-5
33	0	1	2	38.4	20.6	Q9SN95 A0A1P8BFI1 A0A1P8BFL8 B3H4I6 F4KHU8 A0A1P8B345 C0Z2I3 F4JAG3 Q9FIE8 Q9ZV36 Q8VZC0 Q8S8T4 Q9LZI2	UXS5 UXS3 UXS3 UXS1 UXS3 UXS6 UXS4 UXS1 UXS3 UXS6 UXS1 UXS4 UXS2
34	1	0	1	103.9	6.1	A0A1I9LNN9 A0A1I9LNP2 A0A1I9LNP0 F4IXE7	ROS4 ROS4 ROS4 IDM1
35	2	0	0	28.8	7.3	F4JNF1 A0A1P8B4W4 Q43315	FPS2 FPS2 FPS2
36	1	0	1	119.4	6.2	A0A1P8BBL1	At5g15070
37	0	1	1	35.5	23.4	A8MQP1 F4JTV5 F4JTV4 Q9LK36 O23255	HOG1 HOG1 HOG1 SAHH2 SAHH1
38	1	1	0	28.3	6.1	F4II65 F4II66 Q38884	TRIP-1 At2g46290 TIF3I1
39	0	1	1	50.7	13.4	P29515 Q9ASR0 Q56YW9 P29517 P24636 P12411	TUBB7 TUBB3 TUBB2 TUBB9 TUBB4 TUBB1

						P29516 P29514 P29513	TUBB8 TUBB6 TUBB5
40	0	1	1	38.9	6.1	P46011	NIT4
41	0	1	1	41.7	9.9	P53492	ACT7
42	1	0	1	41.7	7.9	P53496	ACT11
43	1	1	0	89.4	6.9	P54609 Q9LZF6 Q9SCN8	CDC48A CDC48E CDC48D
44	2	0	0	36.2	13.1	P68209	At5g08300
45	1	0	1	59.7	31.3	P83484 P83483 Q9C5A9 P19366	At5g08690 At5g08670 At5g08680 atpB
46	2	0	0	38.1	13.1	Q39172 A0A1P8BEE4 Q93Z72 Q9LFK5 F4IE59 Q9M9M7 F4IBH8 Q9C677 Q39173	AER At5g17000 At5g17000 At5g16960 At1g26320 At3g03080 At1g65560 At1g26320 P2
47	1	0	1	40.3	9.4	Q8RUF8	NLP3
48	1	0	1	40.6	7.8	Q945K7	IDH5
49	1	1	0	42.4	12.0	Q9SN86	At3g47520
50	1	0	1	40.6	7.4	Q9SRT9	RGP1
51	1	1	0	42.3	10.5	Q9ZU52	FBA3

Appendix 9: Protein groups identified with ≡Ner in Arabidopsis seedling extract after IGD

Tab. 19 Protein groups identified from the IGD of the *in vitro* labelling of Arabidopsis seedling extract with ≡Ner. Complete list of protein groups obtained after initial filtering to remove irrelevant hits (2.2.5.2) that were identified after IGD (2.2.4.2.1) and LC-MS/MS analysis (2.2.4.4) of the samples obtained from the *in vitro* labelling of Arabidopsis seedling extract with **≡Ner** (2.2.3.3.3). Protein groups (No.) were sorted by total MS/MS counts across all analysed samples. MS/MS counts for each individual sample, MW, Andromeda score, majority protein IDs (UniProt identifier) and gene names are reported for each protein group.

No.	MS/MS Count DMSO	MS/MS Count ≡Ner	MS/MS Count ≡Ner/ Ner	MW [kDa]	Score	Majority protein IDs (UniProt)	Gene names
1	7	6	6	26.9	138.3	F4KE21 Q42533	CAC1 BCCP1
2	9	6	4	64.3	109.9	O49006	PME3
3	0	9	2	42.5	60.8	P25856 F4HNZ6 A0A1P8APR6 Q9LPW0	GAPA1 GAPA-2 GAPA-2 GAPA2
4	2	5	3	35.6	84.7	P93819 P57106	MDH1 MDH2
5	1	7	2	42.9	94.0	Q9SJU4 F4IGL5 F4IGL7	FBA1 FBA1 FBA1
6	3	5	1	53.0	61.1	O03042	rbcL
7	1	7	0	80.5	125.2	Q42523	MCCA
8	0	4	1	43.3	42.0	A0A1P8ATL2 Q9SA52	CRB CSP41B
9	1	4	0	35.6	42.8	F4JU04 Q8H121 F4JU03	At4g19880 At4g19880 At4g19880
10	0	5	0	36.7	83.5	O81299	At4g02340/ T14P8.15
11	1	4	0	36.2	32.0	Q9SYT0	ANN1
12	0	3	1	36.3	26.9	A0A1I9LTP2 Q9S757	CYSC1 CYSC1
13	2	1	0	64.1	17.9	A0A1P8ARX5 Q1JPL7	PMEPCRA PME18
14	0	3	0	40.9	19.9	Q01908	ATPC1
15	0	1	2	56.9	12.5	Q56WF8	SCPL48
16	1	1	1	36.7	6.2	Q7XJK5	AGL90
17	1	1	1	40.3	6.3	Q94AT3	At1g49350
18	0	3	0	37.8	21.6	Q9SF85	ADK1

						Q9LZG0 A0A1P8BAP0	ADK2 ADK2
19	0	0	2	16.2	6.9	F4JL66	At4g22370
20	1	0	1	27.5	5.9	Q84JS4 F4JYN2	MCA23.6 MCA23.6
21	0	2	0	13.7	7.2	Q9LD28 O81826 Q9LHQ5 Q9C681 Q9C944 Q9S9K7 O04848 Q9FJE8 Q94F49	RAT5 At4g27230 At3g20670 At1g51060 At1g52740 At1g54690 At1g08880 At5g59870 At5g27670
22	0	2	0	42.4	12.2	P46283	At3g55800
23	0	2	0	39.2	14.9	Q38799	PDH2
24	1	0	1	36.2	6.4	Q41931	ACO2
25	0	0	2	65.8	9.2	Q501D5	ETG1
26	0	2	0	74.0	6.1	Q93Y06	At5g67200
27	0	2	0	43.0	15.6	Q944G9 F4JUJ5	FBA2 FBA2
28	0	2	0	38.4	12.5	Q9SJQ9 Q9LF98	FBA6 FBA8
29	0	2	0	39.0	12.6	Q9LFG2	DAPF
30	0	2	0	42.4	20.4	Q9SN86	At3g47520
31	1	1	0	53.7	5.9	Q9ZVX4	UGT90A1

Appendix 10: Protein groups enriched with ≡Ner, ≡Ctrl1 and ≡Ctrl2 in Arabidopsis seedling extract after OBD

Tab. 20 Protein groups enriched with ≡Ner that were identified from the OBD of the *in vitro* labelling of Arabidopsis seedling extract. Complete list of protein groups enriched with **≡Ner** compared to the DMSO control (2.2.5.2) that were identified after OBD (2.2.4.2.2) and LC-MS/MS analysis (2.2.4.4) of the samples obtained from the *in vitro* labelling of Arabidopsis seedling extract with **≡Ner** (2.2.3.3.3). Protein groups (No.) were sorted by log_2-fold enrichment with **≡Ner**. Majority protein IDs (UniProt identifier) and gene names are reported for each protein group.

No.	Log_2-fold enrichment	Majority protein IDs (Uniprot)	Gene names
1	5.24003	Q9ZUC1	AOR
2	5.00996	O81299	At4g02340/T14P8.15
3	3.90267	P42734	CAD9
4	3.863	A0A2H1ZE37 Q0WP12	HOL1 HOL1
5	3.73374	P47999	OASB
6	3.45823	Q8LAS8	SFGH
7	3.40845	Q9FJA6 Q9M339 Q9SIP7	RPS3C RPS3B RPS3A
8	3.20364	F4JFY5 Q42592 F4JFY4	SAPX APXS SAPX
9	3.01607	P31265	TCTP1
10	2.94608	P06525	ADH1
11	2.91013	A0A1I9LNS4 Q9M1R2	At3g62120 At3g62120
12	2.87446	Q9S726	RPI3
13	2.8719	Q93WJ8	MDAR2
14	2.71677	Q9SN86	At3g47520
15	2.69674	P48523	CAD4
16	2.60144	Q94AR8	IIL1
17	2.53802	Q42605	UGE1
18	2.50495	A0A1I9LPQ6 Q9LSV0	GLYR1 GLYR1
19	2.49673	P59233 P59232 F4JGM3 A0A1P8BGQ7 F4I9X6 Q3EAA5 Q42202 B9DHA6	RPS27AC RPS27AB UBQ11 UBQ4 UBQ13 UBQ10 RPL40B RPL40A

		Q8RUC6 Q9SHE7 P59271 P0CH33 Q3E7K8 Q3E7T8 Q1EC66 Q9FHQ6 P0CH32 Q8H159 Q39256	RUB2 RUB1 RPS27AA UBQ11 UBQ12 UBQ14 UBQ3 UBQ9 UBQ4 UBQ10 UBQ8
20	2.4505	Q9LZG0 A0A1P8BAP0	ADK2 ADK2
21	2.4266	Q93VR3	At5g28840
22	2.42014	Q9FM97 O65595	MCD7.8 At4g26390
23	2.34892	B9DG17 Q08682	P40 RPSaA
24	2.30241	Q9SF85	ADK1
25	2.29147	P56795	rpl22
26	2.19112	Q93VP3	ELF5A-2
27	2.19016	Q9FJ95	SDH
28	2.15982	Q9C5C8	MSRB2
29	2.12678	Q96255	PSAT1
30	2.07875	Q96533 F4K7D6	ADH2 HOT5
31	2.06828	Q9SIV0	SUR1
32	2.0448	Q9C5R8 A0A1P8BD74	At5g06290 2-Cys Prx B
33	2.02176	P25856	GAPA1
34	1.99068	P52032	GPX1
35	1.96359	F4JRT7 Q9SW21	ACP4 ACP4
36	1.87916	A8MR07 Q94KE3	At3g52990 At3g52990
37	1.86296	Q949U7	PRXIIE
38	1.85686	P49200 Q9STY6	RPS20A RPS20B
39	1.83799	Q9STX2	VEP1
40	1.83001	Q9ZW85 F4IQ61	SSU1 MFL8.15
41	1.82734	O65719	HSP70-3
42	1.75652	Q56WD9	PED1
43	1.73191	Q8LE52	DHAR3
44	1.72809	P60040 A8MRH4 Q9LHP1	RPL7B At2g01250 RPL7D
45	1.72034	Q9SQI8	LTA2

46	1.70241	F4I7I0	ALAAT1
47	1.65048	P49201 Q9SF35	RPS23B RPS23A
48	1.64902	P24636	TUBB4
49	1.62811	Q94K71	CBBY
50	1.61844	Q9LIA8	UGD2
51	1.61409	F4KGV2 F4KGV5 P48349	GRF6 GRF6 GRF6
52	1.61007	Q56WH1 B9DHQ0	TUBA3 TUBA5
53	1.59931	P25858	GAPC1
54	1.59681	F4KDZ4 Q9ZP05 A0A1P8BBQ0 A8MRP1 B3H560	PMDH2 PMDH2 PMDH2 PMDH2 PMDH2
55	1.57455	Q43127	GLN2
56	1.5618	Q9S7B5	TS1
57	1.56172	Q9LRR9 Q2V3V9 A8MS37 B3H4B8	GLO1 GOX1 GOX1 GOX1
58	1.53098	P34788	RPS18A
59	1.50711	A0A1P8APR6 Q9LPW0 F4HNZ6	GAPA-2 GAPA2 GAPA-2
60	1.50701	P56791	rpl2-A
61	1.50701	O80585	MTHFR2
62	1.49626	P48491	CTIMC
63	1.48628	Q9XEX2 F4ID64	PRXIIB TPX1
64	1.46625	Q9LF46	HACL
65	1.45478	Q9XFH8	At3g02730
66	1.44689	Q9SFH9	HEMB1
67	1.4451	Q9FIE8 A0A1P8BFI1 A0A1P8BFL8 F4KHU8 A0A1P8B345 Q9ZV36	UXS3 UXS3 UXS3 UXS3 UXS6 UXS6
68	1.42448	O23254	SHM4
69	1.39708	F4K5C7 Q93VH9 Q8VYK6 P49204 F4IMI7	At5g07090 RPS4A RPS4D RPS4B At2g17360
70	1.3905	Q93VG5	RPS8A

71	1.36664	A0A1I9LT03 A0A1I9LT02 Q9M9P3	UGP1 UGP1 UGP2
72	1.35901	O23627	At1g29880
73	1.35806	P25857	GAPB
74	1.34705	F4HU93 Q05431	APX1 APX1
75	1.33488	F4J849 Q9LFA3	MDAR1 MDAR1
76	1.33258	P56802	rps11
77	1.32181	P46286	RPL8A
78	1.30544	O64650 Q9M2F1	RPS27A RPS27B
79	1.23604	Q9LF98	FBA8
80	1.22061	Q9SJQ0	At2g36580
81	1.16848	Q38799	PDH2
82	1.16149	Q9LTF2 F4JTD3 Q9SW09	RPS10C At4g25740 RPS10A
83	1.15332	Q96291	BAS1
84	1.14989	P62126	rps12-A
85	1.11215	Q8LEM8 Q43292 Q8LFH7	RPL37C RPL37B RPL37A
86	1.11031	P49691 F4KDU5	RPL4D At5g02870
87	1.10489	A0A2H1ZEA9 O65396	At1g11860 GDCST
88	1.10214	Q8W4H7 Q8GTY0 Q0WL56 P0DH99 F4HUA0	A2 A4 A3 A1 At1g07930
89	1.09737	Q9STW6	HSP70-6
90	1.08406	P47998	OASA1
91	1.07417	Q9LRS0 F4JFV6	GLO2 GOX2
92	1.05221	P22953 F4KCE5	HSP70-1 HSC70-1
93	1.05204	Q09152	FPS1
94	1.04993	F4KEX3 Q8H1E2	MCK7.20 At5g58330
95	1.03512	P56792	rpl14
96	1.03147	Q8S4Y1	AAT1
97	1.01884	Q9C5C2	TGG2
98	1.0094	O04603	RPL5
99	0.99698	Q39161	NIR1

100	0.988563	A8MRX2 Q42340 F4JWM1 Q9M8X9	At5g18380 RPS16C At5g18380 RPS16B
101	0.964976	Q9LKR3	BIP1
102	0.947442	Q94A28	ACO2
103	0.93671	Q9SE60	MTHFR1
104	0.913883	P10896 F4IVZ7	RCA RCA
105	0.90954	Q9SW96	SYNC1
106	0.908579	P94072	GER3
107	0.895381	P42795 P42794	RPL11A RPL11B
108	0.871151	Q9SU63	ALDH2B4
109	0.868727	P36428 F4I4Z2	ALATS ALATS
110	0.857579	O48917	SQD1
111	0.856828	Q94CE4	BCA4
112	0.847889	A8MRW5 O65423 B9DGL1	At4g21580 F18E5.200 At4g21580
113	0.834966	P46643	ASP1
114	0.832894	Q2V3X4 Q9SF40	At3g09630 RPL4A
115	0.813545	F4JYE0 O04983 F4JYE1	CAC2 CAC2 CAC2
116	0.811565	F4JJ94 P42643	GRF1 GRF1
117	0.801341	Q9FVT2	At1g57720
118	0.791189	Q94CE5	POP2
119	0.776498	P29197	CPN60
120	0.771742	Q9FFP6	MBK5.16
121	0.771331	P32961 Q8LFU8	NIT1 NIT1
122	0.74973	Q05758	At3g58610
123	0.746127	O04487 C0Z2L8	At1g09640 At1g09640
124	0.744582	P56757	atpA
125	0.724511	Q9CAV0	RPS3AA
126	0.711442	P25696 A0A1P8B1N1	ENO2 LOS2
127	0.700827	O23654	VHA-A
128	0.697371	F4I576 P92947 F4I577	MDAR6 MDAR5 MDAR6
129	0.695816	P11574	VHA-B1

		Q8W4E2	VHA-B3
130	0.694115	P38666 Q42347	RPL24B RPL24A
131	0.693262	Q9LD57	PGK1
132	0.68897	P19366	atpB
133	0.683775	P49688 Q93VB8 Q8L8Y0 Q9SCM3	RPS2C RPS2B RPS2A RPS2D
134	0.680799	F4JBY2 Q8RWV0	AtTKL1 TKL-1
135	0.678804	P53492	ACT7
136	0.666325	P16181 P42733 O65569	RPS11A RPS11C RPS11B
137	0.662912	F4JXD5 Q9ZSK4	ADF3 ADF3
138	0.658798	Q9FPF0	DJ1A
139	0.634582	P42737 A8MQY4 F4K875 F4K873	BCA2 CA2 CA2 CA2
140	0.59978	Q9SRZ6	CICDH
141	0.585492	A0A1P8AY36 P51418 A8MRF3 Q8L7K0	At2g34480 RPL18AB RPL18AA RPL18AA
142	0.536431	Q9SAJ4	PGK3
143	0.507967	A0A1I9LQB3 P27140	CA1 BCA1
144	0.505765	P37702	TGG1
145	0.505679	Q9LR30	GGAT1
146	0.503523	Q9XFT3	PSBQ1
147	0.501989	Q9ZUT9	RPS5A
148	0.500221	Q42403	TRX3
149	0.49773	Q9ZU52	FBA3
150	0.484058	P25697	At1g32060
151	0.479232	Q9ZRW8	GSTU19
152	0.478877	Q9S9M7	At1g16080
153	0.470235	F4I7M5 Q9ZUB3	SPDS1 SPDSYN1
154	0.433234	P51430 F4KGU2	RPS6B EMB3010
155	0.428505	Q42029	PSBP1
156	0.41247	Q9M5K3 Q9M5K2	LPD1 LPD2
157	0.392763	P93819	MDH1

158	0.390861	Q9LYG3	NADP-ME2
159	0.383778	A0A1P8ATL2 Q9SA52	CRB CSP41B
160	0.371054	Q9LVI9	PYD1
161	0.368667	P83484 P83483 Q9C5A9	At5g08690 At5g08670 At5g08680
162	0.315291	F4JD96 Q9SFU1	At3g07110 RPL13AA
163	0.298282	P21238	CPN60A1
164	0.296751	A0A1I9LTP2 Q9S757	CYSC1 CYSC1
165	0.288258	Q8LCE1 F4ID91 F4ID92	GLN1-2 GSR2 GSR2
166	0.287917	Q9ASR1	LOS1
167	0.273215	P17094 A8MQQ1	ARP1 RP1
168	0.263684	Q940B0 P42791 A0A1P8BGQ0 A0A1I9LT16	RPL18C RPL18B At5g27850 RPL18
169	0.238499	O50008	MS1
170	0.233783	Q8H156 P41917 P41916	RAN3 RAN2 RAN1
171	0.231066	Q9LTX9	HSP70-7
172	0.187454	Q9LHA8	HSP70-4
173	0.177591	Q93ZN9	DAP
174	0.162889	P30184 F4INR3	LAP1 LAP1
175	0.156432	Q8LDU4	RCCR
176	0.125459	Q9FKW6 F4JZ46	LFNR1 FNR1
177	0.109308	P55228	APS1
178	0.0803843	Q9SUR0	At4g23670
179	0.0793962	P25851	CFBP1
180	0.0537486	Q9SRX2 P49693	RPL19A RPL19C
181	0.0526366	P25855	GDH1
182	0.0380344	Q9ZP06 A8MQK3 Q9LKA3	At1g53240 mMDH2 At3g15020
183	0.035964	Q944G9 F4JUJ5	FBA2 FBA2
184	0.0244603	Q680P8	RPS29A
185	0.0166211	Q42560 B3H5Y0	ACO1 ACO1

186	0.00551605	P46283	At3g55800
187	0.00108194	Q9SJU4 F4IGL5 F4IGL7	FBA1 FBA1 FBA1
188	0.000453949	Q9SMT7	AAE3

Tab. 21 Protein groups enriched with ≡Ctrl1 that were identified from the OBD of the *in vitro* labelling of Arabidopsis seedling extract. Complete list of protein groups enriched with **≡Ctrl1** compared to the DMSO control (2.2.5.2) that were identified after OBD (2.2.4.2.2) and LC-MS/MS analysis (2.2.4.4) of the samples obtained from the *in vitro* labelling of Arabidopsis seedling extract with **≡Ctrl1** (2.2.3.3.3). Protein groups (No.) were sorted by log_2-fold enrichment with **≡Ctrl1**. Majority protein IDs (UniProt identifier) and gene names are reported for each protein group.

No.	Log_2-fold enrichment	Majority protein IDs (Uniprot)	Gene names
1	1.44715	Q9C5R8 A0A1P8BD74	At5g06290 2-Cys Prx B
2	1.39056	P31265	TCTP1
3	1.17795	P60040 A8MRH4 Q9LHP1	RPL7B At2g01250 RPL7D
4	1.17426	Q96533 F4K7D6	ADH2 HOT5
5	1.10065	P56791	rpl2-A
6	1.04879	P46286	RPL8A
7	1.04316	F4HRW5 P51413	At1g67430 RPL17B
8	1.03676	A0A1I9LT03 A0A1I9LT02 Q9M9P3	UGP1 UGP1 UGP2
9	1.03506	B9DG17 Q08682	P40 RPSaA
10	1.00324	Q9C5C2	TGG2
11	0.972498	O23627	At1g29880
12	0.947996	Q9SR37	BGLU23
13	0.936649	Q9M5K3 Q9M5K2	LPD1 LPD2
14	0.901636	A0A2H1ZE37 Q0WP12	HOL1 HOL1
15	0.901482	P37702	TGG1
16	0.899336	Q9LKR3	BIP1
17	0.898856	P47999	OASB
18	0.889407	Q9C5C8	MSRB2
19	0.87178	Q94AR8	IIL1
20	0.855183	Q949U7	PRXIIE
21	0.834037	P49200 Q9STY6	RPS20A RPS20B
22	0.821805	F4J849 Q9LFA3	MDAR1 MDAR1
23	0.820936	F4KEX3 Q8H1E2	MCK7.20 At5g58330
24	0.816927	Q93VG5	RPS8A

25	0.804275	Q9SN86	At3g47520
26	0.797464	O64650 Q9M2F1	RPS27A RPS27B
27	0.793382	Q9LRR9 Q2V3V9 A8MS37 B3H4B8	GLO1 GOX1 GOX1 GOX1
28	0.762641	Q9FIE8 A0A1P8BFI1 A0A1P8BFL8 F4KHU8 A0A1P8B345 Q9ZV36	UXS3 UXS3 UXS3 UXS3 UXS6 UXS6
29	0.747854	P29197	CPN60
30	0.709095	P25858	GAPC1
31	0.70662	Q8H103	PGI1
32	0.703983	F4KDZ4 Q9ZP05 A0A1P8BBQ0 A8MRP1 B3H560	PMDH2 PMDH2 PMDH2 PMDH2 PMDH2
33	0.686647	P22953 F4KCE5	HSP70-1 HSC70-1
34	0.676039	P24636	TUBB4
35	0.63277	P25696 A0A1P8B1N1	ENO2 LOS2
36	0.632648	P31170	HSP21
37	0.629297	B3H725 F4K0E8	HDS ISPG
38	0.624078	A0A1P8APR6 Q9LPW0 F4HNZ6	GAPA-2 GAPA2 GAPA-2
39	0.609981	A0A1P8ATL2 Q9SA52	CRB CSP41B
40	0.594939	P42795 P42794	RPL11A RPL11B
41	0.592444	P34790	CYP18-3
42	0.572706	Q05758	At3g58610
43	0.569255	Q42522	GSA2
44	0.553118	F4IX28 F4IX26 P34791	ROC4 ROC4 CYP20-3
45	0.545811	Q9SFH9	HEMB1
46	0.536599	Q9ZP06 A8MQK3 Q9LKA3	At1g53240 mMDH2 At3g15020
47	0.511322	A0A2H1ZEA9 O65396	At1g11860 GDCST

48	0.499269	P25856	GAPA1
49	0.496929	F4JYE0 O04983 F4JYE1	CAC2 CAC2 CAC2
50	0.491813	F4JD96 Q9SFU1	At3g07110 RPL13AA
51	0.489732	Q96255	PSAT1
52	0.487216	P48491	CTIMC
53	0.481867	Q9LF98	FBA8
54	0.480611	A0A1I9LTP2 Q9S757	CYSC1 CYSC1
55	0.465261	O23254	SHM4
56	0.464994	A0A1I9LQB3 P27140	CA1 BCA1
57	0.453925	F4JJ94 P42643	GRF1 GRF1
58	0.450572	Q9FKW6 F4JZ46	LFNR1 FNR1
59	0.449829	P21276 F4JRV2	FSD1 FSD1
60	0.449539	Q9LYG3	NADP-ME2
61	0.443737	Q43127	GLN2
62	0.441318	P19366	atpB
63	0.43503	Q9LD57	PGK1
64	0.428835	Q9SRZ6	CICDH
65	0.41838	Q9SUR0	At4g23670
66	0.417166	Q9ZUY6 Q9SGE0	AXS1 AXS2
67	0.415667	Q39161	NIR1
68	0.410247	F4HU93 Q05431	APX1 APX1
69	0.409624	Q9ASR1	LOS1
70	0.40899	Q9STW6	HSP70-6
71	0.408265	P83484 P83483 Q9C5A9	At5g08690 At5g08670 At5g08680
72	0.405225	Q9MAH0	PPC1
73	0.400622	P25697	At1g32060
74	0.398015	Q38946 F4K6P9	GDH2 GDH2
75	0.393696	Q42029	PSBP1
76	0.382944	Q9LRS0 F4JFV6	GLO2 GOX2
77	0.38084	A8MRX2 Q42340 F4JWM1 Q9M8X9	At5g18380 RPS16C At5g18380 RPS16B

78	0.378225	F4K5C7 Q93VH9 Q8VYK6 P49204 F4IMI7	At5g07090 RPS4A RPS4D RPS4B At2g17360
79	0.36649	Q56WH1 B9DHQ0	TUBA3 TUBA5
80	0.35937	Q9SF85	ADK1
81	0.358388	Q9SZJ5	SHM1
82	0.357548	P25857	GAPB
83	0.353781	O23654	VHA-A
84	0.342824	Q8W4H7 Q8GTY0 Q0WL56 P0DH99 F4HUA0	A2 A4 A3 A1 At1g07930
85	0.341197	O50008	MS1
86	0.336875	P46643	ASP1
87	0.334653	Q96291	BAS1
88	0.330473	F4I576 P92947 F4I577	MDAR6 MDAR5 MDAR6
89	0.324706	P56757	atpA
90	0.323192	Q42403	TRX3
91	0.321942	P25851	CFBP1
92	0.320971	Q9LHA8	HSP70-4
93	0.317496	Q1WIQ6 F4INS6 A0A2H1ZE23	ALDH11A3 ALDH11A3 ALDH11A3
94	0.308297	P10796	RBCS-1B
95	0.303079	P42737 A8MQY4 F4K875 F4K873	BCA2 CA2 CA2 CA2
96	0.29892	Q9FWR4 Q9LN39	DHAR1 At1g19550
97	0.288414	P11574 Q8W4E2	VHA-B1 VHA-B3
98	0.281588	Q9LR30	GGAT1
99	0.270581	Q9S726	RPI3
100	0.25586	P38666 Q42347	RPL24B RPL24A
101	0.255649	P10896 F4IVZ7	RCA RCA
102	0.249599	Q8LEM8 Q43292 Q8LFH7	RPL37C RPL37B RPL37A
103	0.245503	Q93ZN9	DAP

104	0.242314	P30184 F4INR3	LAP1 LAP1
105	0.231845	P43287	PIP2-2
106	0.226438	Q9SRX2 P49693	RPL19A RPL19C
107	0.223932	F4JXD5 Q9ZSK4	ADF3 ADF3
108	0.223809	F4JBY2 Q8RWV0	AtTKL1 TKL-1
109	0.221734	P49688 Q93VB8 Q8L8Y0 Q9SCM3	RPS2C RPS2B RPS2A RPS2D
110	0.221065	P10795	RBCS-1A
111	0.218349	P59224	RPS13B
112	0.213772	P21238	CPN60A1
113	0.213349	Q9FPF0	DJ1A
114	0.203617	A0A1P8AY36 P51418 A8MRF3 Q8L7K0	At2g34480 RPL18AB RPL18AA RPL18AA
115	0.20103	Q9SE60	MTHFR1
116	0.200048	P34788	RPS18A
117	0.196061	P53492	ACT7
118	0.190364	P46283	At3g55800
119	0.1853	Q9SJU4 F4IGL5 F4IGL7	FBA1 FBA1 FBA1
120	0.184273	P93819	MDH1
121	0.177232	Q5GM68	PPC2
122	0.171532	Q38882	PLDALPHA1
123	0.166208	Q9SDM9 O04316	NSP1 NSP4
124	0.1657	P55228	APS1
125	0.162848	B9DG18 Q42547 A0A1P8AWT7 F4HUL6 Q2V4M4 A0A1P8AWR0	CAT3 CAT3 CAT3 CAT3 CAT3 CAT3
126	0.159786	P25855	GDH1
127	0.155746	Q9LR75	CPX1
128	0.154009	B3H5S2 P10798 P10797 F4KA76	RBCS3B RBCS-3B RBCS-2B RBCS3B
129	0.151833	P49637 Q9LR33	RPL27AC RPL27AB

130	0.129308	P32961 Q8LFU8	NIT1 NIT1
131	0.120669	P42734	CAD9
132	0.120202	Q9CAV0	RPS3AA
133	0.11477	Q94CE5	POP2
134	0.114625	O65398	GLX1
135	0.112685	Q9SIB9	ACO3
136	0.112216	Q8H156 P41917 P41916	RAN3 RAN2 RAN1
137	0.107793	Q42560 B3H5Y0	ACO1 ACO1
138	0.102271	O23255 F4JTV4 A8MQP1 F4JTV5	SAHH1 HOG1 HOG1 HOG1
139	0.101794	Q9C9W5 A0A1P8ANC0	HPR HPR
140	0.0830946	P25819 F4JM86 A0A1P8B564	CAT2 CAT2 CAT2
141	0.0647278	Q8W493 C0Z2A8	LFNR2 FNR2
142	0.0557504	Q56YA5	AGT1
143	0.0497169	P21240 C0Z361	CPN60B1 CPN60B3
144	0.0456858	Q940B0 P42791 A0A1P8BGQ0 A0A1I9LT16	RPL18C RPL18B At5g27850 RPL18
145	0.0392709	P16181 P42733 O65569	RPS11A RPS11C RPS11B
146	0.0289917	P36428 F4I4Z2	ALATS ALATS
147	0.0275435	Q9ZNZ7	GLU1
148	0.0107551	Q93VT9 Q08770 A0A1P8AUU3	RPL10A RPL10B RPL10B
149	0.0098753	Q944G9 F4JUJ5	FBA2 FBA2

Tab. 22 Protein groups enriched with ≡Ctrl2 that were identified from the OBD of the *in vitro* labelling of Arabidopsis seedling extract. Complete list of protein groups enriched with **≡Ctrl2** compared to the DMSO control (2.2.5.2) that were identified after OBD (2.2.4.2.2) and LC-MS/MS analysis (2.2.4.4) of the samples obtained from the *in vitro* labelling of Arabidopsis seedling extract with **≡Ctrl2** (2.2.3.3.3). Protein groups (No.) were sorted by log_2-fold enrichment with **≡Ctrl2**. Majority protein IDs (UniProt identifier) and gene names are reported for each protein group.

No.	Log_2-fold enrichment	Majority protein IDs (Uniprot)	Gene names
1	1.5495	Q949U7	PRXIIE
2	1.35876	O23515 Q8VYF1	RPL15A RPL15B
3	1.31467	Q9M5K3 Q9M5K2	LPD1 LPD2
4	1.26566	Q96533 F4K7D6	ADH2 HOT5
5	1.2447	P46286	RPL8A
6	1.23491	F4J849 Q9LFA3	MDAR1 MDAR1
7	1.1742	P60040 A8MRH4 Q9LHP1	RPL7B At2g01250 RPL7D
8	1.10053	P56791	rpl2-A
9	1.09575	Q9SN86	At3g47520
10	1.06295	O23627	At1g29880
11	1.01957	F4JTH0 P46248 B9DG21	ASP5 ASP5 ASP5
12	1.01456	P34788	RPS18A
13	1.01447	A0A1I9LNS4 Q9M1R2	At3g62120 At3g62120
14	0.936845	Q8LEM8 Q43292 Q8LFH7	RPL37C RPL37B RPL37A
15	0.908711	Q9LRR9 Q2V3V9 A8MS37 B3H4B8	GLO1 GOX1 GOX1 GOX1
16	0.867611	Q9LKR3	BIP1
17	0.859581	Q9SFH9	HEMB1
18	0.748463	Q38946 F4K6P9	GDH2 GDH2
19	0.738825	O64650 Q9M2F1	RPS27A RPS27B
20	0.737115	P42795 P42794	RPL11A RPL11B

21	0.733943	Q9XFT3	PSBQ1
22	0.724514	P25856	GAPA1
23	0.716988	P56757	atpA
24	0.665207	P47999	OASB
25	0.66504	F4JFY5 Q42592 F4JFY4	SAPX APXS SAPX
26	0.659596	F4KDZ4 Q9ZP05 A0A1P8BBQ0 A8MRP1 B3H560	PMDH2 PMDH2 PMDH2 PMDH2 PMDH2
27	0.635035	P38666 Q42347	RPL24B RPL24A
28	0.627667	O23254	SHM4
29	0.622994	Q56WH1 B9DHQ0	TUBA3 TUBA5
30	0.617138	P83484 P83483 Q9C5A9	At5g08690 At5g08670 At5g08680
31	0.616412	F4JYE0 O04983 F4JYE1	CAC2 CAC2 CAC2
32	0.611983	P46283	At3g55800
33	0.610393	Q38814	THI1
34	0.605227	Q9FIE8 A0A1P8BFI1 A0A1P8BFL8 F4KHU8 A0A1P8B345 Q9ZV36	UXS3 UXS3 UXS3 UXS3 UXS6 UXS6
35	0.59146	Q9LYG3	NADP-ME2
36	0.584435	F4I576 P92947 F4I577	MDAR6 MDAR5 MDAR6
37	0.58075	A0A1I9LT03 A0A1I9LT02 Q9M9P3	UGP1 UGP1 UGP2
38	0.576825	Q8LAS8	SFGH
39	0.559639	Q9MAH0	PPC1
40	0.539378	P25858	GAPC1
41	0.528939	Q9LF98	FBA8
42	0.526075	F4IX28 F4IX26 P34791	ROC4 ROC4 CYP20-3
43	0.521487	Q9SJU4 F4IGL5 F4IGL7	FBA1 FBA1 FBA1

44	0.503589	P37702	TGG1
45	0.49261	A0A1P8ATL2 Q9SA52	CRB CSP41B
46	0.487379	Q9S726	RPI3
47	0.485865	Q38882	PLDALPHA1
48	0.482635	Q39161	NIR1
49	0.469317	Q9SIH0	RPS14A
50	0.468936	Q42403	TRX3
51	0.46651	Q9LD57	PGK1
52	0.460518	P42734	CAD9
53	0.460139	P24636	TUBB4
54	0.450519	Q9SF85	ADK1
55	0.433519	F4JD96 Q9SFU1	At3g07110 RPL13AA
56	0.431185	Q42560 B3H5Y0	ACO1 ACO1
57	0.426615	P11574 Q8W4E2	VHA-B1 VHA-B3
58	0.420186	Q9ZP06 A8MQK3 Q9LKA3	At1g53240 mMDH2 At3g15020
59	0.41275	A0A1I9LQB3 P27140	CA1 BCA1
60	0.406144	P46643	ASP1
61	0.402198	P22953 F4KCE5	HSP70-1 HSC70-1
62	0.401316	Q8S4Y1	AAT1
63	0.393462	Q940B0 P42791 A0A1P8BGQ0 A0A1I9LT16	RPL18C RPL18B At5g27850 RPL18
64	0.392434	P21276 F4JRV2	FSD1 FSD1
65	0.385919	O23654	VHA-A
66	0.380977	P25857	GAPB
67	0.378946	Q9SR37	BGLU23
68	0.377539	Q96291	BAS1
69	0.360254	Q9ASR1	LOS1
70	0.356162	Q9ZRW8	GSTU19
71	0.348707	Q1WIQ6 F4INS6 A0A2H1ZE23	ALDH11A3 ALDH11A3 ALDH11A3
72	0.347888	Q9SZJ5	SHM1
73	0.346995	P49688 Q93VB8 Q8L8Y0 Q9SCM3	RPS2C RPS2B RPS2A RPS2D

74	0.33134	Q42522	GSA2
75	0.330415	F4JJ94 P42643	GRF1 GRF1
76	0.32129	P19366	atpB
77	0.312638	P10896 F4IVZ7	RCA RCA
78	0.308717	Q9STW6	HSP70-6
79	0.30316	P16181 P42733 O65569	RPS11A RPS11C RPS11B
80	0.297802	Q9SE60	MTHFR1
81	0.292348	P93819	MDH1
82	0.290783	Q9C9W5 A0A1P8ANC0	HPR HPR
83	0.282276	P30184 F4INR3	LAP1 LAP1
84	0.279684	Q2V3X4 Q9SF40	At3g09630 RPL4A
85	0.276629	Q93ZN9	DAP
86	0.273704	P25855	GDH1
87	0.271135	A0A1I9LTP2 Q9S757	CYSC1 CYSC1
88	0.26327	Q42029	PSBP1
89	0.257872	P48491	CTIMC
90	0.247867	P32961 Q8LFU8	NIT1 NIT1
91	0.247519	Q9ZU52	FBA3
92	0.246542	Q9LHA8	HSP70-4
93	0.240694	P25696 A0A1P8B1N1	ENO2 LOS2
94	0.239484	Q9LR30	GGAT1
95	0.235527	Q05758	At3g58610
96	0.235126	A0A2H1ZEA9 O65396	At1g11860 GDCST
97	0.231581	Q9S7B5	TS1
98	0.221144	Q9FWR4 Q9LN39	DHAR1 At1g19550
99	0.219966	O50008	MS1
100	0.208766	P21238	CPN60A1
101	0.205052	Q9SUR0	At4g23670
102	0.195379	Q56YA5	AGT1
103	0.193771	P25697	At1g32060
104	0.190621	P55228	APS1
105	0.188367	Q944G9 F4JUJ5	FBA2 FBA2
106	0.186948	Q9FKW6 F4JZ46	LFNR1 FNR1

107	0.18365	Q680P8	RPS29A
108	0.168897	Q94CE5	POP2
109	0.166547	Q9SDM9 O04316	NSP1 NSP4
110	0.16319	P21240 C0Z361	CPN60B1 CPN60B3
111	0.158629	P10796	RBCS-1B
112	0.155865	P25851	CFBP1
113	0.149334	Q8LCE1 F4ID91 F4ID92	GLN1-2 GSR2 GSR2
114	0.147312	P53492	ACT7
115	0.13677	B3H5S2 P10798 P10797 F4KA76	RBCS3B RBCS-3B RBCS-2B RBCS3B
116	0.131192	Q9SRZ6	CICDH
117	0.130916	Q9LXG1 B3H7J6 Q9FLF0	RPS9B At5g15200 RPS9C
118	0.129006	Q43127	GLN2
119	0.126378	Q5GM68	PPC2
120	0.113552	Q8H156 P41917 P41916	RAN3 RAN2 RAN1
121	0.107992	Q9LLC1	BCCP2
122	0.0995526	Q9SIB9	ACO3
123	0.0948062	Q93WN0	SBP2
124	0.091485	O04487 C0Z2L8	At1g09640 At1g09640
125	0.071106	Q9CAV0	RPS3AA
126	0.0619497	F4JBY2 Q8RWV0	AtTKL1 TKL-1
127	0.0610366	Q9SRX2 P49693	RPL19A RPL19C
128	0.055789	O23255 F4JTV4 A8MQP1 F4JTV5	SAHH1 HOG1 HOG1 HOG1
129	0.0542293	Q9ZUT9	RPS5A
130	0.052578	Q03251 F4JVC0 F4JVC1	RBG8 CCR1 CCR1
131	0.048542	P59224	RPS13B
132	0.0434732	Q9ZNZ7	GLU1
133	0.0390124	Q9FPF0	DJ1A
134	0.0036664	P42737 A8MQY4	BCA2 CA2

		F4K875 F4K873	CA2 CA2
135	0.00264263	Q8W4H7 Q8GTY0 Q0WL56 P0DH99 F4HUA0	A2 A4 A3 A1 At1g07930

Appendix 11: Effect of Ner-pretreatment on protein groups enriched with ≡Ner, ≡Ctrl1 and ≡Ctrl2 in Arabidopsis seedling extract after OBD

Tab. 23 Effect of Ner-pretreatment on protein groups enriched with ≡Ner. Results of the *t*-test comparing noncompetition ≡**Ner**-labelled samples with **Ner**-pretreated ≡**Ner**-labelled samples (2.2.5.2) on the complete list of ≡**Ner**-enriched protein groups (Tab. 20) that were identified after OBD (2.2.4.2.2) and LC-MS/MS analysis (2.2.4.4) of the samples obtained from the *in vitro* labelling of Arabidopsis seedling extract with ≡**Ner** (2.2.3.3.3). Protein groups (No.) were sorted by negative log_2-fold enrichment with ≡**Ner** after **Ner**-pretreatment. –Log p-value, majority protein IDs (UniProt identifier) and gene names are reported for each protein group.

No.	Log_2-fold enrichment	-Log p-value	Majority protein IDs (Uniprot)	Gene names
1	-4.89128	4.74926	O81299	At4g02340/ T14P8.15
2	-1.56757	1.32709	Q9SJQ0	At2g36580
3	-1.25438	1.52821	P47999	OASB
4	-0.788035	0.392383	F4JFY5 Q42592 F4JFY4	SAPX APXS SAPX
5	-0.766571	1.73753	P59233 P59232 F4JGM3 A0A1P8BGQ7 F4I9X6 Q3EAA5 Q42202 B9DHA6 Q8RUC6 Q9SHE7 P59271 P0CH33 Q3E7K8 Q3E7T8 Q1EC66 Q9FHQ6 P0CH32 Q8H159 Q39256	RPS27AC RPS27AB UBQ11 UBQ4 UBQ13 UBQ10 RPL40B RPL40A RUB2 RUB1 RPS27AA UBQ11 UBQ12 UBQ14 UBQ3 UBQ9 UBQ4 UBQ10 UBQ8
6	-0.675344	0.57672	F4JD96 Q9SFU1	At3g07110 RPL13AA
7	-0.652622	0.21124	P37702	TGG1
8	-0.617284	0.52485	O64650 Q9M2F1	RPS27A RPS27B
9	-0.600913	0.270762	Q9ZW85 F4IQ61	SSU1 MFL8.15

10	-0.573712	0.319032	P52032	GPX1
11	-0.544948	0.826753	Q42403	TRX3
12	-0.506621	0.216148	P42734	CAD9
13	-0.485396	0.311206	Q42605	UGE1
14	-0.470886	0.336322	Q9XFT3	PSBQ1
15	-0.470681	0.437164	Q38799	PDH2
16	-0.422522	0.408174	Q9XFH8	At3g02730
17	-0.41125	0.345611	Q42029	PSBP1
18	-0.410328	0.379846	Q9FFP6	MBK5.16
19	-0.382432	0.240895	Q8LE52	DHAR3
20	-0.375095	0.214339	Q94K71	CBBY
21	-0.373172	0.469826	P31265	TCTP1
22	-0.368005	0.76412	P25697	At1g32060
23	-0.34731	0.179688	Q9C5R8 A0A1P8BD74	At5g06290 2-Cys Prx B
24	-0.323395	0.123007	Q9C5C2	TGG2
25	-0.279016	0.254539	P60040 A8MRH4 Q9LHP1	RPL7B At2g01250 RPL7D
26	-0.267261	0.295901	P32961 Q8LFU8	NIT1 NIT1
27	-0.253319	0.21957	P34788	RPS18A
28	-0.22194	0.312522	F4I576 P92947 F4I577	MDAR6 MDAR5 MDAR6
29	-0.21748	0.266505	Q9FKW6 F4JZ46	LFNR1 FNR1
30	-0.216695	0.130442	Q94AR8	IIL1
31	-0.204904	0.244642	P25856	GAPA1
32	-0.203472	0.279788	Q8W4H7 Q8GTY0 Q0WL56 P0DH99 F4HUA0	A2 A4 A3 A1 At1g07930
33	-0.200796	0.318738	Q93VG5	RPS8A
34	-0.189758	0.102286	P48523	CAD4
35	-0.187959	0.160752	P56791	rpl2-A
36	-0.170597	0.175085	Q9SIV0	SUR1
37	-0.162061	0.226263	Q9SE60	MTHFR1
38	-0.161837	0.190582	O48917	SQD1
39	-0.157293	0.0688276	A0A2H1ZE37 Q0WP12	HOL1 HOL1
40	-0.146908	0.0952687	Q9ZRW8	GSTU19
41	-0.135891	0.15317	Q8LCE1 F4ID91 F4ID92	GLN1-2 GSR2 GSR2
42	-0.135855	0.183672	A0A1I9LPQ6	GLYR1

			Q9LSV0	GLYR1
43	-0.135011	0.161195	P47998	OASA1
44	-0.134101	0.245756	F4HU93 Q05431	APX1 APX1
45	-0.134017	0.365798	A8MRX2 Q42340 F4JWM1 Q9M8X9	At5g18380 RPS16C At5g18380 RPS16B
46	-0.128358	0.161321	B9DG17 Q08682	P40 RPSaA
47	-0.124937	0.197878	Q9FPF0	DJ1A
48	-0.108447	0.0577549	P38666 Q42347	RPL24B RPL24A
49	-0.0938969	0.0370444	Q9C5C8	MSRB2
50	-0.0843635	0.0832421	P48491	CTIMC
51	-0.0840487	0.106734	O65719	HSP70-3
52	-0.0806966	0.0760344	Q9CAV0	RPS3AA
53	-0.0724249	0.0651122	P56792	rpl14
54	-0.0623865	0.0754369	P42737 A8MQY4 F4K875 F4K873	BCA2 CA2 CA2 CA2
55	-0.0525584	0.0492368	P36428 F4I4Z2	ALATS ALATS
56	-0.0520153	0.0968568	Q43127	GLN2
57	-0.046751	0.0376131	P53492	ACT7
58	-0.0456166	0.040179	P49201 Q9SF35	RPS23B RPS23A
59	-0.0439487	0.0482193	Q9SRZ6	CICDH
60	-0.0346365	0.0205864	Q9LRS0 F4JFV6	GLO2 GOX2
61	-0.0336561	0.0162761	Q9ZUC1	AOR
62	-0.0330434	0.0332217	P17094 A8MQQ1	ARP1 RP1
63	-0.030766	0.0483192	Q9ZUT9	RPS5A
64	-0.0304408	0.0381135	A0A1I9LTP2 Q9S757	CYSC1 CYSC1
65	-0.0302677	0.0283987	F4I7M5 Q9ZUB3	SPDS1 SPDSYN1
66	-0.0280757	0.0164614	Q9SMT7	AAE3
67	-0.024405	0.0218722	Q9SRX2 P49693	RPL19A RPL19C
68	-0.0207772	0.0261669	Q9SUR0	At4g23670
69	-0.00971699	0.00754983	Q9S726	RPI3
70	-0.00117874	0.00142076	A0A1P8APR6 Q9LPW0 F4HNZ6	GAPA-2 GAPA2 GAPA-2

71	-0.000965118	0.00098249	P25857	GAPB
72	0.0107903	0.0157636	P93819	MDH1
73	0.0131516	0.0145128	O04487 C0Z2L8	At1g09640 At1g09640
74	0.0141115	0.0224493	F4J849 Q9LFA3	MDAR1 MDAR1
75	0.0249009	0.0126163	Q9LD57	PGK1
76	0.027987	0.0290152	F4JBY2 Q8RWV0	AtTKL1 TKL-1
77	0.0339499	0.0468038	Q93VP3	ELF5A-2
78	0.0359302	0.0305097	P24636	TUBB4
79	0.0377135	0.0220806	F4KEX3 Q8H1E2	MCK7.20 At5g58330
80	0.0412159	0.0648478	Q9FIE8 A0A1P8BFI1 A0A1P8BFL8 F4KHU8 A0A1P8B345 Q9ZV36	UXS3 UXS3 UXS3 UXS3 UXS6 UXS6
81	0.0417066	0.0443029	A0A2H1ZEA9 O65396	At1g11860 GDCST
82	0.0428205	0.0400157	Q9SQI8	LTA2
83	0.0542154	0.0556677	Q9STX2	VEP1
84	0.0543213	0.0343472	P94072	GER3
85	0.0592794	0.0418931	A0A1P8AY36 P51418 A8MRF3 Q8L7K0	At2g34480 RPL18AB RPL18AA RPL18AA
86	0.0593042	0.0707778	P19366	atpB
87	0.063714	0.1018	Q9LTX9	HSP70-7
88	0.0646448	0.0437881	Q94CE4	BCA4
89	0.0909648	0.037443	F4JRT7 Q9SW21	ACP4 ACP4
90	0.0950432	0.0907888	Q56WH1 B9DHQ0	TUBA3 TUBA5
91	0.0986776	0.179854	F4KGV2 F4KGV5 P48349	GRF6 GRF6 GRF6
92	0.106789	0.147321	Q9SJU4 F4IGL5 F4IGL7	FBA1 FBA1 FBA1
93	0.109306	0.0654108	Q8LDU4	RCCR
94	0.1141	0.330994	Q05758	At3g58610
95	0.115713	0.0717348	O04603	RPL5
96	0.11784	0.179867	P25858	GAPC1
97	0.139706	0.232961	Q944G9 F4JUJ5	FBA2 FBA2

98	0.144582	0.261161	A0A1I9LNS4 Q9M1R2	At3g62120 At3g62120
99	0.147529	0.17649	Q9STW6	HSP70-6
100	0.147755	0.188704	P16181 P42733 O65569	RPS11A RPS11C RPS11B
101	0.150311	0.151998	P56757	atpA
102	0.154481	0.216481	O23254	SHM4
103	0.155036	0.251334	Q9FJA6 Q9M339 Q9SIP7	RPS3C RPS3B RPS3A
104	0.15731	0.378774	F4JJ94 P42643	GRF1 GRF1
105	0.163599	0.215484	Q9SF85	ADK1
106	0.163869	0.162439	Q9LRR9 Q2V3V9 A8MS37 B3H4B8	GLO1 GOX1 GOX1 GOX1
107	0.167354	0.345495	O23654	VHA-A
108	0.167455	0.709335	Q9LIA8	UGD2
109	0.168392	0.309157	P25696 A0A1P8B1N1	ENO2 LOS2
110	0.16996	0.121076	Q940B0 P42791 A0A1P8BGQ0 A0A1I9LT16	RPL18C RPL18B At5g27850 RPL18
111	0.17044	0.192472	Q9SN86	At3g47520
112	0.193082	0.296681	P11574 Q8W4E2	VHA-B1 VHA-B3
113	0.195401	0.244604	A8MR07 Q94KE3	At3g52990 At3g52990
114	0.19656	0.113178	Q93VR3	At5g28840
115	0.202655	0.257916	Q9LF98	FBA8
116	0.203353	0.14346	Q9SFH9	HEMB1
117	0.207645	0.276431	Q949U7	PRXIIE
118	0.209758	0.134133	Q9SAJ4	PGK3
119	0.21118	0.190393	P46286	RPL8A
120	0.211536	0.888337	P55228	APS1
121	0.217359	0.158481	Q680P8	RPS29A
122	0.219254	0.326599	Q9LF46	HACL
123	0.220603	0.268961	Q96255	PSAT1
124	0.224663	0.449437	A0A1I9LT03 A0A1I9LT02 Q9M9P3	UGP1 UGP1 UGP2
125	0.226743	0.290381	Q9LR30	GGAT1
126	0.229014	0.504312	P30184 F4INR3	LAP1 LAP1

127	0.230126	0.151804	P42795 P42794	RPL11A RPL11B
128	0.230283	0.423156	O50008	MS1
129	0.231635	0.704834	P49688 Q93VB8 Q8L8Y0 Q9SCM3	RPS2C RPS2B RPS2A RPS2D
130	0.239193	0.339097	P83484 P83483 Q9C5A9	At5g08690 At5g08670 At5g08680
131	0.239908	0.473949	P06525	ADH1
132	0.243931	0.114376	Q93WJ8	MDAR2
133	0.244891	0.268248	Q42560 B3H5Y0	ACO1 ACO1
134	0.247039	0.154891	P56802	rps11
135	0.253595	0.097926	P10896 F4IVZ7	RCA RCA
136	0.278752	0.670682	Q9ZP06 A8MQK3 Q9LKA3	At1g53240 mMDH2 At3g15020
137	0.28157	0.587441	P25851	CFBP1
138	0.290537	0.817651	Q9ASR1	LOS1
139	0.291175	0.134866	Q8LEM8 Q43292 Q8LFH7	RPL37C RPL37B RPL37A
140	0.294251	0.378479	Q39161	NIR1
141	0.294353	0.547625	Q9ZU52	FBA3
142	0.296181	0.217027	Q9XEX2 F4ID64	PRXIIB TPX1
143	0.310331	0.577016	P22953 F4KCE5	HSP70-1 HSC70-1
144	0.311216	0.238524	Q9S9M7	At1g16080
145	0.312615	0.227039	P49691 F4KDU5	RPL4D At5g02870
146	0.326137	0.311228	A0A1I9LQB3 P27140	CA1 BCA1
147	0.335617	0.494049	Q9S7B5	TS1
148	0.346886	0.358272	P21238	CPN60A1
149	0.356298	0.232215	P29197	CPN60
150	0.367472	1.55773	P25855	GDH1
151	0.367911	0.440086	Q9LYG3	NADP-ME2
152	0.368495	0.4997	Q96291	BAS1
153	0.376338	0.68519	O80585	MTHFR2
154	0.381044	0.935791	F4I7I0	ALAAT1
155	0.383366	0.103998	P56795	rpl22
156	0.384377	0.697438	P51430 F4KGU2	RPS6B EMB3010

157	0.387128	0.296859	F4KDZ4 Q9ZP05 A0A1P8BBQ0 A8MRP1 B3H560	PMDH2 PMDH2 PMDH2 PMDH2 PMDH2
158	0.387244	0.390766	P46643	ASP1
159	0.401307	0.560577	P49200 Q9STY6	RPS20A RPS20B
160	0.401647	0.606016	Q94CE5	POP2
161	0.40332	0.331807	Q9LZG0 A0A1P8BAP0	ADK2 ADK2
162	0.419484	0.395934	Q9M5K3 Q9M5K2	LPD1 LPD2
163	0.430487	1.09301	Q8S4Y1	AAT1
164	0.434128	1.07406	O23627	At1g29880
165	0.435581	1.06011	Q9FM97 O65595	MCD7.8 At4g26390
166	0.440963	0.464244	Q9LHA8	HSP70-4
167	0.447565	0.322901	Q2V3X4 Q9SF40	At3g09630 RPL4A
168	0.465607	0.774014	Q8H156 P41917 P41916	RAN3 RAN2 RAN1
169	0.469532	0.663424	Q9LTF2 F4JTD3 Q9SW09	RPS10C At4g25740 RPS10A
170	0.485183	0.431627	Q9LVI9	PYD1
171	0.499854	1.33423	Q96533 F4K7D6	ADH2 HOT5
172	0.500311	0.822955	Q56WD9	PED1
173	0.501206	0.541837	Q94A28	ACO2
174	0.506311	1.13013	A0A1P8ATL2 Q9SA52	CRB CSP41B
175	0.507377	0.513133	P46283	At3g55800
176	0.507884	0.783601	Q9FVT2	At1g57720
177	0.514157	1.13348	Q93ZN9	DAP
178	0.52466	0.565455	Q9FJ95	SDH
179	0.550586	0.719737	Q9SW96	SYNC1
180	0.563024	0.46568	A8MRW5 O65423 B9DGL1	At4g21580 F18E5.200 At4g21580
181	0.566062	1.13854	F4JXD5 Q9ZSK4	ADF3 ADF3
182	0.586345	0.72547	Q9LKR3	BIP1
183	0.586451	0.511986	Q8LAS8	SFGH
184	0.589188	0.875591	F4JYE0 O04983 F4JYE1	CAC2 CAC2 CAC2

185	0.600116	1.20736	Q9SU63	ALDH2B4
186	0.679328	1.18471	F4K5C7 Q93VH9 Q8VYK6 P49204 F4IMI7	At5g07090 RPS4A RPS4D RPS4B At2g17360
187	0.787977	0.767376	P62126	rps12-A
188	1.04636	1.62243	Q09152	FPS1

Tab. 24 Effect of Ner-pretreatment on protein groups enriched with ≡Ctrl1. Results of the *t*-test comparing noncompetition ≡**Ctrl1**-labelled samples with **Ner**-pretreated ≡**Ctrl1**-labelled samples (2.2.5.2) on the complete list of ≡**Ctrl1**-enriched protein groups (Tab. 21) that were identified after OBD (2.2.4.2.2) and LC-MS/MS analysis (2.2.4.4) of the samples obtained from the *in vitro* labelling of Arabidopsis seedling extract with ≡**Ctrl1** (2.2.3.3.3). Protein groups (No.) were sorted by negative log_2-fold enrichment with ≡**Ctrl1** after **Ner**-pretreatment. –Log p-value, majority protein IDs (UniProt identifier) and gene names are reported for each protein group.

No.	Log_2-fold enrichment	-Log p-value	Majority protein IDs (Uniprot)	Gene names
1	-1.31796	0.643408	P60040 A8MRH4 Q9LHP1	RPL7B At2g01250 RPL7D
2	-1.23	0.541026	B9DG17 Q08682	P40 RPSaA
3	-1.17769	0.5839	F4HU93 Q05431	APX1 APX1
4	-1.14232	0.920739	Q93VG5	RPS8A
5	-0.986384	0.786863	F4HRW5 P51413	At1g67430 RPL17B
6	-0.857336	0.679569	P36428 F4I4Z2	ALATS ALATS
7	-0.803066	0.333081	A0A2H1ZE37 Q0WP12	HOL1 HOL1
8	-0.708397	0.540818	F4KEX3 Q8H1E2	MCK7.20 At5g58330
9	-0.699456	0.90525	B3H725 F4K0E8	HDS ISPG
10	-0.667747	0.944791	P43287	PIP2-2
11	-0.601773	0.359682	Q8LEM8 Q43292 Q8LFH7	RPL37C RPL37B RPL37A
12	-0.598297	0.522145	P16181 P42733 O65569	RPS11A RPS11C RPS11B
13	-0.540084	0.507369	Q8H103	PGI1
14	-0.507978	1.27057	A0A1P8AY36 P51418 A8MRF3 Q8L7K0	At2g34480 RPL18AB RPL18AA RPL18AA
15	-0.503348	0.264481	Q9C5R8 A0A1P8BD74	At5g06290 2-Cys Prx B
16	-0.483788	0.634909	A0A1I9LTP2 Q9S757	CYSC1 CYSC1
17	-0.482382	0.931003	Q05758	At3g58610
18	-0.47101	0.500421	O23627	At1g29880
19	-0.4702	0.372483	Q9LYG3	NADP-ME2

20	-0.461895	0.649604	Q42403	TRX3
21	-0.450259	0.256952	Q9FWR4 Q9LN39	DHAR1 At1g19550
22	-0.446561	0.482677	O23254	SHM4
23	-0.438184	0.264627	Q9MAH0	PPC1
24	-0.437825	0.52441	P49637 Q9LR33	RPL27AC RPL27AB
25	-0.415495	0.288474	Q9SF85	ADK1
26	-0.410475	0.660424	P22953 F4KCE5	HSP70-1 HSC70-1
27	-0.408111	0.404171	P10795	RBCS-1A
28	-0.400003	0.358208	P49200 Q9STY6	RPS20A RPS20B
29	-0.369931	0.19259	P32961 Q8LFU8	NIT1 NIT1
30	-0.368532	0.353233	P47999	OASB
31	-0.325248	0.350677	Q9LRS0 F4JFV6	GLO2 GOX2
32	-0.322868	0.313689	P56791	rpl2-A
33	-0.315262	0.380254	Q9C5C8	MSRB2
34	-0.307872	0.149471	Q9SN86	At3g47520
35	-0.271134	0.185806	P31170	HSP21
36	-0.26781	0.347271	F4JJ94 P42643	GRF1 GRF1
37	-0.266506	0.406285	Q9FIE8 A0A1P8BFI1 A0A1P8BFL8 F4KHU8 A0A1P8B345 Q9ZV36	UXS3 UXS3 UXS3 UXS3 UXS6 UXS6
38	-0.238932	0.160869	P55228	APS1
39	-0.238575	0.245386	A8MRX2 Q42340 F4JWM1 Q9M8X9	At5g18380 RPS16C At5g18380 RPS16B
40	-0.229584	0.0919824	P34788	RPS18A
41	-0.210129	0.106616	B9DG18 Q42547 A0A1P8AWT7 F4HUL6 Q2V4M4 A0A1P8AWR0	CAT3 CAT3 CAT3 CAT3 CAT3 CAT3
42	-0.209356	0.203621	P42795 P42794	RPL11A RPL11B
43	-0.194377	0.158965	Q9LKR3	BIP1
44	-0.183247	0.124088	P34790	CYP18-3
45	-0.166248	0.252632	Q9FPF0	DJ1A
46	-0.165761	0.266563	B3H5S2	RBCS3B

			P10798 P10797 F4KA76	RBCS-3B RBCS-2B RBCS3B
47	-0.162442	0.318749	O23654	VHA-A
48	-0.159733	0.218578	Q9SIB9	ACO3
49	-0.14299	0.282479	Q8W4H7 Q8GTY0 Q0WL56 P0DH99 F4HUA0	A2 A4 A3 A1 At1g07930
50	-0.131103	0.339731	Q43127	GLN2
51	-0.11709	0.139615	F4JD96 Q9SFU1	At3g07110 RPL13AA
52	-0.0960274	0.115816	P25819 F4JM86 A0A1P8B564	CAT2 CAT2 CAT2
53	-0.089756	0.140706	P53492	ACT7
54	-0.0722051	0.118676	P25858	GAPC1
55	-0.0685248	0.0831948	P25697	At1g32060
56	-0.0532241	0.0591244	Q9SR37	BGLU23
57	-0.051013	0.0638204	Q9CAV0	RPS3AA
58	-0.0395346	0.0813229	P29197	CPN60
59	-0.0332365	0.034287	A0A1P8ATL2 Q9SA52	CRB CSP41B
60	-0.0248995	0.0497046	P48491	CTIMC
61	-0.0242453	0.0319127	O50008	MS1
62	-0.00652838	0.0050434	Q9STW6	HSP70-6
63	-0.000889778	0.000800477	P24636	TUBB4
64	0.00241327	0.0028378	O64650 Q9M2F1	RPS27A RPS27B
65	0.00436449	0.00609302	Q42522	GSA2
66	0.00526381	0.0107559	P25696 A0A1P8B1N1	ENO2 LOS2
67	0.00727749	0.0073214	Q9ZP06 A8MQK3 Q9LKA3	At1g53240 mMDH2 At3g15020
68	0.0128469	0.0173958	O23255 F4JTV4 A8MQP1 F4JTV5	SAHH1 HOG1 HOG1 HOG1
69	0.0157561	0.0134226	Q9ZUY6 Q9SGE0	AXS1 AXS2
70	0.0221066	0.0116498	F4KDZ4 Q9ZP05 A0A1P8BBQ0 A8MRP1 B3H560	PMDH2 PMDH2 PMDH2 PMDH2 PMDH2

71	0.0233774	0.0332829	A0A1I9LT03 A0A1I9LT02 Q9M9P3	UGP1 UGP1 UGP2
72	0.0256605	0.0337975	Q8H156 P41917 P41916	RAN3 RAN2 RAN1
73	0.0257678	0.0379916	F4JBY2 Q8RWV0	AtTKL1 TKL-1
74	0.0258961	0.0249299	F4I576 P92947 F4I577	MDAR6 MDAR5 MDAR6
75	0.026639	0.0208946	Q9LR75	CPX1
76	0.0285773	0.0273493	P31265	TCTP1
77	0.0399604	0.0534465	Q5GM68	PPC2
78	0.0408878	0.0499819	A0A1P8APR6 Q9LPW0 F4HNZ6	GAPA-2 GAPA2 GAPA-2
79	0.0451846	0.0257679	F4K5C7 Q93VH9 Q8VYK6 P49204 F4IMI7	At5g07090 RPS4A RPS4D RPS4B At2g17360
80	0.046258	0.0255084	P37702	TGG1
81	0.0529356	0.0394404	Q9LR30	GGAT1
82	0.0531836	0.0792103	P42737 A8MQY4 F4K875 F4K873	BCA2 CA2 CA2 CA2
83	0.0536442	0.0534884	Q940B0 P42791 A0A1P8BGQ0 A0A1I9LT16	RPL18C RPL18B At5g27850 RPL18
84	0.0549493	0.0321937	Q94AR8	IIL1
85	0.0590982	0.198431	Q9LF98	FBA8
86	0.0675087	0.197771	Q9ASR1	LOS1
87	0.0678506	0.0663622	Q9SRZ6	CICDH
88	0.0704732	0.0336893	Q9LRR9 Q2V3V9 A8MS37 B3H4B8	GLO1 GOX1 GOX1 GOX1
89	0.0719957	0.0470673	Q9LD57	PGK1
90	0.0750484	0.067642	P49688 Q93VB8 Q8L8Y0 Q9SCM3	RPS2C RPS2B RPS2A RPS2D
91	0.0803576	0.0608173	A0A1I9LQB3 P27140	CA1 BCA1
92	0.0853572	0.0799226	Q94CE5	POP2

93	0.0935574	0.197913	Q9ZNZ7	GLU1
94	0.0970016	0.120619	P10796	RBCS-1B
95	0.101232	0.209963	P25856	GAPA1
96	0.103846	0.152213	Q949U7	PRXIIE
97	0.116382	0.152425	Q9SZJ5	SHM1
98	0.12009	0.155263	P25857	GAPB
99	0.126925	0.181222	Q9SDM O04316	NSP1 NSP4
100	0.130996	0.163868	P56757	atpA
101	0.131116	0.207704	P19366	atpB
102	0.131376	0.118908	Q96255	PSAT1
103	0.132542	0.10056	Q9LHA8	HSP70-4
104	0.136878	0.194105	Q42029	PSBP1
105	0.139619	0.189429	P21276 F4JRV2	FSD1 FSD1
106	0.144697	0.114814	P59224	RPS13B
107	0.148185	0.242115	P93819	MDH1
108	0.149098	0.0935188	P25851	CFBP1
109	0.150737	0.132789	F4JXD5 Q9ZSK4	ADF3 ADF3
110	0.158584	0.196	Q9SFH9	HEMB1
111	0.161695	0.320947	Q9SE60	MTHFR1
112	0.164926	0.388724	Q42560 B3H5Y0	ACO1 ACO1
113	0.167572	0.361938	P25855	GDH1
114	0.180357	0.2985	Q9FKW6 F4JZ46	LFNR1 FNR1
115	0.182771	0.124833	O65398	GLX1
116	0.187399	0.347905	Q9SRX2 P49693	RPL19A RPL19C
117	0.192944	0.444479	P11574 Q8W4E2	VHA-B1 VHA-B3
118	0.196404	0.247725	A0A2H1ZEA9 O65396	At1g11860 GDCST
119	0.196862	0.139639	P46283	At3g55800
120	0.20225	0.173682	Q93VT9 Q08770 A0A1P8AUU3	RPL10A RPL10B RPL10B
121	0.213466	0.355444	Q96533 F4K7D6	ADH2 HOT5
122	0.214823	0.492213	P46643	ASP1
123	0.216931	0.214736	P38666 Q42347	RPL24B RPL24A
124	0.217277	0.15201	Q9M5K3 Q9M5K2	LPD1 LPD2
125	0.218587	0.243252	P21240 C0Z361	CPN60B1 CPN60B3

126	0.219735	0.463902	F4IX28 F4IX26 P34791	ROC4 ROC4 CYP20-3
127	0.222168	0.589931	Q9SJU4 F4IGL5 F4IGL7	FBA1 FBA1 FBA1
128	0.222465	0.546667	Q1WIQ6 F4INS6 A0A2H1ZE23	ALDH11A3 ALDH11A3 ALDH11A3
129	0.225177	0.358476	Q38882	PLDALPHA1
130	0.226384	0.256716	Q56YA5	AGT1
131	0.227036	0.125816	Q9C5C2	TGG2
132	0.230606	0.103848	Q38946 F4K6P9	GDH2 GDH2
133	0.231488	0.19582	P42734	CAD9
134	0.237883	0.462812	F4JYE0 O04983 F4JYE1	CAC2 CAC2 CAC2
135	0.241947	0.236201	Q9C9W5 A0A1P8ANC0	HPR HPR
136	0.24859	0.596295	P83484 P83483 Q9C5A9	At5g08690 At5g08670 At5g08680
137	0.276107	0.489281	P30184 F4INR3	LAP1 LAP1
138	0.281412	0.301602	F4J849 Q9LFA3	MDAR1 MDAR1
139	0.295867	0.546602	Q56WH1 B9DHQ0	TUBA3 TUBA5
140	0.306068	0.686485	Q8W493 C0Z2A8	LFNR2 FNR2
141	0.309851	0.973424	Q944G9 F4JUJ5	FBA2 FBA2
142	0.317099	0.335146	Q39161	NIR1
143	0.334916	0.493151	P21238	CPN60A1
144	0.348115	0.712513	Q93ZN9	DAP
145	0.368116	0.147591	P10896 F4IVZ7	RCA RCA
146	0.370843	0.356911	P46286	RPL8A
147	0.424725	0.486792	Q9S726	RPI3
148	0.431695	0.528392	Q9SUR0	At4g23670
149	0.438473	0.545624	Q96291	BAS1

Tab. 25 Effect of Ner-pretreatment on protein groups enriched with ≡Ctrl2. Results of the *t*-test comparing noncompetition ≡**Ctrl2**-labelled samples with **Ner**-pretreated ≡**Ctrl2**-labelled samples (2.2.5.2) on the complete list of ≡**Ctrl2**-enriched protein groups (Tab. 22) that were identified after OBD (2.2.4.2.2) and LC-MS/MS analysis (2.2.4.4) of the samples obtained from the *in vitro* labelling of Arabidopsis seedling extract with ≡**Ctrl2** (2.2.3.3.3). Protein groups (No.) were sorted by negative log_2-fold enrichment with ≡**Ctrl2** after **Ner**-pretreatment. –Log p-value, majority protein IDs (UniProt identifier) and gene names are reported for each protein group.

No.	Log_2-fold enrichment	-Log p-value	Majority protein IDs (Uniprot)	Gene names
1	-1.24159	0.906666	O23515 Q8VYF1	RPL15A RPL15B
2	-1.23858	1.78618	Q8LCE1 F4ID91 F4ID92	GLN1-2 GSR2 GSR2
3	-0.895714	0.856114	P47999	OASB
4	-0.743895	0.395542	P46283	At3g55800
5	-0.73259	0.315542	Q03251 F4JVC0 F4JVC1	RBG8 CCR1 CCR1
6	-0.713881	0.789551	P56791	rpl2-A
7	-0.712182	0.716179	Q42403	TRX3
8	-0.590641	0.314196	O23627	At1g29880
9	-0.549078	0.972211	F4JTH0 P46248 B9DG21	ASP5 ASP5 ASP5
10	-0.521255	0.267324	Q9SIB9	ACO3
11	-0.513369	0.883263	Q9FIE8 A0A1P8BFI1 A0A1P8BFL8 F4KHU8 A0A1P8B345 Q9ZV36	UXS3 UXS3 UXS3 UXS3 UXS6 UXS6
12	-0.498034	0.258942	O04487 C0Z2L8	At1g09640 At1g09640
13	-0.473485	0.913664	Q940B0 P42791 A0A1P8BGQ0 A0A1I9LT16	RPL18C RPL18B At5g27850 RPL18
14	-0.462414	0.802849	Q9SE60	MTHFR1
15	-0.459542	0.146151	P37702	TGG1
16	-0.416134	0.313137	A0A1I9LNS4 Q9M1R2	At3g62120 At3g62120
17	-0.389469	0.261685	B3H5S2 P10798 P10797 F4KA76	RBCS3B RBCS-3B RBCS-2B RBCS3B

18	-0.355742	0.903535	F4J849 Q9LFA3	MDAR1 MDAR1
19	-0.316467	0.195411	Q9SN86	At3g47520
20	-0.302581	0.238751	P42734	CAD9
21	-0.277894	0.385813	Q9STW6	HSP70-6
22	-0.269217	0.0690009	Q8LEM8 Q43292 Q8LFH7	RPL37C RPL37B RPL37A
23	-0.267777	0.321012	Q96533 F4K7D6	ADH2 HOT5
24	-0.263839	0.271583	O23254	SHM4
25	-0.263251	0.298389	Q93WN0	SBP2
26	-0.259599	0.473067	P25857	GAPB
27	-0.257818	0.296768	Q9SDM9 O04316	NSP1 NSP4
28	-0.253353	0.21682	F4JYE0 O04983 F4JYE1	CAC2 CAC2 CAC2
29	-0.235004	0.302684	Q9LR30	GGAT1
30	-0.232312	0.162076	F4JFY5 Q42592 F4JFY4	SAPX APXS SAPX
31	-0.227809	0.218125	Q8LAS8	SFGH
32	-0.216956	0.112138	Q9SFH9	HEMB1
33	-0.196738	0.194622	Q9ZUT9	RPS5A
34	-0.196373	0.165613	Q38814	THI1
35	-0.195157	0.551101	O64650 Q9M2F1	RPS27A RPS27B
36	-0.194641	0.289152	Q38882	PLDALPHA1
37	-0.193147	0.150339	F4I576 P92947 F4I577	MDAR6 MDAR5 MDAR6
38	-0.190006	0.395686	A0A2H1ZEA9 O65396	At1g11860 GDCST
39	-0.189031	0.335872	Q93ZN9	DAP
40	-0.173135	0.18717	P10796	RBCS-1B
41	-0.166266	0.161257	P30184 F4INR3	LAP1 LAP1
42	-0.164724	0.0910317	Q9ZRW8	GSTU19
43	-0.161933	0.156173	Q9LD57	PGK1
44	-0.160653	0.213663	Q9LYG3	NADP-ME2
45	-0.149259	0.278397	P38666 Q42347	RPL24B RPL24A
46	-0.148941	0.262426	Q9LXG1 B3H7J6 Q9FLF0	RPS9B At5g15200 RPS9C
47	-0.147491	0.172592	P22953	HSP70-1

			F4KCE5	HSC70-1
48	-0.146504	0.211375	Q9LLC1	BCCP2
49	-0.145234	0.369358	P16181 P42733 O65569	RPS11A RPS11C RPS11B
50	-0.142955	0.0896057	P34788	RPS18A
51	-0.133503	0.153256	P32961 Q8LFU8	NIT1 NIT1
52	-0.126213	0.489824	P42737 A8MQY4 F4K875 F4K873	BCA2 CA2 CA2 CA2
53	-0.125919	0.116104	Q949U7	PRXIIE
54	-0.119252	0.115688	P46286	RPL8A
55	-0.116745	0.2138	Q9SJU4 F4IGL5 F4IGL7	FBA1 FBA1 FBA1
56	-0.116505	0.132733	Q9M5K3 Q9M5K2	LPD1 LPD2
57	-0.106397	0.108022	Q9LRR9 Q2V3V9 A8MS37 B3H4B8	GLO1 GOX1 GOX1 GOX1
58	-0.106029	0.176279	Q9CAV0	RPS3AA
59	-0.105464	0.0667637	Q42029	PSBP1
60	-0.100007	0.170365	P25697	At1g32060
61	-0.0929718	0.102073	A0A1I9LQB3 P27140	CA1 BCA1
62	-0.0817394	0.169969	P56757	atpA
63	-0.078783	0.0931304	Q8S4Y1	AAT1
64	-0.0632858	0.100803	Q9ASR1	LOS1
65	-0.0611024	0.0764329	P25856	GAPA1
66	-0.0484724	0.0806277	F4KDZ4 Q9ZP05 A0A1P8BBQ0 A8MRP1 B3H560	PMDH2 PMDH2 PMDH2 PMDH2 PMDH2
67	-0.0479369	0.0387084	P42795 P42794	RPL11A RPL11B
68	-0.0473766	0.0257253	F4JJ94 P42643	GRF1 GRF1
69	-0.0370274	0.0532617	P48491	CTIMC
70	-0.0244884	0.0311249	Q9LF98	FBA8
71	-0.0223074	0.0341878	Q05758	At3g58610
72	-0.0181823	0.0189772	Q94CE5	POP2
73	-0.0128589	0.0312486	Q9ZNZ7	GLU1
74	-0.0110993	0.0121861	F4JD96 Q9SFU1	At3g07110 RPL13AA

75	-0.0101576	0.0117759	Q9FPF0	DJ1A
76	-0.00452852	0.00485793	A0A1P8ATL2 Q9SA52	CRB CSP41B
77	-0.00349426	0.00402476	P19366	atpB
78	-0.00259542	0.00178335	Q9LHA8	HSP70-4
79	-0.00137663	0.00113529	P55228	APS1
80	-0.000420094	0.000630593	A0A1I9LTP2 Q9S757	CYSC1 CYSC1
81	-0.000109196	0.000162207	Q9S7B5	TS1
82	0.0000734329	0.0000870244	Q9SF85	ADK1
83	0.00749254	0.00573147	Q9SR37	BGLU23
84	0.0113263	0.00774497	P25855	GDH1
85	0.0117288	0.0168713	Q42522	GSA2
86	0.0148039	0.0230482	F4JBY2 Q8RWV0	AtTKL1 TKL-1
87	0.025022	0.0201945	Q5GM68	PPC2
88	0.0273771	0.030725	O23654	VHA-A
89	0.0301681	0.0330748	O50008	MS1
90	0.0339279	0.0285932	P59224	RPS13B
91	0.0393033	0.0363175	P11574 Q8W4E2	VHA-B1 VHA-B3
92	0.0401316	0.0334569	Q9LKR3	BIP1
93	0.0488815	0.0655489	P49688 Q93VB8 Q8L8Y0 Q9SCM3	RPS2C RPS2B RPS2A RPS2D
94	0.070406	0.0701657	Q9XFT3	PSBQ1
95	0.0706487	0.106498	Q9SIH0	RPS14A
96	0.081223	0.0708052	Q56WH1 B9DHQ0	TUBA3 TUBA5
97	0.0857306	0.0338899	Q38946 F4K6P9	GDH2 GDH2
98	0.0894403	0.086268	Q9SRX2 P49693	RPL19A RPL19C
99	0.0919371	0.20395	Q1WIQ6 F4INS6 A0A2H1ZE23	ALDH11A3 ALDH11A3 ALDH11A3
100	0.0920444	0.0474933	Q9S726	RPI3
101	0.0956602	0.166599	Q56YA5	AGT1
102	0.0960455	0.175208	Q944G9 F4JUJ5	FBA2 FBA2
103	0.0987277	0.0796521	P24636	TUBB4
104	0.106728	0.147719	Q9C9W5 A0A1P8ANC0	HPR HPR
105	0.110296	0.176222	Q43127	GLN2
106	0.112763	0.141311	Q8H156 P41917	RAN3 RAN2

			P41916	RAN1
107	0.12862	0.176083	Q9FKW6 F4JZ46	LFNR1 FNR1
108	0.144341	0.1676	P25858	GAPC1
109	0.144534	0.194011	Q9SZJ5	SHM1
110	0.147252	0.0713571	P10896 F4IVZ7	RCA RCA
111	0.147673	0.216975	Q9SRZ6	CICDH
112	0.152167	0.163767	Q9SUR0	At4g23670
113	0.158977	0.26939	Q9MAH0	PPC1
114	0.162076	0.158726	P83484 P83483 Q9C5A9	At5g08690 At5g08670 At5g08680
115	0.173208	0.200395	Q96291	BAS1
116	0.1801	0.394299	Q9ZP06 A8MQK3 Q9LKA3	At1g53240 mMDH2 At3g15020
117	0.180435	0.320778	P25696 A0A1P8B1N1	ENO2 LOS2
118	0.189483	0.189104	P60040 A8MRH4 Q9LHP1	RPL7B At2g01250 RPL7D
119	0.202006	0.348456	A0A1I9LT03 A0A1I9LT02 Q9M9P3	UGP1 UGP1 UGP2
120	0.209308	0.25629	Q8W4H7 Q8GTY0 Q0WL56 P0DH99 F4HUA0	A2 A4 A3 A1 At1g07930
121	0.211982	0.322416	P21238	CPN60A1
122	0.223153	0.456018	Q9FWR4 Q9LN39	DHAR1 At1g19550
123	0.248878	0.26021	O23255 F4JTV4 A8MQP1 F4JTV5	SAHH1 HOG1 HOG1 HOG1
124	0.252473	0.247653	P46643	ASP1
125	0.266829	0.39629	Q42560 B3H5Y0	ACO1 ACO1
126	0.292183	0.517282	Q9ZU52	FBA3
127	0.318673	0.56042	P21240 C0Z361	CPN60B1 CPN60B3
128	0.322927	0.505886	P21276 F4JRV2	FSD1 FSD1
129	0.347615	0.260568	Q2V3X4 Q9SF40	At3g09630 RPL4A
130	0.383655	0.437904	P93819	MDH1

131	0.410829	0.341698	Q680P8	RPS29A
132	0.4694	0.543427	F4IX28 F4IX26 P34791	ROC4 ROC4 CYP20-3
133	0.523161	0.537975	Q39161	NIR1
134	0.591287	0.85992	P25851	CFBP1
135	1.09846	0.459025	P53492	ACT7

Appendix 12: Compound composition of the used chemical kinase inhibitor library

Tab. 26 Complete list of kinase inhibitors employed in the screen for SA agonist in *PR1p::GUS* Arabidopsis seedlings. The chemical name for all used kinase inhibitors is given alongside with the respective number and the library they originate from.

Library	Number	Chemical name
BML-2832	1	PD-98059
BML-2832	2	U-0126
BML-2832	3	SB-203580
BML-2832	4	H-7·2HCl
BML-2832	5	H-9·HCl
BML-2832	6	Staurosporine
BML-2832	7	AG-494
BML-2832	8	AG-825
BML-2832	9	Lavendustin A
BML-2832	10	RG-1462
BML-2832	11	Tyrphostin 23
BML-2832	12	Tyrphostin 25
BML-2832	13	Tyrphostin 46
BML-2832	14	Tyrphostin 47
BML-2832	15	Tyrphostin 51
BML-2832	16	Tyrphostin 1
BML-2832	17	Tyrphostin AG 1288
BML-2832	18	Tyrphostin AG 1478
BML-2832	19	Tyrphostin AG 1295
BML-2832	20	Tyrphostin 9
BML-2832	21	Hydroxy-2-naphthalenylmethylphosphonic acid
BML-2832	22	PKC-412
BML-2832	23	Piceatannol
BML-2832	24	PP1
BML-2832	25	AG-490
BML-2832	26	AG-126
BML-2832	27	AG-370
BML-2832	28	AG-879
BML-2832	29	LY 294002
BML-2832	30	Wortmannin
BML-2832	31	GF 109203X

BML-2832	32	Hypericin
BML-2832	33	Ro 31-8220 mesylate
BML-2832	34	(D)-*erythro*-Sphingosine
BML-2832	35	H-89·2HCl
BML-2832	36	H-8
BML-2832	37	HA-1004·2HCl
BML-2832	38	HA-1077·2HCl
BML-2832	39	2-Hydroxy-5-(2,5-dihydroxybenzylamino)benzoic acid
BML-2832	40	KN-62
BML-2832	41	KN-93
BML-2832	42	ML-7·HCl
BML-2832	43	ML-9·HCl
BML-2832	44	2-Aminopurine
BML-2832	45	N9-isopropyl-olomoucine
BML-2832	46	Olomoucine
BML-2832	47	Iso-olomoucine
BML-2832	48	Roscovitine
BML-2832	49	5-Iodotubericidin
BML-2832	50	LFM-A13
BML-2832	51	SB-202190
BML-2832	52	PP2
BML-2832	53	ZM 336372
BML-2832	54	SU 4312
BML-2832	55	AG-1296
BML-2832	56	GW 5074
BML-2832	57	Palmitoyl-(DL)-carnitine
BML-2832	58	Rottlerin
BML-2832	59	Genistein
BML-2832	60	Daidzein
BML-2832	61	Erbstatin analog
BML-2832	62	Quercetin·2H_2O
BML-2832	63	SU1498
BML-2832	64	ZM 449829
BML-2832	65	BAY 11-7082
BML-2832	66	5,6-dichloro-1-β-(D)-ribofuranosylbenzimidazole
BML-2832	67	HBDDE
BML-2832	68	SP 600125
BML-2832	69	Indirubin
BML-2832	70	Indirubin-3'-monooxime
BML-2832	71	Y-27632·2HCl
BML-2832	72	Kenpaullone

BML-2832	73	Terreic acid
BML-2832	74	Triciribine
BML-2832	75	BML-257
BML-2832	76	SC-514
BML-2832	77	BML-259
BML-2832	78	Apigenin
BML-2832	79	BML-265
BML-2832	80	Rapamycin
Hand picked	81	PD 153035
Hand picked	82	Canertinib
Hand picked	83	Vandetinib
Hand picked	84	Erlotinib
Hand picked	85	Gefitinib
Hand picked	86	Neratinib
Hand picked	87	Lapatinib
Hand picked	88	Pelitinib
Hand picked	89	Mubritinib
Hand picked	90	Salicylic acid (internal control)

Appendix 13: Chemical synthesis of ≡Ner, ≡Ctrl1 and ≡Ctrl2

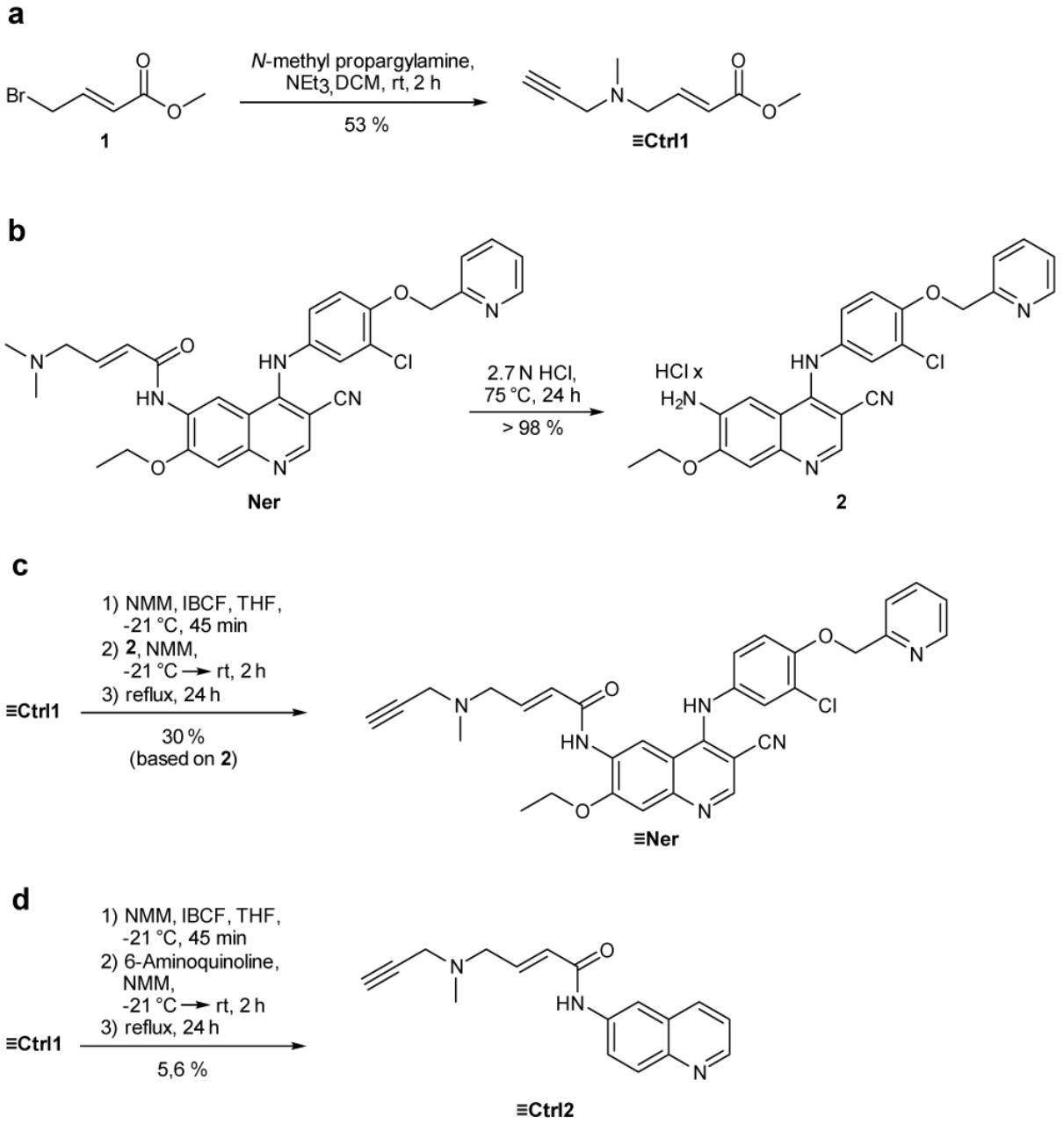

Fig. 38 Chemical synthesis of ≡Ner, ≡Ctrl1 and ≡Ctrl2. (a) Methyl-*trans*-4-(*N*-methyl propargyl)-2-butenoate (**≡Ctrl1**) was prepared from methyl *trans*-4-bromo-2-butenoate (**1**) and *N*-methyl propargylamine. (b) Acid-catalysed hydrolysis of the amino butenoate moiety of **Ner** yielding **2** (c). **≡Ner** is prepared by the coupling of **≡Ctrl1** with **2**. (d) Synthesis of **≡Ctrl2** from **≡Ctrl1** and 6-aminoquinoline.

Appendix 14: Site-directed mutagenesis of AtEH7

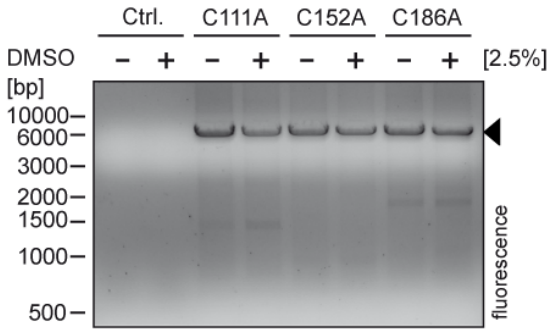

Fig. 39 Control of DNA amplification after PCR-based site-directed mutagenesis of AtEH7. To check for the successful amplification of the *eh7*::pET-59-DEST template plasmid DNA using the designed primer pairs during site-directed mutagenesis (2.2.2.2), 20 µL of the digested PCR products were analysed by agarose gel electrophoresis (2.2.2.3).

Appendix 15: Purification of recombinant mutant AtEH7

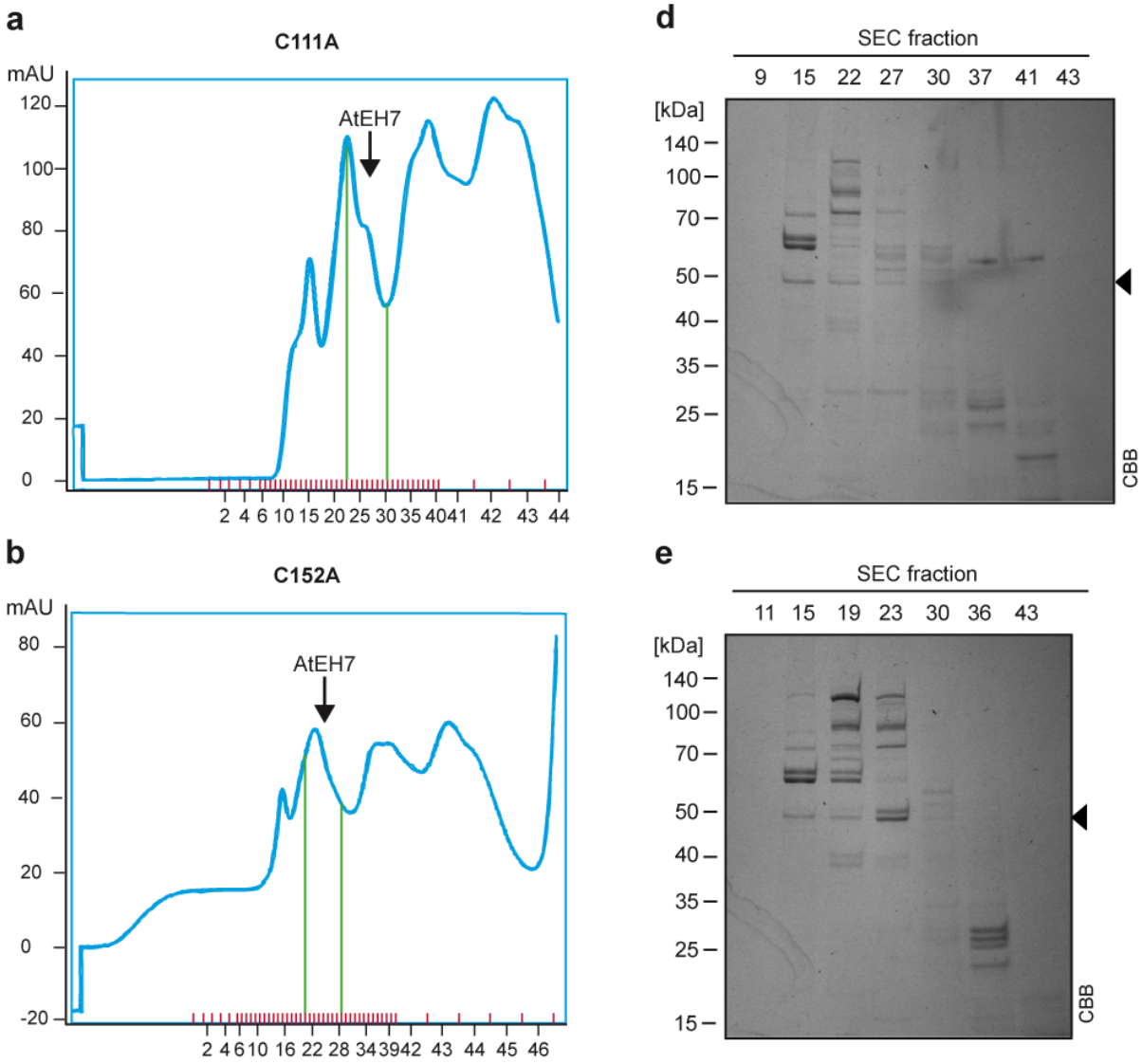

[Continued]

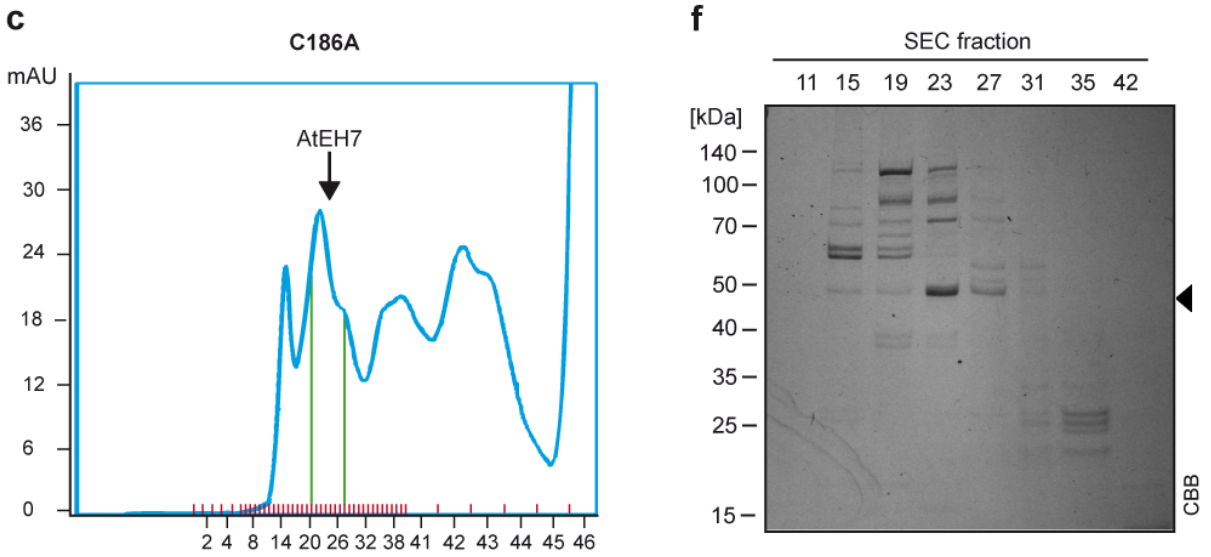

Fig. 40 SEC purification of recombinant mutant AtEH7. (a) Recombinant mutant C111A, C152A and C186A AtEH7 which was produced in (2.2.1.5) and extracted from *E. coli* (2.2.1.6.1) was purified by SEC (2.2.3.1.3) following IMAC using a NI-IDA resin (2.2.3.1.2). SEC of the pooled AtEH7 elution was performed on a Superdex™ column using IMAC200 buffer as eluent. (b) SEC fractions were analysed by gel electrophoresis (2.2.3.6) and subsequent staining with a colloidal Coomassie solution (2.2.3.9). AtEH7 was confirmed to be present on gel and SEC fractions containing large amounts of AtEH7 (as indicated in (a)) were combined to yield the final enzyme purification that was utilised in chemical labelling experiments (2.2.3.3.3) as well as in enzyme assays (2.2.3.10).

Appendix 16: Control gel for the labelling of recombinant AtEH7 with ≡Ner

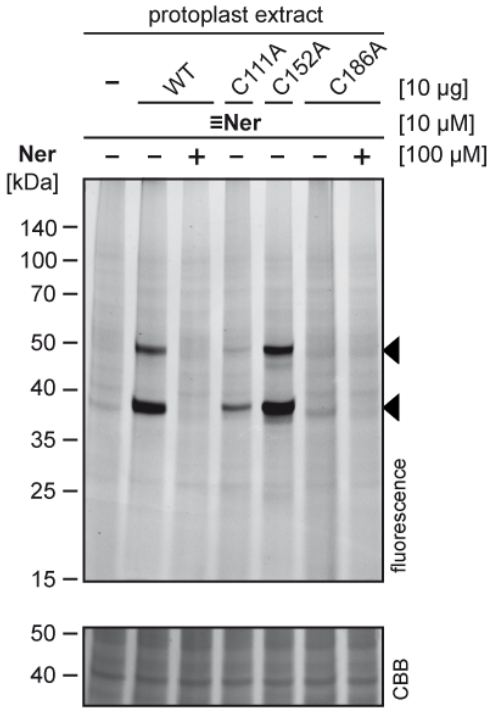

Fig. 41 Control gel for the labelling of WT and mutant AtEH7 with ≡Ner. *In vitro* labelling of Arabidopsis protoplast extract as well as recombinant WT and mutant AtEH7 spiked to Arabidopsis protoplast extract with **≡Ner** visualised by fluorescence detection. 10 µg of WT or mutant AtEH7 was spiked to 50 µg Arabidopsis protoplast extract whereas 50 µg of protoplast extract alone were additionally utilised for the labelling. A final probe concentration of 10 µM **≡Ner** was used. Preincubation with **Ner** was done at a final concentration of 100 µM, if applicable. Expression and purification of recombinant WT and mutant AtEH7 (2.2.1.5, 2.2.1.6.1 and 2.2.3.1), disruption of Arabidopsis plant material (2.2.1.6.3), protein concentration determination (2.2.3.2), *in vitro* labelling (2.2.3.3.3), methanol-chloroform precipitation (2.2.3.4) and 'click' reaction (2.2.3.5) were performed as described in the methods section. For the sample separation by gel electrophoresis (2.2.3.6), 13.3 µL of the samples (10 µg of total protein from Arabidopsis chloroplasts, 2 µg of recombinant AtEH7) and 7 µL of protein ladder were loaded on an 11 % Bis-Tris gel. The fluorescence of the fluorophore Cy3 ($\lambda_{ex.}$ = ~550 nm excitation, $\lambda_{em.}$ = ~570 nm emission) was detected using Cy3-DIGE settings (green laser $\lambda_{em.}$ = 532 nm, BPG1 band pass green filter 560-580 nm) of the laser scanner (2.2.3.7). Equal loading of the gel was confirmed by staining with a colloidal Coomassie solution (2.2.3.9).

Appendix 17: Sequence homology comparison of Arabidopsis EHs

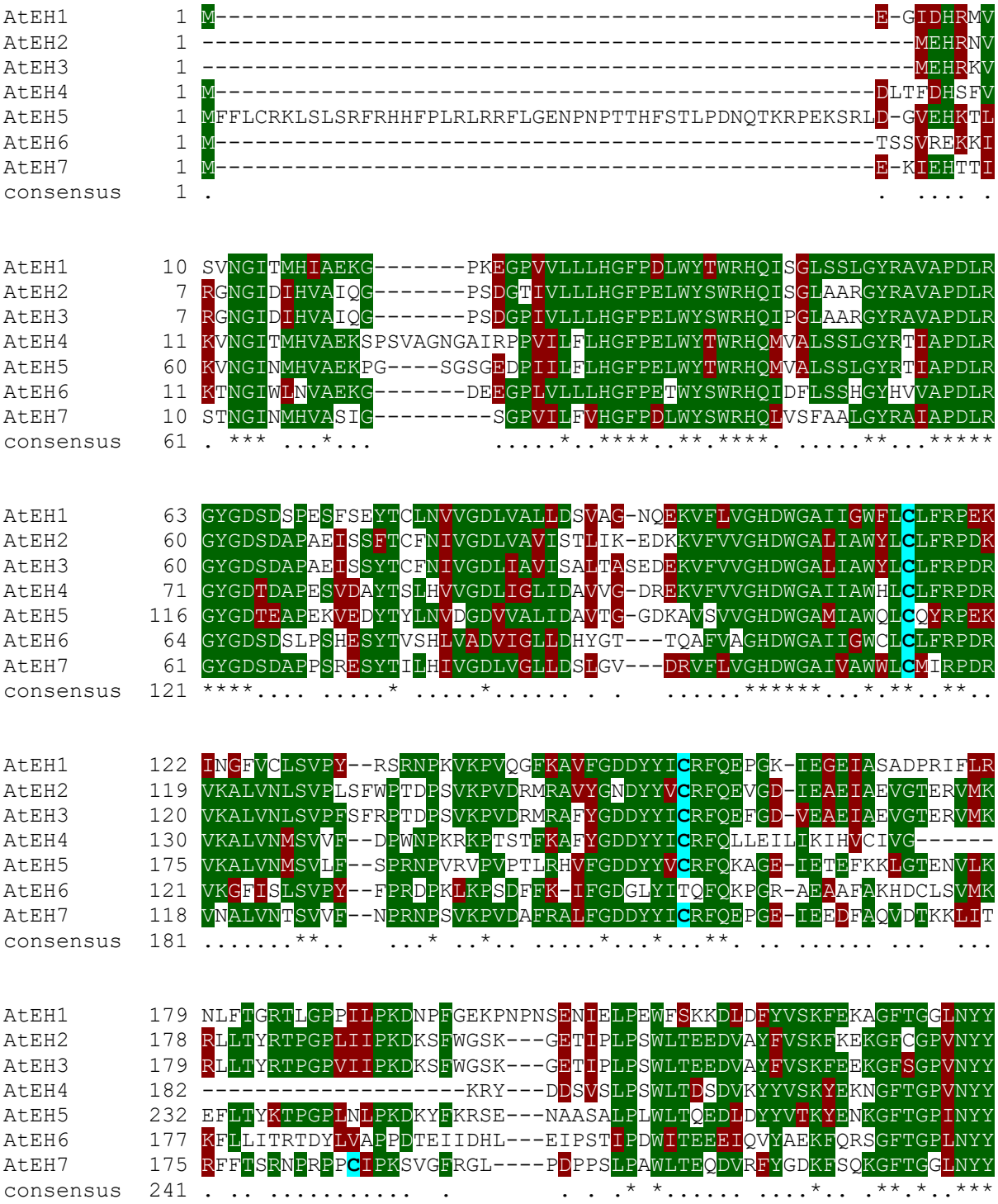

[Continued]

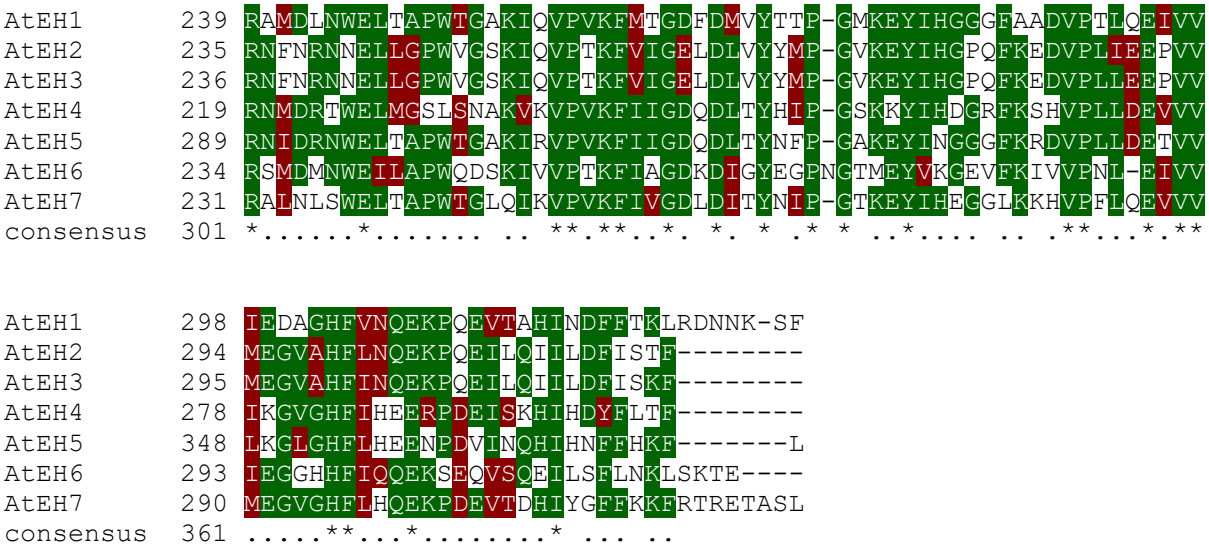

Fig. 42 Sequence homology comparison of Arabidopsis EHs. The sequences of all seven loci from Arabidopsis that exhibit EH activity were compared by MSA (2.2.5.4). The three cysteine residues present in the sequence of AtEH7 are highlighted in light blue. Numbering of Arabidopsis EHs is in accordance with Pineu *et al*.[188].

Appendix 18: Sequence homology comparison of AtEH7 with NbEH2.1 and NbEH2.2

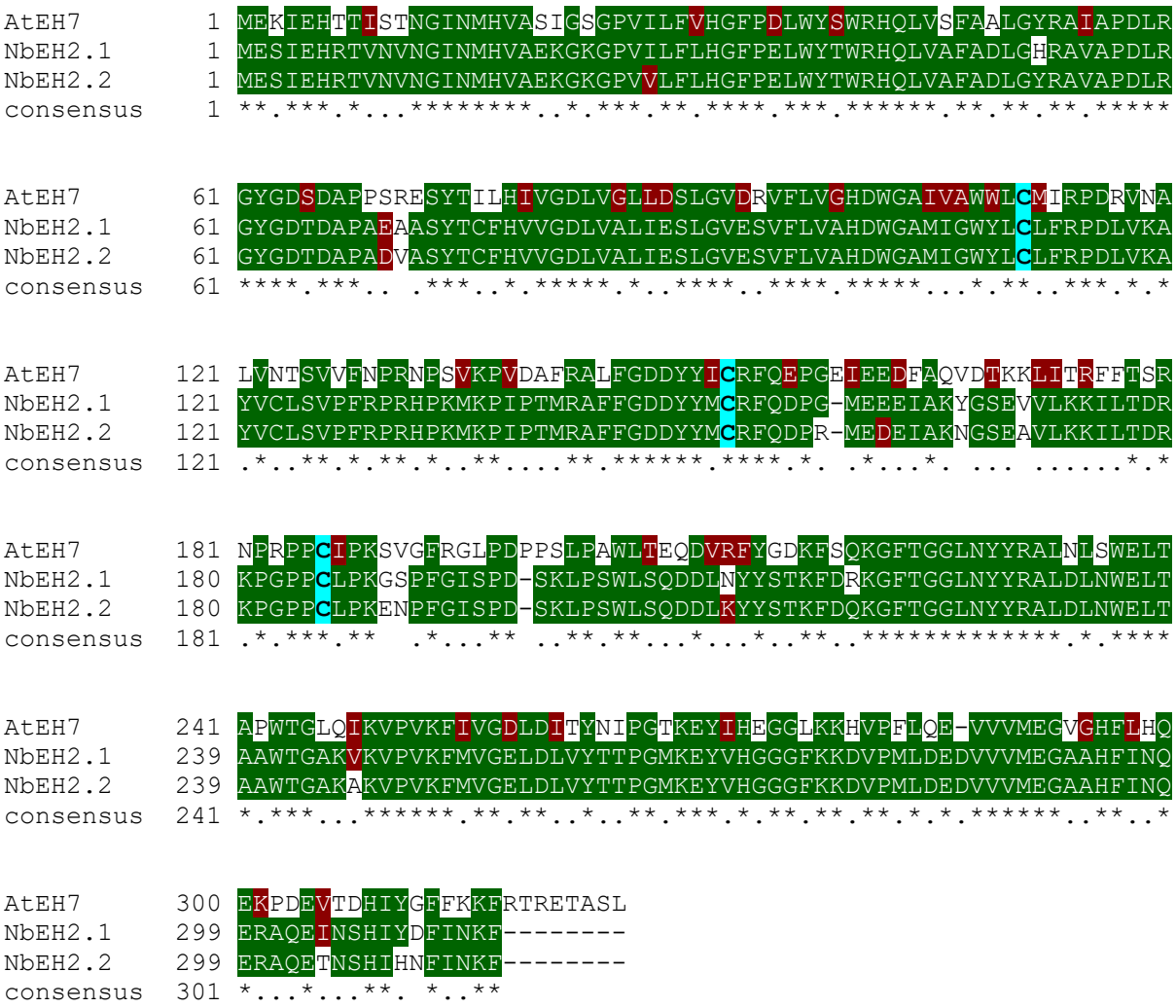

Fig. 43 Sequence homology comparison of AtEH7 and *N. benthamiana* EHs. MSA (2.2.5.4) of Arabidopsis AtEH7 with the two peroxisomal EHs NbEH2.1 and NbEH2.2 from *N. benthamiana*. The three conserved cysteine residues are highlighted in light blue.

Danksagung

An dieser Stelle möchte ich mich bei all denjenigen Menschen bedanken, die aktiv oder auch passiv eine wichtige Rolle bei der Entstehung dieser Arbeit gespielt haben. Besonders danken möchte ich Prof. Dr. Markus Kaiser, der mich von Beginn meiner wissenschaftlichen Arbeit an stets mit einem offenen Ohr begleitet und unterstützt hat und mir die Möglichkeit geboten hat, meine Doktorarbeit in seiner Arbeitsgruppe schreiben zu dürfen. Weiterhin möchte ich mich bei Prof. Dr. Bettina Siebers für die langjährige gute Zusammenarbeit sowie für die Übernahme des Zweitgutachtens bedanken.

Bedanken möchte ich mich ebenfalls bei allen aktuellen und ehemaligen Mitgliedern der AGs Kaiser & Saccà, mit denen ich über die ganzen letzten Jahre zusammenarbeiten durfte und die entweder zu meiner Arbeit beigetragen oder einfach nur den Laboralltag und die Mittagspausen drum herum bereichert haben. Danke an Dr. Jan Krahn und Sarah Resch für die Synthese der in dieser Arbeit verwendeten chemischen Sonden. Danke auch an Svenja Kernchen für ihre superschnelle Hilfe bei allen bürokratischen Angelegenheiten von A bis Z, an Svenja Heimann für die Hilfe bei der Vorbereitung der MS Proben und an Jenny Bormann für ihre Hilfe bei der Etablierung des Enzymassays. Vielen Dank auch an Dr. Farnusch Kaschani für seine Unterstützung bei allen Belangen rund um die Massenspektrometrie. Und danke an alle anderen für die super Atmosphäre innerhalb der Arbeitsgruppe, denn ohne Euch hätte es definitiv nur halb so viel Spaß gemacht.

Danke auch an die AG Ehrmann, vor allem an Helmut Tourné, der mir immer tatkräftig mit Chemikalien und Verbrauchsmaterialien ausgeholfen hat, wenn mal wieder dringend etwas besser noch gestern als heute benötigt wurde. Mein weiterer Dank geht an Dr. Vivek Halder, der mit mir an diesem Projekt gearbeitet und alle meine pflanzenbiologischen Fragen geduldig beantwortet hat.

Ein besonders großes Dankeschön gilt meinen lieben Freunden, die mich nicht nur in der Zeit der Entstehung dieser Arbeit immer bestärkt und aufgemuntert haben. Hier möchte ich vor allem auch meinen fleißigen Korrekturlesern dieser Arbeit für Ihre Zeit und Mühe und die daraus resultierenden konstruktiven Ratschläge danken.

Mein größter Dank aber gilt meiner Familie, insbesondere meinen Eltern, die mich stets bedingungslos unterstützt und immer an mich geglaubt haben. Ich habe euch lieb!

Lebenslauf

[Der Lebenslauf ist in der Online-Version aus Gründen des Datenschutzes nicht enthalten.]

[Der Lebenslauf ist in der Online-Version aus Gründen des Datenschutzes nicht enthalten.]

[Der Lebenslauf ist in der Online-Version aus Gründen des Datenschutzes nicht enthalten.]

Erklärungen

Erklärung:

Hiermit erkläre ich, gem. § 7Abs. (2) d) + f) der Promotionsordnung der Fakultät für Biologie zur Erlangung des Dr. rer. nat., dass ich die vorliegende Dissertation selbständig verfasst und mich keiner anderen als der angegebenen Hilfsmittel bedient, bei der Abfassung der Dissertation nur die angegeben Hilfsmittel benutzt und alle wörtlich oder inhaltlich übernommenen Stellen als solche gekennzeichnet habe.

Essen, den _____ _____

Unterschrift des/r Doktoranden/in

Erklärung:

Hiermit erkläre ich, gem. § 7Abs. (2) e) + g) der Promotionsordnung der Fakultät für Biologie zur Erlangung des Dr. rer. nat., dass ich keine anderen Promotionen bzw. Promotionsversuche in der Vergangenheit durchgeführt habe und dass diese Arbeit von keiner anderen Fakultät/Fachbereich abgelehnt worden ist.

Essen, den _____ _____

Unterschrift des/r Doktoranden/in

Erklärung:

Hiermit erkläre ich, gem. § 6 Abs. (2) g) der Promotionsordnung der Fakultät für Biologie zur Erlangung der Dr. rer. nat., dass ich das Arbeitsgebiet, dem das Thema „Chemoproteomics as a versatile approach for the study and identification of the target enzymes of neratinib in *Arabidopsis thaliana*“ zuzuordnen ist, in Forschung und Lehre vertrete und den Antrag von Sabrina Ninck befürworte und die Betreuung auch im Falle eines Weggangs, wenn nicht wichtige Gründe dem entgegenstehen, weiterführen werde.

_____

Name des Mitglieds der Universität Duisburg-Essen in Druckbuchstaben

Essen, den _____ _____

Unterschrift eines Mitglieds
der Universität Duisburg-Essen